ROLE OF RND EFFLUX PUMPS AND BIOFILM IN CONFERRING ANTIMICROBIAL RESISTANCE (AMR)

A THESIS TO BE SUBMITTED TO

THE UNIVERSITY OF TRANS-DISCIPLINARY HEALTH SCIENCES AND TECHNOLOGY

FOR THE AWARD OF THE DEGREE OF

DOCTOR OF PHILOSOPHY

BY

PURNENDU BHOWMIK

UNDER THE GUIDANCE OF

DR. VASANTHI RAMACHANDRAN AND

&

DR. NAGAKUMAR BHARATHAM

BUGWORKS RESEARCH INDIA PVT. LTD.

AUGUST 2024

THE UNIVERSITY OF TRANS-DISCIPLINARY HEALTH SCIENCES AND TECHNOLOGY

Private University Established in Karnataka by ACT 35 of 2013

BENGALURU - 560064

DECLARATION BY THE CANDIDATE

I declare that this thesis entitled "**Role of RND Efflux Pumps and Biofilm in Conferring Antimicrobial Resistance (AMR)**", submitted for the award of Doctor of Philosophy to THE UNIVERSITY OF TRANS-DISCIPLINARY HEALTH SCIENCES AND TECHNOLOGY, Bengaluru is my original work, conducted under the supervision of my guide, **Dr VASANTHI RAMACHANDRAN** and co-guide, **Dr NAGAKUMAR BHARATHAM**. I also wish to inform that no part of the research has been submitted for a degree or examination at any university. References, help and material obtained from other sources have been duly acknowledged.

I hereby confirm the originality of the work and that there is no plagiarism in any part of the dissertation.

Place: Bengaluru **Signature of the Candidate**

Date: August 13, 2024

Name of candidate: Purnendu Bhowmik

Registration No. and Date of Registration: 20220021188 dated February 20, 2020.

THE UNIVERSITY OF TRANS-DISCIPLINARY HEALTH SCIENCES AND TECHNOLOGY

Private University Established in Karnataka by ACT 35 of 2013

BENGALURU - 560064

CERTIFICATE

This is to certify that the work incorporated in this thesis "**Role of RND efflux pumps and biofilm in conferring antimicrobial resistance (AMR)**" submitted by **Purnendu Bhowmik** was carried out under my supervision. No part of this thesis has been submitted for a degree or examination at any university. References, help and material obtained from other sources have been duly acknowledged. I hereby confirm the originality of the work and that there is no plagiarism in any part of the dissertation.

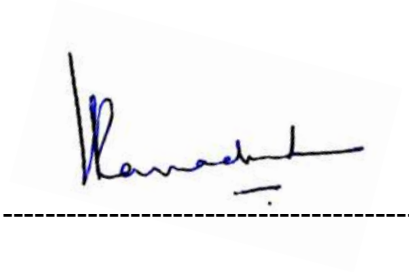

Research Supervisor

Date: August 13, 2024

Dr. Vasanthi Ramachandran

Vice President, Collaborations

Bugworks Research India Pvt. Ltd.

3rd Floor, C-CAMP, NCBS-TIFR,

GKVK-UAS Campus, Bellary Road,

Bengaluru 560065, Karnataka, India

THE UNIVERSITY OF TRANS-DISCIPLINARY HEALTH SCIENCES AND TECHNOLOGY

Private University Established in Karnataka by ACT 35 of 2013

BENGALURU - 560064

CERTIFICATE

This is to certify that the work incorporated in this thesis **"Role of RND efflux pumps and biofilm in conferring antimicrobial resistance (AMR)"** submitted by **Purnendu Bhowmik**, "Role of RND efflux pumps and biofilm in conferring antimicrobial resistance (AMR)", submitted by Purnendu Bhowmik, was carried out under my supervision. No part of this thesis has been submitted for a degree or examination at any university. References, help and material obtained from other sources have been duly acknowledged. I hereby confirm the originality of the work and that there is no plagiarism in any part of the dissertation.

Co-Supervisor

Date: August 13, 2024

Dr. Nagakumar Bharatham

Principal Scientist, Transition Bio,

Cambridge, United Kingdom.

Acknowledgement

"The journey of a thousand miles begins with a single step…(Chinese Proverb)"

The journey towards securing a PhD spans thousands of miles, and I was very fortunate to traverse this path. Whenever I sought help, I received plenty of support and encouragement from several people around me, who offered their unconditional support in making this dream a reality. In this section, I would like to duly acknowledge their timely help and guidance in all possible ways.

First and foremost, I would like to express my gratitude to Dr Anand Anandkumar, Dr Balasubramanian V., and Dr Santanu Datta (Bugworks Research Inc.) for giving me this opportunity to undertake this PhD research programme. Their commitment to bridging academia and industry has allowed me to explore real-world challenges while contributing to the advancement of knowledge. I am also grateful to them for allowing me to conduct this research and contribute towards their vision of addressing and finding solutions to one of the major global challenges of humanity while working at Bugworks. Their constant motivation helped me to push my boundaries, widen my knowledge base, and hone my skills while conducting all the challenging studies. The valuable mentorship of Dr Santanu Datta has always encouraged me to think outside the box and understand and address complex scientific problems with more basic, straightforward approaches.

I owe my gratitude to my supervisors, Dr Vasanthi Ramachandran and Dr Nagakumar Bharatham, for their unwavering guidance, mentorship and support. Their deep insights, critical feedback, and extensive experience have been instrumental in shaping the direction and quality of this thesis. Moreover, their constant support and scientific inputs have been an absolute learning experience in research, critical analysis, scientific writing and publications. I am also thankful to the members of my Doctoral Advisory Committee (DAC) members, Dr Shahul P Hameed and Dr Nainesh Katagihallimath, whose expertise and constructive feedback have added tremendous value to this work. My senior colleagues, Mr Ranga Rao, Dr Harish Kaushik Kotakonda, Dr Biswanath Majumdar, Dr Vasan Sambandamurthy and Ms Leela Maitreyee, have been guiding pillars throughout the journey of my PhD with their insightful suggestions and guidance.

The success of any scientific discovery lies in the collaborative efforts of people from multiple disciplines, and words would be limited to express my gratitude to all the

authors who have contributed to the scientific discoveries reported in this thesis and published in the scientific community. I extend my heartfelt appreciation to Dr. Victoria Hmar for her contributions to my published work on biofilm. Her work on target gene KOs and qRT-PCR in clinical isolates has significantly enriched the outcome of my research. I am also grateful to Prof. Satoshi Murakami for his collaborative research, critical insights, and shared inputs, which have enriched the research process and broadened the perspectives of this research work.

The success of this journey would be incomplete without acknowledging the collective contributions of my lab mates at Bugworks, who have been instrumental in carrying out my day-to-day research work. While it would be difficult to thank everyone in the lab individually, I would like to express my gratitude to all for their constant support and encouragement and for making the lab space "*my second home*" to conduct my research work comfortably. All my colleagues at Bugworks have been there with me throughout the entire tenure of my PhD, and their cooperation, critical analysis, and scientific inputs have enriched my research work significantly. I have always considered myself fortunate to have a friend and colleague, Anirudh P Shanbhag. I could not thank him enough in words for his unwavering support, both personally and professionally, which has helped me achieve my goals and complete this journey. I am also thankful to Mr. Ravikumar G, Assistant Registrar, TDU, for his guidance and assistance with the academic formalities of TDU.

Last but not least, I would like to thank my friends and family (both old and new) for their unwavering support and understanding throughout this academic journey. My wife, Sanjukta, has been a true companion in this journey and a constant source of inspiration. I am also thankful to my brother and mother for their continuous support and for keeping the dream of completing the PhD alive in their hearts, which has always encouraged and motivated me. Their endless affection, support, love, and encouragement have been a constant source of my strength throughout this challenging journey. Their confidence and faith in me have not only shaped me into who I am today but also made them an integral part of my academic achievements.

Dedicated to my Family…

List of Contents

List of Tables

List of Tables: Appendix

List of Figures

List of Figures: Appendix

List of Abbreviations

Sl. No.	Abbreviation	Full Form
1	ABC	ATP-binding cassette (ABC)
2	AbgT	p-Aminobenzoyl-glutamate transporter
3	ADP	Adenosine diphosphate
4	AI-2	Autoinducer-2
5	AMP	Adenosine monophosphate
6	AMR	Antimicrobial resistance
7	ATP	Adenosine triphosphate
8	CA	Colanic Acid
9	cAMP	Cyclic- AMP
10	c-di-GMP	Cyclic-di-GMP
11	CIP/CIPRO	Ciprofloxacin
12	CLSI	Clinical and Laboratory Standard Institute
13	DNA	Deoxyribonucleic acid
14	Eco	*Escherichia coli*
15	EPI	Efflux Pump Inhibitor
16	EPS	Extra-cellular polymeric substances/ Exopolymeric Substance
17	ERY	Erythromycin
18	ESBL	Extended Spectrum Beta-Lactamases
19	ESKAPE	*Enterococcus faecium, Staphylococcus aureus, Klebsiella pneumoniae, Acinetobacter baumannii, Pseudomonas aeruginosa, and Enterobacter sp*.
20	FBA	Flux Balance Analysis
21	FQ	Fluoroquinolone
22	GDP	Guanosine diphosphate
23	GMP	Guanosine monophosphate
24	GTP	Guanosine triphosphate
25	HGT	Horizontal Gene Transfer
26	IMP	Inner Membrane Protein
27	IRMA	Irreversible Mass Action
28	kb	Kilobase
29	KD	Knockdown
30	KO	Knockout
31	Kpn	*Klebsiella pneumoniae*
32	L	Litre
33	LEVO	Levofloxacin
34	LPS	lipopolysaccharides
35	LZD	Linezolid
36	MATE	Multidrug And Toxic Compound Extrusion

Sl. No.	Abbreviation	Full Form
37	MBL	Metallo-Beta-Lactamases
38	MDR	Multidrug-resistant/Multidrug resistance
39	MFP	Membrane Fusion protein
40	MFS	Major Facilitator Superfamily
41	mg	Milligram
42	MHB	Muller-Hilton Broth
43	MIC	Minimum Inhibitory Concentration
44	min	Minute
45	mM	Millimolar
46	MOXI	Moxifloxacin
47	MRSA	Methicillin-Resistant *Staphylococcus aureus*
48	NOR	Norfloxacin
49	NOV	Novobiocin
50	ODE	Ordinary Differential Equation
51	OE	Overexpression
52	OLA	Olaquindox
53	OMP	Outer Membrane channel Protein
54	PACE	Proteobacterial Antimicrobial Compound Efflux
55	Pae	*Pseudomonas aeruginosa*
56	PAβN	Phenylalanine-arginine β-naphthylamide
57	PBPs	Penicillin-Binding Protein
58	PCR	Polymerase chain reaction
59	PGA	poly-beta-1,6-N-acetyl-D-glucosamine
60	QRDR	Quinolone-Resistance-Determining Region
61	qRT-PCR	Quantitative Real-Time Polymerase Chain Reaction
62	RIF	Rifampicin
63	RMA	Reversible Mass Action
64	RNA	Ribonucleic acid
65	RNase	Ribonuclease
66	RND	Resistance Nodulation and Division
67	rpm	Rotation per minute
68	rRNA	Ribosomal RNA
69	S.E.	Standard Error
70	s/sec	Seconds(s)
71	SA	*Staphylococcus aureus*
72	SD	Standard Deviation
73	SMR	Small Multidrug Resistance
74	SP	Structural proteins
75	UPEC	Uropathogenic *Escherichia coli*

Sl. No.	Abbreviation	Full Form
77	VRE	Vancomycin-resistant *Enterococci*
78	VRSA	Vancomycin-resistant *S. aureus*
79	WHO	World Health Organization
80	WT	Wild-type
81	β -Lactam	Beta-Lactam
82	μg	Microgram
83	μM	Micromolar

Synopsis of the Thesis

In recent years, antimicrobial resistance (AMR) has emerged as a worldwide threat that is worrying and increasingly becoming an imminent danger to global health and the well-being of humanity. This crisis has been quietly gathering momentum, raising concerns among scientists, healthcare professionals, and policymakers alike. Throughout history, antimicrobial agents have been the cornerstone of modern medicine, enabling us to conquer infectious diseases that once claimed countless lives. However, with the continuous evolution of microbes, along with the overuse and misuse of the available antibiotics, AMR development is also growing at an alarming rate. The situation has worsened to such an extent that many of the treatment regimens, once considered effective and reliable, are gradually being rendered obsolete today.

Microbes employ a diverse array of defence mechanisms to counter the inhibitory effect of antibiotics and help them to survive. Among these, efflux pumps and biofilms significantly contribute to the AMR phenomenon. While the former contributes to the extrusion of toxic metabolites and antibiotics out of the bacterial planktonic form, the latter provides an impervious barrier and confers protection to the bacterial population per se at a community level. The association of both of these factors in pathogens responsible for hospital-acquired infections further indicates their significance in the development of the multi-drug resistance that impedes successful treatments in healthcare setups.

The focus of the present work on AMR development aims to understand the role of the key contributing factors contributing to efflux-mediated and biofilm-driven AMR. The first aspect of the work is based on the structural and functional explorations of efflux pump members belonging to the RND family. Furthermore, explorative research on the characterization of the structural and functional aspects of OqxB, the not-so-well-characterized RND efflux pump in *Klebsiella pneumoniae*, adds significant knowledge to our current understanding of their roles in multi-drug efflux, especially the fluoroquinolones. Another aspect of the study is focused on understanding the interplay of factors contributing to biofilm formation in *Escherichia coli*. The validated *in silico* platform developed and reported in this work would certainly enhance our current understanding of the roles of different pathways, signalling molecules and cellular components, which drive the transition of the bacteria from their motile

planktonic phase to sessile biofilm forms. Overall, the outcomes of this research would significantly aid in designing agents that could interfere with efflux pump inhibition and/or disruption of biofilms, with specific applications in different industrial sectors, including healthcare.

The research findings of the present work are comprehensively detailed in six chapters, encompassing the significance of RND efflux pumps and biofilms in antimicrobial resistance (AMR), and their roles in promoting resistance mechanisms, as discussed below:

Chapter 1 provides a comprehensive review of the literature on antibiotics, their mode of action and the mechanisms behind the emergence of antimicrobial resistance (AMR) among various classes of antibiotics observed in the recent decade. It provides the basis for the urgent need to address issues and develop countermeasures against drug-resistant microbes that are posing imminent threats in critical care. This chapter also touches upon an alternate lifestyle called biofilms adopted by pathogenic bacteria to escape harsh growth conditions. Surprisingly, there is a clear link between AMR and biofilms, especially in device-associated and chronic infections. This chapter sets the stage for the current research work, highlighting the significance of understanding AMR to devise strategies to combat the growing threat of antibiotic-resistant infections.

Chapter 2 explores the vital role of the RND efflux pump family in bacterial systems. It investigates their functions and examines the intriguing promiscuity of permeases and MFPs despite substantial differences in sequence homology. The chapter showcases that MexAB from *Pseudomonas aeruginosa* and OqxAB from *Klebsiella pneumoniae*, have a remarkable ability to drive antibiotic efflux in efflux compromised background of *E. coli* system, thereby demonstrating functional overexpression of pumps in heterologous bacteria. This research sheds light on the potential mechanisms, including the possibility of horizontal gene transfer to spread antibiotic resistance. There is a clear need for understanding efflux pumps to devise strategies for combating bacterial infections.

Chapter 3 revolves around structural and functional investigations aimed at structural and functional explorations, leading to the characterization of OqxB, the RND efflux pumps found in *Klebsiella pneumoniae*. While crystal structure analysis helps in revealing its distinct structural architecture, *in silico* and *in vitro* studies offer valuable

insights into the functional aspects of OqxB and the potential mechanisms behind its ability to efflux a wide range of antibiotics, including fluoroquinolones. This research sheds light on the molecular basis of antibiotic resistance, providing crucial information for understanding and combatting multidrug-resistant infections caused by *K. pneumoniae*.

Chapter 4 extends the research from Chapter 3 and focuses on identifying and characterizing the roles of crucial charged and uncharged residues at the substrate binding pocket of OqxB. Through site-directed mutagenesis studies, this chapter investigates their role in binding and the subsequent efflux of fluoroquinolones. The identification of key residues has led to an enhanced understanding of OqxB's functional mechanisms and provides valuable insights for developing targeted approaches to combat antibiotic resistance associated with efflux pumps.

Chapter 5 is dedicated towards exploring the critical role of biofilms in antimicrobial resistance (AMR). Using *E. coli* as the model organism, the developed validated *in silico* dynamic model is one of the significant attempts to have a holistic understanding of the events associated with biofilm formation. The chapter sheds light on the involvement of key structural components and regulatory players, including efflux pumps, within the biofilm architecture of *E. coli*., by integrating various signalling and regulatory pathways related to biofilms. The roles of different key components are thoroughly investigated in the model, and by identifying potential and novel target genes (*miaA, ydeO and ygiV*) against biofilms, this research offers promising avenues to combat AMR and enhance antimicrobial therapies. The chapter emphasizes the clinical relevance of studying biofilms, as understanding their mechanisms is crucial in tackling persistent infections and improving patient outcomes.

Chapter 6 includes a comprehensive summary of the key findings and underscores the importance of this study in developing effective strategies to counter drug resistance. By elucidating the interplay between efflux pumps, biofilms, and AMR, this work not only contributes to advancing antimicrobial therapies but also significantly aids in the fight against the global challenge of antibiotic resistance, emphasizing the critical role of this research in the scientific community.

List of Publications

- Name of the Candidate: **Purnendu Bhowmik**
- Date of Registration and Registration number: **20/02/2020, 20220021188**
- Name of Institution: **Bugworks Research India Pvt. Ltd., Bangalore, India.**
- No. of Publications: **3**
- Link to Scopus Profile: https://www.scopus.com/authid/detail.uri?authorId=57202033037

1. Nagakumar Bharatham, **Purnendu Bhowmik**, Maho Aoki, Ui Okada, Sreevalli Sharma, Eiki Yamashita, Anirudh P. Shanbhag, Sreenath Rajagopal, Teby Thomas, Maitrayee Sarma, Riya Narjari, Savitha Nagaraj, Vasanthi Ramachandran, Nainesh Katagihallimath, Santanu Datta & Satoshi Murakami. **Structure and function relationship of OqxB efflux pump from *Klebsiella pneumoniae***. ***Nature Communications***. *Volume 12, Article number: 5400 (2021)*. doi: 10.1038/s41467-021-25679-0; PMID: 34518546. Publication Date: September 13, 2021. (Impact Factor: 11.878)

2. **Purnendu Bhowmik**, Sreenath Rajagopal, Rothangamawi Victoria Hmar, Purnima Singh, Pragya Saxena, Prakruthi Amar, Teby Thomas, Rajani Ravishankar, Savitha Nagaraj, Nainesh Katagihallimath, Ramanujan Kadambi Sarangapani, Vasanthi Ramachandran, and Santanu Datta. **Validated *In Silico* Model for Biofilm Formation in *Escherichia coli*. *ACS Synthetic Biology***. *2022, 11, 2, 713–731*. https://doi.org/10.1021/acssynbio.1c00445; PMID: 35025506. Publication Date: January 13, 2022. (Impact Factor: 5.249)

3. **Purnendu Bhowmik**, Nagakumar Bharatham, Satoshi Murakami, Vasanthi Ramachandran, Santanu Datta. **Identification of key amino acid residues in OqxB mediated efflux of fluoroquinolones using site-directed mutagenesis**. ***Research in Microbiology.*** *Volume 174, Issue 4, May 2023, 104039.* doi: 10.1016/j.resmic.2023.104039; PMID: 36738814. Publication Date: February 03, 2023 (Impact Factor: 2.6)

List of Conferences/Paper presentations

Oral Presentation

1. Validated *in silico* model for biofilm formation in *Escherichia coli*. Presented at "Advances in Microbial Biotechnology: Current Trends And Future Prospects". Organized by the Department of Microbiology, Biotechnology & Food Technology in Association with Microbiologists Society, India (MSI), Bangalore University (April 28-29, 2022).

2. Structure and function relationship of OqxB efflux pump from *Klebsiella pneumoniae*. Presented at 62nd Annual International Conference of Association of Microbiologists of India (AMI) "Microbiology and Society: Current Trends and Future Prospects" (MSCTFP-2022). Organized by University of Mysore, in association with CSIR-CFTRI, DRDO-DFRL, KSTA and JSS AHER Mysuru (September 21-23, 2022).

Conference Participation

1. "Antimicrobial resistance (AMR) Man Vs Microbes: Race of the Century". International symposium on Antimicrobial resistance, Biocrest 2021. Organized by School of Biotechnology at Amritha Vishwa Vidyapeetham, CHARM at University of California (San Diego), Bugworks Research Inc. and C-CAMP (February 24-26, 2021).

Chapter 1

Antimicrobial Resistance (AMR): An Emerging Global Threat

1.1 Antibiotics: Origins and the journey so far

The use of the term antibiotic can be traced back to 1890, when the word "*antibiose*" was first used by Paul Vuillemin in his publication to describe the antagonistic action between different microorganisms (for example, fungi vs bacteria; bacteria vs protozoa), as an antonym to the symbiotic relationship between microorganisms (Nicolaou & Rigol, 2017). However, the term is being used with a broader meaning nowadays to include specially designed small molecules or drugs for treating infections via inhibition of microbial growth, survival, and spread. Antibiotic-producing bacteria have been used to treat open wounds in Serbia, China, Greece, and Egypt for more than 2000 years, demonstrating the long history of their usage in disease prevention. The oldest medical text that exists today is Eber's papyrus from 1550 BC, which lists cures, including mouldy bread and medicinal soil. In addition, an Anglo-Saxon recipe described 1000 years ago has recently been demonstrated to kill methicillin-resistant *Staphylococcus aureus* (MRSA) (Harrison et al., 2015). In 1907, Paul Ehrlich introduced the term' magic bullet', referring to a theoretical drug that could have an adverse effect only on a target pathogen without harming either its host or causing any collateral damage to the surrounding environment. Ehrlich envisioned a drug that would precisely hit its target with complete accuracy, thus eliminating the pathogen without any unintended consequences (J. Blair, 2017). Later, in 1910, the deployment of the first synthetic antibiotic, the arsenic-based pro-drugs salvarsan (Arsphenamine) and neo-salvarsan, to treat *Treponema pallidum*, the causal organisms of syphilis became a milestone event in the history of discovery of antibiotics. As a result, Paul Ehrlich is widely credited for his remarkable contributions to the development of the first anti-infective drugs and the fundamental idea of chemotherapy (Hutchings et al., 2019). The serendipitous discovery of penicillin by Sir Alexander Fleming in 1928 further revolutionized the era of antibiotics and started the golden age of discoveries of natural-product-based antibiotics that peaked in the mid-1950s. Since then, various classes of antibiotics have been discovered, which find their uses for treating a wide range of infections caused by multiple microorganisms. In the last century, antibiotics have clearly transformed the course of modern medicine, positively impacting the quality of human lives and extending the average lifespan by almost 23 years. Moreover, antibiotics have consistently played a crucial role in advancing medical science, benefiting modern medical procedures, including critical surgeries,

cancer therapy, organ transplantations, open-heart surgery and many more (Hutchings et al., 2019).

The time period between the 1950s and the 1980s was often considered the "golden era" of antibiotic discovery. From the introduction of tetracyclines in 1948, macrolides in 1952, nitrofuran in 1953, quinolones in 1960, and oxazolidinones in 1987, new antibiotics were discovered at a steady pace. However, the antibiotic pipeline has ironically become lean, as no new classes of antibiotics have been discovered globally in the last few decades (**Figure 1.1)**. Drug resistance continues to pose a menace to society, with many lives lost due to life-threatening infections caused by these continuously emerging resistant strains that spread much more rapidly than our efforts to either limit their dissemination or eradicate them completely. Considering the current rate of the rise of the AMR phenomena worldwide, we are rapidly heading towards the dark ages of the "post-antibiotic era", in which conventional antibiotics would no longer be effective, leading to massive public health emergencies and human crises. Sadly, when the need has logarithmically risen worldwide owing to the rapid evolution of drug-resistant pathogens, so-called 'superbugs', antibiotic discovery efforts have drastically diminished. Moreover, in recent times, most big pharma companies have decided to abandon this area owing to poor return on investment and broken market dynamics. The treatment course is brief, often limited to a week or two, limiting the market share, unlike lifestyle diseases or cancer therapy, which require much longer, often life-long duration. There is, however, a glimmer of hope as a few selected public-private partnership (PPP) ventures have been instrumental in supporting innovation, providing funding opportunities for SMEs (Small and Medium Enterprises) for the discovery of conventional small molecule drugs or non-traditional agents right from the basic science up to clinical trials without dependence on the market share. Such projects encompass identifying molecules that are not only the typical direct-acting small molecule antibacterial agents but could also be anti-regulators, anti-signal transduction, anti-virulence, anti-toxin, engineered bacteriophages, or microbiome modulators that are now viewed as possible game-changers in combatting antibiotic-resistant bacteria (Hutchings et al., 2019; Stephens et al., 2020; Taneja et al., 2019; Uddin et al., 2021; C. H. Wang et al., 2020). Such 'push' incentives have now been complemented with 'pull' directives (Årdal et al., 2017; Global AMR R&D Hub & WHO, 2023) by various Governments that guarantee revenue to the SME irrespective of market sales, thus mitigating risks and losses. Both of these have indeed re-vitalised efforts to address the

unmet need for developing novel antibiotics to stall the emergence and spread of superbugs.

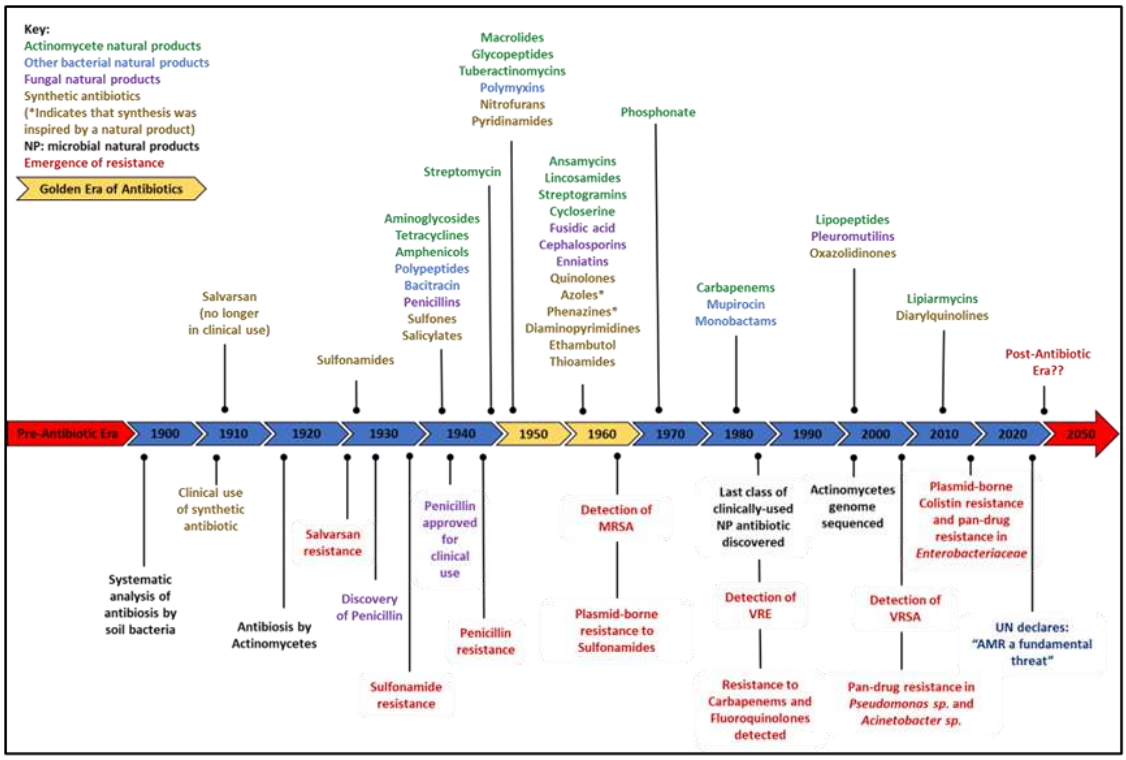

Figure 1.1 Era spanning multiple decades of development of different antibiotics and the resultant development of antimicrobial resistance consequent to their regular usage in the clinic. Different colours encode the source of the respective antibiotics: Green: Actinomycetes, Blue: other bacteria, Purple: Fungi, and Orange: Synthetic. Critical time points linked to the discovery of antibiotics and the development of antimicrobial resistance are listed at the bottom of the timeline, including the first report of drug-resistant strains such as methicillin-resistant *S. aureus* (MRSA) and Vancomycin-resistant *S. aureus* (VRSA), plasmid-borne colistin resistance in *Enterobacteriaceae* and Vancomycin-resistant *Enterococci* (VRE); Adapted from (Hutchings et al., 2019).

1.2 AMR and a lean antibiotics pipeline?

The recent outbreak of the COVID-19 pandemic, which crippled nations worldwide, emphasized an urgent assessment and deployment of measures, including administering vaccines to minimise the loss of lives and curtail the occurrence of any such pandemics in the future. Incidentally, it was noted that a significant sub-group of COVID-19 patients with a high mortality rate had secondary microbial infections

(Rehman, 2023). Moreover, a recent report showed that about 5 million deaths were associated with AMR in 2019 (Murray et al., 2022). With the current rate of the widespread rise in multidrug resistance among bacterial pathogens, it is estimated to hit an annual toll of over 10 million deaths by 2050 (de Kraker et al., 2016; Jim O'Neil, 2014). It was indeed a matter of concern that we had failed to react to the alarm bells due to AMR, aptly coined "the silent pandemic". World Health Organization (WHO) has recognised AMR as one of the top ten Global threats that must be addressed with utmost urgency. A list of 12 bacterial families was published recently as priority pathogens based on their severity of infection, the inherent drug resistance and classified under priority/critical and severe category by WHO, thereby highlighting the urgent need for new treatment options to combat AMR (Mulani et al., 2019; Tacconelli et al., 2018; World Health Organization, 2017).

1.3 Factors contributing to AMR

Bacteria and other microorganisms can survive under diverse environmental conditions and, thus, eventually acclimatize to whichever environment they are exposed to. With a relatively short generation time of 20-30 minutes, their primary goal is survival, multiplication, and spreading rapidly. As a result, microorganisms find strategies and means to rapidly adapt to their surroundings and evolve in ways that ensure optimal survival. Factors challenging or inhibiting their growth, such as exposure to an antibiotic or other environmental adversaries, would lead to phenotypic or genetic changes, allowing the bacteria to cope or become immune to the stress and helping them to live until the return of a conducive milieu (Tan et al., 2022). Overall, the factors contributing to the phenomenon of AMR could be broadly categorized into intrinsic and extrinsic factors (**Figure 1.2**).

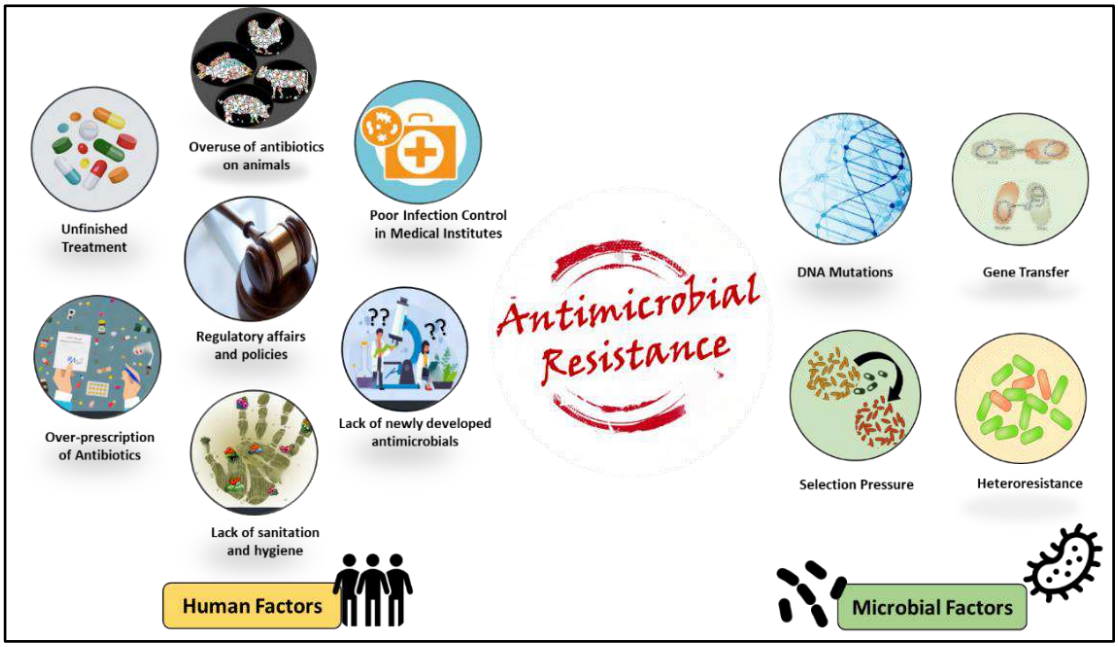

Figure 1.2 Extrinsic (human) and intrinsic (microbial) factors contributing to the development of AMR.

1.3.1 Intrinsic factors: Role in AMR

Several properties of microorganisms that are intrinsic to their biological makeup enable them to withstand the effects of antimicrobial agents. These include genetic traits as well as physiological attributes. These innate factors, as depicted in **Figure 1.2**, are explained below:

Genetic mutations

In microorganisms, the genetic variability arising from a mutation plays a crucial role in developing antibiotic resistance. Mutations are usually spontaneous and can occur in a bacterial cell at any time of its life cycle. Most often, the accumulation of small and limited mutations within a bacterial population provides adaptive benefits with better fitness and survival chances, especially in a clinical situation (Salverda et al., 2017). Multiple factors, including antibiotic exposure, could influence the nature of these mutations. The genetic alterations occurring spontaneously or induced by factors contribute to antibiotic resistance. For instance, in methicillin-resistant *Mycobacterium tuberculosis* or *Staphylococcus aureus*, resistance to rifampicin can be acquired through genetic mutations in the β-subunit of the RNA polymerase (Coculescu, 2009).

Transfer of genetic materials

The exchange of genetic material works as a powerful means to allow bacteria to acquire and share genes, including antibiotic resistance genes (e.g., efflux pumps, antibiotic degradation enzymes, etc.), contributing to enhanced resistance and consequently leading to treatment failures. Intra-specific or inter-specific (polymicrobial) transfer of resistance genes occurs within a bacterial population or between non-identical bacterial species, respectively. For instance, such horizontal gene transfer (HGT) of plasmids carrying the resistant genes (NDM-1 that encodes New Delhi Metallo-protease-1, a subclass of β-lactamases (MBL) and MCR-1, that confers resistance to colistin) across different bacterial systems has led to the global emergence of "superbugs" (D. Sun et al., 2019).

Plasmids are transferred predominantly through transformation, in which bacteria take up extracellular DNA (eDNA) from the environment. Alternatively, the source of this eDNA could also include DNA fragments released from dead bacteria, indicating the possibility of transferring genetic materials across different cells in a population (Castañeda-Barba et al., 2023; Jian et al., 2021). In addition, conjugation, which utilises a type IV secretion system or transduction, also aids in transferring DNA across bacteria (Christie & Vogel, 2000).

Selection pressure

Antibiotic selection pressure occurs when the administration of antibiotics exerts a selective influence on bacterial populations, causing preferential survival, expansion, spread and evolution of pre-existing resistant strains even in the presence of antimicrobial agents. In the presence of sublethal concentrations of antibiotics, adaptive responses may be induced in bacteria, promoting the acquisition and expression of resistance genes (Skalet et al., 2010; Xiong et al., 2015).The overall bacterial dynamics and landscape get altered, reducing the susceptible pool and enabling resistant strains to gain a competitive advantage and thrive within the community.

Heteroresistance

Unlike conventional resistance, where all bacteria in a population are uniformly resistant, heteroresistance (HR) involves the presence of a small subpopulation of resistant cells within a larger population of susceptible cells. These resistant cells have the ability to rapidly replicate in the presence of antibiotics, distinguishing them from persister cells, which remain dormant when exposed to drugs. Notably, the resistant

subpopulation in HR lacks stable mutants; as a result, heteroresistance is challenging to detect and study due to its phenotypic and genetic instability. Although multiple studies have reported the existence of heteroresistance and its clinical relevance, both in Gram-positive (*Staphylococcus aureus*, *Enterococcus faecium*) as well as Gram-negative bacteria (*Klebsiella pneumoniae*, *Escherichia coli*, *Enterobacter spp.*, and *Acinetobacter baumannii*), further research is needed to elucidate their concrete mechanisms and implications in the context of AMR (Band & Weiss, 2021; El-Halfawy & Valvano, 2015; Roch et al., 2023; Stojowska-swędrzyńska et al., 2022). Overall, the interplay between the various bacterial factors and the emergence of pan-resistant strains contribute significantly to the spread of AMR and its potential amplification.

1.3.2 Extrinsic factors contributing to AMR

A wide variety of human activities further enhances the occurrence of AMR. Antibiotic misuse and abuse, inexact diagnosis, incorrect antibiotic prescribing, patient self-medication, inadequate healthcare environments, poor personal hygiene, and excessive usage of antibiotics in agricultural practices, poultry and cattle feed are some of the examples. The limited availability and development of new antibiotics are further constrained by various factors such as technical difficulties, inadequate knowledge, and challenges in combating the complex physiology of bacteria, including the Gram-negative cell wall. Additionally, financial and regulatory hurdles limit the availability of new antibiotics. As a result, the problem of AMR has exacerbated, resulting in the rapid development of resistance in a relatively short period (Uddin et al., 2021).

1.4 Mode of action of antibiotics

Antibiotics are best categorised based on their inhibition mechanisms against specific essential components or targets, leading to reduced synthesis of one of the major macromolecules. The antibiotics are further delineated as narrow or broad spectrum, depending on whether the inhibitory activity is limited to a few or exerted on a wide variety of bacterial species.

1.4.1 Precision targeting of vital bacterial components: Impact limited only to either microbial growth (stasis) or extended to killing (cidality)

Most antibiotics discovered so far mediate their antimicrobial effect via various mechanisms. Primarily, the target of their action involves inhibition of synthesis of one or more of the essential and critical components of the bacterial cell, which then directly

ensures cessation of the bacterial growth and at times, culminates in cell death (Baran et al., 2023; Etebu & Arikekpar, 2016; Kapoor et al., 2017; Uddin et al., 2021). Some of the commonly used antibiotics and their targets are depicted in **Figure 1.3**. Briefly, the multiple strategies through which the antibacterial effect is brought about are described below:

Inhibition of cell wall synthesis

The bacterial cell wall is an integral and essential component that maintains the cell's overall structure. Antibiotics belonging to the beta-lactam class, including penicillins, cephalosporins, carbapenems, and certain glycopeptides, like vancomycin, interfere with bacterial cell wall synthesis. They target enzymes involved in the synthesis of peptidoglycan components or their cross-linking, leading to the weakening of the cell wall structure and bacterial cell lysis (Sarkar et al., 2017).

Disruption of protein synthesis

Antibiotics like chloramphenicol, macrolides, tetracyclines, and aminoglycosides block protein synthesis and prevent bacterial growth by targeting the bacterial ribosome subunits (30S or 50S) or by interfering with the initiation or elongation of protein synthesis (Arenz & Wilson, 2016).

Inhibition of nucleic acid synthesis (DNA replication and transcription)

Quinolones like nalidixic acid, a non-fluorinated first-generation quinolone, fluoroquinolones like ciprofloxacin, norfloxacin, and aminocoumarins like novobiocin target bacterial DNA gyrase and topoisomerases, enzymes involved in DNA replication and transcription. By interfering with these essential target enzymes, these antibiotics disrupt replication and transcription, causing DNA damage and ultimately inhibiting bacterial growth (van Eijk et al., 2017). Gepotidacin and zoliflodacin are novel bacterial topoisomerase inhibitors which inhibit gyrases and topoisomerase, albeit using a mechanism different from that of fluoroquinolones (Schuster et al., 2021). Other antibiotics, such as rifampin, inhibit RNA polymerase, an essential enzyme required for bacterial transcription (Hardie & Fenn, 2022; Wehrli, 1983).

Disruption of membrane integrity

Certain antibiotics, such as polymyxins (like polymyxin B and colistin, also known as polymyxin E) and lipopeptide antibiotics (like daptomycin), disrupt the integrity of bacterial cell membranes. They interact with the lipopolysaccharide

component of Gram-negative bacteria or the phospholipids in bacterial membranes, leading to membrane destabilisation and cell death (Ledger et al., 2022).

Inhibition of metabolic pathways

Antibiotics that target essential metabolic pathways are designed to interfere with specific enzymes involved in bacterial metabolism, leading to disruption of vital cellular functions and, ultimately, affecting bacterial survival. Sulfonamides (like sulfamethoxazole, sulfamerazine, sulfadimethoxine, and sulphanilamide) and trimethoprim target dihydropteroate synthase and dihydrofolate reductase, respectively, are required for the synthesis of folic acid, a crucial component for bacterial DNA and protein synthesis. By competitively binding to the enzyme involved in folic acid synthesis, sulfonamides prevent the production of this essential metabolite, thus hindering bacterial growth (Ovung & Bhattacharyya, 2021; Sköld & Swedberg, 2017).

In recent times, efforts have also been directed towards the discovery of non-conventional alternatives. Such an arsenal covers bacteriophages, biologics including monoclonal antibodies and peptides, antisense oligonucleotides, biofilm inhibitors, etc., with the understanding that these may provide the benefit of delayed resistance development (MacNair et al., 2023). However, these are still in nascent stages, and how they perform in the clinic needs to be seen. Thus, to summarise, it is important to note that different classes of antibiotics vary in terms of their chemical makeup and have different mechanisms of action. Their effectiveness would depend on their entry, efflux and other pre-existing resistance mechanisms in the target bacteria. All of these contribute to the specific bacterial potency of the antibiotic (**Appendix Table S1.1**).

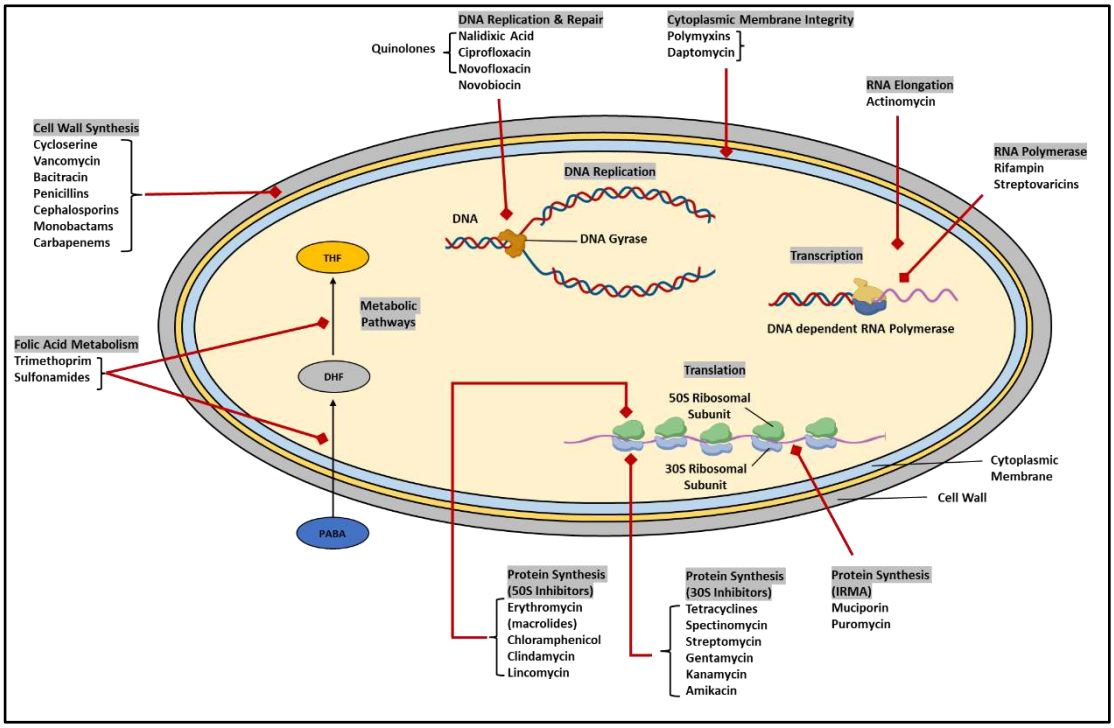

Figure 1.3 Comparative overview of various antibiotics and their targeted mechanisms of action within bacteria. Illustration depicting a range of antibiotics and their specific targets within bacteria. The diagram highlights key mechanisms, such as inhibition of cell wall synthesis, protein synthesis, nucleic acid synthesis, replication, and metabolic pathways, providing a comprehensive overview of antibiotic actions for combating bacterial infections.

1.5 Resistance in bacteria: Intrinsic mechanisms contributing to AMR

Single-celled bacteria are one of the most advanced living entities when it comes to adapting to a changing growth milieu. They need to continuously evolve and equip themselves with advanced defense mechanisms to overcome and nullify the effects of harsh environmental conditions, including exposure to immune systems and antibiotics within the human host while establishing infection and during treatment. Among the different types of bacteria that are frequently associated with serious, debilitating and life-threatening outcomes, the majority belong to the ESKAPE pathogens group (representing *Enterococcus faecium*, *Staphylococcus aureus*, *Klebsiella pneumoniae*, *Acinetobacter baumannii*, *Pseudomonas aeruginosa*, and *Enterobacter species)*, that cause a significant proportion of multidrug-resistant hospital-acquired infections including pneumonia, sepsis, urinary tract infections, and surgical site infections (Denissen et al., 2022; Peleg & Hooper, 2010; Pendleton et al., 2013; Rice, 2010).

The mechanisms of action of different classes of antibiotics are specific and precise. However, with usage over some time, the bacteria counter their action by employing diverse arrays of strategies which help to gain resistance, neutralise the detrimental effects and ensure their survival in the presence of the antibiotics (**Figure 1.4**). Often, these may encompass a single or a combination of armaments (Abushaheen et al., 2020; Darby et al., 2022; De Oliveira et al., 2020; Santajit & Indrawattana, 2016). Some of the common mechanisms are discussed below:

Target mutations and modifications

Target alterations driven primarily by genetic mutations are among the most effective resistance mechanisms frequently exhibited by bacterial systems. The structure of the target or binding affinity could get altered; consequently, the bacterium becomes less susceptible to the drug's action. For example, fluoroquinolones target type II topoisomerases (DNA gyrase and topoisomerase IV) that maintain the DNA topology during replication and transcription. *gyrA* and *gyrB* encode DNA gyrase, while *parC* and *parE* code for topoisomerase IV. There are significant sequence similarities between *gyrA* and *parC* and *gyrB* and *parE*. Amino acid substitutions in GyrA and ParC result in fluoroquinolone resistance. Several resistance mutations in *Escherichia coli* have been identified, with the bulk of these occurring in the quinolone resistance-determining region (QRDR), defined as the codons 67-106 in *gyrA* (predominant mutations in codons 67, 81, 82, 83, 84, 87 and 106) and 56-108 in *parC* (numbering as in *E. coli*). A single mutation in *gyrA* can effectively provide high-level resistance to nalidixic acid. On the other hand, additional mutations in *gyrA* or other type II topoisomerase genes are required for high-level resistance to ciprofloxacin. Similar target mutations were also reported in quinolone resistance variants of *Pseudomonas aeruginosa* and *Salmonella sp*. (Bruchmann et al., 2013; Ruiz, 2003).

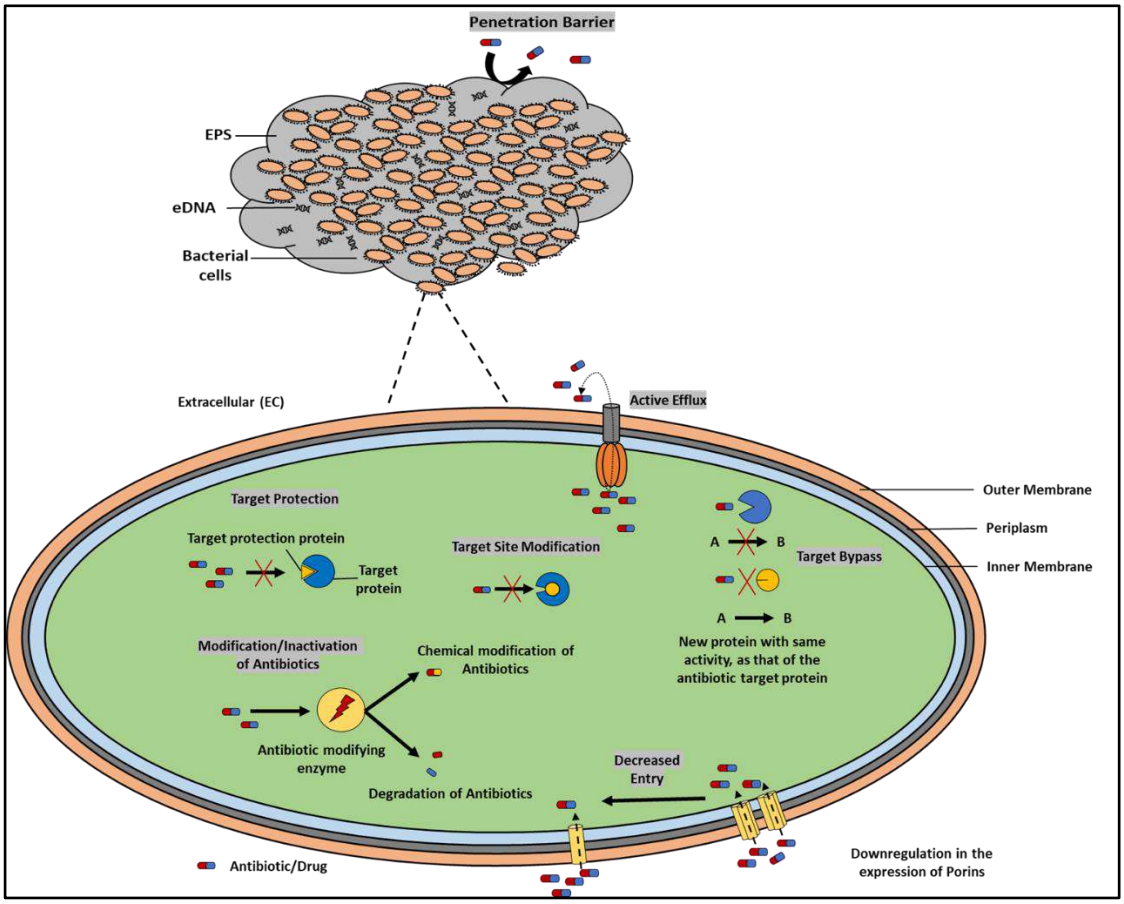

Figure 1.4 Overview of the molecular mechanisms of antibiotic resistance in bacteria. Bacterial resistance mechanisms acquired by (A) community-based resistance by sessile bacterial forms embedded in a thick impervious matrix of exopolymeric substance (EPS) in biofilm, which forms a penetration barrier, and (B) different molecular mechanisms deployed by the individual planktonic cells to tackle antibiotic stress.

Surface modifications leading to reduced permeability

The outer membrane of many Gram-negative bacteria comprises open, water-filled protein channels spanning the outer membrane called porins that act as gatekeepers and control the passage of small hydrophilic molecules, including antibiotics such as carbapenems, β-lactams and fluoroquinolones into the cell. Upon exposure to antibiotics, sometimes the outer membrane undergoes remodelling, resulting in an altered distribution profile of these porins. Such changes could result in reduced expression of wild-type porins and expression of mutated porins with reduced affinity and selectivity, often becoming a permeability barrier for the antibiotic. As

porins are selective in the size of molecules they allow to pass through, these alterations could also restrict the entry of specific antibiotics. For example, studies on the major porins in *E. coli* OmpF and OmpC revealed that OmpF expression is switched on (and OmpC is turned off) in response to carbapenems and tetracycline. In contrast, following exposure to nalidixic acid or 3% ethanol, OmpC expression is activated (while OmpF is inhibited). Similarly, porin alterations were also observed in the clinical isolates of *Klebsiella pneumoniae* (OmpK35, OmpK36), *Neisseria gonorrhoeae* (PorA, PorB), and other bacteria (Pagès et al., 2008; Prajapati et al., 2021; Rosas & Lithgow, 2022).

Enzymatic inactivation and degradation of antibiotics

Some bacteria possess enzymes that degrade antibiotics into inactive metabolites, thus rendering them incapable of target binding and loss of antibacterial activity. One of the most prominent examples of such degrading enzymes is represented by beta-lactamases, which are widely distributed among the resistant Gram-positive and Gram-negative bacteria. These enzymes are responsible for the hydrolysis of the amide bond of the β-lactam ring, making the drug ineffective. Although the first β-lactamase was described in the early 1940s, even before the discovery of penicillin, to date, there are more than 1000 different kinds of β-lactamases reported so far, and many more are likely to evolve. Members of this enzyme family can hydrolyse and inactivate antibiotics belonging to the beta-lactam family, which includes penicillins, carbapenems and cephalosporins, rendering them ineffective for treating bacterial infections. For example, the enzyme TEM-3 can hydrolyse third-generation cephalosporins and aztreonam. The plasmid-encoded ESBL, CTX-M, commonly found in *K. pneumoniae*, *E. coli*, and other *Enterobacteriaceae spp.* contribute significantly to a large proportion of cephalosporin resistance in *E. coli* and *K. pneumoniae*. Recently, a new class of carbapenemase was discovered, NDM-1 (New Delhi metallo-β-lactamase 1). It is found in resistant variants of *E. coli* and *K. pneumoniae* with enhanced resistance against a broad spectrum of antibiotics, including carbapenems, macrolides, quinolones, rifampin, etc., thus associated with multidrug-resistance (Al-Abdely et al., 2021; Liang et al., 2011; Munita & Arias, 2016).

Modification of antibiotics

Certain bacteria can produce specialised enzymes responsible for modifying the antibiotics, leading to their complete inactivation or reduced potency. These enzymes can modify specific functional groups on the antibiotic molecule, leading to a loss of its

antimicrobial activity or transfer of a functional moiety to the antimicrobial molecule, resulting in structural alterations that lead to steric hindrance, loss of activity and elevated minimum inhibitory concentrations (MICs). This mechanism of drug inactivation by modification is found in both Gram-negative and Gram-positive bacteria and is an established mechanism of acquired antibiotic resistance. Notably, most antibiotics susceptible to enzymatic modifications act on ribosomes and bring about inhibition of protein synthesis (Wilson, 2013). Various types of modifying enzymes and their activities have been identified. Among these, the most prevalent catalysed reactions include acetylation (aminoglycosides, chloramphenicol, streptogramins), phosphorylation (macrolides, aminoglycosides, chloramphenicol), and adenylation (aminoglycosides, lincosamides). Irrespective of the specific response, the resulting impact often involves steric hindrance that reduces the drug's affinity for its target, leading to enhanced resistance, as reflected by the elevated minimum inhibitory concentrations (MICs) in bacteria. For example, the genes encoding the chloramphenicol acetyltransferases (CATs) in *E. coli* CAT-III and Class B CAT in *P. aeruginosa* (xenobiotic acetyltransferase; PaXAT) are well characterised for their roles in chloramphenicol resistance. Similarly, genes encoding macrolide kinases (MPHs) like *mphA* and *mphB* from *E. coli* and *mphBM* (also known as *mphC*) from *S. aureus* were identified and characterised for their roles in phosphorylating and thereby inactivating macrolides and conferring resistance (Munita & Arias, 2016; Wright, 2005).

Apart from those described above, bacteria successfully exploit other strategies to escape antibiotic action. Studies pertaining to such bacterial countermeasures will form the basis of this doctoral work, describing two prominent mechanisms that contribute significantly to enhanced antibiotic resistance development.

Efflux pump mediated reduction of intracellular antibiotic concentration.

Efflux pumps are membrane transporters that can extrude a wide array of substrates, including toxic metabolites, salts, inducer molecules and many more substrates out of bacterial cells (Amaral et al., 2014; Liangxing Fang et al., 2016; Nikaido & Pagès, 2012; J. Sun et al., 2014). Apart from these, efflux pumps can expel multiple classes of antimicrobial agents, thereby aiding the bacteria to escape their lethal action. Efflux pumps through this strategy allow bacterial survival by reducing the effective intracellular drug concentration (Webber & Piddock, 2003). These pumps are

thus instrumental in contributing to drug resistance and, at times, indirectly influencing physiological processes adopted as an alternate mode of growth, e.g., biofilms, persisters, single-cell variants, etc. Thus, multiple factors acting in a concerted manner may contribute to the occurrence of AMR in the clinic. (Huang et al., 2022).

Bacterial systems exhibit a diverse array of efflux pumps, which are broadly classified into five prominent families, namely, the ATP-binding cassette (ABC) superfamily, the multidrug and toxic compound extrusion (MATE) family, the major facilitator superfamily (MFS), the small multidrug resistance (SMR) family, and the resistance/nodulation/division (RND) superfamily. The activity of an efflux pump depends on the different types of energy sources each system uses: ABC transporters are fuelled by ATP hydrolysis; MFS, RND, and SMR use the proton-motive force, and MATE transporters consist of Na^+/H^+ drug antiport systems. Except for the RND superfamily, which is found predominantly in Gram-negative bacteria, efflux systems of the other four families, MFS, ABC, SMR and MATE, are widely distributed in both Gram-positive and Gram-negative bacteria (Nair et al., 2016; Orelle & Jault, 2016; Sapula & Brown, 2016; J. Sun et al., 2014). Depending on the specific classes they belong to, efflux pumps are either single-component transporters like the SMR and MFS family of efflux pumps or multiple-component systems containing not only an inner membrane transporter but also an outer membrane channel and a periplasmic adaptor protein, such as the RND type efflux pumps (Neuberger et al., 2018; Sapula & Brown, 2016). Some of the major families of bacterial efflux pumps and the classes of antibiotics they confer resistance to, are represented in **Figure 1.5** below.

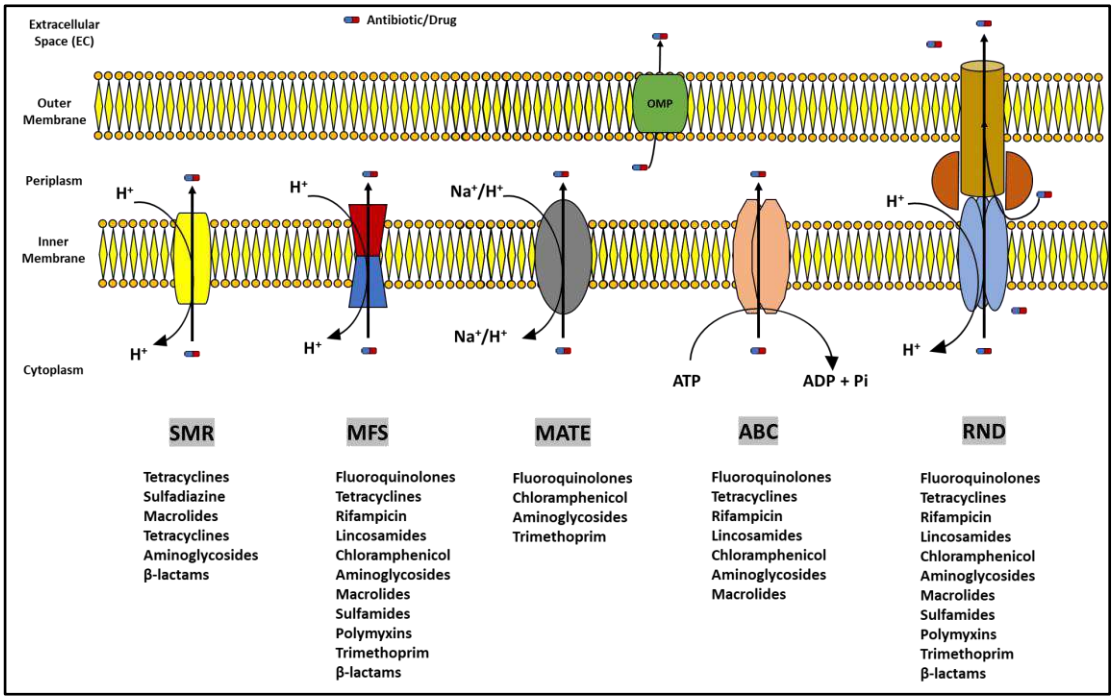

Figure 1.5 Major superfamilies of bacterial efflux pumps and their role in antimicrobial resistance. A schematic representation of an overview of the complex interplay between efflux systems and antibiotics, highlighting the specificities exhibited by different efflux pump families towards distinct antibiotic classes leading to resistance development, is represented. (SMR: small multidrug resistance protein; MFS: major facilitator superfamily; MATE: multidrug and toxic compound extrusion superfamily; ABC: ATP- binding cassette transporter and RND: resistance nodulation division superfamily).

The bacterial efflux pumps reveal a complex interplay between these cellular transporters and the vast array of antibiotics used to combat bacterial infections. Through their remarkable diversity and specificities, efflux pumps play a crucial role in bacterial resistance by actively pumping antibiotics out of the cell, thereby reducing their intracellular concentrations. The different classes of antibiotics are subjected to the action of various efflux pumps, which may exhibit preferences for certain antibiotics based on their chemical structures and modes of action. This specificity further highlights the dynamic and adaptive nature of bacterial resistance mechanisms.

Biofilm

So far, we have looked at changes occurring via multiple approaches at the genetic level that allow the bacteria to escape the inhibitory activity of the antibiotic. Apart from acquiring such strategies, many bacterial species are known to resort to alternate forms of growth to tide over nutrient deprivation and harsh environmental conditions, which in turn aid in building resistance to diverse agents, including antibacterials. Biofilms, one of such multi-cellular lifestyle adaptations, are specialised, well-defined, three-dimensional (3D) structures that enable bacteria to thrive under stressful conditions. In addition to posing a significant threat to the healthcare and food industries, biofilms also cause biofouling, thus leading to a loss of revenue in multiple industrial sectors (Flemming et al., 2016; Sharma et al., 2019). Biofilms are protected and hard-to-permeate self-encapsulated bacterial aggregates anchored to biotic or abiotic substrates. Such transformations in lifestyle confer growth-related advantages and refractoriness to stressful conditions, immune responses, and, more importantly, equip bacteria to evade antibiotic action. Understanding the key players in biofilm formation contributing to AMR forms the next part of this doctoral work.

1.6 Significance of studying the mechanisms leading to the emergence of AMR

Studies associated with the explorations of the mechanisms contributing to AMR offer opportunities to understand the course of multi-drug resistant infections and design appropriate countermeasures that are essential for optimal healthcare management. The emergence and spread of antibiotic resistance pose a significant threat to global public health, wherein supposedly successful treatments are rendered ineffective, causing increased morbidity, mortality, and healthcare costs. Listed below are a few significant benefits of such investigations:

Development of novel and Effective Treatment Strategies

Understanding how bacteria develop resistance mechanisms is essential for designing effective treatment strategies. Additionally, such explorations would drive innovation and pave the path for designing molecules with novel mechanisms to combat resistance or enhance the efficacy of existing antibiotics using adjunct therapies.

Prevention and Control of Resistance

By identifying the determinants and transmission patterns of resistance, policymakers can establish control measures and ensure the implementation of

programs that curtail infection. This information would also aid the development of surveillance programs to detect and monitor resistant strains. This information would guide public health policies and interventions, enabling proactive strategies to limit the transmission and impact of resistant infections.

Preservation of Antibiotics and One Health Perspective

Antibiotics are a finite resource, and the emergence of resistance threatens their effectiveness. As emphasized in the earlier sections, with the overuse or abuse of antimicrobials, the current trends indicate rising antimicrobial resistance and very few options available for treating infections, thereby demanding immediate action with utmost urgency. This is where antimicrobial stewardship (AMS) comes to our rescue. AMS refers to a set of rational actions that promotes the responsible use of antimicrobials. Prescribing appropriately by doctors and educating patients to use responsibly as per the advice and emphasizing to colleagues, including the administering nurses, dosage designed by pharmacists, testing by microbiology staff and epidemiologists who track the performance of antibiotics and the emergence of resistance on the proper use of this increasingly scarce medical resource would go a long way to protect our current and future patients and more importantly, minimize resistance development and reduce health care costs.

The principles of AMS also apply to bar the usage of antimicrobials in animal and agriculture sectors as growth-promoting agents. Aligning to the "One Health" perspective, which emphasises the vital link and dependency between humans, animals, and the environment in contributing towards preventing the inappropriate use of antibiotics while stopping the spread of infection, is required to minimise the looming threat effectively in a holistic manner. (Collignon & McEwen, 2019).

1.7 Future of Antibiotic Development

Understanding how bacteria develop resistance paves the path for the design and development of specific antimicrobial agents that essentially delay such a course as much as possible during its use. By elucidating the exact mechanisms bacteria employ to evade antibiotics, researchers can identify vulnerable targets that lack cross-resistance to current drugs and possess very low resistance frequencies. Effectively, there is a need to extend its life cycle and safeguard the future of healthcare. Adopting suitable Stewardship Program measures along with the implementation of 'push' and

'pull' incentives would go a long way in ensuring suitable financial support to agencies embarking on this 'not so profitable' yet 'scientifically challenging' journey.

1.8 Scope of the present investigation

The preceding sections provided a comprehensive review of the multiple facets of antibiotics, ranging from the diverse mode of action to bacterial strategies employed for evading inhibitory action through multiple mechanisms of resistance and the concomitant rise of antimicrobial resistance in recent times. While propelling efforts towards discovering novel therapeutics is a must, along with optimal formulation of policies by the concerned authorities to contain the global AMR situation, explorations should also continue to unequivocally decipher the basic tenets of specific molecular mechanisms that the bacteria very smartly develop to thwart antibiotic action. The latter needs thorough investigation as it unravels how superbugs evolve. Thus, considering the complex nature of AMR, the current doctoral thesis work was embarked upon to fill some gaps in our understanding of AMR development either via efflux pumps or through specific pathways during biofilm formation.

The first part of the work is focussed on studying the roles of RND efflux pump components from three important Gram-negative pathogens, known causative agents of drug-resistant hospital-acquired infections from the ESKAPE group, namely AcrB from *Escherichia coli*, MexB from *Pseudomonas aeruginosa* and OqxB from *Klebsiella pneumoniae*. As these efflux pumps significantly contribute to multi-drug resistance, the first study was initiated to understand how they function in a non-native heterologous host system. Such an evaluation would enhance our knowledge of the transmission of efflux pump encoding resistant gene markers across different bacterial systems via horizontal gene transfer. Further, the study provided here describes the structural and functional characterisation of OqxB from *K. pneumoniae*, one of the recently reported but less explored RND efflux pumps and its role in conferring resistance to antibiotics.

The next aspect focuses on studying the complexities of a surface-associated alternate bacterial lifestyle, i.e., biofilms with acquired resistance, adopted by various bacteria to escape harsh environments and to confer phenotypic resistance to antibiotics. Using *E. coli* as the model organism, a validated *in silico* model based on ordinary differential equation (ODE) was constructed. Such a platform provided an insight into the interplay of various interconnected genes, regulators and metabolites alongside the

structural and functional components, which concertedly drive the transition of the motile planktonic bacterial form to a sessile biofilm state. Moreover, although efflux pumps are well-known for their roles in extruding toxic metabolites and antibiotics out of the cells, they also play a crucial role in mediating quorum sensing and driving the progression toward biofilm formation. The outcome of such studies would add value to our current understanding of biofilm dynamics and its role in virulence and AMR. Such explorations could help in providing a link between efflux pumps and biofilm targets. Along with direct-acting antibiotics, specific adjunct therapeutics against biofilm targets could be a part of combinatorial therapy to address and combat serious MDR infections.

Chapter 2

Functional explorations of the role of RND Efflux Pumps in AMR: A Heterologous Complementation Study in *E. coli*

2.1 RND Efflux Pumps: An Overview

Efflux pumps are one of the most powerful tools employed by bacterial hosts to overcome antibiotic stress, and thus, they play a significant role in contributing towards the overall generation and maintenance of AMR. Among the various families of efflux pumps discussed briefly in the earlier chapter, members of the Resistance Nodulation and Division (RND) superfamily hold special significance. Owing to their wide range of distribution across ESKAPE pathogens, a broad array of substrate specificities, including antibiotics, dyes, and heavy metals, and their tripartite composition, which allows the direct extrusion of various drugs from cytosol or periplasmic space to the outside of bacterial cells, their contribution to AMR has garnered significant attention (Zwama & Nishino, 2021).

2.2. General architecture of RND efflux pumps

Most members of the various efflux pump families (such as SMR, MFS, PACE, MATE, AbgT) found in bacteria are located in the cytoplasmic membrane and possess the ability to expel drugs and other molecules rapidly into the periplasm. However, these drug molecules often have the tendency to re-enter the cytosol through spontaneous diffusion. In contrast, members belonging to the RND family of efflux pumps, along with a few exceptional pumps from other families (like ABC and MFS, acting as inner membrane complexes), which are found predominantly in Gram-negative bacteria, exhibit a tripartite structural assembly, that spans both the outer membrane (OM) and the inner membrane, resembling the protein-secreting apparatus observed in Gram-negative bacteria (Henderson et al., 2021; Okada & Murakami, 2022; J. Sun et al., 2014). This complex includes a permease protein positioned in the inner membrane, a periplasmic adaptor protein belonging to the MFP family and finally, an outer membrane protein belonging to the Outer Membrane Factor (OMF) family, as illustrated in **Figure 2.1** below; this arrangement enables bacteria to directly expel drug molecules into the external environment. This also confers a significant advantage to bacteria, as the drugs present in the external medium must traverse the less permeable OM to re-enter the cells, unlike the drug molecules in the periplasm that can easily penetrate the highly permeable inner membrane. Consequently, the tripartite RND pumps effectively generate drug resistance in a concerted manner along with the outer membrane barrier (Nikaido, 2011).

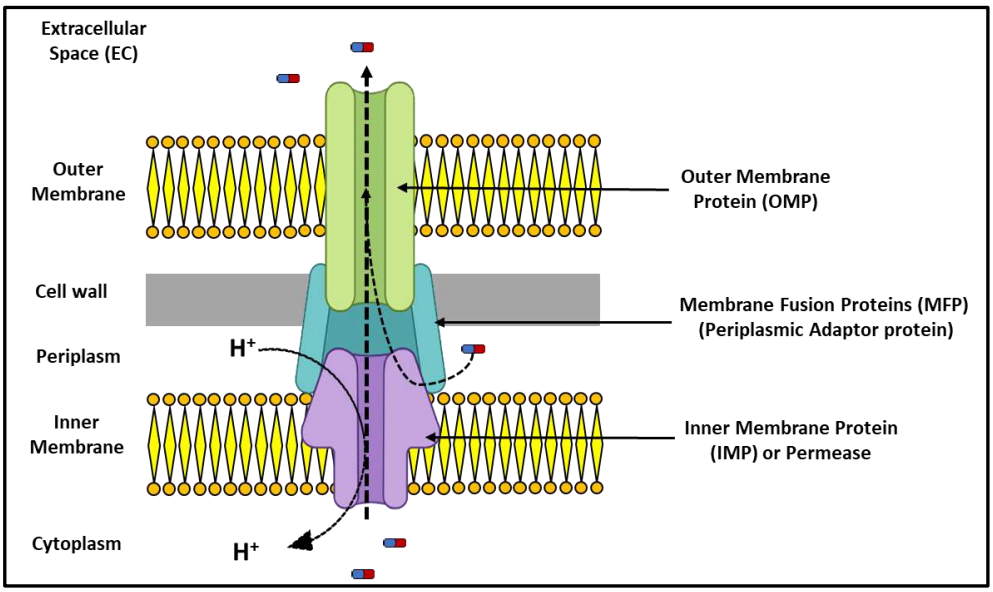

Figure 2.1 General architecture of the tripartite assembly of RND efflux pumps in bacterial systems. A general illustration of the general architecture of RND (Resistance-Nodulation-Division) efflux pumps, highlighting the tripartite assembly of the efflux pump components. The inner membrane protein (IMP) or the permease spans the inner membrane and actively transports substrates from the cytoplasmic compartment and the periplasmic space. The Membrane Fusion protein (MFP) is a periplasmic adaptor that links the IMP protein and the outer membrane channel protein (OMP) in the outer membrane. These components, together, form a channel or transmembrane pore through which the substrates are expelled to the external environment (generated using https://www.biorender.com/).

Some of the well-reported members in different Gram-negative bacteria from the ESKAPE spectrum are the AcrB in *Escherichia coli* (J. M. A. Blair et al., 2015; Du et al., 2014; Murakami et al., 2006), MexB in *Pseudomonas aeruginosa* (Sennhauser et al., 2009; Tsutsumi et al., 2019) and AdeB in *Acinetobacter baumannii* (Ornik-Cha et al., 2021; Su et al., 2019). Another member of the efflux pump family is OqxB, which is primarily studied in *Klebsiella pneumoniae* and is frequently found to be associated with AMR (Yuan et al., 2012). In addition, OqxB has also been reported to have a similar pivotal role in AMR in other Gram-negative bacteria like *E. coli*, *Enterobacter cloacae* and *Salmonella spp.,* (Johannesen et al., 2004; J. Li et al., 2019). A detailed understanding of the role and function of OqxB and its contribution to multi-drug efflux would add value to otherwise sparse information on OqxB.

The overall architecture of tripartite assembly for all members of RND efflux pumps, which are distributed across different bacterial systems, is usually similar across all organisms. These RND pumps are found in various bacterial species, including *Escherichia coli*, *Pseudomonas aeruginosa*, *Klebsiella pneumoniae* and *Acinetobacter baumannii*, which are all critical pathogens commonly associated with antibiotic resistance. For instance, the RND efflux pump complex in *E. coli* is composed of the inner membrane protein AcrB, periplasmic membrane fusion protein AcrA, and the outer membrane protein TolC, leading to the assembly of the functional pump (AcrB-AcrA-TolC). This is one of the most well-characterized and studied efflux pump systems in bacteria and is responsible for the extrusion of a broad spectrum of metabolites and antibiotics such as chloramphenicol, penicillins, cephalosporins, macrolides, etc., (Du et al., 2014; Murakami et al., 2002; Nikaido & Zgurskaya, 2001; Pos, 2009; Seeger et al., 2006; Z. Wang et al., 2017). Studies have shown that mutations in the *acrB*, which encodes the inner membrane transporter of the AcrAB-TolC pump, can lead to increased resistance to these antibiotics (Trampari et al., 2023). Another member of this efflux pump family in *E. coli* is AcrD, which associates with the MFP component AcrF and the OMF protein TolC and is capable of extruding substrates like aminoglycosides, fusidic acid and novobiocin (Nikaido, 2009).

Similarly, the RND efflux pump system composed of MexB-MexA-OprM complex in *P. aeruginosa* is well known for its ability to efflux a diverse spectrum of substrates including crystal violet, acriflavine, ethidium bromide and antibiotics like aminoglycosides, trimethoprim, triclosan and many more (Sakurai et al., 2019; Tsutsumi et al., 2019). Overexpression studies of MexAB-OprM in *P. aeruginosa* have also established the role of these pumps in conferring multi-drug resistance (Shigemura et al., 2015). Moreover, multiple efflux pumps can be present in many bacteria and work together to confer antibiotic resistance. These multi-drug efflux systems are more complex and more challenging to inhibit than a single one. For example, the efflux pumps MexAB–OprM, MexCD–OprJ, MexEF–OprN, and MexXY are found to be overexpressed in cystic fibrosis isolates of *P. aeruginosa*, which work together to extrude a wide range of drugs, including beta-lactams, aminoglycosides, and quinolones (M. Singh et al., 2017).

OqxAB and AcrAB pumps in *Klebsiella pneumoniae* are some of the significant members of the RND efflux pump systems that are clinically relevant for their roles in AMR (Bialek-Davenet et al., 2015). Especially, the pump OqxB is capable of extruding

a wide range of drugs, including fluoroquinolones, tetracyclines, and macrolides, and is widely considered a threat in the transmission of AMR phenotype among clinical isolates of *Klebsiella spp*., as well as across different bacteria (J. Li et al., 2019). Other notable members belonging to this family, which are often encountered as key contributors of multi-drug resistance in the clinic, are the AdeABC and AdeIJK of *Acinetobacter baumannii* (Sugawara & Nikaido, 2014; C. Xu et al., 2019). Several additional RND multi-drug transporters have been reported in various bacterial species, including AmrB in *B. pseudomallei*, AcrF (EnvD), AcrD, and MdtF (YhiV) in *E. coli*, HI0895 in *H. influenzae*, and MexD or MtrD in *N. gonorrhoeae*. Although the distribution of the RND efflux pumps was widely accepted to be restricted to the inner membrane of Gram-negative organisms, recent findings have confirmed the presence of these pumps in numerous Gram-positive bacteria, such as *S. aureus*, *Corynebacterium glutamicum*, *C. difficile*, and *B. subtilis* (Spengler et al., 2017).

In spite of sharing marked resemblance in terms of the overall structural architecture and assembly, members of the RND efflux pump families differ in gene sequences and consequently in the encoded proteins, thereby attributing to varied substrate specificities and functional diversities. Sequence-based homology studies and phylogenetic trees of various characterized efflux pumps indicate that they are clustered closer to each other in different clades. For example, the clinically relevant OqxB, which is known to expel different substrates, belongs to a separate and structurally unexplored clade as compared to AcrB, MexB, TriC, and AdeB (**Appendix Figure S2.1)**, which are reported to lie in different clusters (Bharatham et al., 2021). The variations among the members of the RND efflux pumps range from differences in substrate specificity, drug resistance profile, and even structural features. Some RND efflux pumps have additional domains that can confer resistance to specific compounds, such as heavy metals or detergents. Additionally, some RND efflux pumps are regulated by distinct signalling pathways or transcriptional regulators, which can affect their expression and activity. Overall, the diversity of RND efflux pumps is evident in their structure, function, distribution, and mechanisms to confer resistance to antibiotics. As the versatility among bacterial RND efflux pumps significantly contributes to the development of antibiotic resistance, an improved understanding would pave for new strategies to combat AMR (Zwama & Nishino, 2021).

2.3 Diverse roles of RND Efflux pumps

Some of the multifaceted functionality of these efflux pump systems, which encompasses several key areas, are discussed below:

Plant–Bacteria Interactions

Multi-drug resistance (MDR) pumps have been found to play a vital role in the plant-microorganism interaction, from colonization to survival within plant tissues. For example, the RND efflux pump IfeAB in *Agrobacterium tumefaciens* is involved in the competitive colonization of alfalfa roots by reducing cellular accumulation of isoflavonoids and flavonoids like coumestrol (an antimicrobial root-exudated flavonoid), which serves as both substrate and an inducer (Alvarez-Ortega et al., 2013; Martinez et al., 2009).

Role in Bacterial Virulence

Another intriguing aspect of RND efflux pumps is their involvement in the transport of virulence factors. These pumps facilitate the secretion of virulence determinants (e.g., toxins, adhesins, and tissue-degrading enzymes), which enhance the pathogenicity of bacteria, allowing them to invade host tissues, colonize, and cause infections. By exporting virulence factors, RND efflux pumps contribute to the ability of bacteria to establish and sustain infections. For example, the efflux pump inhibitor (EPI) Phe-Arg-β-naphthylamide (PAβN) brings about a reduction in the *in vivo* virulence of the *P. aeruginosa* (Rampioni et al., 2017).

Transport of Toxic Compounds

RND efflux pumps also transport various toxic compounds out of the bacterial cell, which could otherwise restrict bacterial growth and survival. By expelling these harmful agents, the pumps protect the bacterium from environmental stressors and maintain cellular homeostasis. For instance, both the virulent as well as avirulent variants of *E. coli*, which inhabit the digestive tract of animals, possess AcrAB, which helps the bacteria to withstand the deadly bile salts in their surrounding milieu along with protecting them from decanoate on mucosal surfaces (Martinez et al., 2009). Similarly, CzcCBA, which belongs to the HME (Heavy Metal Efflux) family, provides enhanced tolerance to *P. aeruginosa* against excess zinc in the environment (Ducret et al., 2020).

Export of Endogenous Metabolites

RND efflux pumps participate in the export of endogenous metabolites. They prevent the accumulation of toxic molecules within the bacterial cell by actively transporting them out to help maintain the overall metabolic balance and ensure optimal cellular functioning. For example, the MexGHI-OpmD efflux pump system in *P. aeruginosa* extrudes anthranilate, a toxic precursor of the Pseudomonas quinolone signal (PQS) and other endogenously produced phenazine antibiotics (Sakhtah et al., 2016).

Quorum Sensing

RND (Resistance-Nodulation-Division) efflux pumps have been found to export quorum-sensing molecules from bacterial cells. RND efflux pumps can contribute to the efflux of these signalling molecules, such as acylated-homoserine lactones (AHLs), autoinducing peptides (AIPs), and other signalling molecules, to communicate with one another, affecting their concentration and distribution within the bacterial population, and thus helping in influencing their differential gene expression and, overall lifestyle. For example, studies have revealed the involvement of MexAB-OprM efflux pump in *Pseudomonas aeruginosa* in mediating selective AHLs-driven quorum-sensing pathways and its associated pathogenicity (Minagawa et al., 2012).

Biofilm Formation

Additionally, RND efflux pumps are implicated in the regulation of biofilm formation in various environments, including medical devices, industrial settings, and natural habitats. These pumps influence the production and secretion of biofilm components, affecting their formation, structure, and maintenance. Studies have shown that RND efflux pumps exert their effects, including the release of exopolymeric substances (EPS), efflux of quorum sensing (QS), and/or quorum quenching (QQ) molecules to regulate QS and facilitate biofilm matrix formation. Indirectly, they could be involved in the efflux of harmful molecules, like antibiotics and metabolic intermediates, and affecting aggregation by promoting or inhibiting adhesion to surfaces (Alav et al., 2018).

Role in drug efflux and AMR

RND efflux pumps are notorious for their role in conferring antibiotic resistance. They recognize and pump out a wide variety of antibiotics thereby reducing their

effective intracellular concentrations. This efflux mechanism enables bacteria to evade the effects of antibiotics, leading to treatment failure and the emergence of multidrug-resistant strains. Furthermore, they are also considered the hotspot of AMR driving factors through various mechanisms, such as mutations in genes that encode the pumps, overexpression, or the presence of multiple efflux pumps in a single cell.

Continuous exploration in the field of efflux pumps is an ongoing research endeavour, with the development and implementation of novel approaches aimed at enhancing our understanding of these pumps. Genetic studies involving overexpression, knockout, site-directed mutagenesis and subunit swapping of target genes of RND efflux pumps often contribute valuable insights related to antibiotic susceptibility and substrate specificity patterns for a given efflux pump. Knockout studies involve creating a genetic mutation or deletion that inactivates the gene encoding a particular protein, in this case, an RND efflux pump. This allows researchers to study the effects of the absence of the protein on cellular physiology (Cudkowicz & Schuldiner, 2019; Murata et al., 2002; Yoneyama et al., 1998). On the other hand, over-expression studies involve increasing the amount of a particular protein, which helps in understanding the effects of an excess of the protein on cellular physiology, which further corroborates the effect of overexpression of these pumps in clinical isolates (Green et al., 2023; Shigemura et al., 2015). Furthermore, studies involving site-directed mutagenesis and mutations in wild-type genes also aid in identifying the role of critical amino acid residues, protein domains/pockets, crucial interactions, etc., which contribute to the binding of the substrate and its subsequent extrusion, thereby deciphering the mechanism of action of the efflux pump (Alav et al., 2022; Krishnamoorthy et al., 2008). Structural knowhow about the assembly of efflux pumps wherein reconstituted complexes with native efflux pump components from *E. coli* (AcrA-AcrB-TolC) and *P. aeruginosa* (MexA-MexB-OprM) using lipid nanodisc systems (Daury et al., 2016) have also been reported.

Another novel approach, which is being explored extensively, involves studies on the expression of efflux pumps with components from heterologous origins. In the work by Tikhonova et al., chimeric RND transporters were designed and expressed using different domain components (N-terminal residues of AcrB from *E. coli* and C-terminal residues of MexB from *Pseudomonas aeruginosa*) of the major RND efflux pumps. These chimeric protein complexes were then co-expressed to study the susceptibility of *E. coli* as well as to understand the interactions of the different components of the tripartite assembly (Tikhonova et al., 2002).

Along similar lines, a heterologous expression system was developed and evaluated in the present work. In this system, the RND permease (B-homologue) and the periplasmic component (A-homologue) were overexpressed in an efflux pump-deleted *E. coli* background. Considering the reported events related to the transmission of resistance across different bacterial systems (J. Li et al., 2019), studying the assembly and functional translation in terms of antimicrobial susceptibility of the host against different antibiotics would be a worthy exploration, not only in terms of understanding the biology but also its clinical significance. For these reasons, RND efflux pump components from three members of the ESPKAPE group, namely, AcrA-AcrB from *E. coli*, MexA-MexB from *P. aeruginosa* and OqxA-OqxB from *Klebsiella pneumoniae*, were selected. The selection of antibiotics for such explorations was based on their inhibitory effects, primarily on Gram-positive organisms but poorly on Gram-negative ones. As Gram-negative microorganisms are known to exhibit resistance across a wide spectrum of antibiotics, owing to their advanced efflux systems. Therefore, antibiotics such as linezolid, novobiocin, and erythromycin were chosen for the present work due to their different mechanisms of action and high efflux liabilities. Another key point for the selection of these organisms is that while AcrB and MexB share a sequence homology of greater than 70%, this number drops down to a mere 40% in the case of OqxB (**Appendix Figure S2.2 and Table S2.1**). Despite these differences, the presence of OqxB in *E. coli* and other bacteria and the consequent impact leading to enhanced resistance makes it a subject for further investigation.

2.4 Materials and Methods

2.4.1 Protein structures, homology modelling and sequence analysis

Structures of all the efflux pumps viz. AcrB (5V5S) (Z. Wang et al., 2017), MexB (6IOK) (Tsutsumi et al., 2019) and OqxB (7CZ9) (Bharatham et al., 2021) were downloaded from the PDB database (https://www.rcsb.org/). Furthermore, the latter has been characterized in this treatise (**Chapter 3**). The structural superimposition was done using PyMol (DeLano, 2002). Consequently, the RMSD value between the aligned structures was noted to determine the efficiency of superimposition. OqxA was modelled against the crystal structure of AcrA (2F1M) (Mikolosko et al., 2006), using SwissModel (https://swissmodel.expasy.org/) and energy minimization was done using the Chiron server (Ramachandran et al., 2011). The phylogenetic analysis was done in

ClustalΩ (Sievers et al., 2011) using the sequences obtained from the PDB IDs of the proteins. This helped compare the residues and understand the similarities and variations among the different RND efflux pump components.

2.4.2 Cloning of single and double overexpression system

The cloning for the single overexpression complementation systems, consisting of the inner membrane transporter (B-Subunit) protein only, involved the cloning of respective genes into the *pET21a* vector. For the construction of double overexpression systems, which consisted of both the periplasmic adaptor protein (A-subunit) and the inner membrane transporter (B-Subunit) for different RND pump components, a modified vector backbone derived from *pTrc99a* (Genscript) was utilized. This modified vector contained only the 2.4kb fragment obtained after vector digestion, which included the Ampicillin (Amp^r) marker, the *pBR322* origin, and the terminator sequence. The genes *acrB*, *mexB* and *oqxB,* polycistronic *acrAB,* and *oqxAB* were PCR amplified with specific primers from the genomic DNA isolated from the respective hosts, namely, *E. coli BW25113*, *P. aeruginosa* ATCC 27853 and *K. pneumoniae* ATCC 13883, using high-fidelity Phusion DNA Polymerase (Thermo Fisher Scientific), as shown in **Figure 2.2**. Specific primers (enlisted in **Appendix Tables S2.2 and S2.3**) were designed for the PCR amplification process to ensure the constitutive expression of these genes upon heterologous expression. The amplicons for the complementation studies for *acrB, mexB* or *oqxB* were cloned between the NdeI and XhoI restriction sites of the *pET21a* (Invitrogen) expression vector. At the same time, the *acrAB, mexAB* and *oqxAB,* along with a constitutive promoter sequence, were fused with the modified vector backbone from *pTrc99a*, using the NdeI and HindIII restriction sites. The clones containing the plasmids with the gene of interest, as depicted in **Table 2.1** below, were further confirmed by restriction digestion and Sanger sequencing.

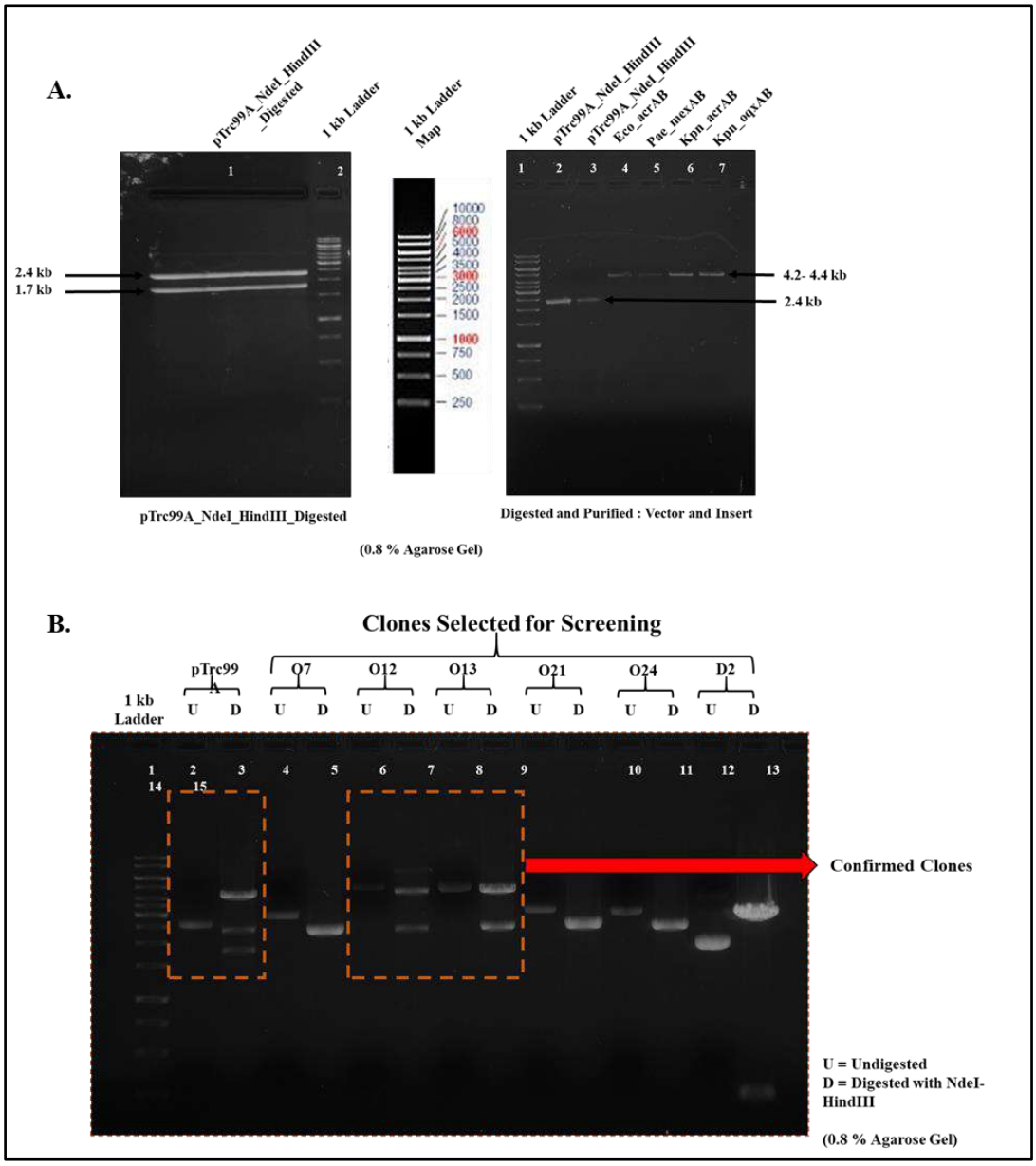

Figure 2.2 Cloning of the RND efflux pump homologues from different Gram-negative organisms. (A) Extraction of *pTrc99a* Vector backbone and PCR products of the gene inserts of *Eco_acrA-acrB*, *Pae_mexA-mexB*, and *Kpn_oqxA-oqxB*, amplified from the genomic DNA of the hosts, namely *E. coli BW25113*, *P. aeruginosa* ATCC 27853 and *K. pneumoniae* ATCC 13883 respectively (B) Confirmation of the positive clones for *Kpn_oqxA-oqxB* from the selected colonies, was done by restriction digestion with HindIII and NdeI. The selected clones were further confirmed for the presence of the gene of interest by Sanger sequencing. A similar approach was followed for screening *Eco_acrA-acrB* and *Pae_mexA-mexB* positive clones (data not shown).

Table 2.1 Plasmids and constructs used for complementation studies

Plasmids	Description	Reference or Source
pET21a	Cloning Vector	Invitrogen
pTrc99a	Cloning Vector	Genscript
pEcoB	*pET21a* carrying His_6-Tagged *E. coli acrB*; Amp^r	This Study
pMexB	*pET21a* carrying His_6-Tagged *P. aeruginosa mexB*; Amp^r	This Study
pOqxB	*pET21a* carrying His_6-Tagged *K. pneumoniae oqxB*; Amp^r	This Study
pEcoAB	*pTrc99a* derivative carrying *E. coli acrA* & *acrB*; Amp^r	This Study
pMexAB	*pTrc99a* derivative carrying *P. aeruginosa mexA* & *mexB*; Amp^r	This Study
pOqxAB	*pTrc99a* derivative carrying *K. pneumoniae oqxA* & *oqxB*; Amp^r	This Study

2.4.3 Strains and growth conditions for complementation studies

The bacterial strains used in this study are listed in **Table 2.2**. The strains were grown in cation-adjusted Mueller Hinton Broth (MHB No.2 Control Cations Hi-Media) or on 1.5% Luria Bertani Agar Miller (Hi-Media) plates. Antibiotics like Amp 100µg/mL (Ampicillin sodium salt; Sigma-Aldrich, Catalogue no.# A9518) or Kan 30µg/mL (Kanamycin sulphate; HiMedia, Catalogue no.# MB105) were used for selection wherever required. *E. coli C43(DE3)* (Miroux & Walker, 1996) *ΔacrB* (*acrB* deletion strain) was constructed by transduction with P1 phage that was prepared using the *BW25113ΔacrB* (JW0451) from the Keio collection (Baba et al., 2006), as the donor. Kanamycin-resistant transductants were verified to be *acrB* deletion mutants by PCR. Double Knockout *ΔacrA-ΔacrB* strain in *E. coli BW25113* was generated by homologous recombination (Datsenko & Wanner, 2000). *E. coli* Top10 F' strain (Thermo Fisher Scientific) was used for DNA cloning and plasmid amplification. All the cultures were grown at 37 °C under aerobic conditions.

Table 2.2 Bacterial strains used

Strains	Reference or Source
*E. coli K-12 BW25113 (*Wild-type)	(Baba et al., 2006)
E. coli K-12 BW25113 ΔacrB::kan	(Baba et al., 2006)
*E. coli C43(DE3) (*Wild-type)	(Miroux & Walker, 1996)
E. coli C43(DE3) ΔacrB::kan	This Study
E. coli K-12 BW25113 ΔacrA ΔacrB::kan (ΔacrAB)	This Study
E. coli C43(DE3) ΔacrB carrying *pET21a*	This Study
E. coli C43(DE3) ΔacrB carrying *pEcoB* = (+ *acrB*)	This Study
E. coli C43(DE3) ΔacrB carrying *pMexB* = (+ *mexB*)	This Study
E. coli C43(DE3) ΔacrB carrying *pOqxB* = (+ *oqxB*)	This Study
E. coli K-12 BW25113 ΔacrB::kan carrying *pTrc99a*	This Study
E. coli K-12 BW25113 ΔacrAB carrying *pEcoAB* = (+ *acrA* + *acrB*)	This Study
E. coli K-12 BW25113 ΔacrAB carrying *pMexAB* = (+ *mexA* + *mexB*)	This Study
E. coli K-12 BW25113 ΔacrAB carrying *pOqxAB* = (+ *oqxA* + *oqxB*)	This Study

2.4.4 RNA isolation and real-time quantitative PCR (qRT-PCR)

Total RNA was extracted from mid-log phase cultures by a phenol extraction method, as discussed elsewhere (Chatterjee et al., 2012). Following DNase1 treatment and extraction, spectrophotometric analysis ensured the RNA was free of DNA, protein, and solvent contamination. This total RNA was used for cDNA synthesis, and quantification of the target genes, *acrB, mexB* and *oqxB,* was done using gene-specific primers listed in **Appendix Table S2.4**. The cDNA synthesis was performed following the manufacturer's protocol from the iTaq Universal SYBR Green One-Step Kit (Bio-rad Catalog #172-5151). The quantitative-PCR (qPCR) amplification was done using an Applied Biosystems Thermocycler and 384-well optical plates. The qPCR was performed in triplicates for each of the samples using the following conditions: an initial

holding temperature of 50 °C for 10 minutes for cDNA synthesis and a second hold of 95 °C for 30 sec for the initial denaturation, followed by 40 cycles of 15 sec at 95 °C and 60 °C for 1 min. The cycling was then terminated with an additional extension of 60 °C for 30 sec. Fluorescence detection was performed at the annealing phase, and the dissociation curves were analyzed to confirm the amplification of a single product. The Ct values for the Threshold cycles were determined using QuantStudioTM Design and Analysis Software v1.5.1. All real-time PCR quantifications were performed simultaneously for the target genes encoding the permeases (*acrB, mexB and oqxB*), MFPs (*acrA, mexA* and *oqxA*), housekeeping gene *dnaK* and no template controls (NTC).

2.4.5 Nile Red Efflux Assays

The efflux liability and functionality of the reconstituted and heterologous overexpression systems were assessed further using Nile Red efflux assay, as reported elsewhere (Bohnert et al., 2010). Briefly, single colonies for all the bacterial strains were streaked on LB-Agar plates from glycerol stocks maintained at −80 °C and grown overnight at 140-150 rpm, 37 °C in a shaker incubator. The next day, cells were diluted in fresh LB broth (1:10) in an Erlenmeyer flask and continued to grow on a shaker (140 rpm; 37 °C) for 14 to 16 h. A 10-ml portion of this culture was then centrifuged at 4,400 rpm for 10 min at room temperature. The pellet was resuspended in 20 mM potassium phosphate buffer (pH 7.0) containing 1 mM $MgCl_2$ (PPB), and the final cells were adjusted to a final OD_{600nm} of 1.0 in PPB. All subsequent steps were performed at room temperature unless mentioned. 2ml aliquots of the cells were then transferred to Pyrex 15-ml conical centrifugation tubes, and CCCP (5 mM stock solution in 50% DMSO) was added to a final concentration of 10 μM. After 15 min, Nile Red (a stock solution of 5 mM in 10% dimethyl formamide-90% ethanol [vol/vol]) was added to a final concentration of 5 μM, and the cell suspension was incubated in the presence or absence of the competitor drug (antibiotic in this case) on a shaker (140 rpm; 37 °C) for 3h. The cells were left at room temperature for 60 min and then centrifuged for 5 min at 4,400 rpm. The supernatant was thoroughly removed, and the cells were resuspended in 2 ml PPB. Immediately thereafter, 100 μl of cells were aliquoted into 96 well-clear bottom black plates (Corning). The fluorescence of the cell suspension was recorded with Ex/Em: 556/662nm over 100 seconds, using a Tecan Infinite Pro 200 plate reader.

Efflux was monitored for an additional 200 seconds after Nile Red efflux was induced by rapid energization with 10µl of 1 M glucose.

2.4.6 Evaluation of Antibiotic susceptibility on solid media

The sensitivity of different strains was assessed by incorporating fixed concentrations of standard antibiotics in agar media (Wiegand et al., 2008) . Briefly, novobiocin (NOV), linezolid (LZD), and erythromycin (ERY) were added separately to molten LB agar media (Luria Bertani Agar, Miller; Hi-media) to achieve different concentrations (20,10 and 2.5µg/ml) and poured on to petri-plates. Isopropyl β-d-1-thiogalactopyranoside (IPTG; Catalogue no.# I6758, Sigma-Aldrich) was used at a final concentration of 100 µM for the induction of single complementation systems in *E. coli C43(DE3)* host with the *pET21a* expression system. The strains were initially streaked from glycerol stocks maintained at −80 °C onto LB-Agar plates with Ampicillin (100 µg/mL) and allowed to grow for 16-18 hours at 37 °C. A single colony of each of the strains was picked and grown in fresh LB broth (Luria Bertani Broth, Miller; Hi-media) at 37 °C, with shaking at 200 rpm, and allowed to grow for 6-8 hours. The cells were diluted to a final cell number equivalent to ~ 1*10^6 CFU/ml, and 10ul (~1*10^4 cells) was streaked onto the surface of the solid agar plates with respective antibiotics and allowed to grow overnight at 37 °C. The next day, plates were checked for bacterial growth.

2.4.7 Determination of Minimum Inhibitory Concentration (MIC)

MIC was determined according to guidelines, as discussed elsewhere (CLSI, 2018). Briefly, the strains from glycerol stocks maintained at −80 °C were streaked on LB-Agar plates with Ampicillin (100 µg/mL) and allowed to grow overnight at 37 °C. A single colony of each strain was picked from freshly streaked plates and grown in MHB No.2 Control Cations Hi-Media (MHB) with Ampicillin (100 µg/mL). Phe-Arg-β-naphthylamide (PAβN; Sigma-Aldrich, Catalogue no.# P4157), wherever mentioned, was used at a final concentration of 25 µg/mL. Isopropyl β-d-1-thiogalactopyranoside (IPTG; Catalogue no.# I6758, Sigma-Aldrich) was used at a final concentration of 100 µM for the induction of single complementation systems in the *pET21a* vector backbone. In contrast, the *acrB/acrAB, mexB/mexAB,* and *oqxB/oqxAB* expression systems in the modified *pTrc99a* vector backbone were constitutively expressed. The AcrAB, MexAB, and OqxAB were constitutively expressed, whereas induction with 100 µM of IPTG was required for AcrB, MexB, and OqxB expressing strains

(Amresco, Catalogue no.# 0487-10G). Serial, two-fold dilutions of stock solutions for different antibiotics such as linezolid (LZD), novobiocin (NOV), erythromycin (ERY) and rifampicin (RIF), which was used as a negative control due to its relatively lower efflux liability) were prepared in DMSO. 3µL compound from each of the dilutions and 150 µl (3–7*10^5 CFU/ml) of bacterial culture were added to a flat bottom 96 well microtiter plates to obtain final antibiotic concentrations as mentioned below (**Table 2.3**).

Table 2.3 Final concentration range (in µg/mL) for different antibiotic solutions used in the MIC assays

LZD	400	160	80	40	20	10	5	2.5	1.25	0.625	0.3
NOV	400	160	80	40	20	10	5	2.5	1.25	0.625	0.3
ERY	160	80	40	20	10	5	2.5	1.25	0.625	0.3	0.15
RIF	80	40	20	10	5	2.5	1.25	0.625	0.3	0.15	0.075

The plates were packed in gas-permeable polythene bags and incubated at 37 °C for 16-18h. MIC was determined as the concentration at which no bacterial growth was observed and ascertained by absorbance (OD_{600nm}) with a spectrophotometer. In the case of the wild-type strain and clinical isolates, 90% growth inhibition was used for MIC determination. For recombinant strains, the growth is compromised partially due to the presence of a plasmid and gene over-expression. Here, an 80% growth inhibition results in the reduction of the test OD values to that of the media control levels, which is used for MIC determination. All experiments were performed in triplicates, and the data reported in the present work is representative of the same.

2.5 Results

2.5.1 Structural studies based on modelling

Understanding the basis behind complementation or replacement from a different bacteria entails a thorough structural and sequence analysis of their RND efflux pumps. Further, the conservation of crucial residues helps to understand the basis and better probability of a functional heterologous efflux pump. As horizontal gene transfer is a means of transfer of permeases across the species barrier, the battle against AMR only gets more complex than previously imagined. Therefore, the conservation

of residues among permeases among MFP helps to confirm functional complementation and, hence, a confirmation of "in theory transmission" of AMR.

An examination of the structural conservation of the permeases and membrane fusion proteins (MFPs) selected for the present work was done across *E. coli* (AcrA-AcrB), *P. aeruginosa* (MexA-MexB), and *K. pneumoniae* (OqxA-OqxB) RND pumps. Based on the available structural information in published literature and the reported crystal structures, a sequence-based homology modelling approach was followed to understand the possible assembly of the efflux pump complex upon overexpression as a heterologous system. As the assembly of AcrB-AcrA-TolC in *E. coli* (5V5S) and MexB-MexA-OprM in *P. aeruginosa* (6IOK) are well reported in the literature, the same were considered as templates for the modelling studies. The evaluation of both single (**Figure 2.3 A-D**) and double complementation (**Figure 2.4 A-D**) clearly demonstrates the 'theoretical' assembly of the tripartite complex and the subsequent likely functional complementation of these proteins. Furthermore, it was also observed that TolC exhibits significant conservation with its analogue OprM in *P. aeruginosa*, which was found to complement MexA specifically (**Figure 2.5**).

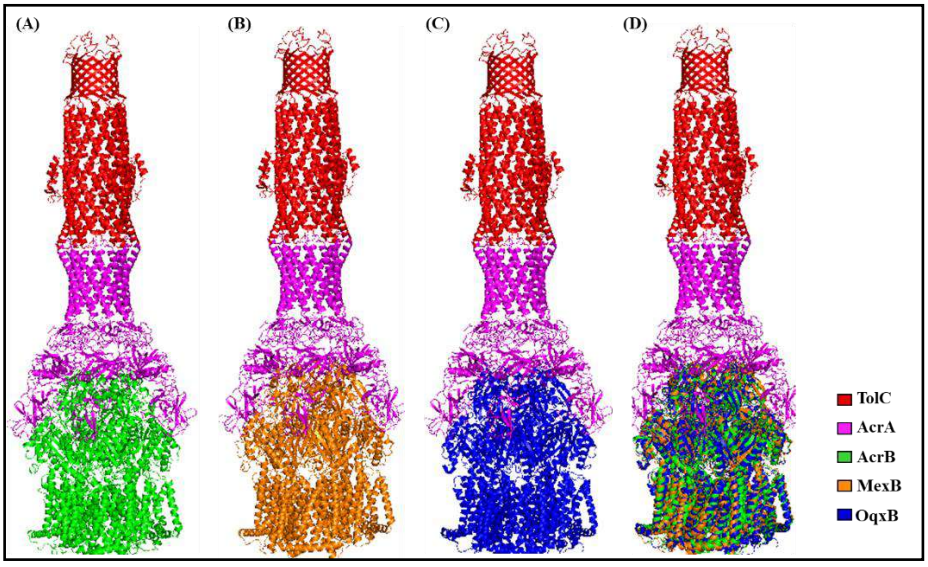

Figure 2.3 Structural assembly of the permeases from *E. coli, P. aeruginosa* and *K. pneumoniae* in a single complementation system. TolC (5V5S; Red) complements with AcrA (2F1M; Magenta), which, in turn, complements with permeases from other organisms (A) AcrB (5V5S; in Green), (B) MexB (6IOK; Orange) and (C) OqxB (7CZ9; Blue) respectively. (D) The superimposition of the permeases demonstrates the structural conservation and assembly of all the overexpressed efflux pumps in single complementation systems from different organisms.

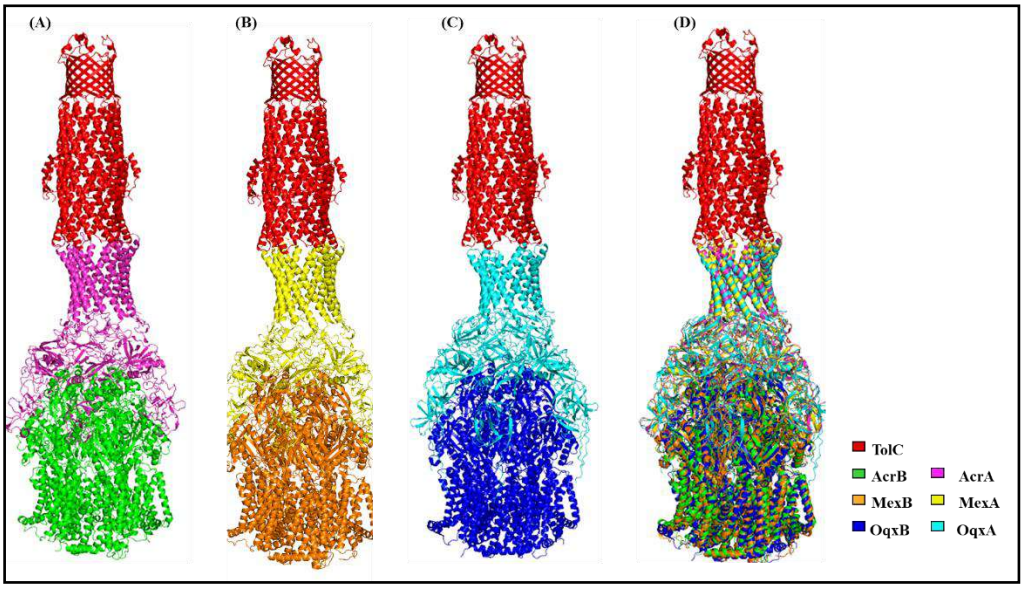

Figure 2.4 Structural assembly of the permeases and MFPs from *E. coli, P. aeruginosa* and *Klebsiella pneumoniae* in a double complementation system. TolC (Red) complements with (A) AcrA (Magenta) and AcrB (Green), (B) MexA (Yellow) and MexB (Orange) and (C) OqxA (Cyan) and OqxB (Blue) respectively. The superimposed image (D) demonstrates the overall structural conservation and assembly of all the overexpressed efflux pumps in double complementation systems from different organisms.

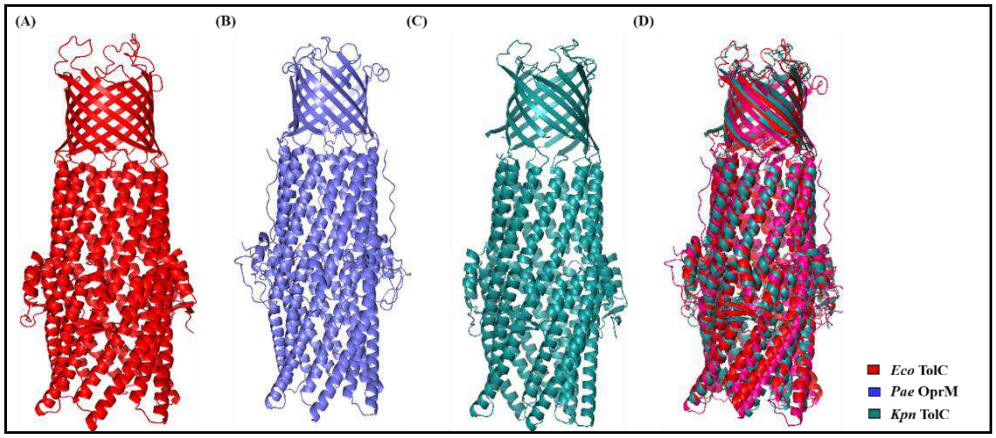

Figure 2.5 Structural similarity and conservation of the OMP components. TolC (5V5S) in *E. coli* (Red) (A) and OprM (Blue) (6IOK) in *Pseudomonas aeruginosa* (B) and *Klebsiella pneumoniae* TolC (C) superimposition of all the outer membrane protein components from the three organisms, depicting their overall structural conservation.

To analyze the relationships between MFPs, distance-based trees (**Figure 2.6**) were constructed using their sequences. These trees demonstrate a substantial degree of closeness in the MFP components of the different Resistance-Nodulation-Division (RND) pumps (**Figure 2.6 A**). However, upon examination of the permease domain, which is responsible for facilitating the transport of substances across membranes, noticeable differences were observed among the different members of the RND superfamily in *E. coli*, *P. aeruginosa* and *K. pneumoniae* (**Figure 2.6 B**). The existence of these variations could be the determining factor that governs the overall transport mechanisms and the different substrate specificities exhibited by each of the respective pump systems.

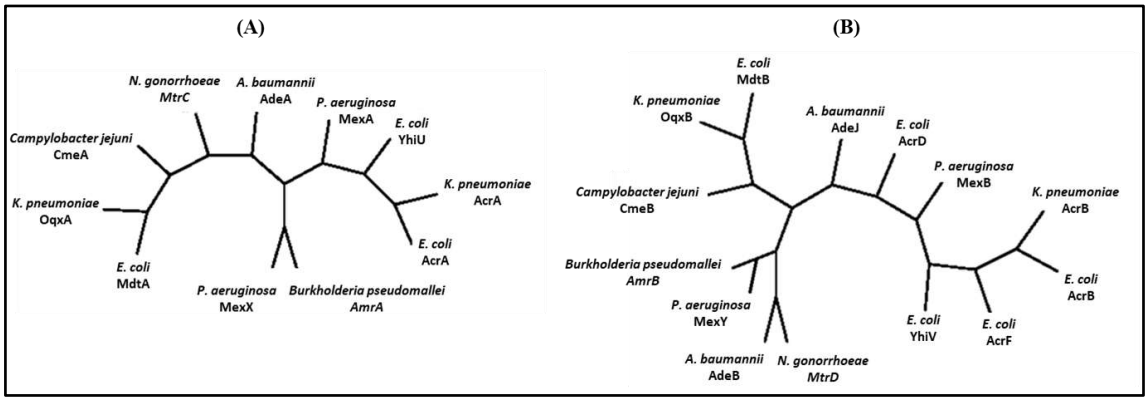

Figure 2.6 Distance-based phylogenetic tree for different permeases and MFPs. Illustrative depiction of the sequence alignment-based phylogenetic tree demonstrating the similarities and divergence among related biological sequences for different MFPs (A) and Permeases (B) of the RND efflux pumps in different Gram-negative bacteria.

Furthermore, the conservation of residues among the sequences was checked using the Consurf server for various MFPs in *E. coli* (Ashkenazy et al., 2016), which describes the amino acids conserved across permeases (**Figure 2.7**). It is noteworthy that the TolC complements with multiple proteins specifically, with RND (AcrA, AcrE, EmrA, EmrK) and ABC (MdtE, MacA) membrane fusion proteins in *E. coli* (Horiyama & Nishino, 2014; Zgurskaya et al., 2011). Based on the analysis, the conserved serine residue (S102 in AcrA, S106 in MexA, and S131 in OqxA) interacts with the threonine (T363) of TolC to form the complex successfully. The serine residue is present in the 'hairpin' tip of MFPs and is reported to form a complex with TolC (H. M. Kim et al., 2010). The superimposition of AcrA, MexA and OqxA shows structural conservation,

with RMSD values of 0.235 for AcrA: OqxA and 2.023 for AcrA: MexA. This implies a possibility of complex formation among the heterologous MFPs with TolC. Interestingly, the essentiality of AcrA for AcrB: TolC complex formation can be voided by mutating interacting residues to form disulfide linkage. However, such association has not been reported in nature, thereby cementing the position of MFPs as an important constituent for the overall functioning of the RND efflux pump (Hayashi et al., 2016; Tamura et al., 2005). Furthermore, the C-terminal region of AcrA, which is sensitive to proteolysis, is crucial for its association with the inner membrane protein AcrB. This has been demonstrated through chimera studies using AcrA residues 290-357 and direct binding studies using an AcrA fragment comprising residues 172-397 (Elkins & Nikaido, 2003).

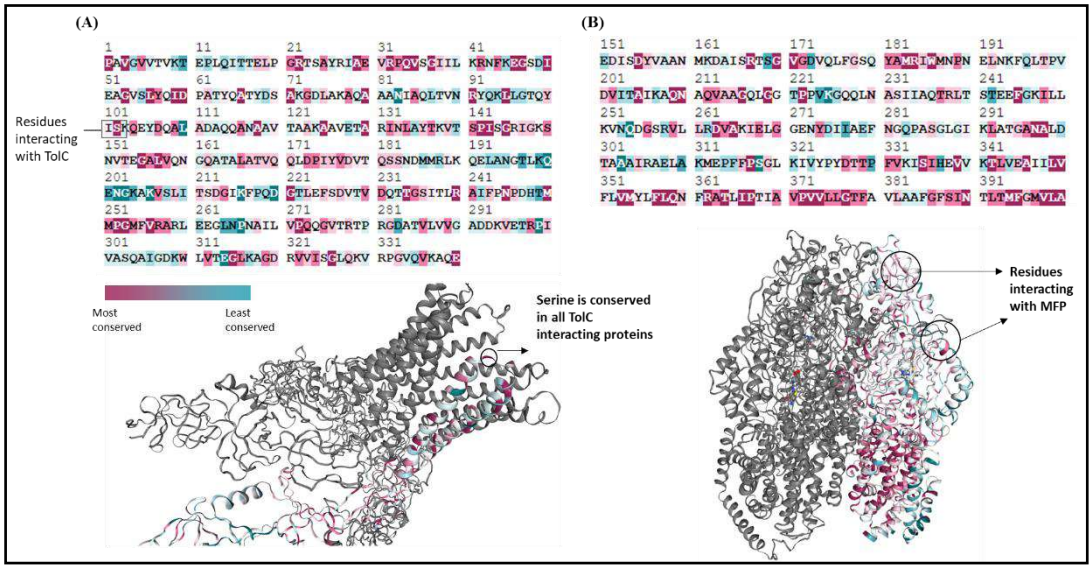

Figure 2.7 Conservation of TolC interacting residues across AcrAB, MexAB and OqxAB. (A) Consurf analysis shows the MFP encompassing the conserved residue Serine in the hairpin loop, which is essential for MFP: TolC complex formation. (B) Similarly, the region in permeases interacting with MFP exhibits comparable conservation.

From the structural studies, we can infer that despite the variations in their sequences and individual structures, the overall assembly of the functional tripartite is similar in both the single and the double expression complementation systems. However, to further ascertain the functionality of the predicted assembly in these reconstituted efflux pumps, certain functional assays were also performed to assess their

potentiality to extrude out some of the common antibiotics and affect the overall antibiotic susceptibility profiles of the host.

2.5.2 Expression of AcrB/AcrA-AcrB, MexB/MexA-MexB and OqxB/OqxA-OqxB as a heterologous system.

In order to establish the role of different efflux pump components, reconstituted efflux pump complex from the selected Gram-negative organisms, namely AcrB/AcrA-AcrB from *E. coli*, MexB/MexA-MexB from *P. aeruginosa* and OqxB/OqxA-OqxB from *K. pneumoniae*, each of the genes were overexpressed as a single/double complementating overexpression system respectively, in an efflux deficient *E. coli* background. The overexpression of the target genes in the respective host strains was further confirmed by quantitative real-time PCR in both the single and double complementation systems (**Figures 2.8 and 2.9**). These overexpression strains were further used to assess the efflux liability assays for different antibiotics.

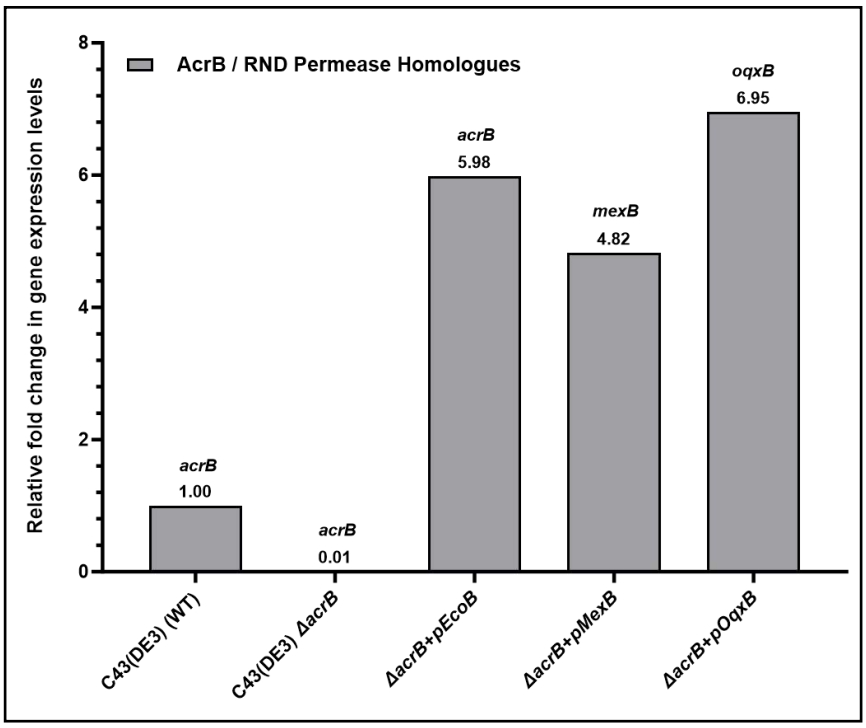

Figure 2.8 Estimation of gene expression levels in single complementation systems by qRT-PCR. The relative expression levels for the genes *acrB, mexB* and *oqxB* in *E. coli C43(DE3)* wild-type (WT), *ΔacrB* background and each of the heterologous systems, overexpressing the target genes AcrB (+ *pEcoB*), MexB (+ *pMexB*) or OqxB (+ *pOqxB*). Each point represents the ratios of the fold change for each of the target genes relative to the expression level of *acrB* in the *E. coli* wild-type system without

any complementation, as observed from two independent biological experiments (n=2) in technical triplicates. *dnaK* was used as the housekeeping control gene for internal normalization (**Appendix Table S2.5**).

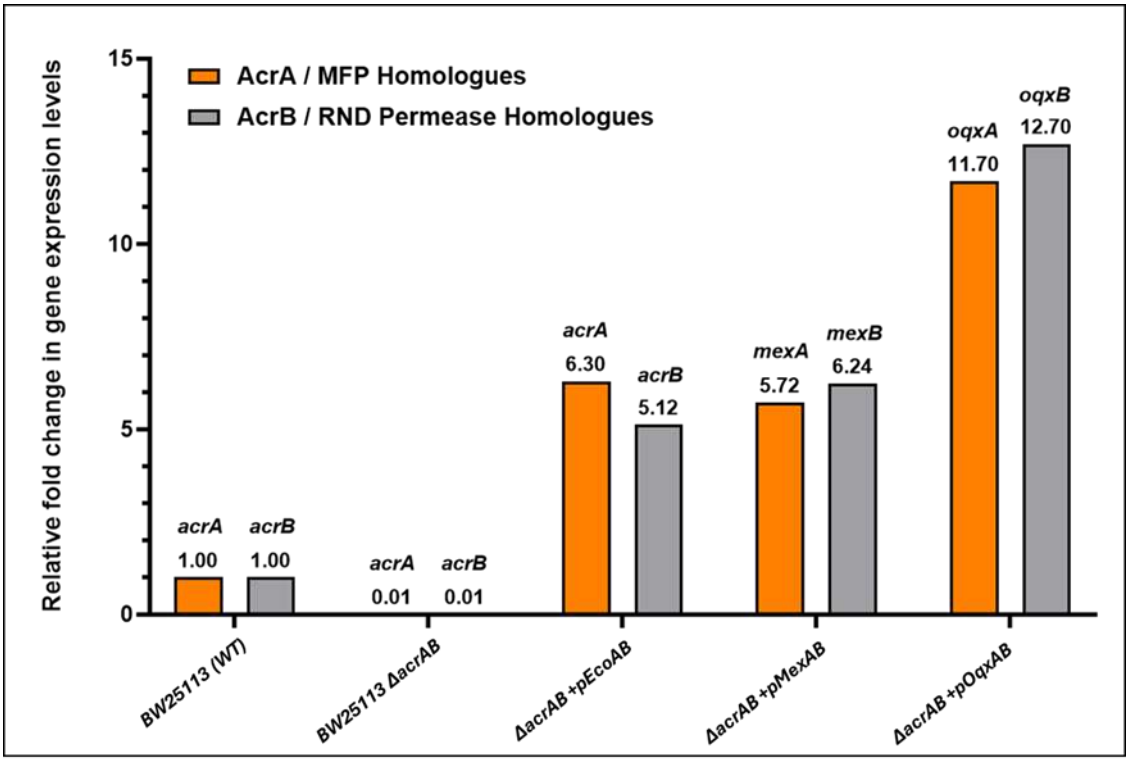

Figure 2.9 Estimation of gene expression levels in double complementation systems by qRT-PCR. The relative expression levels for the genes encoding the different permeases (*acrB, mexB* and *oqxB*) and MFPs (*acrA, mexA and oqxA*) in *E. coli BW25113* wild-type (WT), *ΔacrB* background and each of the heterologous systems, overexpressing the target genes *acrA-acrB* (+ *pEcoAB*), *mexA-mexB* (+ *pMexAB*) or *oqxA-oqxB* (+ *pOqxAB*). Each point represents the ratios of the fold change for each of the target genes relative to the expression level of *acrB* in the *E. coli* wild-type system without any complementation, as observed from two independent biological experiments (n=2) in technical triplicates. *dnaK* was used as the housekeeping control gene for internal normalization (**Appendix Table S2.6 A and B).**

2.5.3 Estimation of efflux complementation by Nile-Red Assay

Efflux monitoring assays with lipophilic membrane dyes, like Nile Red, are frequently utilized as gold standard assays for assessing the extent of drug extrusion by

efflux pumps (Bohnert et al., 2010). This assay is based on the competitive binding of the dye Nile Red and the drug molecules with the efflux pumps, followed by their release into the extra-cellular milieu. The compound competes with Nile red, resulting in a delay in the efflux of the dye, and the efflux liability is determined through the measurement of $T_{efflux50}$, which represents the time (in seconds) required to efflux half of the Nile red from the cells. In the present work, the ability of the efflux pump components from three key Gram-negative organisms to form a heterogenous tri-partite pump complex and extrude antibiotics was assessed by the Nile Red efflux assays.

The efflux-deficient mutants *E. coli C43(DE3) ΔacrB* and *E. coli BW25113 ΔacrA-ΔacrB* were used as controls. The $T_{efflux50}$ values of Nile red in these controls were greater than 300, indicating the absence or non-functionality of RND pumps. In contrast, the wild-type and the *ΔacrB* strain overexpressing the native *E. coli* AcrB overexpressed cells exhibited a comparable $T_{efflux50}$ and Nile red efflux profile (**Figure 2.10**), indicating the successful efflux complementation of the AcrB protein in the AcrB knockout (**Figure 2.11**). Furthermore, efflux of Nile red was observed in strains overexpressing AcrB, MexB, and OqxB in a *ΔacrB* background, as well as in AcrAB, MexAB, and OqxAB strains in a *ΔacrA-ΔacrB* background.

Complementation assays were also conducted against both RND and RND with MFP co-expressing strains in the presence of compounds such as linezolid, novobiocin, and erythromycin. The efflux liability of the compounds was also observed in these assays, with $T_{efflux50}$ values for the wild-type strain exceeding 300s for linezolid and novobiocin. Ciprofloxacin exhibits a partial liability at 260s, while erythromycin is less liable at 140s. These findings were further mirrored in the antibiotic susceptibility assays. Interestingly, overexpression of the efflux pump results in slightly less competition and lower $T_{efflux50}$ values for all compounds due to reduced competition with Nile Red. The $T_{efflux50}$ for erythromycin remains similar to the wild-type, suggesting the compound's ability to counteract all three efflux pumps. The $T_{efflux50}$ values for the compounds in single complementation, i.e., RND with the native MFP, are slightly lower (**Figure 2.10**). In contrast, the relatively lower $T_{efflux50}$ values for the double complementation systems, expressing the RND and the MFP components from the respective organisms (*P. aeruginosa* and *K. pneumoniae*) into the *E. coli* system exhibited a slightly higher efflux pattern, as compared to the single overexpressed ones. This indicates that while MFP plays a structural role in enhancing the functionality of the RND pumps, its overall contribution is minimal. Overall, the results of these assays

indicated that strains overexpressing different (heterologous) pump components were found to effectively extrude Nile red and other antibiotics, similar to that of the wild-type, indicating the assembly of a functional tri-partite system in efflux-deficient *E. coli* (**Figure 2.11**).

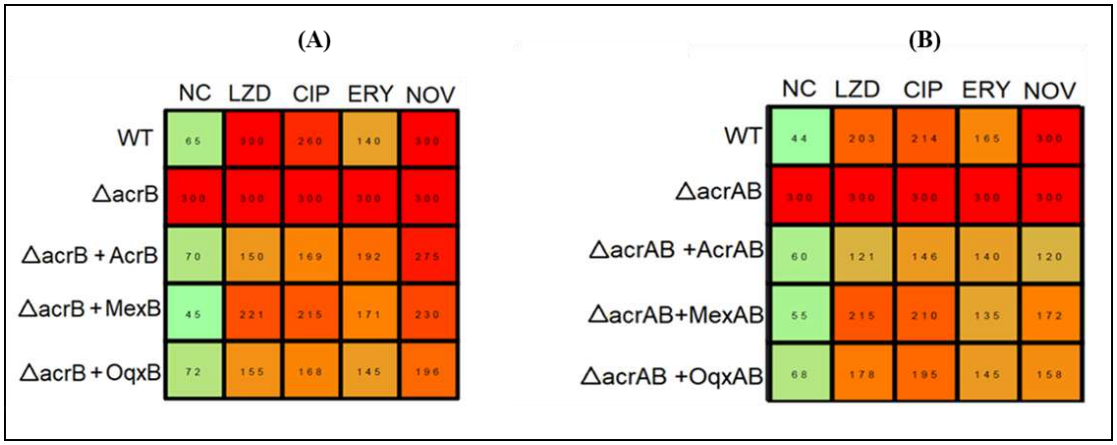

Figure 2.10 Nile Red $t_{efflux50}$ values for different complementation systems. Illustrative representation of the Nile red $t_{efflux50}$ values and heat map for the Nile red efflux assays. (A) Single complementation (RND expressing cells) in *E. coli C43(DE3)* wild-type, *ΔacrB and acrB (+pEcoB)*, *mexB (+pMexB)* and *oqxB (+pOqxB)* overexpressing systems. (B) Double complementation (i.e. RND and MFP expressing cells) in *E. coli BW25113*, *ΔacrAB and acrAB (+ pEcoAB)*, *mexAB (+pMexAB)* and *oqxAB (+pOqxAB)* overexpressing systems. In the presence of antibiotics, the $t_{efflux50}$ for Nile Red increases due to competition, as depicted in shades of red. The efflux pattern of the double overexpressed strain is higher compared to the single overexpressed ones.

NC: No Compound; **LZD:** Linezolid, **CIP:** Ciprofloxacin, **ERY:** Erythromycin, **NOV:** Novobiocin

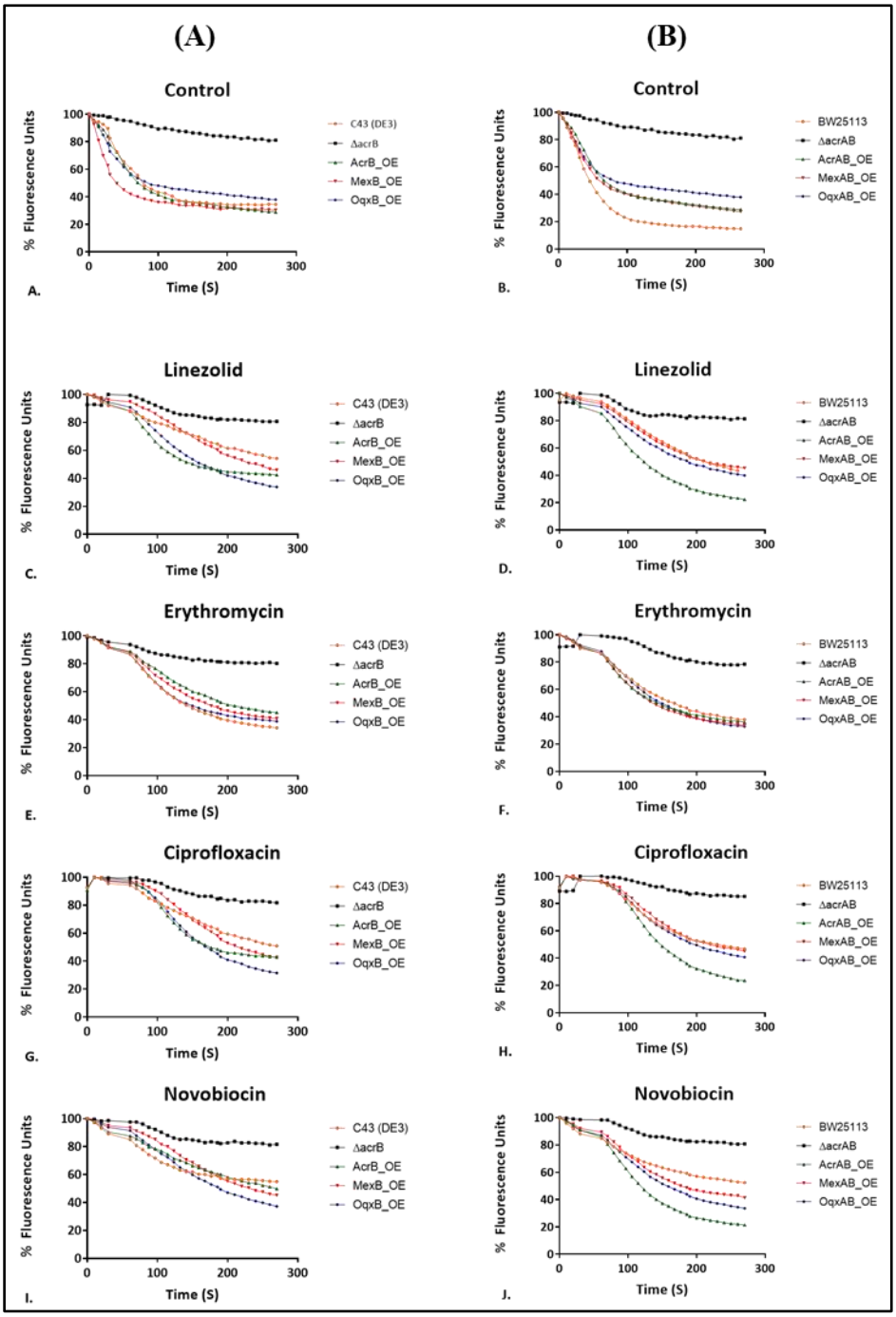

Figure 2.11 Nile red-based efflux assays in the wild-type and efflux deficient *ΔacrB/ΔacrAB* strains and their complementation. Inhibition of Nile Red efflux by competitor antibiotics with high efflux liability in (A) *E. coli C43(DE3)* (WT) and its single knockout background of *ΔacrB*, complemented with single overexpression systems of native AcrB or heterologously expressed MexB and OqxB (B) *E. coli BW25113* (WT) and its double knockout background of *ΔacrAB*, complemented with double overexpression systems of native AcrAB or heterologously expressed MexAB and OqxAB.

2.5.4 Antibiotic susceptibility and complementation assays

The functionality and antibiotic susceptibilities of all the overexpressing heterologous systems were further tested by evaluating growth in solid media containing fixed concentrations of antibiotics and also by determining their minimum inhibitory concentrations (MICs) on solid media and liquid broth, as per the CLSI guidelines (CLSI, 2018; Wiegand et al., 2008). For these studies, a panel of antibiotics, such as linezolid (LZD), novobiocin (NOV) and erythromycin (ERY), were considered, which inhibit different targets and consequently differ in their mechanisms of action. Although these antibiotics are well known for their antimicrobial effects against most of the Gram-positive bacteria, they exhibit poor efficacy in Gram-negative bacteria due to their high efflux liabilities. Rifampicin (RIFA) was considered a negative control in the panel due to its low efflux liability. Susceptibility patterns using solid media indicated a direct correlation between the expression of the efflux pumps and bacterial survival under different antibiotic concentrations. As depicted in **Figure 2.12**, the wild-type *E. coli C43(DE3)* exhibited visible growth under all the antibiotic conditions (LZD, NOV, ERY), with concentrations ranging from as high as 20µg/ml to as low as 2.5µg/ml. However, the loss of the native efflux pump AcrB resulted in enhanced sensitivity of the host strain towards these antibiotics, leading to an inhibited growth phenotype. Interestingly, complementation with either the native efflux pump or non-native pump components like MexB from *P. aeruginosa* and OqxB from *K. pneumoniae* resulted in complete restoration of the wild-type phenotype, as indicated by the visible growth, even at the highest concentrations of all the antibiotics, under the tested conditions. Only in the case of 2.5 µg/ml (novobiocin and erythromycin) growth was notably less, possibly indicating MIC may be different on solid media Vs the broth.

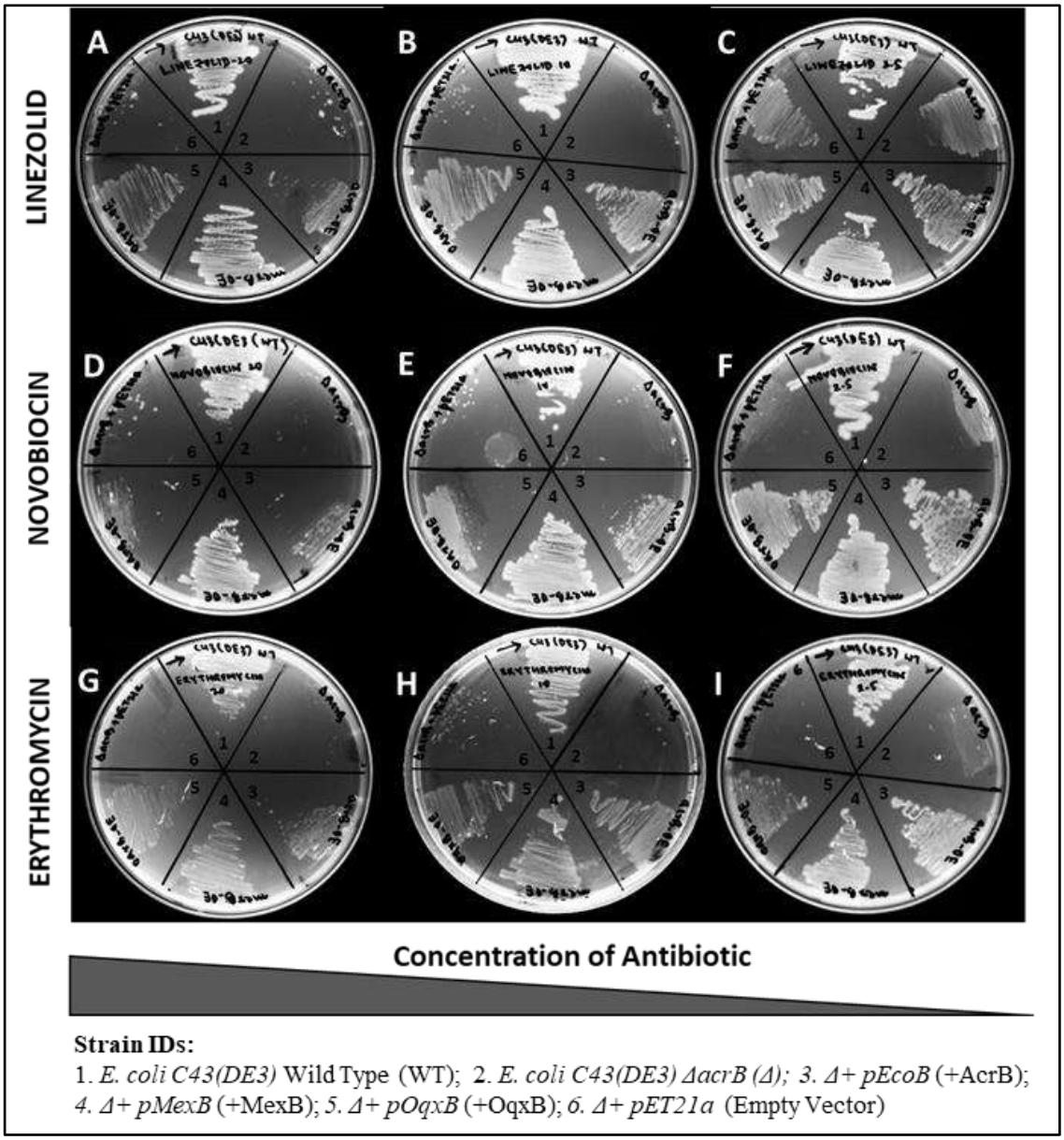

Figure 2.12 Antibiotic susceptibility on solid media. Antibiotic susceptibility assay was done on solid agar plates to check for complementation by *overexpressing acrB, mexB and oqxB* in *E. coli C43(DE3)* Δ*acrB* background**.** Different concentrations (20µg/ml, 10µg/ml and 2.5µg /ml) of compounds like linezolid (LZD): Plates A-C; novobiocin (NOV): Plates D-F and erythromycin (ERY): Plates G-I, were tested to check for sensitivity and growth of the strains expressing different pumps in *E. coli C43(DE3)* Δ*acrB*.

The functionality of all the overexpressing heterologous systems was further tested by determining their antibiotic susceptibilities by estimating their minimum inhibitory concentrations (MICs) in broth, as per the CLSI guidelines (CLSI, 2018). For these studies, a panel of antibiotics, such as linezolid (LZD), novobiocin (NOVO), and erythromycin (ERY), were considered. These antibiotics have different targets and mechanisms of action and are known for their high efflux liabilities in Gram-negative bacteria. Rifampicin (RIF) was included in the panel as a negative control due to its relatively lower efflux liability.

The results of the MIC experiments further corroborated both the output from the Nile Red efflux assays and growth on solid media containing antibiotics. The absence of the native efflux pump component in wild-type systems in either *C43(DE3) ΔacrB* or *BW25113 ΔacrAB* background resulted in potent MICs for all the tested antibiotics by 8 to 16-fold, thus confirming its role in the extrusion of these antibiotics. However, growth was restored with an increased shift in MICs by 8 to 32-fold and, in some cases, back to the wild-type levels following over-expression of native AcrB/AcrA-AcrB and upon complementation with the efflux pump components, MexB/MexA-MexB, and OqxB/OqxA-OqxB in similar background. (**Tables 2.4 and Table 2.5**). These results indicate that the non-native or heterologous overexpressed efflux pump components not only can form a functional pump complex but are also capable of compensating for the loss of the native *E. coli* pump component by effectively mediating the efflux of the tested antibiotics.

Table 2.4 MIC values (with fold change with respect to *ΔacrB*) in *E. coli C43(DE3) ΔacrB* background: AcrB, MexB and OqxB single complementation

	C43 (DE3)	***ΔacrB***	***ΔacrB +pET21a***	***ΔacrB +pEcoB***	***ΔacrB +pMexB***	***ΔacrB +pOqxB***
LZD	200 (16)	12.5	25 (2)	100 (8)	100 (8)	200 (16)
NOV	400 (32)	12.5	25 (2)	400 (32)	200 (16)	100 (8)
ERY	80 (8)	10	10 (1)	160 (16)	80 (8)	160 (16)
RIF	5 (1)	5	10 (2)	5 (1)	5 (1)	5 (1)

LZD: Linezolid; **NOV:** Novobiocin; **ERY:** Erythromycin; **RIFA:** Rifampicin.
(MIC values in µg/mL; Fold change calculated with respect to the MIC in efflux deficient background *ΔacrB*)

E. coli C43(DE3) (WT: wild-type) and its *ΔacrB* deletion strain were used for MIC; *pET21a* (empty vector), *pEcoB* (*+acrB), pMexB (+mexB) and pOqxB (+oqxB)*: complementation with the plasmid carrying the respective genes.

Table 2.5 MIC values (with fold change with respect to *ΔacrAB*) in *E. coli BW25113 WT* background: AcrA-AcrB, MexA-MexB and OqxA-OqxB double complementation

	BW25113	***ΔacrAB***	***ΔacrAB +pTrc99a***	***ΔacrAB +pEcoAB***	***ΔacrAB +pMexAB***	***ΔacrAB +pOqxAB***
LZD	200 (8)	25	25 (1)	100 (4)	100 (4)	200 (8)
NOV	400 (16)	25	25 (2)	200 (8)	400 (16)	200 (8)
ERY	160 (4)	40	20 (2)	160 (4)	80 (2)	160 (4)
RIF	5 (2)	2.5	2.5 (1)	5 (2)	5 (2)	5 (2)

LZD: Linezolid; **NOV:** Novobiocin; **ERY:** Erythromycin; **RIFA:** Rifampicin.

(MIC values in µg/mL; Fold change calculated with respect to the MIC in efflux deficient background *ΔacrB*)

E. coli BW25113 (WT: wild-type) and its *ΔacrAB* deletion strain were used for MIC. *pTrc99a* (empty vector), *pEcoAB* (*+ acrAB), pMexAB (+mexAB) and pOqxAB* (*+oqxAB*): complementation with the plasmid carrying the respective genes.

Additionally, the assembly and the functionality of the reconstituted efflux pump complexes were further tested by inhibition of AcrB and the other non-native efflux pump systems with efflux pump inhibitors (EPIs) like phenylalanine-arginine-β-naphthylamide (PaβN). The inhibition of the efflux pump component by EPIs significantly improved the activity of all the tested antibiotics, and the MICs were 10 to 20-fold more potent, indicating that the mechanism of action of the functional tri-partite efflux pump components of heterologous origin is similar to that of the native one (**Table 2.6 A and B**).

A. Single overexpression complementation assays in *E. coli C43(DE3) ΔacrB* background

	PAβN	***C43(DE3)***	***ΔacrB***	***ΔacrB +pTrc99a***	***ΔacrB +pEcoB***	***ΔacrB +pMexB***	***ΔacrB +pOqxB***
LZD	-	200	12.5	25	100	100	200
	+	12.5	25	12.5	12.5	25	25

B. Double overexpression complementation assays in *E. coli BW25113 ΔacrAB* background

	PAβN	***BW25113***	***ΔacrAB***	***ΔacrAB +pTrc99a***	***ΔacrAB +pEcoAB***	***ΔacrAB +pMexAB***	***ΔacrAB +pOqxAB***
LZD	-	200	12.5	25	100	100	100
	+	25	25	12.5	25	12.5	25

Table 2.6 Effect of EPIs on minimum inhibitory concentrations in single and double component complemented overexpression. MIC values (with fold change relative to the - PaβN system) of the antibiotics tested for their efflux liabilities in (A) single and (B) double component overexpression systems of the reconstituted efflux pump systems.

MIC values (in µg/mL); PAβN: Phenylalanine-Arginine-beta-Naphthylamide (PAβN); 25µg/ml; **LZD**: Linezolid.

2.6 Conclusion

The results of the current study demonstrated the salient structural and functional aspects of RND efflux pumps, which are likely to be the mechanism of AMR transmission across bacterial systems. The efflux pump components, chosen from the three key members of the ESKAPE pathogens, shared varying degrees of sequence homologies. The homology for the permease component (B-subunit) ranged from 70% (AcrB Vs MexB) to as low as 40% (AcrB Vs OqxB), and the same varied for the MFP component (A-subunit) as well. While AcrA and MexA share a homology of over 50%, this number is even lower for AcrA and OqxA (40%). Despite these differences, the expressed efflux pump components from heterologous sources in efflux pump component deleted *E. coli* could form a functional complex with the native *E. coli* TolC

and extrude antibiotics efficiently. These findings indicate their possible promiscuity and potential to mediate antibiotic efflux in non-native host organisms. Among factors responsible for causing an increase in AMR and transmitted via horizontal gene transfer, overexpression of efflux pumps is often considered one of the significant contributors. The outcome of this work elucidates the plausible underlying mechanisms in the transmission and establishment of AMR across different bacteria. Confirming the reconstitution of functional pumps by non-native efflux pump components in *E. coli* by structural assembly information, Nile Red assay and MIC determinations thus opens up newer opportunities for further explorations to probe the workings of different RND-type transporters and their associated MFPs.

The next phase of the research work focuses on the detailed characterization of OqxB, the RND efflux pump in *K. pneumoniae*, which has not been studied so well. Contrary to its counterparts, AcrB in *E. coli* and MexB in *P. aeruginosa*, the structural and functional aspects of OqxB have not been well characterized so far. The pump is considered important, especially with regard to its clinical relevance and broad distribution across different bacteria that possess varying levels of multi-drug resistance. Additionally, the transmissibility of the gene *oqxB*, encoding this efflux pump to other bacteria via horizontal gene transfer and its ability to extrude a wide spectrum of antibiotics makes it an important efflux pump to be embarked upon for detailed explorative studies. The key findings of the explorative research work are elucidated in the subsequent chapters (Chapters 3 & 4).

Chapter 3

Unveiling the Secrets of OqxB: The RND Efflux Pump in *Klebsiella pneumoniae*

Note 1: Part of the text in this chapter is included in the published manuscript: Bharatham, N., **Bhowmik, P**., Aoki, M. et al. *Nat. Commun.* 12, 5400 (2021). (DOI: https://doi.org/10.1038/s41467-021-25679-0)

Note 2: This project was done in collaboration with **Prof. Satoshi Murakami**, Department of Life Science and Technology, Tokyo Institute of Technology, Yokohama, Japan, and **St. Johns Research Institute**, Bengaluru, Karnataka, India.

3.1 Introduction

Klebsiella pneumoniae is a Gram-negative opportunistic pathogen, frequently encountered as the causal organism associated with multiple hospital-acquired infections, including pneumonia, urinary tract infections (UTIs), bloodstream infections, wound and surgical site infections, meningitis, etc., (Asri et al., 2021). This pathogen is also known to cause secondary infections. One of the recent studies found that a significant proportion of COVID-19 patients, with a high mortality rate of 56.7%, had secondary microbial infections caused predominantly by the multidrug-resistant variant of this pathogen (Vijay et al., 2021). As mentioned earlier, *Klebsiella pneumoniae* belongs to the ESKAPE group of pathogens (Gram-positive bacteria, including *Enterococcus faecium* and *Staphylococcus aureus*; and Gram-negative bacteria, including *Klebsiella pneumoniae, Acinetobacter baumannii, Pseudomonas aeruginosa, Enterobacter sp*.), that are continuously evolving to develop enhanced resistance against different types of antibiotics (De Oliveira et al., 2020; Pak-Leung Ho et al., 2016; Pendleton et al., 2013). The increasing mortality due to infections caused by resistant variants of *K. pneumoniae* has triggered a global health alarm. Although carbapenems were expected to potentially be effective, 8% of the bloodstream-related infections caused by *Klebsiella pneumoniae* were resistant to carbapenems, raising the danger of deaths associated with these unmanageable infections. As a result, the World Health Organization (WHO) has also recognized and declared *K. pneumoniae* a priority pathogen, for which there is an urgent need to develop next-generation antibiotics (World Health Organization, 2017, 2023). Antibiotics previously found to exhibit high potencies like nitrofurantoin, β-lactams, aminoglycosides, quinolones, tigecycline, and colistin (Bassetti et al., 2018; Ferreira et al., 2019; Holmes et al., 2016; Q. Xu et al., 2019; Zowawi et al., 2015), are now proving to be ineffective against *K. pneumoniae*, a phenomenon usually attributed to the increased expression of efflux pumps. It is widely reported that Gram-negative bacteria possess a wide array of efflux pumps, which contribute to intrinsic or acquired resistance against multiple classes of antibiotics by reducing the intracellular concentrations of antibiotics (Blanco et al., 2016; Hernando-Amado et al., 2016; J. Sun et al., 2014). Among them, the members of the RND family of efflux pumps are significant contributors to AMR (Alvarez-Ortega et al., 2013; Murakami, 2016; Nikaido & Takatsuka, 2009).

Protein crystal structures are crucial in understanding the complex biological interactions involving substrate/inhibitor binding. They provide atomic-level insights

with regard to biological function, allowing the designing of drugs to alter protein function (Jaskolski et al., 2014). *E. coli* AcrB, the efflux transporter protein, is no exception in this regard. The discovery of its structure offered information regarding substrate/inhibitor binding pockets and possible routes of substrate entry and exit (Du et al., 2018). The first crystal structure of *E. coli* AcrB was solved and reported as a symmetric trimer with each protomer composed of a 70Å protruding headpiece and a transmembrane region 50Å thick (Murakami et al., 2002). The *E. coli* AcrB transporter's structure facilitated the understanding of the efflux pump mechanisms in other Gram-negative bacteria from the ESKAPE family, such as MexB in *P. aeruginosa*, AcrB in *K. pneumoniae* and AdeB in *A. baumannii*, due to their high degree of sequence homology. Later work elucidated the asymmetric trimeric structure of *E. coli* AcrB, in which each domain has a different conformation corresponding to one of the three functional states: access/loose, binding/tight and extrusion/open conformations, of the transport cycle (Murakami, 2008; Murakami et al., 2006; Seeger et al., 2006). These structures indicated that the export of drugs is carried out via a three-step rotational mechanism in which substrates bind sequentially before being expelled out into the extracellular milieu. These asymmetric trimer structures also aided in modelling AcrA and TolC interactions with AcrB (Pos, 2009; Symmons et al., 2015). The subsequent work further helped to identify and reveal the substrate-binding mechanisms and the dynamic participation of crucial amino acid residues in the efflux mechanism (Lu et al., 2014; Schuster et al., 2014; Z. Wang et al., 2015; Zhou et al., 2015). Computational approaches, such as molecular docking and MD simulations, used this structural data to decipher binding modes and to understand antibiotic export mechanisms (Takatsuka et al., 2010; A. V. Vargiu & Nikaido, 2012). Furthermore, the drug-bound peristaltic movement and the corresponding conformational changes in the trimeric efflux pump were linked using tMD (targeted Molecular Dynamics) simulations (Jamshidi et al., 2016; Matsunaga et al., 2018; Ruggerone et al., 2013; A. V. Vargiu et al., 2018; Zuo et al., 2016). The crystal structure and computational models were utilized to create several effective and potent inhibitors that prevent conformational changes and, thereby, drug efflux (Aron & Opperman, 2016; Sjuts et al., 2016; A. V. Vargiu et al., 2014). The structural knowledge was also used to better understand the binding modes and interaction patterns of new antibacterial agents with AcrB, which led to medicinal chemistry inputs that reduced the efflux liability (Hameed P et al., 2018). Recent advances in cryo-electron microscopy (EM) in resolving multi-

subunit complexes to their atomic features have shifted paradigms in comprehending the intricacies of these sophisticated pumps (Z. Wang et al., 2017).

In this chapter, the key findings from the detailed crystal structure of the *K. pneumoniae* OqxB efflux pump, along with the salient features of its substrate-binding pocket, are described. This structure was then used to determine the critical amino acids involved in the efflux of fluoroquinolones. We further investigated its efflux proclivity using gene complementation and biochemical tests. We opine that this research will help to understand the role of OqxB transporters better so as to effectively interfere and prevent the OqxB-mediated efflux and thus reduce the AMR threat posed by its action.

3.2 Materials and Methods

3.2.1 Plasmids and constructs for complementation studies.

The plasmids and the constructs used in this study were generated and used, as discussed earlier (Chapter 2, **Section 2.4.2, Table 2.1**).

3.2.2 Strains and growth conditions for complementation studies.

The bacterial strains used in this study were generated as discussed earlier (Chapter 2, **Section 2.4.3)** and listed in **Table 3.1** below. The overexpression strains in the *E. coli BW25113* background were generated by transforming the respective overexpressing plasmids in the host strain. All the strains used were grown at 37 °C under aerobic conditions, with their respective selection markers, as discussed earlier.

Table 3.1 Bacterial strains used

Strains	Reference or Source
*E. coli K-12 BW25113 (*Wild-type)	(Baba et al., 2006)
E. coli K-12 BW25113 ΔacrB::kan	(Baba et al., 2006)
*E. coli C43(DE3) (*Wild-type)	(Miroux & Walker, 1996)
E. coli C43(DE3) ΔacrB::kan	This Study
E. coli K-12 BW25113 ΔacrA ΔacrB::kan (ΔacrAB)	This Study
E. coli C43(DE3) ΔacrB carrying *pET21a*	This Study
E. coli C43(DE3) ΔacrB carrying *pEcoB* = (+ *acrB*)	This Study

Strains	Reference or Source
E. coli C43(DE3) ΔacrB carrying *pOqxB* = (+ *oqxB*)	This Study
E. coli K-12 BW25113 carrying *pTrc99a*	This Study
E. coli K-12 BW25113 carrying *pEcoAB* = (+ *acrA* + *acrB*)	This Study
E. coli K-12 BW25113 carrying *pOqxAB* = (+ *oqxA* + *oqxB*)	This Study

3.2.3 RNA isolation and real-time quantitative PCR (qRT-PCR)

The isolation of total RNA, synthesis of cDNA and the quantification of the target genes *acrB* and *oqxB* were done using the protocols, as discussed earlier (Chatterjee et al., 2012)), using the gene-specific primers listed in **Appendix Table S2.4**.

3.2.4 Determination of MIC

MIC (Minimum Inhibitory Concentration) was determined following CLSI guidelines, as discussed elsewhere (CLSI, 2018). Briefly, the strains were streaked on LB-Agar plates with Ampicillin (100 µg/mL) from glycerol stocks maintained at −80 °C and allowed to grow overnight at 37 °C. A single colony of each strain was picked from the fresh plates and grown in MHB No.2 Control Cations Hi-Media (MHB) with Ampicillin (100 µg/mL). Phe-Arg β-naphthylamide (PAβN; Sigma-Aldrich, Catalogue no.# P4157) was used at a final concentration of 20 µg/mL, wherever mentioned. The AcrAB and OqxAB expression is under a constitutive promoter, and AcrB and OqxB were induced with 100 µM of IPTG (Amresco, Catalogue no.# 0487-10G). Antibiotics and their two-fold dilution series were prepared in DMSO. 3µL compound from each of the dilutions and 150 µl (3–7*10^5 CFU/ml) of bacterial culture were added to a flat bottom 96 well microtiter plates to obtain final antibiotic concentrations ranging from 0.03 µg/mL to 160 µg/mL. The plates were packed in gas-permeable polythene bags and incubated at 37 °C for 16-18h. MIC was determined as the concentration at which no bacterial growth was observed, as ascertained by absorbance (OD_{600nm}) with a spectrophotometer. In the case of the wild-type strain and clinical isolates, 90% growth inhibition was used for MIC determination. In the recombinant strains, the growth is partially compromised due to a plasmid and gene over-expression. Here, an 80% growth inhibition results in the reduction of the test OD values to that of the media control levels, which is used for the computation of MIC.

All experiments were performed in triplicates, and the data reported in the present work represents the same.

3.3 Results

This work was conducted in collaboration with Prof. Satoshi Murakami from the Department of Life Science and Technology at the Tokyo Institute of Technology in Yokohama, Japan, and St. John's Research Institute in Bengaluru, Karnataka, India. Consequently, only the key findings from the research conducted at these collaborative labs were highlighted. However, the thesis provides a comprehensive discussion of all the work undertaken as a part of the present doctoral research work, including detailed descriptions of the methods, protocols, and results.

3.3.1 Crystal structure of the OqxB

The crystal structure of the protein OqxB from *K. pneumoniae* was solved (Department of Life Science and Technology at the Tokyo Institute of Technology in Yokohama, Japan) at 1.85Å resolution after purification (**PDB ID: 7CZ9**). Each of the six monomers/protomers of the asymmetric unit of OqxB protein is composed of 1040 amino acid residues. The overall fold of the trimer resembles the other HAE1 subfamily of the RND (resistance nodulation-cell division) class of efflux pumps such as AcrB and MexB. Each OqxB monomer comprises twelve trans-membrane (TM) helices (TM1 to TM12), and the four porter subdomains (PN1, PN2, PC1, and PC2) comprise OqxB's periplasmic domain. The PN2 and PC2 sub-domains are further extended to the DN and DC docking sub-domains, respectively. These docking sub-domains are essential for the binding of OqxA and the formation of the trimer of the functional pump. Structural studies involving the superimposition of the OqxB monomer onto the asymmetric trimer of AcrB revealed that it is similar to AcrB binding/tight monomer conformation. The observations were similar for all the other protomers of the OqxB structure.

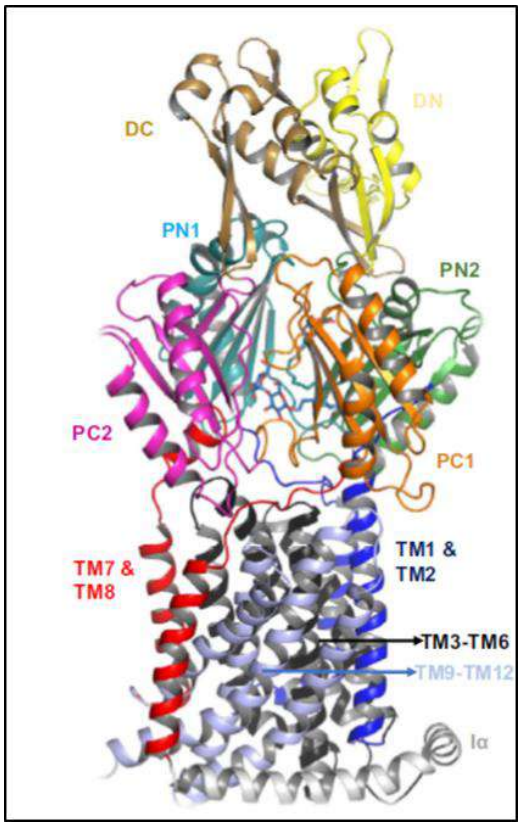

Figure 3.1. OqxB structural features. The OqxB structure is represented as a single protomer with important sub-domains highlighted with varied colours and labelled accordingly. The porter sub-domains PC1, PC2, PN1, and PN2 are highlighted with orange, magenta, cyan, and green coloured cartoons, respectively.

3.3.2 Substrate-binding pocket in OqxB: Comparison with other RND pumps

The outcome of the studies with the substrate binding domain of OqxB reveals its resemblance and the distinguishing salient features in comparison to other RND efflux pumps. The OqxB substrate/drug-binding pocket was compared with other known RND pumps, in particular, MexB, which is preferred over *E. coli* AcrB, due to the availability of the MexB crystal structure bound with DDM in its substrate-binding pocket (PDB ID: 3W9I) (Nakashima et al., 2013). In addition to the difference in the orientation of the binding of the DDM molecule, the substrate binding pocket of OqxB exhibited marked differences in comparison to MexB. The phenylalanine cage in MexB is primarily composed of hydrophobic residues such as F136, F178, F610, F615, F617 and F628, along with a few hydrophilic residues such as S48, S180 and Q185. In contrast, the substrate binding pocket of OqxB has a different architecture comprising both hydrophobic and hydrophilic or polar residues. The pocket is composed of

hydrophobic residues like F180, L280, F618, and L621, F295, F626 and F636, L138, V141, F295 and F626. In addition, the presence of polar residues such as S48, Q46, R48, Q125, Q134 and Q178 in the substrate-binding pocket of OqxB is unique, which is not observed in other RND pumps (**Figure 3.2**). Furthermore, both AcrB and MexB pumps have a small hydrophilic serine residue (S155), which is replaced by the R157 residue in the OqxB molecule. Even marked differences were observed in the gate loops (g-loop), which is important in facilitating the entry of the substrate molecules into the substrate-binding pocket and the subsequent efflux process (Cha et al., 2014). In comparison to AcrB and MexB, the g-loop in OqxB is longer by two residues (16 vs 14 g-loop residues), with the presence of two proline residues (P619 and P630), contrary to the g-loop in AcrB which comprises of four glycine residues (G614, G616, G619 and G621), and in MexB comprising of three glycine residues (G614, G616, and G621) (**Figure 3.3**). The two phenylalanine residues (F615 and F617) on the g-loop of both AcrB and MexB, which are crucial for substrate binding, were replaced with hydrophobic residues such as L621, A623 and F626, thereby contributing to the phenylalanine cage architecture. These overall structural differences contribute to the different binding modes of substrate molecules at the OqxB substrate-binding pocket compared to MexB. A comparative visualization of the sequences and residue variations for AcrB, MexB and OqxB could be referred in **Appendix Figure S2.2**.

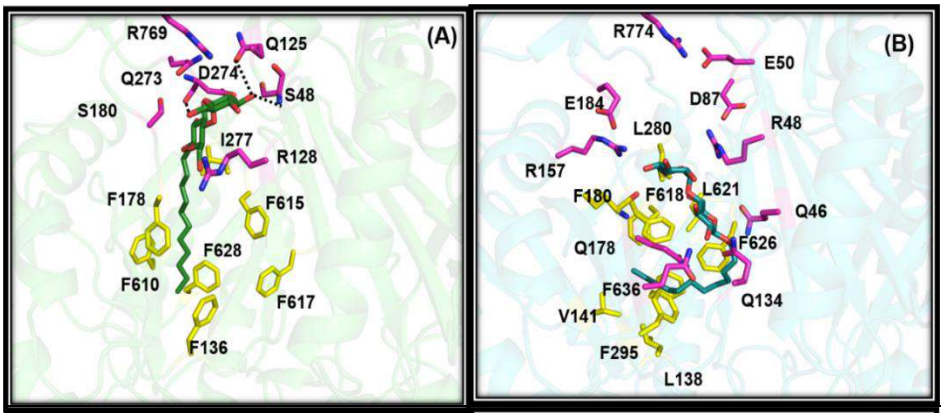

Figure 3.2 Key variations in substrate binding pocket. The differences in the binding mode of DDM molecule at the substrate binding pocket, as experimentally determined with MexB (A) and OqxB (B) structures compared. Hydrophobic residues are shown as yellow sticks, whereas hydrophilic residues are depicted as magenta sticks and labelled accordingly.

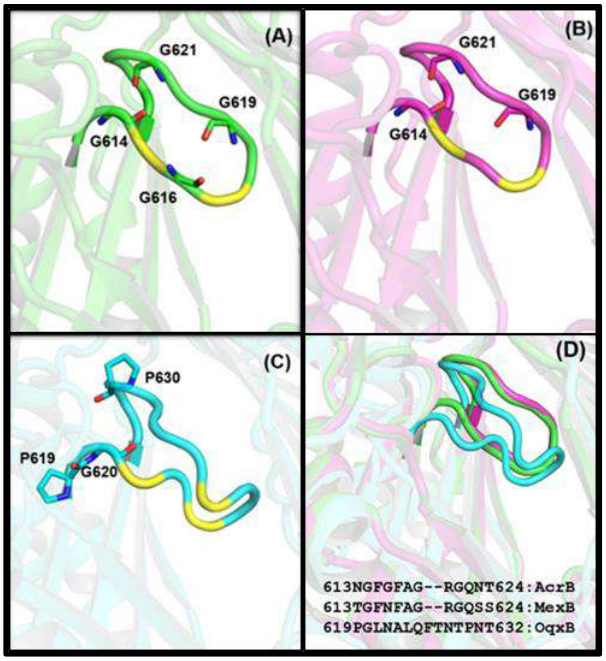

Figure 3.3 The gate loop (g-loop) variations. Structural and sequence level differences of the g-loop are shown by highlighted loop structure and critical residues of (A) AcrB, (B) MexB and (C) OqxB. The glycine or proline residues present on AcrB, MexB and OqxB of the g-loop are highlighted. (D) superimposed image to emphasize the g-loop orientational differences of OqxB compared to the other two structures. Sequences of g-loop aligned to highlight the extra residues of OqxB.

3.3.3 Role of efflux pumps in fluoroquinolone resistance

OqxB, the RND efflux pump component, is frequently associated with the increased resistance found in the clinical isolates of *E. coli* and *K. pneumoniae* (Hong et al., 2009). The efflux liability for fluoroquinolones in the clinical isolates of *E. coli* was, therefore, determined and evaluated in 84 recent isolates by MIC experiments. As per the findings made at St. John's Medical Hospital, Bengaluru, India, the MIC of ciprofloxacin against most of these clinical strains of *E. coli* ranged from 0.015 to >8 mg/mL. Sanger sequencing studies revealed that the resistance phenotype was associated with the mutations in the Quinolone-Resistance Determining Regions (QRDR) of *gyrA* and *parC* for the majority of the screened strains (**Appendix Table S3.2**). However, four of the outlier strains (with MIC values varying from 0.015 to 0.25 g/mL) were also found to be devoid of the ciprofloxacin resistance mutations (S83L and D87N of *gyrA*, S80I or S80R, as well as E84V or E84G of *parC*). From these clinical

strains, MIC experiments were further performed using an efflux pump inhibitor, PaβN (Phenylalanine-Arginine beta-Naphthylamide), on a panel of nine isolates (five with the above *gyrA* and *parC* mutations and four without any target mutations) to measure the contribution of efflux towards resistance. Except for one susceptible clinical strain (SEC032) that showed a 4-fold reduced MIC, none of the other strains showed an altered MIC in the presence or absence of PAβN (**Appendix Table S3.3**). In contrast, PAβN inhibition of AcrB potentiated linezolid and reduced its MIC by 10 to 20-fold. This data unequivocally indicated that ciprofloxacin has minimal efflux liability through the efflux pump AcrB in these strains. Further analysis by PCR and target sequencing was done to detect the presence of the *oqxB* gene amongst these 84 clinical isolates. Surprisingly, three of the screened isolates were found to possess the gene (**Appendix Table S3.4**). The accompanying mutations in the QRDR region of these strains precluded their use in establishing the role of OqxB in the efflux of the fluoroquinolones. Therefore, complementation experiments in "sensitive strains" were undertaken to probe further the role of OqxB in efflux towards fluoroquinolone resistance.

3.3.4 Efflux of fluoroquinolones by OqxB: MIC-based Complementation Studies

Studies based on molecular docking and MD simulations revealed that fluoroquinolone molecules such as ciprofloxacin, levofloxacin, and moxifloxacin could bind and subsequently be extruded by OqxB. The three negatively charged residues (E50, D87, and E184) and three positively charged residues (R48, R157, and R774) together constitute the OqxB hydrophilic pocket for the binding of these molecules. Other notable residues, such as S182, also play a key role in the binding of the fluoroquinolones at the substrate binding pocket. Furthermore, the important charged residue pairs (E50:R774 and R157:E184) were observed to stabilize the binding of the substrate molecules via intra-molecular interactions. Another striking characteristic not observed in any other RND efflux pumps is the highly charged OqxB hydrophilic pocket. The corresponding pocket in AcrB and MexB is majorly composed of hydrophilic residues like serine and threonine and possesses fewer charged residues.

In order to further ascertain the role of OqxB in the efflux of fluoroquinolones, complementation studies through antibiotic susceptibility assays were done with overexpression of OqxB from heterologous bacteria in wild-type *E. coli* and its

corresponding *ΔacrB* strain. Overexpression of *K.pneumoniae* OqxAB in *E. coli BW25113* wild-type, as confirmed by quantitative real time-PCR (**Figure 3.4**), led to an increased shift of 8 to 32 fold in the MICs for quinolones like ciprofloxacin, moxifloxacin and levofloxacin **(Table 3.2)**, indicating its involvement in their efflux. Similar results were observed when heterologous (*K.pneumoniae*) OqxB was over-expressed as a single complementation system in *E. coli C43 (DE3) ΔacrB* (**Table 3.3**). The outcomes from the complementation assays align completely with our earlier findings from the Nile red assay, as discussed earlier, in which the reconstituted efflux pumps with OqxB and OqxAB in *E. coli* efflux deficient system successfully extruded ciprofloxacin (**Chapter 2, Figures 2.10 & 2.11**) The lower $T_{efflux50}$ values in OqxB complemented systems, in comparison to the wild-type systems further indicates the high efflux liability of fluoroquinolone molecules by OqxB. Overall, these findings suggest that OqxB can form a functional complex with the *E. coli* AcrA-TolC and further confirm its role in conferring antibiotic resistance, as reported elsewhere (Hansen et al., 2007). It is noteworthy that the fluoroquinolone resistance due to efflux by AcrB is less than that caused by OqxB, as shown in studies conducted here with the high efflux liabilities in bacterial systems containing OqxB.

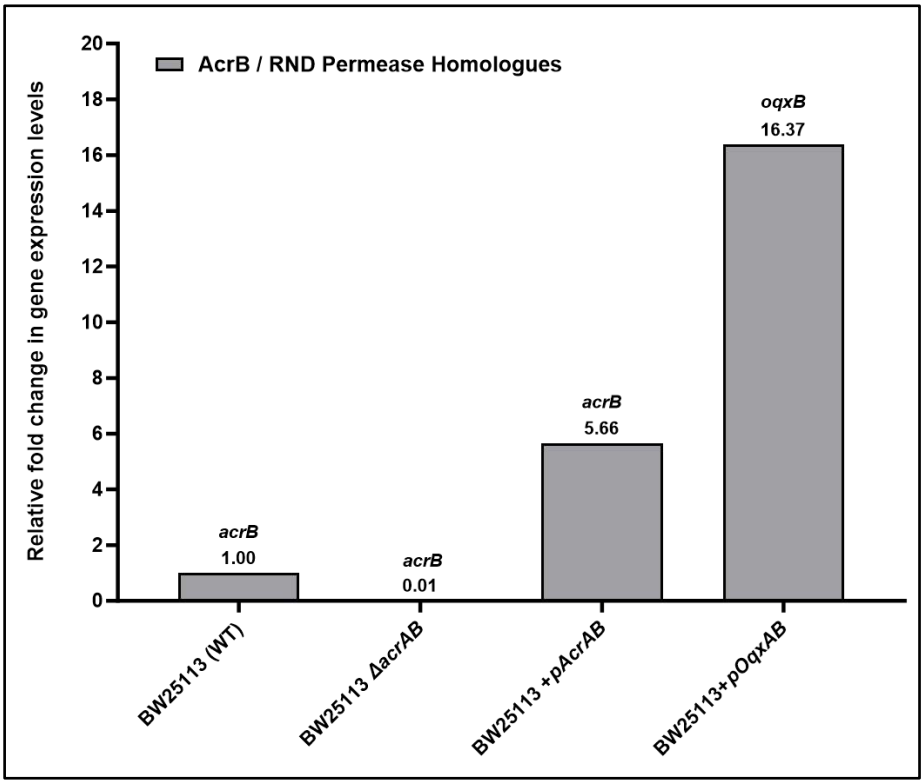

Figure 3.4 Estimation of gene expression levels in complementation systems by qRT-PCR. The relative expression levels for the genes *acrB* and *oqxB* in each of the overexpression systems, (A) *E. coli K-12 BW25113* wild-type, BW(WT); (B*)* WT carrying *pEcoAB* (overexpressing *acrA*-*acrB*) and (C) WT carrying *pOqxAB* (overexpressing *oqxA*-*oqxB*), was estimated by quantitative Real-Time PCR (qRT-PCR). Each point represents the ratios of the fold change for each of the target genes (*acrB* and *oqxB*) relative to the expression level of *acrB* in *E. coli* wild-type system, without any complementation, as observed from two independent biological experiments (n=2) in technical triplicates. *dnaK* was used as the housekeeping control gene for internal normalization (**Appendix Table S3.5**).

Table 3.2 MIC values (with fold change) in *E. coli BW25113 WT* background: AcrA-AcrB and OqxA-OqxB double complementation

Compounds	*E. coli BW25113* (WT)	*ΔacrAB*	WT + *pTrc99a*	WT + *pEcoAB*	WT + *pOqxAB*
CIPRO	0.0125 (2)	0.00625	0.00625 (1)	0.00625 (1)	0.05 (8)
LEVO	0.025 (2)	0.00625	0.0125 (2)	0.0125 (2)	0.2 (32)
MOXI	0.025 (2)	0.0125	0.025 (2)	0.025 (2)	> 0.4 (16)
RIFA	10 (2)	5	5 (1)	10 (2)	10 (2)

CIPRO: Ciprofloxacin; **LEVO:** Levofloxacin; **MOXI:** Moxifloxacin; **RIFA:** Rifampicin.

(MIC values in µg/mL; Fold change calculated with respect to the MIC in efflux deficient background *ΔacrAB*); *E. coli BW25113* (WT: wild-type) and its *ΔacrAB* deletion strain were used for MIC; *pTrc99a* (empty vector), *pEcoAB* (+*Eco_acrAB*), *pOqxAB* (+*oqxAB*): complementation with the plasmid carrying the respective genes.

Table 3.3 MIC values (with fold change) in *E. coli C43(DE3) ΔacrB* background: AcrB and OqxB single complementation

Compounds	*E. coli C43 (DE3)*	*ΔacrB*	*ΔacrB* + *pET21a*	*ΔacrB* + *pEcoB*	*ΔacrB* + *pOqxB*
CIPRO	0.00625 (1)	0.00625	0.00625 (1)	0.00625 (1)	0.1(16)
LEVO	0.00625 (0.5)	0.0125	0.00625 (1)	0.0125 (2)	0.1 (8)
MOXI	0.00625 (0.5)	0.0125	0.0125 (1)	0.025 (2)	0.2 (16)
RIFA	5 (1)	5	5 (1)	5 (1)	5 (1)

CIPRO: Ciprofloxacin; **LEVO:** Levofloxacin; **MOXI:** Moxifloxacin; **RIFA:** Rifampicin.

(MIC values in µg/mL; Fold change calculated with respect to the MIC in efflux deficient background *ΔacrB*); *E. coli C43(DE3)* (WT: wild-type) and its *ΔacrB* deletion strain were used for MIC; *pET21a* (empty vector), *pEcoB* (+ *acrB*), *pOqxB* (+*oqxB*): complementation with the plasmid carrying the respective genes.

3.4 Discussion

OqxB and other RND efflux pumps, such as AcrB and MexB, have little sequence identity in comparison (**Appendix Table S2.1**). However, the findings of the present work revealed that their architectural features are comparable. Several studies revealing the structures of RND efflux pumps have reported asymmetric trimeric forms, with each protomer having a distinct conformation: access/loose, binding/tight, and extrusion/open. In contrast, OqxB has a symmetric structure in which all three protomers are found to be present in the binding or tight protomer state. Furthermore, sequence and structural comparisons also provided crucial evidence that OqxB might also exist as an asymmetric trimer.

Antibiotics belonging to the class of fluoroquinolones were extruded more effectively by OqxB (around 8-16-fold) than AcrB, as found in our complementation studies. The lack of impact by efflux pump inhibitors like PAβN on the MIC for ciprofloxacin in clinical isolates of *E. coli* further indicated the limited efflux liability by AcrB. The susceptibility studies using *E. coli* and *P. aeruginosa* efflux pump knockout data, as reported previously (Piddock, 2006), also showed a moderate shift, which aligns with our observations. This increased efflux of fluoroquinolones by OqxB could be attributed to the charged residues in the substrate binding pocket. As none of the structurally well-characterized efflux pumps reported so far possesses such charged residues in the substrate-binding pocket/phenylalanine cage, we also propose that the zwitterionic fluoroquinolones interact with these oppositely charged R157 and E50 side chains. Together, these findings support our hypothesis that charged residues are essential for fluoroquinolone molecules to bind optimally in the hydrophobic cage of the RND class of efflux pumps.

Our current work on the OqxB crystal structure from *Klebsiella pneumoniae* uncovered several crucial structural attributes of this pump. These include the salient features of the substrate binding pocket, including the g-loop variations and the contribution of F626 in substrate binding. Though the phenylalanine cage of the substrate binding pocket is comparatively intact, the pocket's hydrophilic portion has several charged residues showing significant variations with other RND pumps. To our knowledge, none of the known RND efflux pumps demonstrates such high charge propensity. It is also important to reiterate that intra-molecular interaction between E50 and R774 residues may play a crucial role in the substrate efflux process. The presence of R157 residue and its elongated side chain's projection towards the substrate-binding

pocket is also a unique feature of OqxB. Such unique structural features near the substrate-binding pocket and associated rearrangements signify the possibility of altered substrate specificity. However, these interactions and the contribution of these unique charged residues cannot be captured only from structural *in silico* studies with the apo structures or homology modelling techniques and need further functional investigations. Therefore, additional functional studies were performed to further validate the role of these predicted charged residues in the extrusion of fluoroquinolone molecules. The next chapter captures detailed information related to the design of these studies and their subsequent outcomes.

Overall, the present work reports the first high-resolution crystal structure of OqxB, which provides opportunities for an in-depth understanding of OqxB-related efflux and hopefully can aid the discovery and development of antibiotics with reduced efflux liabilities.

3.5 Data availability

The OqxB efflux pump crystal structure solved and reported in this study has been deposited in the Protein Data Bank under accession code **PDB 7CZ9.**

Chapter 4

Deciphering the impact of key amino acid residues on OqxB-mediated efflux of fluoroquinolones: insights from site-directed mutagenesis

Note: Part of the text in this chapter is included in the published manuscript:

Bhowmik, P., *et al*. *Res Microbiol*. 2023 May;174(4):104039.

(DOI: 10.1016/j.resmic.2023.104039)

4.1 Introduction.

The role of OqxB in conferring multidrug resistance across a spectrum of bacterial systems and its ability to extrude a wide variety of antibiotics, such as quinolones, nitrofurantoin, chloramphenicol, quinoxalines, tigecycline, disinfectants and detergents, is a well-established phenomenon (Hong et al., 2009; J. Li et al., 2019; Ni et al., 2020; Pak-Leung Ho et al., 2016; Rodríguez-Martínez et al., 2013; Wyres & Holt, 2018; Q. Xu et al., 2019; Yuan et al., 2012). Recently, the crystal structure of OqxB at 1.85Å resolution was reported, along with insights into its unique substrate-binding site and its contribution to the efflux of fluoroquinolones (Bharatham et al., 2021). Although the overall structural assembly of OqxB is similar to the well-studied and characterized RND efflux pump components from other bacterial systems, like AcrB in *E. coli* and MexB in *Pseudomonas aeruginosa*, the distinctive architecture of its substrate-binding site makes it unique and also versatile. The substrate-binding domains of RND pumps like AcrB in *E. coli* and MexB in *P. aeruginosa* feature primarily aromatic phenylalanine cages with non-polar hydrophobic or uncharged polar residues. However, the domain of OqxB comprises unique residues, including some conserved ones from the phenylalanine cage, incorporating hydrophobic, polar uncharged like phenylalanine, alanine, valine, leucine, along with some unique polar and charged amino acids such as glutamine, aspartate, arginine, and lysine. Our earlier studies based on docking and molecular dynamics simulations indicated that the interactions of different fluoroquinolone molecules with both the polar as well as non-polar residues at the substrate-binding pocket are crucial for their successful binding and subsequent extrusion (Bharatham et al., 2021).

In the present study, we report the contributions of critical amino acid residues of the substrate binding domain of OqxB, as predicted by docking studies and MD simulations from our earlier work (Bharatham et al., 2021) in mediating efflux of fluoroquinolones. Moreover, with the studies conducted, we could also establish that interactions of the charged substitutions on the substrate with the polar/charged groups of phenylalanine cage were equally crucial along with that of the hydrophobic interactions with the non-polar hydrophobic residues, for the imminent efflux of fluoroquinolones. In order to understand the role of specific residues of OqxB in mediating the latter, MICs were determined against different fluoroquinolones following overexpression of both wild-type and mutated *K. pneumoniae* OqxB generated via site-directed mutagenesis (SDM) and transformation of *E. coli*. We

propose that the results from this study could lead to a better understanding of the mode of efflux mechanisms employed by OqxB and consequently yield valuable insights on how to counter the associated challenge of AMR.

4.2 Materials and Methods

4.2.1 Bacterial Strains

All the bacterial strains used in the present study are listed in **Table 4.1** below. The strains were grown and cultured on either 1.5% Luria Bertani Agar Miller (Hi-Media) plates or in Mueller Hinton Broth MHB No.2 Control Cations (MHB No.2 Control Cations, Hi-Media). Selection pressure with antibiotics like Ampicillin (Ampicillin sodium salt; Sigma-Aldrich, Catalog no.# A9518), Amp 100 µg /ml or Kanamycin (Kanamycin sulfate; HiMedia, Catalog no.# MB105), Kan 30 µg/mL, were used, wherever required. Double Knockout *ΔacrA-ΔacrB* strain in *E. coli BW25113* was generated by homologous recombination, as discussed elsewhere (Datsenko & Wanner, 2000). *E. coli* Top10 F' strain (Thermo Fisher Scientific) was used for DNA cloning and plasmid amplification. All the cultures were grown at 37 °C under aerobic conditions.

Table 4.1 Bacterial strains used for site-directed mutagenesis studies

Bacterial Strains	Reference or Source
E. coli K-12 BW25113	(Baba et al., 2006)
E. coli K-12 BW25113 ΔacrAB ΔacrB::kan	This Study
E. coli K-12 BW25113 carrying *pEcoAB* = (+ acrA + acrB)	(Bharatham et al., 2021)
E. coli K-12 BW25113 carrying *pOqxAB* = (+ oqxA + oqxB)	(Bharatham et al., 2021)
E. coli K-12 BW25113 carrying *pOqxA-OqxB (R157A)*	(Bharatham et al., 2021)
E. coli K-12 BW25113 carrying *pOqxA-OqxB (R48A)*	This Study
E. coli K-12 BW25113 carrying *pOqxA-OqxB (E50A)*	This Study
E. coli K-12 BW25113 carrying *pOqxA-OqxB (D87A)*	This Study
E. coli K-12 BW25113 carrying *pOqxA-OqxB (F180A)*	This Study
E. coli K-12 BW25113 carrying *pOqxA-OqxB (E184A)*	This Study

Bacterial Strains	Reference or Source
E. coli K-12 BW25113 carrying *pOqxA-OqxB (L280A)*	This Study
E. coli K-12 BW25113 carrying *pOqxA-OqxB (L621A)*	This Study
E. coli K-12 BW25113 carrying *pOqxA-OqxB (F626A)*	This Study
E. coli K-12 BW25113 carrying p*OqxA-OqxB (R774A)*	This Study

4.2.2 Plasmids and Constructs

The plasmids used in the current study are listed in **Table 4.2.** Each of the constructs was designed and made, as discussed previously (Bharatham et al., 2021; Braman et al., 1996), for the heterologous expression of the efflux pump components. The polycistronic *acrAB* and *oqxAB* were amplified using genomic DNA templates from *E. coli BW25113* and *K. pneumoniae* ATCC 13883 genomic DNA, respectively, using high-fidelity Phusion DNA Polymerase (Thermo Fisher Scientific). The amplicons for the complementation studies for *acrA-acrB* and *oqxA-oqxB,* along with a constitutive promoter sequence, were fused with a vector backbone containing the *pBR322*-origin and Ampicillin resistance gene (from the vector *pTrc99a*, Genscript) using the NdeI and HindIII restriction sites. The strains used for the complementation assays were generated by transforming these plasmids, as described in **Table 4.1.**

Table 4.2. Plasmids and constructs used for site-directed mutagenesis (SDM) studies

Plasmids	Description	Reference or Source
pTrc99a	Cloning Vector	Genscript
pEcoAB	*pTrc99a* derivative carrying *E. coli acrA* & *acrB*; Amp^r	(Bharatham et al., 2021)
pOqxAB	*pTrc99a* derivative carrying *K. pneumoniae oqxA* & *oqxB*; Amp^r	(Bharatham et al., 2021)
pOqxA-OqxB (R157A)	*pTrc99a* derivative carrying *K. pneumoniae oqxA* & *oqxB* with mutation R157A; Amp^r	(Bharatham et al., 2021)

Plasmids	Description	Reference or Source
pOqxA-OqxB (R48A)	*pTrc99a* derivative carrying *K. pneumoniae oqxA* & *oqxB* with mutation R48A; Amp^r	This Study
pOqxA-OqxB (E50A)	*pTrc99a* derivative carrying *K. pneumoniae oqxA* & *oqxB* with mutation E50A; Amp^r	This Study
pOqxA-OqxB (D87A)	*pTrc99a* derivative carrying *K. pneumoniae oqxA* & *oqxB* with mutation D87A; Amp^r	This Study
pOqxA-OqxB (F180A)	*pTrc99a* derivative carrying *K. pneumoniae oqxA* & *oqxB* with mutation F180A; Amp^r	This Study
pOqxA-OqxB (E184A)	*pTrc99a* derivative carrying *K. pneumoniae oqxA* & *oqxB* with mutation E184A; Amp^r	This Study
pOqxA-OqxB (L280A)	*pTrc99a* derivative carrying *K. pneumoniae oqxA* & *oqxB* with mutation L280A; Amp^r	This Study
pOqxA-OqxB (L621A)	*pTrc99a* derivative carrying *K. pneumoniae oqxA* & *oqxB* with mutation L621A; Amp^r	This Study
pOqxA-OqxB (F626A)	*pTrc99a* derivative carrying *K. pneumoniae oqxA* & *oqxB* with mutation F626A; Amp^r	This Study
pOqxA-OqxB (R774A)	*pTrc99a* derivative carrying *K. pneumoniae oqxA* & *oqxB* with mutation R774A; Amp^r	This Study

4.2.3 Site-directed mutagenesis (SDM) for OqxB

The contribution of the polar residues at the substrate binding site of OqxB in the efflux of fluoroquinolones was studied by generating and using mutants, in which the polar residues were replaced with a non-polar alanine residue. The strategy of rapid PCR-based site-directed mutagenesis of double-stranded DNA was followed, as discussed previously, to generate the desired mutants (Bharatham et al., 2021; Braman et al., 1996). Each of the desired mutations was introduced in the *oqxB* gene by amplifying the plasmid-carrying genes *oqxA-oqxB*, using mutagenic primers for *oqxB*, as described in **Appendix Table S4.1.** The synthesis of the mutant strand was carried out in a Thermal Cycler (Biorad) with the cycling program of 1 hold of 95 °C for 5min, 15 cycles of 95 °C for 30 s, 55 °C for 1min, 68 °C for 6 min and final extension of 68 °C for 10min. Subsequently, the amplified product was digested with DpnI (Thermo

Fisher Scientific) at 37 °C for 1h to eliminate methylated plasmid substrate. The mixture was then transformed into *E. coli* Top10 F' strain (Thermo Fisher Scientific) competent cells and selected on Ampicillin (100 µg/mL) containing plates. Plasmids from individual colonies were screened for the presence of desired mutations by sequencing. Following confirmation of the mutation's presence, the plasmids were transformed in *E. coli BW25113* strains and subsequently used for complementation assays.

4.2.4 Determination of Minimal Inhibitory Concentration (MIC)

MIC was determined, following the guidelines of CLSI, as discussed elsewhere (CLSI, 2018). All the strains were streaked on LB-Agar plates with either Ampicillin (100 µg/mL) or Kanamycin (30 µg/mL) for the respective strains carrying the selection marker from glycerol stocks maintained at −80 °C and allowed to grow overnight at 37 °C. A single colony of each strain was picked from the fresh plates and grown in MHB No.2 Control Cations Hi-Media (MHB) with the selected antibiotic, Ampicillin (100 µg/mL) or Kanamycin (30 µg/mL). As both AcrAB and OqxAB expression are under a constitutive promoter, no additional induction was required to trigger their expression. All the antibiotic stock solutions and their two-fold dilutions were prepared in DMSO. 3µl of each compound dilution was added to 150 µL of bacterial culture (with (3–7 × 10^5 CFU/mL) in flat bottom 96-well microtiter plates for obtaining final antibiotic concentrations ranging from 160µg/ml to as low as 0.03µg/ml. The plates were packed in gas-permeable polythene bags and incubated overnight (16-18 hours) at 37 °C. The next day, absorbance was measured for each of the wells at 600nm using a spectrophotometer, and MIC was determined as the concentration at which no bacterial growth was observed. A 90% growth inhibition cut-off for wild-type strains was used for MIC determination. However, in the recombinant strains, as the growth was compromised partially due to the presence of a plasmid and overexpression of target genes, a cut-off of 80% growth inhibition with respect to their control levels was used for determining the MICs. All experiments were performed in triplicates, and the data reported in the present work is representative of the same.

4.3 Results and Discussion

Earlier *in silico* studies using molecular docking simulations, along with the comparison of structural features of OqxB with that of the well-studied efflux pumps like AcrB and MexB, aided in the identification of putative amino acid residues likely to have a critical impact around the n-dodecyl-β-D-maltoside (DDM) binding pocket of

OqxB (Bharatham et al., 2021). To extend this understanding further, we predicted and identified the roles of these residues in the binding and subsequent efflux of quinoxalines, e.g., olaquindox and various fluoroquinolones such as ciprofloxacin, norfloxacin levofloxacin, and moxifloxacin (**Figure 4.1).**

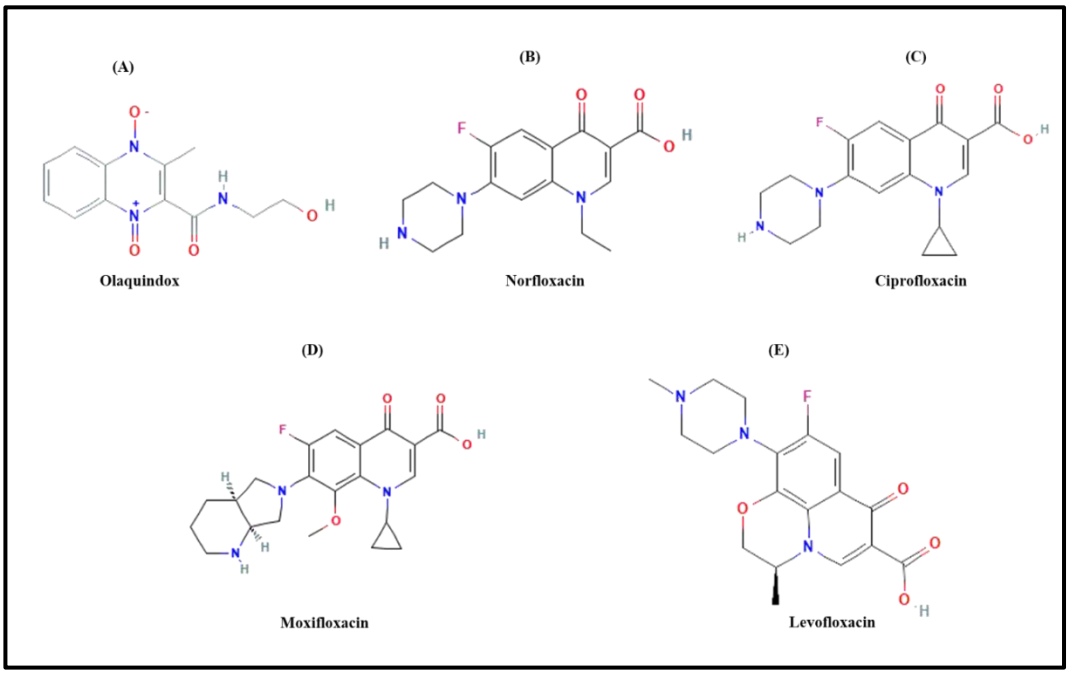

Figure 4.1 2D structures of the common quinoxaline and fluoroquinolones used. (A) Olaquindox, OLA; (B) Ciprofloxacin, CIPRO; (C) Norfloxacin, NOR; (D) Moxifloxacin, MOXI and (E) Levofloxacin, LEVO.

As evident from several structural and mutant generation studies reported earlier, F178 in AcrB and MexB is one of the key and central aromatic residues interacting with most antibiotic/substrate molecules (Gervasoni et al., 2022; Sjuts et al., 2016). Moreover, our earlier investigations with nitro-containing compounds also revealed that I277 is a crucial residue in the hydrophobic substrate binding pocket (Hameed P et al., 2018). In the case of OqxB, however, an identical residue, F180, is present instead of F178 of AcrB and MexB, along with a similar hydrophobic residue, L280, which is present instead of I277. The predicted binding modes of olaquindox and fluoroquinolones (**Figure 4.2**) showed that these two residues are likely to be involved in substrate binding. The g-loop (gate loop) also plays a crucial role in permeation into substrate binding pocket or phenylalanine cage, demonstrating differences with AcrB and MexB (PDB ID: 4DX5 and 3W9I, respectively) in studies reported earlier (Bharatham et al., 2021). Compared to AcrB and MexB, the g-loop is extended by two

extra residues, and additionally, the key F615 and F617 residues are replaced by L621 and A623 in OqxB. Surprisingly, our DDM bound OqxB structure (PDB ID: 7CZ9) indicated that the orientation of the F626 side chain is such that it occupies the space of F617 of AcrB and MexB, thereby plausibly playing a similar role in substrate binding/positioning in phenylalanine cage.

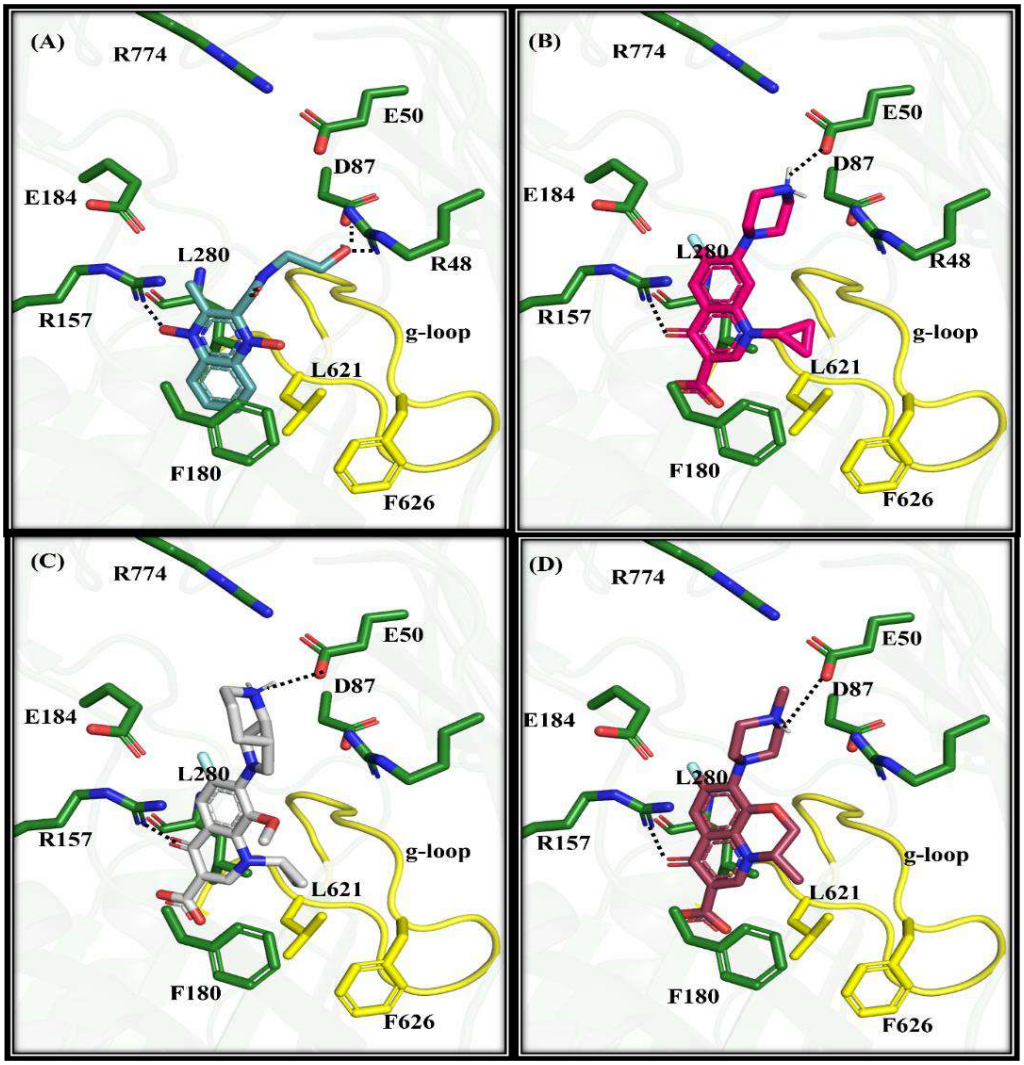

Figure 4.2 Molecular docking for the predicted binding modes of olaquindox and other fluoroquinolone derivatives. Predicted binding modes of olaquindox (A) and ciprofloxacin (B), moxifloxacin (C), and levofloxacin (D) at the substrate binding pocket or phenylalanine cage of OqxB. Olaquindox is depicted as dark cyan, whereas all three fluoroquinolones, ciprofloxacin (magenta), levofloxacin (brown) and moxifloxacin (grey) sticks. Important interacting residues and ion pairs are shown as dark green sticks, and hydrogen bond interactions between protein and ligand are shown as broken lines. The g-loop (gate loop) key for substrate entry into the phenylalanine

cage is highlighted in yellow, and the two critical hydrophobic residues are shown as sticks.

To validate the roles of crucial hydrophobic residues of OqxB in quinolone binding, site-directed mutagenesis of the four residues (F180, L280, L621 and F626), and MIC-based complementation assays were conducted. For these studies, the heterologous system comprising of *K. pneumoniae* wild-type or mutated OqxB was constitutively overexpressed in *E. coli BW25113*. Since most of the studies using clinical isolates of *Klebsiella spp.*, *E. coli* and *Salmonella spp.* that exhibit fluoroquinolone resistance are usually found to be associated with the presence or transmission of plasmid-mediated quinolone resistance (PMQR) of OqxB via horizontal gene transfer (Bharatham et al., 2021; Jingjing Zhao et al., 2010; J. Li et al., 2019), *E. coli* wild-type was chosen as the host strain for our studies, instead of the efflux pumps deleted double knockout strains (*ΔacrAB*), to mimic the possible scenario frequently encountered among the clinical isolates in the human host environment. For the complementation studies, host cells transformed with *pTrc99a* served as the control system. Surprisingly, *E. coli BW25113 ΔacrAB* transformed with native *E. coli* AcrA-AcrB showed an insignificant impact with respect to the efflux of fluoroquinolones. Complementation studies with wild-type and mutated *K. pneumoniae* OqxB in *E. coli BW25113* system exhibited an altered resistance pattern, indicating a specificity towards fluoroquinolones. The overexpression of wild-type OqxA-OqxB in *E. coli* significantly enhanced the MIC values, resulting in an enhanced shift of 8-16-fold (compared to wild-type *E. coli*). However, the substitution of the hydrophobic residues with alanine using site-directed mutagenesis resulted in a complete reversion of the fluoroquinolone extrusion ability of the OqxB efflux pump, as evidenced from the restored MIC values, similar to that seen with wild-type *E. coli BW25113* (**Figure 4.3)** These observed outcomes are also in agreement with the previously published work on OqxB, wherein the involvement of residues F180 and F626 in binding with compounds like olaquindox and ciprofloxacin was reported in *E. coli BL21* (S. Xu et al., 2020). In contrast, the overexpression of the native AcrA-AcrB in *E. coli* did not show any considerable shift in the MIC values for antibiotics like olaquindox, ciprofloxacin, norfloxacin, moxifloxacin, and levofloxacin, further confirming the specificity of OqxB in extrusion of fluoroquinolones **(Table 4.3**).

Table 4.3 Minimum Inhibitory Concentrations of OqxA-OqxB overexpressing (wild-type or mutagenic OqxB) complementation systems in *E. coli BW25113*

Strains	MIC Values (in µg/ml)					
	OLA	**NOR**	**CIPRO**	**LEVO**	**MOXI**	**RIFA**
E. coli K-12 BW25113 (WT)	40	0.05	0.0125	0.05	0.025	10
ΔacrAB	20	0.025	0.00625	0.025	0.0125	5
WT + *pTrc99a*	40	0.05	0.0125	0.025	0.025	5
WT + *pEcoAB*	40	0.05	0.0125	0.025	0.025	5
WT + *pOqxAB*	160	0.4	0.05	0.4	0.4	10
WT + *pOqxA-OqxB* (F180A)*	40	0.05	0.0125	0.05	0.05	10
WT + *pOqxA-OqxB* (L280A)*	40	0.1	0.025	0.05	0.05	5
WT + *pOqxA-OqxB* (L621A)*	20	0.05	0.0125	0.05	0.025	5
WT + *pOqxA-OqxB* (F626A)*	40	0.05	0.0125	0.05	0.025	5
WT + *pOqxA-OqxB* (R48A)#	40	0.05	0.0125	0.05	0.05	5
WT + *pOqxA-OqxB* (E50A)#	40	0.05	0.0125	0.05	0.05	5
WT + *pOqxA-OqxB* (D87A)#	40	0.05	0.025	0.05	0.05	5
WT + *pOqxA-OqxB* (R157A)#	40	0.05	0.0125	0.05	0.05	5
WT + *pOqxA-OqxB* (E184A)#	40	0.05	0.0125	0.05	0.05	10
WT + *pOqxA-OqxB* (R774A)#	40	0.05	0.0125	0.05	0.05	5

The minimal inhibitory concentrations of *E. coli* WT systems overexpressed with either OqxAB or OqxA-OqxB (SDM) against quinoxaline and other fluoroquinolones; Rifampicin was used as a negative control.

E. coli K-12 BW25113 (WT: wild-type) or its *ΔacrAB* strain used for MIC.
pTrc99a, *pEcoAB* (+*acrAB*), *pOqxAB* (+*oqxAB*) and *pOqxA-OqxB(SDM)* (+*oqxA*+*oqxB-SDMs*): complementation with a plasmid carrying the respective genes or the gene with indicated mutations.

OLA: Olaquindox; **NOR**: Norfloxacin; **CIPRO**: Ciprofloxacin; **LEVO**: Levofloxacin; **MOXI**: Moxifloxacin; **RIFA**: Rifampicin
*SDM in Hydrophobic residues; #SDM in Polar/ Hydrophilic residues

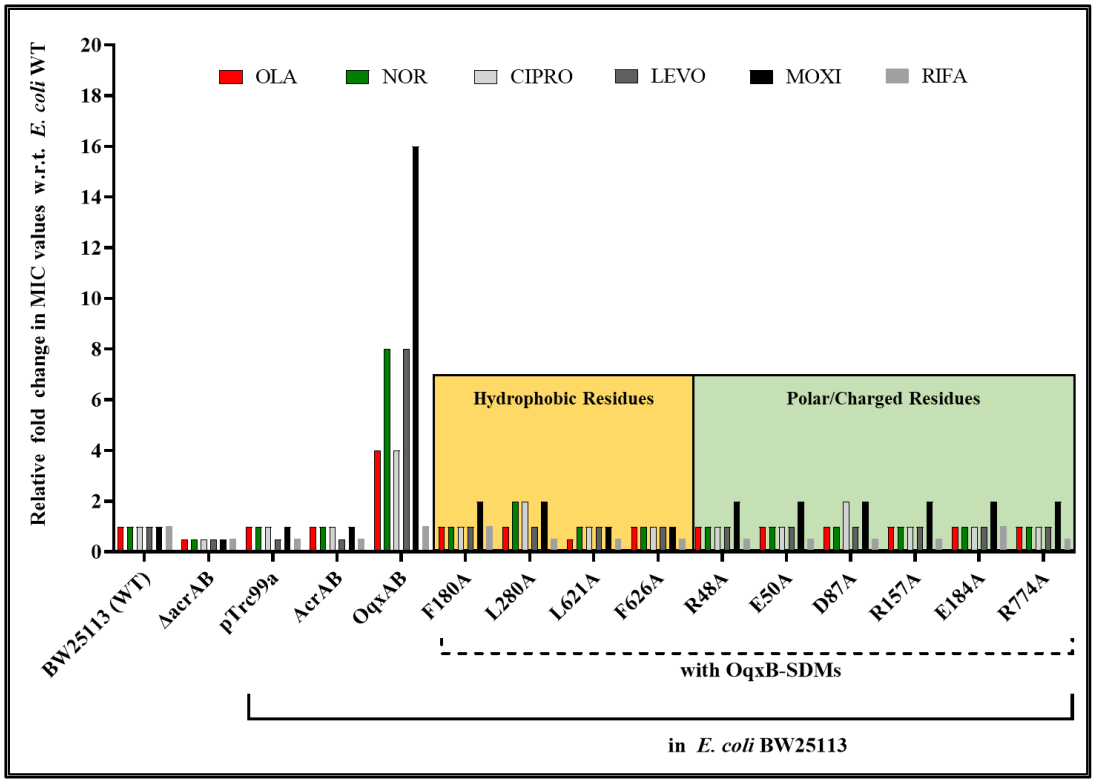

Figure 4.3 Relative Fold-change in MIC values of olaquindox and other fluoroquinolones. The relative fold change for the MIC Values of olaquindox and different fluoroquinolones in *E. coli BW25113* (WT) complemented with either *K. pneumoniae* OqxA-OqxB or OqxA-OqxB (with SDMs) overexpression systems; Rifampicin was used as a negative control.

pTrc99a, *pEcoAB* (+AcrAB), *pOqxAB* (+OqxAB) and *pOqxA-OqxB(SDM)* (+OqxA+OqxB-SDMs): complementation with a plasmid carrying the respective genes or the gene with indicated mutations.

OLA: Olaquindox; **NOR**: Norfloxacin; **CIPRO**: Ciprofloxacin; **LEVO**: Levofloxacin; **MOXI**: Moxifloxacin; **RIFA**: Rifampicin

Although the substrate binding pocket of the well-characterized RND efflux pumps, like AcrB and MexB, is majorly composed of hydrophobic/aromatic residues, hydrophilic residues like serine and threonine are also found to be present at the upper portion of the cage or the opening of the exit tunnel. However, in addition to the conventional hydrophobic/aromatic residues in the phenylalanine cage, the OqxB pocket also possesses few hydrophilic residues, including the three ion pairs of complementary charged residues (E50:R774, D87:R48, and R157:E184). These ion

pairs within the substrate binding pocket are unique to OqxB and have not been found in any other efflux pumps. Docking simulations revealed that the guanidino side chain of residue R157 was oriented towards the substrate binding pocket and had been found to interact with the carbonyl group of quinolones. Furthermore, MD simulations confirmed the additional and stable interactions of R157 with carbonyl and the terminal carboxyl group of quinolone derivatives. Another small hydrophilic residue, S152, present in both AcrB and MexB efflux pumps, is replaced with the positively charged arginine (R157) in OqxB (Bharatham et al., 2021). Furthermore, these hydrophilic residues are replaced with two sets of complementary charged residues (D87: R48 and E50:R774) in the corresponding pocket of OqxB. The negatively charged side chains of E50 and D87 residues are predicted to be crucial in interacting with positively charged substitutions of quinolones and the terminal hydroxyl group of olaquindox, respectively. Additionally, the guanidino side chain of R48 was found to interact with the oxygen of the hydroxyl group (**Figure 4.2**). Although our earlier studies had established the OqxB-mediated efflux of fluoroquinolones (Bharatham et al., 2021), the contributions of these predicted charged residues needed further validation. Therefore, to establish the validity of these predictions and assign the role of these unconventional ion pairs in efflux activity, we selected five additional charged residues (R48, E50, D87, E184 and R774) for site-directed mutagenesis (SDM) studies and complementation assays. As discussed earlier, substituting these polar residues with alanine resulted in complete inactivation of the OqxB mediated efflux of fluoroquinolones in *E. coli BW25113* background, transformed with the heterologous *K. pneumoniae* OqxA-OqxB. The MIC values for olaquindox, moxifloxacin, levofloxacin, norfloxacin and ciprofloxacin showed a significant reduction of 4-8-fold, in comparison to that of wild-type OqxA-OqxB overexpressing system, thus further confirming the role of these hydrophilic residues in the efflux of fluoroquinolones (**Table 4.3)**.

Overall, the reported residues in the substrate binding pocket of OqxB are crucial for the effective positioning, binding, and subsequent efflux of fluoroquinolones. The aromatic ring of the quinolone makes pi-cation as well as charged-charged or hydrogen bond interactions with the guanidino side chain of R157. The charged residue pairs (E50:R774 and R157:E184) are further involved in intra-molecular interactions and are crucial for stabilizing the binding of fluoroquinolones with the OqxB binding pocket. In contrast, residue E50 is associated with the H-bond interactions with the piperazine ring derivatives of the fluoroquinolones, thereby

causing stabilization of its binding. The hydrophobic interactions between the side chain of fluoroquinolones and the pocket comprising residues like F180, L280, L621, and F626 further facilitate effective positioning and binding to the substrate binding pocket of OqxB.

4.4 Conclusion

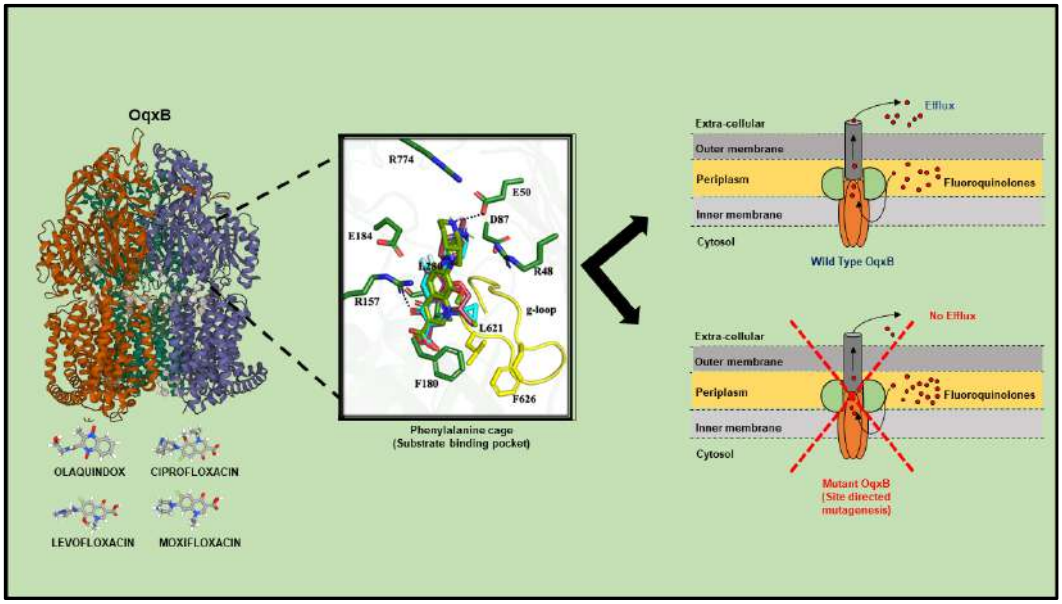

Figure 4.4. Graphical representation of the site-directed mutagenesis study in OqxB. Olaquindox and other fluoroquinolone derivatives (ciprofloxacin, Moxifloxacin and Levofloxacin) bind successfully at the substrate binding pocket of OqxB, leading to their subsequent efflux. However, the introduction of point mutations by site-directed mutagenesis leads to mutant OqxB, which is compromised in its ability to bind and efflux these molecules.

In summary, we report the detailed characterization of the structural architecture of the OqxB efflux pump and the identification of unique amino acid residues within its substrate binding pocket. In the current study, we have also identified the crucial interactions of olaquindox and various fluoroquinolones like ciprofloxacin, norfloxacin, levofloxacin and moxifloxacin at the substrate binding pocket. Further, we established the importance of the positively charged residues (R48, R157, and R774) and the negatively charged residues (E50, D87 and E184). Contrary to the other RND efflux pumps, we report here that the effective binding of the substrate involves the combined contributions of the hydrophobic pocket with residues like F180A, L280, L621and

F626, as well as the charged residues of OqxB. Based on the predictions by docking studies and MD simulations, the contributions of these critical residues in the binding and efflux of fluoroquinolones were ascertained and validated using site-directed mutagenesis and MIC-based complementation assays (**Figure 4.4**). This work implicated that the unique structural components of the OqxB efflux pumps could be the influencing factor, which comprises features such as a combination of aromatic ring systems with charge, along with zwitterionic/hydrophilic substitutions, which in turn dictates its ability to extrude certain classes of antibiotics. These are the key recognition features antibiotics share, as demonstrated in these studies. Observations from such investigations promise a build-up of the knowledge base of the mechanisms employed by pumps like OqxB, which could aid in the design of agents countering efflux-associated AMR.

In the next chapter, the explorative work done to study the impact of biofilms, another crucial contributing factor of AMR in bacterial systems, is elaborately discussed. Although, at first glance, biofilm formation seems to be an individual standalone mechanism of resistance, the overall process involves the contributions of multiple factors and deeply interconnected pathways. Among the interplay of all these factors, efflux pumps also play a crucial role in this overall phenomenon. Using *E. coli* as a model organism, this work consisted of the development of a dynamic and validated *in silico* model, which simulated the functionally interconnected networks of critical components of biofilms. The focus of this study was to find not-so-far-identified targets against which potent inhibitors can be designed to disrupt biofilms.

Chapter 5

Escherichia coli biofilm: A validated *in silico* model development

Note: Part of the text in this chapter is included in the manuscript

Bhowmik et al. *ACS Synthetic Biology* 2022, 11 (2), 713-731.

(DOI: 10.1021/acssynbio.1c00445)

5.1 Introduction

5.1.1 What are Biofilms?

Biofilms are self-encapsulated bacterial aggregates associated with biotic or abiotic substrates that are well-protected and difficult to permeate (Hall-Stoodley et al., 2004; Jefferson, 2004; Stoodley et al., 2002). These three-dimensional structures, which exist in a wide range of environments, are rarely beneficial and most often have undesirable consequences. Biofilms cause biofouling in ship hulls, plumbing lines, reservoirs, etc. and also contaminate food industry equipment surfaces, resulting in irreparable damage and revenue loss (Characklis, 1981). More importantly, biofilms pose a significant threat to the healthcare industry. According to the National Institutes of Health, biofilms are involved in more than 80% of all microbial infections in developed countries. Furthermore, biofilms have been shown to be 100-1000 times more resistant to antibiotics than their planktonic counterparts (Ballén et al., 2022; Soto, 2014; Vestby et al., 2020). In biofilms, bacterial cells are embedded in a heterogeneous matrix of extracellular polymeric substances (EPS), which includes structural proteins such as curli (Evans & Chapman, 2014; Kikuchi et al., 2005), flagella (Guttenplan & Kearns, 2013; Pratt & Kolter, 1998), fimbriae (Avalos Vizcarra et al., 2016; Van Houdt & Michiels, 2005)), polysaccharide components (such as cellulose, poly-N-acetyl-D-glucosamine, beta-1,6-GlcNAc, or PGA), colanic acid, LPS (Branda et al., 2005; Danese, Pratt, & Kolter, 2000; Flemming et al., 2007; Hufnagel et al., 2015; Hung et al., 2013; Sutherland, 2001; Vu et al., 2009), and extracellular DNA, eDNA (Nijland et al., 2010; Okshevsky et al., 2015). Biofilms can also be polymicrobial (Peters et al., 2012), as seen in cystic fibrosis patients with persistent lung infections (Koo et al., 2017). These polymicrobial communities are distinguished by clearly stratified via gradients of nutrient availability, oxygen levels, and pH, which result in the formation of niche spaces wherein bacteria adopt distinct physiological states to survive (Quinn et al., 2018).

Biofilms have gained notoriety as the primary cause for colonising medical implants and devices, in addition to being the cause of chronic infections. The infection site frequently determines which opportunistic organism will infiltrate these devices. Pathogens like coagulase-negative *Staphylococcus spp*., *Enterococcus spp*., *Candida sp*., *Escherichia coli*, and *Klebsiella sp*. inhabit intravascular devices and prosthetic joints, whereas *E. coli*, *Candida sp*., and *Enterococcus sp.* form biofilms and cause

catheter-associated urinary tract infections (Uruén et al., 2020; Van Epps & Younger, 2016). The latter account for the majority of nosocomial infections, which contribute to significant morbidity in hospitalised patients (Römling & Balsalobre, 2012; Wenzel, 2007). Urinary tract infections that affect both children and the elderly do recur as a result of relapse or re-infection (Soto et al., 2006).

Antibiotics, which effectively kill actively growing cells, do not kill the metabolically altered slow growers that make up the biofilms (Bisht & Ann Wakeman, 2019). When present as biofilms, the latter could inadvertently render an otherwise effective drug ineffective in clearing the same pathogen. Surprisingly, the same pathogen behaves differently depending on whether it causes acute or chronic infections (García-Betancur et al., 2017). The organisms that form biofilms gain the ability to withstand an immune attack, making them difficult to be eliminated from the host (A. Ghosh et al., 2020; Kostakioti et al., 2013). As a result, there is an urgent need to develop combination therapies that include potent broad-spectrum-acting drugs against emerging multi-drug-resistant planktonic forms and novel entities that can address the threat posed by biofilms.

Several changes occur prior to the transition from planktonic to a multicellular form. A number of factors govern the altered physiological and structural features that lead to the various stages of biofilm formation. Secondary messengers such as cyclic-di-GMP (c-di-GMP) (Hengge, 2013; Sondermann et al., 2012; Weber et al., 2006), cyclic-AMP (cAMP) (Jackson, Simecka, et al., 2002; Liu et al., 2020; Sutrina et al., 2015), and alarmone molecules such as guanosine pentaphosphate or tetraphosphate ((p)ppGpp) (Hauryliuk et al., 2015; Hobbs & Boraston, 2019; Potrykus & Cashel, 2008) serve as crucial secondary messengers in signalling and playing vital roles in events associated with biofilm formation and bacterial pathogenesis (Kalia et al., 2013). Quorum sensing also plays an important role in mediating cell-cell communication during the biofilm formation cascade (Laverty et al., 2014; Lazar, 2011; Y. H. Li & Tian, 2012). AHL (J. Lee et al., 2009), auto-Inducer-2 (AI-2) (González Barrios et al., 2006; J. Li et al., 2007), and indole (J. Lee et al., 2007; Pandey et al., 2013) are molecules that coordinate intercellular communication signalling and dictate the sequential expression of specific subsets of genes (Beloin et al., 2004; Domka et al., 2007; Prüß et al., 2006). All these processes result in a series of events that govern the transition of the bacteria from normal planktonic phase to non-motile biofilm form. The different stages of this transition can be classified broadly as different stages of biofilm

formation (**Figure 5.1**), namely (a) Initial or reversible attachment: bacterial cells adhere to a surface, forming a monolayer; (b) Microcolony formation or strong irreversible attachment: the bacteria multiply, forming small clusters or microcolonies, (c) Early maturation: microcolonies merge and become encased in an extracellular matrix, (d) Late biofilm maturation: a mature biofilm develops, with a complex three-dimensional structure, and finally (e) Dispersal: Bacteria detach from the biofilm and disperse, potentially colonizing new surfaces (Guzmán-Soto et al., 2021; Sauer et al., 2022). Among the different bacterial species, *E. coli* is known to form stable biofilms. During the multi-stage transformation process, differential expression of over 300 non-essential genes has been identified to be involved in *E.coli* biofilm formation (Niba et al., 2007; Schembri et al., 2003).

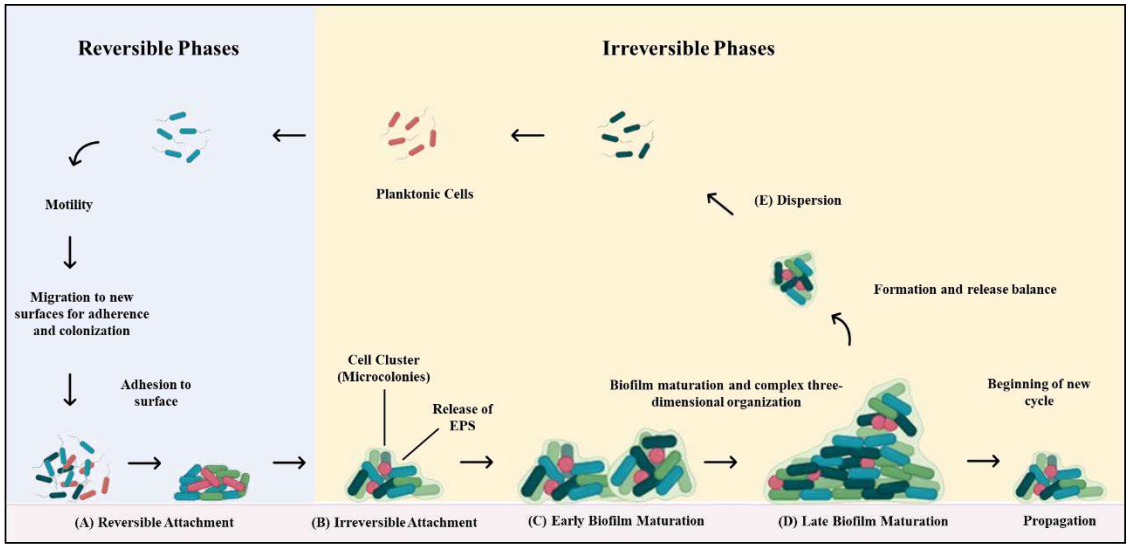

Figure 5.1 Different stages of biofilm formation. The transition of bacteria from planktonic to biofilm form progresses through five major stages, namely (a) reversible attachment: adsorption, (b) strong irreversible attachment: surface colonization and micro-colonies development, (c) early maturation: complex three dimensional structural organization, (d) late maturation: macro-colonies formation, and finally (e) dispersion (created using BioRender.com).

5.1.2 Efflux Pumps: Role in Biofilms

Efflux pumps form an important link, connecting events related to quorum sensing, biofilm formation and antimicrobial resistance (AMR). Apart from conferring resistance to planktonic forms by mediating the extrusion of toxic substrates, including

antibiotics and metabolites, bacterial efflux pumps also confer resistance, ensuring the survival of sessile forms, like biofilms, under adverse environmental conditions (Alav et al., 2018). As illustrated in **Figure 5.2**, the contributions of efflux pumps in biofilm formation could be broadly characterized into four types: (a) efflux of EPS components and quorum sensing molecules, which facilitate biofilm matrix formation and regulate QS (b) indirect regulation of genes involved in biofilm formation (c) efflux of harmful molecules, such as antibiotics and metabolic intermediates and (d) influencing aggregation through promoting or preventing adhesion to surfaces and other cells (Alav et al., 2018).

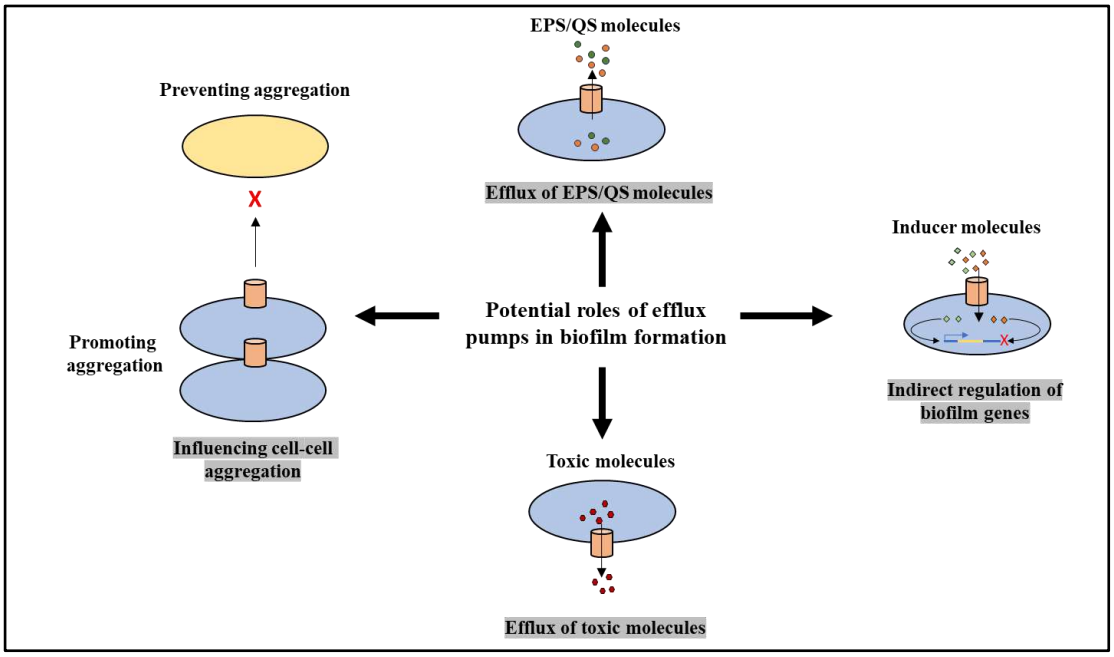

Figure 5.2 Schematic illustration of the potential roles of efflux pumps in different events of biofilm formation. Efflux pumps influence various events of biofilm formation, such as cell-cell aggregation, extrusion of toxic metabolites, quorum sensing molecules, EPS components and regulatory molecules, which indirectly affects the gene expression pattern of the bacterial cell, driving the overall process of development and stability of biofilm communities.

Biofilm formation is a community-coordinated behaviour dependent on quorum sensing, and efflux pumps exert a multi-pronged impact on this phenomenon. For instance, the genes encoding efflux pumps *mdtF* and *lsrA*, belonging to RND and ABC superfamilies, respectively, were reported to be expressed at significantly higher levels

during biofilm growth in comparison to the exponential- and stationary-phase grown *E. coli*. Recent studies have also revealed that efflux pumps, like AcrAB-TolC in *E. coli* and AdeFGH in *A. baumannii*, play crucial roles in biofilm formation (Alav et al., 2018; Byrd et al., 2021). Similarly, knockout studies for genes encoding efflux pumps such as *emrD, emrE, emrK, acrD, acrE* and *mdtE* in *E. coli K-12*, exhibited a reduction in the overall biofilm formation, in comparison to the wild-type strains (Matsumura et al., 2011). The significance of efflux pumps in biofilm formation is also emphasized further by the fact that many anti-biofilm treatments are often combined with efflux pump inhibitors, resulting in both disruption of biofilms and a decline in the overall resistance (Alav et al., 2018; Kvist et al., 2008). Similar observations were made in biofilms formed in Gram-positive organisms, like *Staphylococcus aureus*, in which the members of the MFS family, NorA and NorB, are overexpressed. The role of efflux pumps in biofilms is significantly enhanced in polymicrobial communities. The inter-species and inter-kingdom communication, driven primarily by efflux pumps, is crucial in mediating the cross-talks within the complex organization and in the extrusion of "foreign" autoinducer molecules from the cell. These inter-species communications, in turn, also emerge as a potential defence mechanism employed by the bacteria against other neighbouring bacteria, which might be competing to coexist in the same community (Moore-Machacek et al., 2023).

P. aeruginosa employs an array of virulence factors to invade host cells, subvert host defences, and cause tissue damage. Among these factors, the secretion of extracellular proteases and lipases within the biofilm formers plays a crucial role in enhancing its pathogenicity, facilitating the invasion of host cells, subverting host defences and thus, causing tissue damage. The release of these virulence factors, predominantly done by efflux pumps, also plays a crucial role in altering mucosal integrity by degrading mucosal lipids and phospholipids on the epithelial surface, promoting continuous invasion. Moreover, clinical isolates of *P. aeruginosa* frequently exhibit antibiotic resistance, which has been linked to biofilm formation and the activation of efflux pump activities. The biofilm structure protects the pathogen from the effects of antibiotics, rendering treatment less effective. Concurrently, enhanced activities of efflux pumps like MexAB-OprM, a member of the RND superfamily, are crucial in active extruding mechanisms, mediating poor permeability and increased virulence factor productions, thereby conferring enhanced resistance during the course of *P. aeruginosa* infections (Akinduti et al., 2023).

In *E. coli*, the events leading to the expression of efflux pumps and biofilm development are also interconnected and regulated at multiple levels. For example, the protein SdiA, responsible for cell division in a cell density-dependent or quorum-sensing manner, also regulates the expression of AcrAB efflux pumps in *E. coli.* SdiA has been found to positively regulate the AMR phenotype by facilitating the overexpression and increased levels of the AcrAB pump (Rahmati et al., 2002). SdiA in *E. coli* has also been reported to be associated with the regulatory network of quorum sensing mediated by AHL (Acylated Homo-Serine Lactones) from other bacteria like *Pseudomonas aeruginosa*, as well as responds to its self-signalling via indole. These quorum-sensing molecules also exert an inhibitory effect on *E. coli* biofilm formation (J. Lee et al., 2009). In addition, indole is also known to increase drug resistance by inducing the expression of efflux pump genes (*mdtEF* and *acrD*) in *E. coli* (J. Kim & Park, 2015; J. H. Lee & Lee, 2010). Similarly, RND efflux pumps like *acrE* and *acrF* in *E. coli* are found to be associated with the efflux of indole, which also exerts an inhibitory role on biofilm formation (Kawamura-Sato et al., 1999). Overall, the mechanism of multi-drug resistance and biofilm formation in *E. coli* is driven by the coordination and balance of the quorum sensing molecules, regulatory signals, and the efflux pumps in the system.

5.1.3 *In silico* modelling of biofilm formation

A wide range of mathematical modelling approaches have been used to monitor and follow the biofilm formation process quantitatively. Bacterial growth and response modelling strategies can range from genetic modelling and FBA (Flux Balance Analysis) to statistical inference and kinetic growth models (T. Zhang, 2017). Development of *in silico* biofilm models was also done using Boolean logic networks (Shalá et al., 2011) and logical and stochastic principles (Yousef et al., 2015). Furthermore, agent-based models (Koshy-Chenthittayil et al., 2021), particle-simulation models (Acemel et al., 2018; P. Ghosh et al., 2015), partial differential equations (P. Ghosh et al., 2013; Klapper & Dockeryt, 2010; Mattei et al., 2018), and three-dimensional (3D) models (Hartmann et al., 2019) were developed for the better understanding of biofilm formation in *Pseudomonas aeruginosa*, *Bacillus subtilis*, and *Vibrio cholerae in vitro*. Several other methods for acquiring a comprehensive and detailed understanding of the dynamics of biofilm formation at spatial and temporal levels have also been reported. These range from one-dimensional (1D) mass transfer

models to multi-dimensional models based on microbial ecology diversity (Horn & Lackner, 2014; Joao B Xavier et al., 2005; Thomen et al., 2020), as well as those that considered the roles of extracellular polymeric substances, quorum sensing signals, and secondary metabolites (Q. Li et al., 2017). Recently, confocal laser scanning microscopy images were captured to build an *in vivo* three-dimensional biofilm model for non-typeable *Haemophilus influenzae* (NTHI), which was a modification of the agent-based modelling (J. R. Brown et al., 2019; Das et al., 2017).

In an earlier study reported by Barve et al., an *in silico* platform based on Ordinary Differential Equations (ODE) was developed in order to evaluate the vulnerability of anti-bacterial targets by utilising the metabolic pathways in the planktonic phase of *E. coli* (Barve et al., 2010). Following this effort, a similar model interconnecting the metabolic and signalling networks in *Mycobacterium tuberculosis* was built to study the effect of intracellular perturbations on biomass levels caused by the activities of various anti-mycobacterial drug combinations (R. Singh et al., 2015). However, these modelling approaches did not consider the contributions of various non-essential genes involved in biofilm formation.

The present work involves a complementary exercise in which the genes involved in biofilm formation were interconnected via the ODE network. A platform was developed considering the roles of these genes in various signalling pathways and their associations with various structural components for further investigations (**Figure 5.3A**). Data curation, mapping pathways, connecting networks, and evaluating the effect of multiple perturbations were included as part of this strategic approach. The development of such a model entailed capturing the interactions among various components such as structural and functional proteins, autoinducers, nutrients, metabolites, and important events such as quorum sensing and EPS formation (**Figure 5.3B**).

(A)

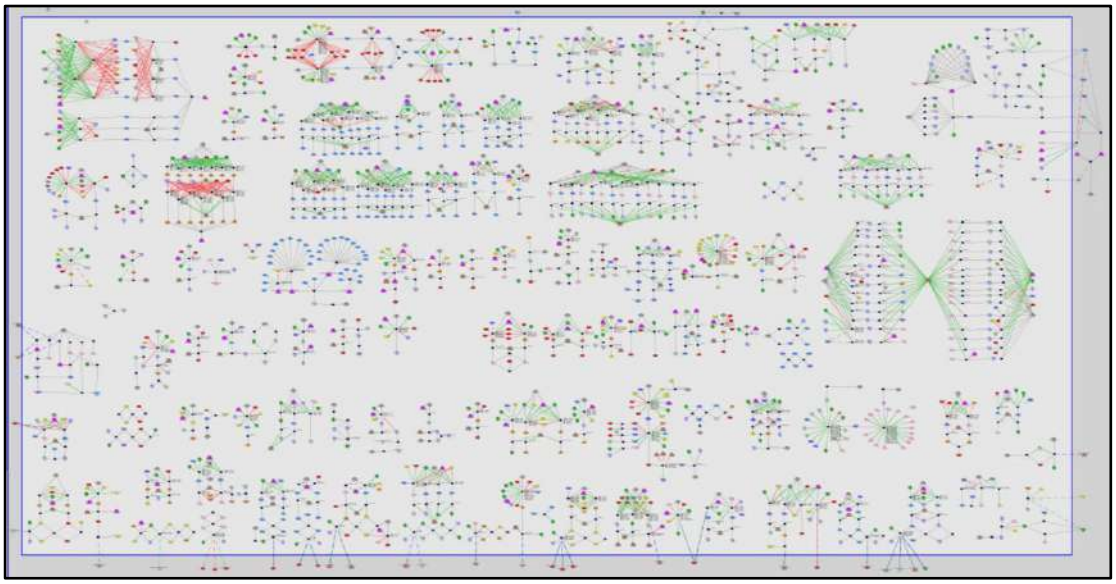

(B)

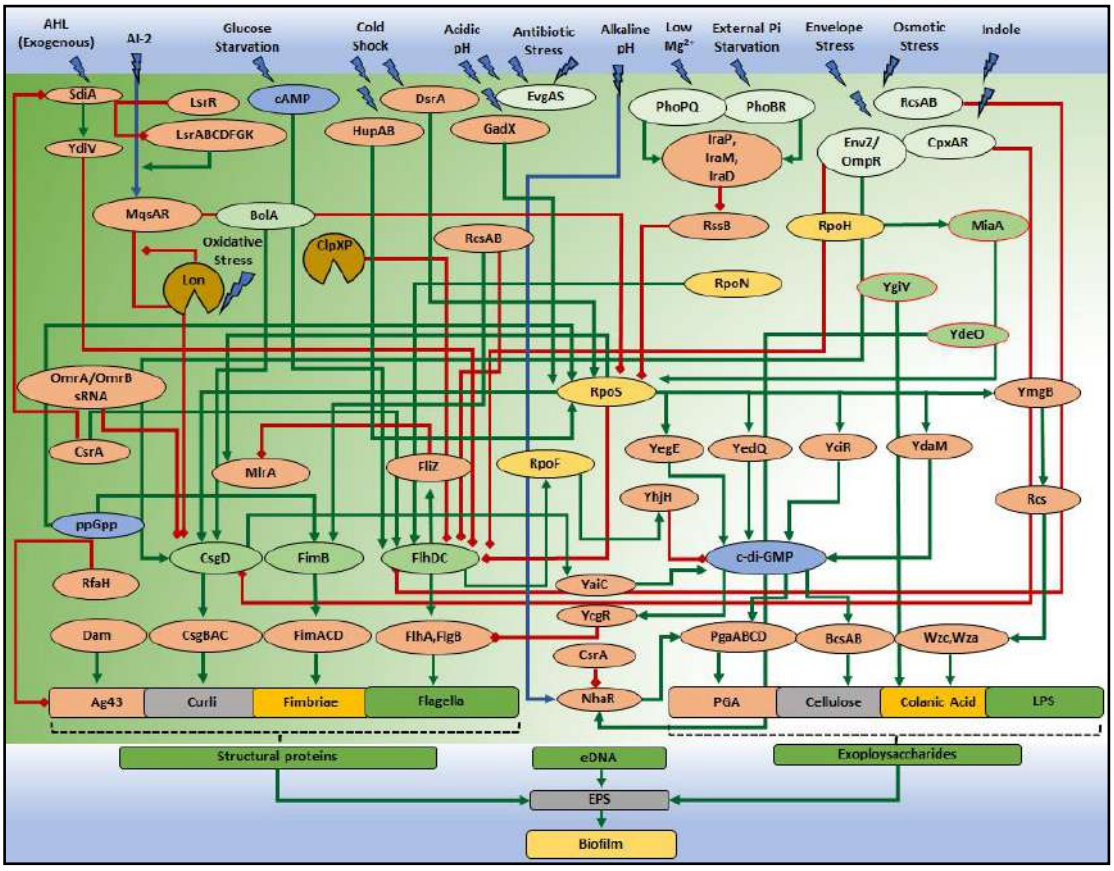

Figure 5.3 ***In silico*** **modeling of** ***E. coli*** **biofilm formation with model outlook, major components and signalling pathways used.** The *in silico* model of biofilm formation in *E. coli* was developed with an interactive network of over 200 genes. An

overall snapshot of the ODE biofilm model (A) and the key model components (B) consisting of structural components like flagella, curli and fimbriae and polysaccharide components like PGA, cellulose, colanic acid, etc., along with eDNA that contribute to the overall extracellular polymeric substance (EPS) of biofilm. In addition, the model also represents the roles of secondary metabolites (cyclic-di-GMP), quorum sensing molecules (AI2) and signalling pathways of the various two-component signal transducing systems (like PhoP-PhoQ, RcsA-RcsB etc.)

The findings from the model simulations were aligned and validated with literature reports that provided insights into the roles of these biofilm-associated proteins. As a result, a few critical target proteins, such as MiaA, YdeO, and YgiV, were identified as crucial in biofilm formation. These findings were then confirmed *in vitro* by testing the biofilm-forming abilities of the corresponding gene knockouts (KOs) from the *E. coli* Keio collection (Baba et al., 2006). In order to understand their relevance in a clinical setting, gene knockouts of the identified targets produced by P1 transduction in pathogenic *E. coli* (*CFT073*, UPEC) were studied. Such a strategy would clearly confirm the model's robustness, giving more confidence in the model's simulation capability, especially with the specific goal of identifying targets for designing novel biofilm disruptors. qRT-PCR studies to monitor transcript levels in a biofilm-forming clinical isolate provided additional evidence of the relevance of the identified key targets. **Figure 5.4** and **Figure S5.1** in **the Appendix section** depict the overall strategy for this study.

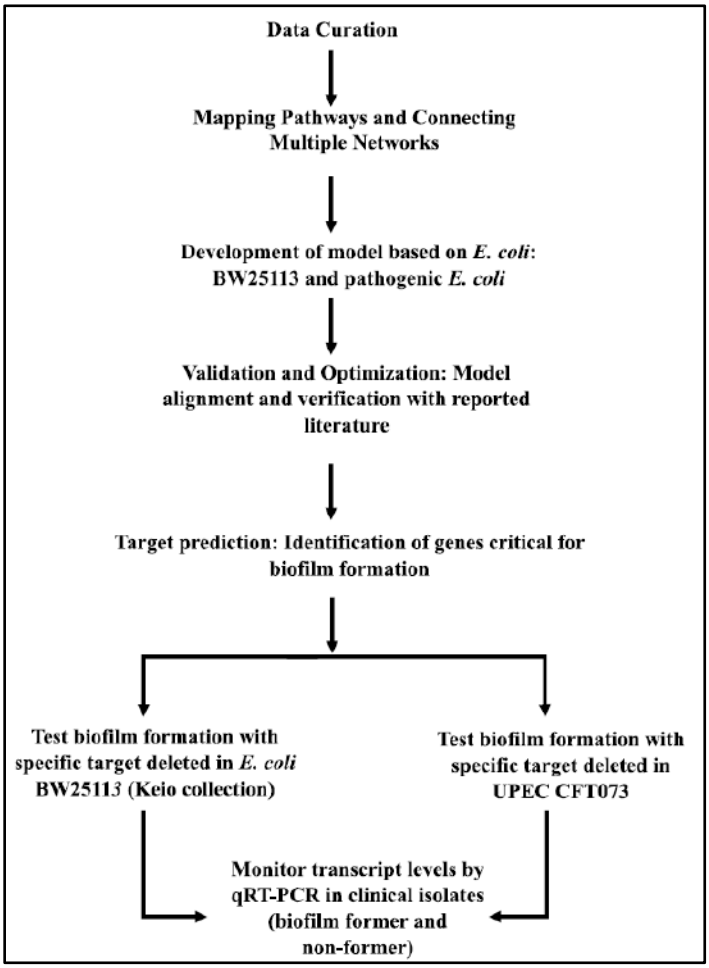

Figure 5.4 Strategy for model development for *E. coli* biofilm. Different stages included in the development of a validated *in silico* model of *E. coli* biofilms and identification of novel targets via predictive simulation studies. The predicted targets from the model were further validated for their roles in biofilm formation using specific target gene deletions in *E. coli* strains and by checking their transcript levels in UPEC CFT073 and *E. coli* clinical isolates.

5.2 Materials and Methods

5.2.1 Bacterial strains and media

E. coli BW25113 was procured from the Coli Genetic Stock Centre (CGSC). KO strains with gene deletions in the wild-type strain, *E. coli BW25113* (available as part of the *E. coli* Keio collection library (Baba et al., 2006) were selected based on the targets predicted in the model for their roles in biofilm formation. These strains were then verified *in vitro* for biofilm formation using the Crystal Violet (CV) assay

(O'Toole, 2011). To extend and substantiate these findings in a clinically relevant pathogenic strain, the assay was also performed with the same KO strains of *E. coli* UPEC strain CFT073 ATCC 700928 generated using P1 phage transduction. Clinical isolates of *E. coli* (SEC54, SEC59) were collected for this study from the Microbiology Department of St. John's Medical Hospital, Bangalore, India. These were isolated as part of their microbiological investigations from patients with suspected urinary tract infections. The inoculum used to grow these bacteria was derived from a single seed lot maintained as glycerol stocks at -80 °C and sub-cultured on LB plates for isolated colonies. A single colony of each strain was inoculated and was grown at 37 °C in 1X M9 Minimal medium supplemented with 0.4% Glucose and 0.2% casamino acids (M9GC). 0.5X of M9GC was used to grow the cultures for the CV assay.

5.2.2 Estimation of biofilm formation by Crystal Violet assay

A single colony from fresh LB agar plates was inoculated into 1X M9GC media and incubated at 37 °C, 200 rpm. When the respective cultures reached an OD_{600nm} of 0.3 to 0.4, the culture was diluted to 0.5X M9GC media to get a cell count of 1 x 10^7 CFU/ mL as a starter inoculum for the biofilm assay. 200µL of the inoculum was aliquoted into 96 well microtiter plates, and each plate was incubated for 24-48 hours at 30 °C (static condition). On completion of incubation, the plates were read at 600nm and further processed for the Crystal Violet assay as described previously (O'Toole, 2011). The culture was discarded, and the plates were washed twice with 250µL of 1X PBS, followed by one wash with 250µL distilled water. After each wash, the plates were tapped on a tissue to remove excess water. 220µL of 0.1% aqueous crystal violet solution was added to the plates, followed by incubation at room temperature for 30-40 minutes. The crystal violet solution was removed from the wells, and the plates were washed thrice with 250µL of distilled water. After each wash, the plates were tapped on a tissue to remove excess water. 250µL of 30% acetic acid solution was then added, and the plates were incubated at room temperature for 15-20 minutes, after which they were read at 590nm against 250µL acetic acid as background control. The readings were subtracted from the average A_{590nm} value of 30% acetic acid blank.

5.2.3 Development of *in silico* model

Model Components

The current ODE-based *in silico* platform includes the major regulatory and signalling pathways involved in the biosynthesis of biofilm components in *E. coli*. These include structural components such as curli, fimbriae, and flagella and exopolysaccharide constituents such as cellulose, PGA, colanic acid, and eDNA. On this platform, the entire networking of these interconnected signalling pathways was done using information curated from published literature. All of these elements were thought to be direct contributors to the formation of biofilm biomass. A static map of all signalling and regulatory pathways and their associated operons was also created. Despite the inclusion and modelling of various regulatory proteins and metabolites, the precise molecular mechanisms of their regulation were not considered for model development. Furthermore, the models for the expression of genetic regulators were properly integrated to represent a complete regulatory network. Since the formation of biofilm is induced by a wide array of environmental changes and stress-inducing factors such as osmotic stress, low pH, low temperature, membrane shock, low oxygen, and nitrogen starvation, these were also considered, along with multiple two-component signal transfer systems (e.g., RcsBCD-RcsA, EvgAS, ArcAB-ArcZ), which triggers biofilm formation. Various small regulatory non-coding RNAs (OxyS, RprA, DsrA) were included as post-transcriptional regulatory mechanisms for gene expression. Additional pathways involving quorum-sensing molecules such as AHL, AI-2, and indole, as well as secondary messengers such as c-di-GMP and cAMP and their regulatory mechanisms, were also modelled in the *in silico* platform.

The *in silico E. coli* biofilm model development process began with data curation from published reports and the creation of a static map of network pathways using the open-source Cytoscape platform (Shannon et al., 2003). The static model was transformed into a dynamic platform by defining an ODE for each flux. The entire model was created in R software using the deSolve package (R Core Team, 2014; Soetaert et al., 2010), and the package's Vode solver was used to solve the ODE system (P. N. Brown et al., 1989). Using the flux of the cellular components, the differential equations defined the change in the amount of the cellular components over time. For the sake of simplicity, modified Reversible Mass Action Kinetics was used instead of the standard Michelis Menten's Equation to define all parameters.

All model components were organized into a multi-tier hierarchy based on our current understanding of their biological roles in the overall process of biofilm formation. In this context, the framework was built by taking into consideration the biological significance of each component rather than any computational advantage. The overall effect of the components of one level in promoting or inhibiting biofilm formation is solely determined by the regulatory effect of that component on the process of biofilm development. Generally, components of higher Levels (e.g., Level III and Level IV) have a more significant contribution to biofilm formation, considering their global impact on the overall phenomenon. The effect on biofilm formation by the components at different levels may act independently or could have a cumulative effect on biofilm formation, depending upon the levels of the components. For example, *csgA* (encoding CsgA, curli, major subunit) has been positioned as a Level I component, *csgD* (encoding the master regulator CsgD) which regulates expression of genes of curli biosynthesis is present at Level II whereas *rpoS* (encoding the stationary phase sigma factor RpoS;) is appropriately placed at Level III. However, their mode of action and impact on the biofilm network and its formation vary as causing cumulative impact or a direct-independent effect. While the effects of components of Level I are direct, components of higher levels (Level II, III and IV) exert a cumulative effect, depending upon the network they regulate. For instance, although both CsgA and CsgD affect the biosynthesis of curli (a Level 0 component), CsgD is more of a cumulative one because of its regulatory effect on other genes of curli biosynthesis. Similarly, the effect of RpoS on biofilm formation is more complex owing to its global regulation in the expression of genes involved in Curli biosynthesis and other biofilm components as well, like flagella, fimbriae, etc. All the cellular components were assigned with a minimal initial concentration, constituting initial values. The simulations were carried out for an interval between t=0 to t=3600 seconds, and the steady-state levels of all the cellular components were ensured during the given simulation interval. Analysis and visualisation, including the changes in the amounts of the cellular components with respect to time, were carried out in Python using the pandas and the plotly packages (McKinney, 2010; Plotly Technologies Inc, 2015; Rossum & Drake, 2009). Subsequent models were built using the control simulation model as the base to study the effects of target levels due to knockdown (KD), knockout (KO) and over-expression (OE) on any of the components present in the biofilm platform. An automated program was designed in Python to parse the base model and information collected from the user (component

to be KO/KD/OE) to design the respective model(Rossum & Drake, 2009). These models were simulated and studied to check the effects of various model perturbations on biofilm and its components. All cellular components were kept at a minimal concentration which was then changed as a function of time. The levels of all the cellular components were maintained at steady-state-steady state for simulations under controlled conditions. Further details related to the considerations and the key terminologies associated with model development and organization could be referred to in the **Appendix** section (**Supplementary Note S5.1- S5.4**).

Kinetics of *in silico* model development

Biochemical reactions in the pathways are catalysed by enzymes, which, in turn, are governed by various regulators that dictate their transcription and translation within the cell. The kinetics for all enzymatic reactions is usually governed by Michaelis-Menten (MM) Kinetics (**equation 5.1**). For example, for an enzyme (E) catalysed reaction, where the substrate [S] is converted to product [P] by flux V, the Michaelis Menten's (MM) equation could be represented by:

$$\mathbf{V} = \frac{(\mathbf{Vmax} * [\boldsymbol{S}])}{\mathbf{Km} + [\boldsymbol{S}]} \qquad \textbf{(5.1)}$$

where, V= Flux; Vmax = [E]*k_{cat}; [E] = enzyme concentration and k_{cat} = turnover number of the enzyme and [S]= substrate concentration.

However, for the current scenario of modelling, the kinetics of all fluxes in the model are driven by a modified Reversible Mass Action kinetics (RMA) instead of the usual MM equation. This is to avoid the requirement of complex kinetic parameters and equations and use relatively simpler ones. The MM equation includes multiple kinetic parameters like Km, kcat, enzyme concentration, etc. Often, the values of these kinetic parameters are not available in the literature. Besides, most of the information available is based on *in vitro* assays, which may be far from actual biological values. Finally, equations used for fluxes involving multiple substrates, activators, or inhibitors with different modes of regulations used in MM kinetics are quite complicated as compared to RMA. For any given reaction, where a substrate, [S], is converted to product, [P], the general RMA equation could be represented as **equation (5.2)** below:

$$\mathbf{V = Kf * [S] - Kr * [P]} \quad \textbf{(5.2)}$$

where V= Flux; Kf = rate of forward reaction; Kr = Rate of backward reaction; [S]=substrate concentration; [P]=product concentration.

RMA uses relatively simpler equations and does not involve complex kinetic parameters. In addition, to consider the role of various regulators (activators/inhibitors), modified RMA kinetics (equations 5.3, 5.4, **and 5.5**) are used in the model. The mathematical representation of a general RMA reaction used in the model could be given as:

$$\mathbf{V = ((Kf * S.Concentration) - (Kr * P.Concentration))*Volume} \quad \textbf{(5.3)}$$

where, [V] = Flux; [S] = substrate concentration; [P] = product concentration; Kf = rate of forward reaction; Kr = rate of backward reaction.

For a flux F, representing a reaction in which a substrate S is converted to product P, catalysed by activators A1 & A2, and inhibited by inhibitor I1 (**Figure 5.5**), the rate of forward reaction, Kf is given as a function of time, by the following modified equations (**equations 5.4 and 5.5**):

$$\mathbf{Kf\ (t) = max(0, min(1,((A1.Concentration\hat{}(1/A1\_action))} \\ \mathbf{+ (A2.Concentration\hat{}(1/A2\_action)))} \\ \mathbf{- (I1.Concentration\hat{}(1/I1\_action)))} \quad \textbf{(5.4)}$$

where, the A1_action, A2_action and I1_actions refer to the relative regulatory contribution of A1, A2 and I1 respectively, in the overall flux F.

$$\mathbf{Kf\ \_app\ (t) = Kf * (1 + ((A1.\ Concentration\ /A1\_action)} \\ \mathbf{+ (A2.\ Concentration\ /A2\_action)} \\ \mathbf{- (I1.\ Concentration\ /\ I1\_action)))} \quad \textbf{(5.5)}$$

where Kf_app is the final effective Kf value for the flux F, with the regulatory contributions of A1, A2 and I1, same as mentioned for **equation 5.4**.

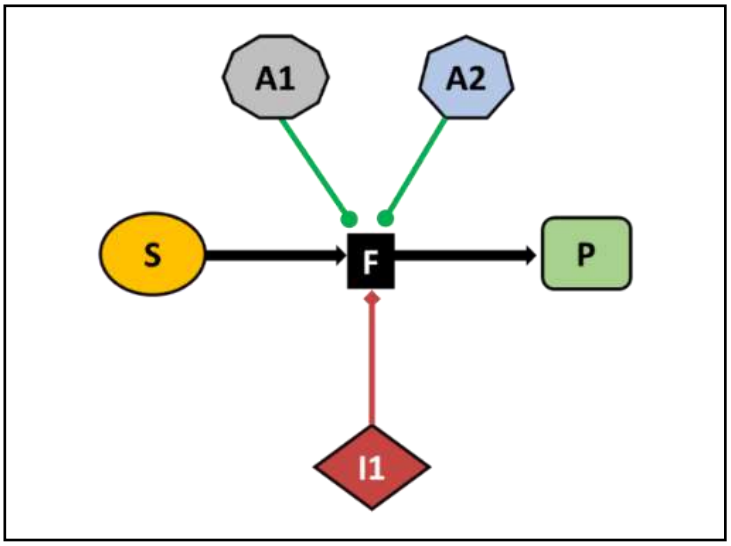

Figure 5.5 General representation of a hypothetical flux used for modeling. Representation of a hypothetical flux F, in which a substrate S, is converted to product P. Regulators A1 and A2 activate the flux, whereas I1 is an inhibitor. The overall flux is determined by the cumulative effect of the contributions of the activators and the inhibitor on the flux.

Relative Contributions of Different Regulators for a given flux

The process of biofilm formation is regulated by the concerted roles of multiple regulators, which can be activators or repressors. The action of these regulators is governed by multiple factors, like the nutritional state, environmental conditions, or various stress conditions affecting the cell. Therefore, the actions of these regulators in the model have been classified into five different categories: *Very strong*, *Strong*, *Linear*, *Weak*, and *Very weak*. A typical response curve obtained by using these equations is shown in **Figure 5.6**.

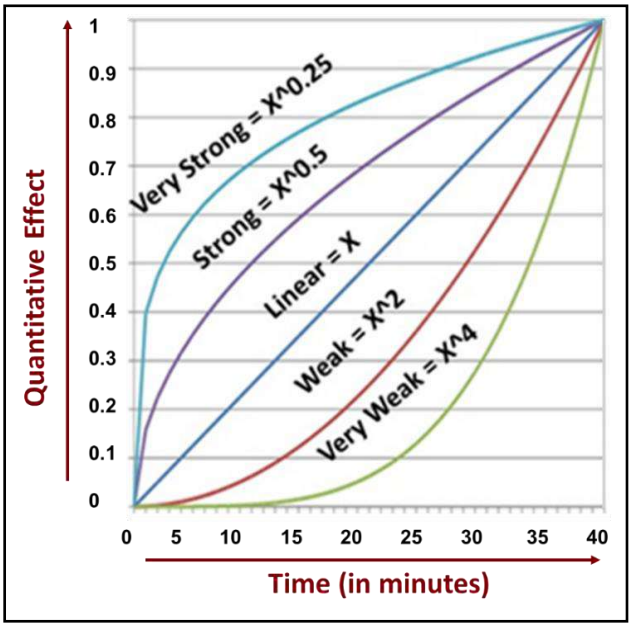

Figure 5.6 General representation of the response curve for the effects of different regulators in the model. A typical response curve showing the effects of modified flux parameters /equations in the model (details in the text). The relative contribution of each of the regulators is determined by considering each of their different action values, resulting in a range of overall regulatory effects.

The kinetics of the fluxes, along with the individual contributions of the various contributing regulators, are classified in **Table 5.1**. For the equations, the power terms *0.25, 0.5, 1, 2, and 4 represent very strong, strong, linear, weak, and very weak regulators,* respectively. The function "*max, min*" ensures that the magnitude of the flux is not negative and that the Kf values do not increase above 1. The activator and inhibitor concentrations are multiplied by action values, which determine the strength of activation or inhibition of the various regulators acting on a particular flux. The differential roles of the regulators could be further determined by modifying the action values for the respective regulator. For optimal biological responses, the levels of all the components in the model were kept ideally in the middle range of 0-1. The values that lie at the extremities do not represent the natural scenarios and may point towards an error in the network. The power terms or the "action values" were decided based on the extent to which a regulator activates or represses the expression levels of a given gene. In some instances where literature data is not available, the action values were decided based on the desired physiological responses to be achieved. The model

is available as an open-source platform for downloading and for any further analysis, development, and evaluation.

Table 5.1 Modified kinetics defined based on the relative contribution of different regulators on the overall flux

Response Level / Contribution	Modified kinetics
Linear Regulation	(max(0,min(1,(activator - inhibitor))))
Strong Regulation	(max(0,min(1,(activator^0.5 - inhibitor^0.5))))
Very Strong Regulation	(max(0,min(1,(activator^0.25 - inhibitor^0.25))))
Weak Regulation	(max(0,min(1,(activator^2 - inhibitor^2))))
Very Weak Regulation	(max(0,min(1,(activator^4 - inhibitor^4))))

The regulatory effects of different regulators on a given flux are represented by modified equations. Depending upon the values of the "action" parameter (see text for details), the overall effect of a given regulator on a flux could be varied across the five-point effector levels, namely Linear, Strong, Very Strong, Weak and Very Weak. The relative contribution of all the regulators is determined by either information available from published literature or model optimization and alignment for a given physiological response.

5.2.4 Real-Time PCR Methodology

Processing of bacterial samples for RNA Isolation

A single colony of each strain (*E. coli* UPEC CFT073 ATCC 700928, SEC54, SEC59) was picked from a freshly isolated LB agar plate, inoculated in M9G media, and then incubated at 37 °C. For RNA analysis, the cultures were sampled at 24 hours. The same number of bacterial cells was collected for each sample (as measured by OD_{600nm}) and immediately stabilized by treating with 10% (v/v) ice-cold stop solution (10% buffer saturated phenol in ethanol) to avoid degradation and any further change in the mRNA levels. This was followed by centrifugation at 4000 x g for 10 min at 4 °C. The cell pellet was then flash-frozen in liquid nitrogen and stored at -80 °C until required.

Isolation of Total RNA

The isolation of total RNA from bacterial cells was done as described previously (Chatterjee et al., 2012). Briefly, the cell pellet was thawed on ice and resuspended in 500 ul of TE buffer, pH 8. Total RNA was extracted using an equal volume of pre-heated water-saturated phenol (pH 7). The cell lysates were mixed gently, followed by incubation at 64 °C for 6 min with frequent mixing every 90 sec. The tubes were immediately chilled on ice and spun at 10,000 x g for 10 min at 4 °C. The aqueous layer was collected from each lysate, and an equal volume of chloroform was added and centrifuged under similar conditions. The upper aqueous layer was collected and precipitated with 2.5 volumes of ethanol and 300 mM sodium acetate, pH 5.2. The pellet obtained (mixture of DNA and RNA) was washed with 70% ethanol and resuspended in 100uL of DEPC water. DNase I (RNase free; New England Biolabs) was added (according to the manufacturer's manual) for the removal of genomic DNA contamination. The RNA was re-extracted with an equal volume of phenol-chloroform isoamyl alcohol (25:24:1) followed by ethanol precipitation. The final pellet obtained was dissolved in 50µL of DEPC-treated water.

Synthesis of cDNA from total RNA

The isolated total RNA from each fraction was estimated quantitatively using NanoDrop 2000 (Thermo Fischer, USA), and the purity (260nm/280nm and 260nm/230nm) was checked. The conversion of mRNA to cDNA was carried out from 1µg of total RNA using SuperScript^{TM} III Reverse Transcription Kit (Invitrogen, USA) according to the manufacturer's manual. Gene-specific primers were used for the first-strand cDNA synthesis. The prepared cDNAs were stored at -80 °C.

Primer Designing

All biofilm-related genes were designed using the software Primer3 (Untergasser et al., 2012), considering the size of the amplicon to be limited to approximately 150-200 bp. The complete sequences of these genes were obtained from the EcoCyc database (Keseler et al., 2017). The housekeeping gene, *dnaK*, was chosen as a control for normalizing the transcript levels in the qRT-PCR experiments. The primers were custom-ordered from Sigma Aldrich. All the primers used for the study are included in the Appendix section, **Table S5.2**.

Quantitative Real-time PCR

Real-time PCR was done using Applied Biosystems 7900 HT (Thermo Fischer Scientific, USA) and iTaq^{TM} Universal SYBR Green Supermix (Bio-Rad, USA). A PCR master mix containing 5µl of 2X SYBR master mix and 0.5µl of each forward and reverse primer (500 nM) per sample was prepared and combined with 1µl of each cDNA. The volume was made up to 10µl with RNase-free water in a 384-well plate (Thermo Fischer Scientific, USA). The plate containing the reaction mixture was centrifuged briefly so that the reaction mixture settled to the bottom prior to placing it in the chamber of the Applied Biosystems equipment. Each reaction was run in triplicate. For each real-time PCR run, NTC (no template control) was prepared without adding cDNA for each target gene and run along with the target gene sample to measure interference from primer dimer formation. The PCR conditions included initial denaturation at 95 °C (30 sec) followed by 40 cycles each of denaturation (95 °C for 15 sec), annealing/extension (60 °C for 25 sec) and assessed by melting curve analysis. Using the transcript levels of the housekeeping *dnaK* gene as the internal reference standard for normalization, the expression levels of the test genes were calculated (Livak & Schmittgen, 2001).

5.3 Results

5.3.1 Model Validation

Multiple simulations were run using data extracted from published literature and databases. Specific gene OE, KDs, and KOs were simulated in the model to affirm its alignment, robustness, and predictive capacity in comparison to reported observations. When the results were comparable, and the manipulations produced similar results, the model was further tested by running simulations to predict new targets important for biofilm development and maintenance. The following are some of the different simulation outputs for validating the model:

CsrA disruption leads to enhanced biofilm formation.

The carbon storage regulator protein, CsrA, is a well-known carbohydrate metabolism global regulatory protein (Sabnis et al., 1995). Additionally, it is also known for its role as a translational inhibitor of the *pgaABCD* operon (X. Wang et al., 2005), which is responsible for the production of the polymer of beta-1,6-N-

acetylglucosamine residues (PGA), an essential component of the biofilm matrix components. Hence, a *csrA* deleted mutant will exhibit an increased biofilm formation due to the de-repression of the *pgaABCD* operon and the resultant rise in PGA levels (Jackson, Suzuki, et al., 2002). The role of CsrA in the model was determined by simulating a gradual decrease in CsrA concentrations (50%, 75%, and 99% of WT levels) and monitoring the resulting effect on biofilm levels. As expected, an inverse trend, i.e., a systematic decrease in CsrA, leading to a concomitant increase in biofilm formation, was observed after such a simulation. **(Figure 5.7)**.

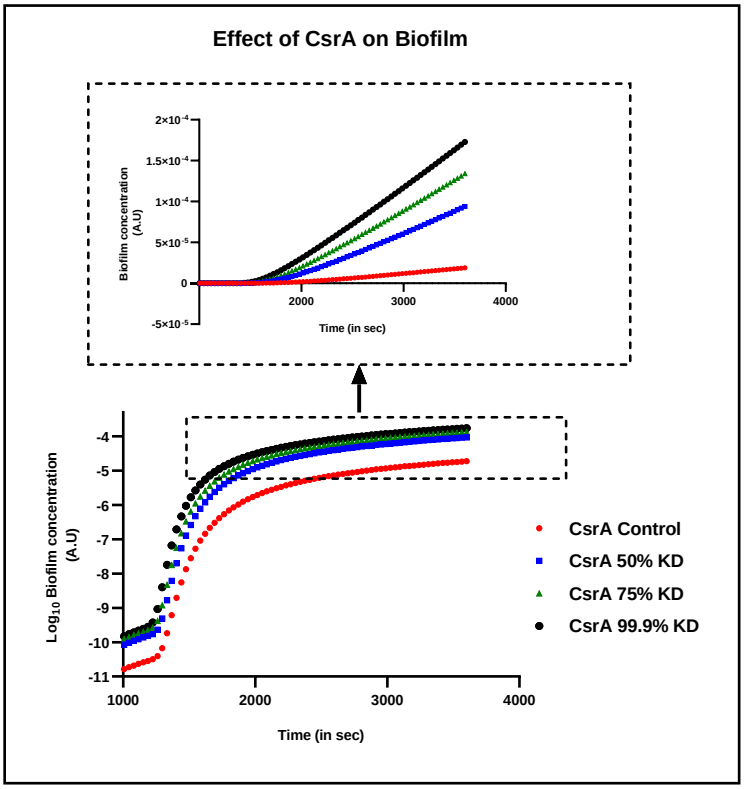

Figure 5.7 Effect of CsrA perturbation on biofilm formation. The role of CsrA in biofilm formation was validated in the model by simulating the model with a graded knockdown (KD) of 50%, 75% and 99.9% (equivalent to knockout-KO) in comparison to the control or wild-type (WT) levels. A gradual decrease in the levels of CsrA in the system resulted in a concomitant increase in biofilm levels. The plots represented here are the simulation output from the *in silico* platform because of the graded knockdown of the protein levels in the model. A logarithmic scale has been used for better representation of the data. (Inset**:** Effect of CsrA graded perturbation on biofilm formation, represented in a linear scale).

Control: Represents wild-type (WT) or control simulations; **50% KD**: 50% knockdown; **75% KD**: 75% knockdown; **99.9% KD**: 99.9 % knockdown (equivalent to knockout, KO); All graded KD with respect to Control Levels, represents a reduction in protein levels.

A.U: Arbitrary Unit; used for the representation of the relative levels of model output.

NhaR positively regulates biofilm formation.

The transcription factor NhaR (Na^+/H^+ antiporter Regulator) has multiple effects in response to different conditions. It regulates the transcription of genes involved in the adaptation to Na^+ and alkaline pH (Carmel et al., 1997; Padan et al., 1999), and functions as a transcriptional activator of the *pgaABCD* operon under adverse conditions (Cerca & Jefferson, 2008; Toesca et al., 2001), promoting biofilm formation. This phenomenon was validated in the model by varying NhaR levels and examining the effect on PGA levels (**Figure 5.8A**) and biofilm (**Figure 5.8B**). Furthermore, the influence of NhaR was also confirmed in the model by simulating both overexpression (OE) and Knockdown (KD) of NhaR in control or wild-type (WT) and csrA KO background simultaneously (**Figure 5.9**). The results from the *in silico* studies with NhaR OE and KD, in WT and Δ*csrA* strain background were in total agreement with the data published previously (Goller et al., 2006). A decrease in the levels of NhaR resulted in the reduction of PGA adhesin levels, leading to a decline in biofilm formation. At the same time, simulating NhaR overexpression by 2-to-4-fold (2X, 4X) over the control (X) levels in the model led to an increase in PGA and biofilm levels.

A.

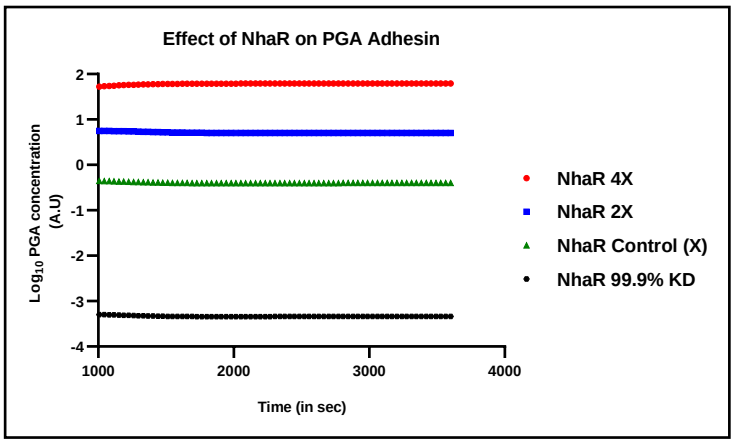

B.

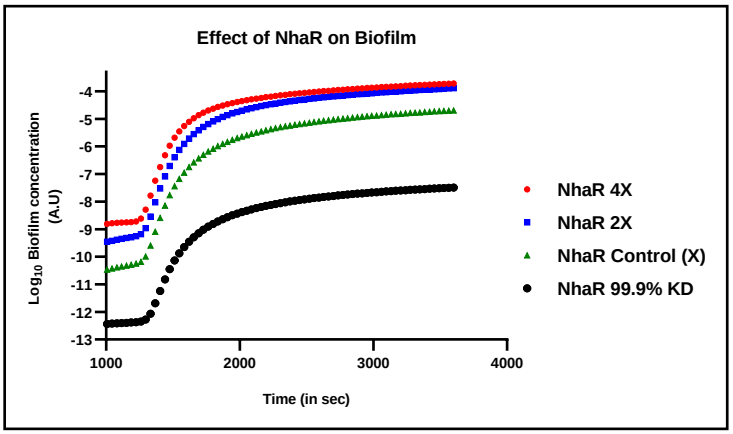

Figure 5.8 Effect of NhaR on PGA (Adhesin) levels and Biofilm formation. The role of NhaR in the synthesis of (A) PGA (Adhesin) and (B) Biofilm formation was validated by simulating the model for a 99.9% knockdown (NhaR 99.9% KD, equivalent to Knockout or KO) and graded overexpression of NhaR levels with respect to Control (X) which refers to the wild-type simulation levels. NhaR, 99.9% knockdown, resulted in a decrease in the levels of biofilm, whereas overexpression of NhaR resulted in an increase in adhesin levels and hence biofilm. The plots represented here are the simulation output from the *in silico* platform because of the graded knockdown of the protein levels in the model. A logarithmic scale has been used for better representation of the data.

Control (X): represents wild-type (WT) or Control simulations; **99.9% KD**: 99.9% knockdown (equivalent to knockout, KO), **2X**: 2-fold overexpression and **4X**: 4-fold overexpression with respect to Control levels (X).

A.U: Arbitrary Unit; used for the representation of the relative levels of model output.

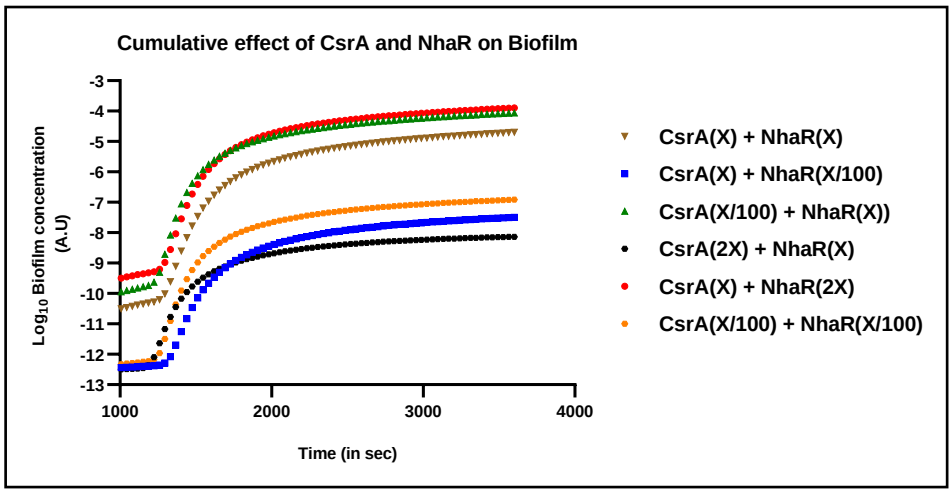

Figure 5.9 Cumulative effect of CsrA and NhaR perturbations on Biofilm formation. The effect of simultaneously perturbing the levels of both CsrA and NhaR on biofilm formation was validated in the model by running regulatory loop runs with respect to the Control levels (X). The cumulative effect of these perturbations was validated by both the overexpression and knockdown of NhaR and CsrA individually, in comparison to Control levels (X) for each of the species. Additionally, a combined loop run was also simulated for double knockout of NhaR and CsrA to check the cumulative effect of these gene knockouts on biofilm formation. The overall output from the model is in accordance with the published literature (see text for details). The plots represented here are the simulation output from the *in silico* platform because of the graded knockdown of the protein levels in the model. A logarithmic scale has been used for better representation of the data.

Control (X): represents wild-type (WT) or Control simulations; **99.9% KD**: 99.9% knockdown (equivalent to knockout, KO), with respect to Control levels; **2X**: 2-fold overexpression with respect to WT levels (X)

A.U: Arbitrary Unit; used for the representation of the relative levels of model output.

Effect of Low pH on biofilm formation

E. coli can withstand a wide range of harsh environmental conditions, including acidic stress. When *E. coli* is exposed to low pH, the acid tolerance response (Šeputiene et al., 2006) of the bacterial system is activated, inducing biofilm formation (X. S. Zhang et al., 2007) via a cascade of signalling pathways. When acid stress is introduced into the system, the two-component signal transduction system EvgS/EvgA inside the

cell is activated (Itou et al., 2009). As a result, a transcriptional cascade of acid and multidrug resistance genes is initiated, which involves transcriptional regulators such as YdeO and GadE. While YdeO indirectly enhances PGA synthesis, GadE also activates RpoS(Ma et al., 2003), a master regulator of gene expression under stationary phase and biofilm formation. This phenomenon was confirmed in the model by a gradual increase in biofilm in response to acid stress (X/100, X and 2X, where X represents the control or wild-type levels in the model; **Figure 5.10**).

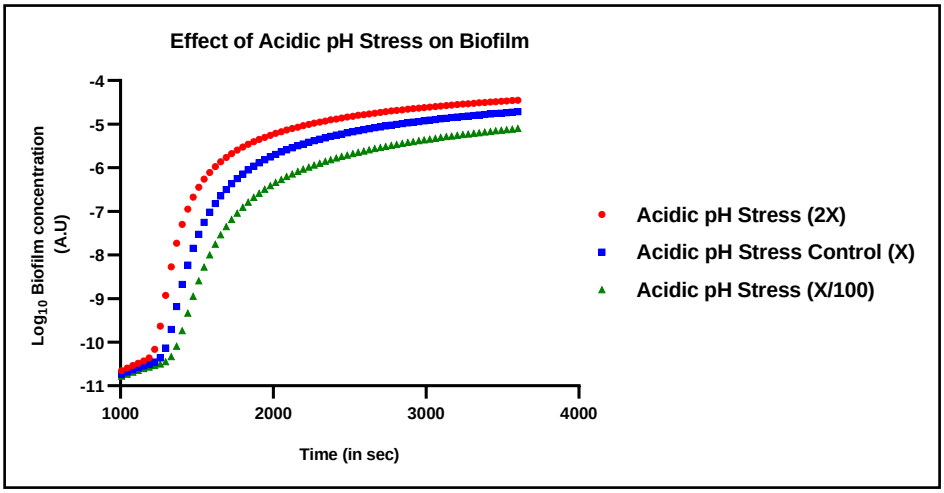

Figure 5.10 Biofilm formation under acidic stress. The role of acidic stress on biofilm formation was validated in the model by introducing an acid stress (hypothetical) component in the model, which mimics biofilm formation in *E. coli* under low pH conditions. The effect of acidic stress was simulated in the model by perturbing the levels of acid stress from as low as **X/100 (0.01X)** to as high as **2X** levels with respect to the control or wild-type levels (**X**). The plots represented here are the simulation output from the *in silico* platform. A logarithmic scale has been used for better representation of the data.

Control (X): Represents Control simulations; **X/100**: 100-fold reduction in the levels, with respect to Control levels; **2X**: 2-fold overexpression with respect to Control levels (X).

A.U: Arbitrary Unit; used for the representation of the relative levels of model output.

Role of extra-cellular DNA (eDNA) in biofilm formation

Extracellular DNA (eDNA) is well established as a structural component of biofilm matrix(Vorkapic et al., 2016; Whitchurch et al., 2002). eDNA is released as a component of genomic DNA due to bacterial cell death or lysis, providing stability to the overall biofilm architecture. This function has been studied and established in a variety of bacterial systems, including *P. aeruginosa*, S. *aureus*, and *E. coli BW25113* (Bayles, 2007; Zhao et al., 2013). DNase I treatment or repressing eDNA release into extracellular media reduces biofilm formation (Nijland et al., 2010). To determine the role of eDNA, the model was simulated for the graded decrease in eDNA levels (50%, 75%, and 99.9% of control wild-type levels). Reduced eDNA levels resulted in a dose-dependent decrease in biofilm formation (**Figure 5.11**).

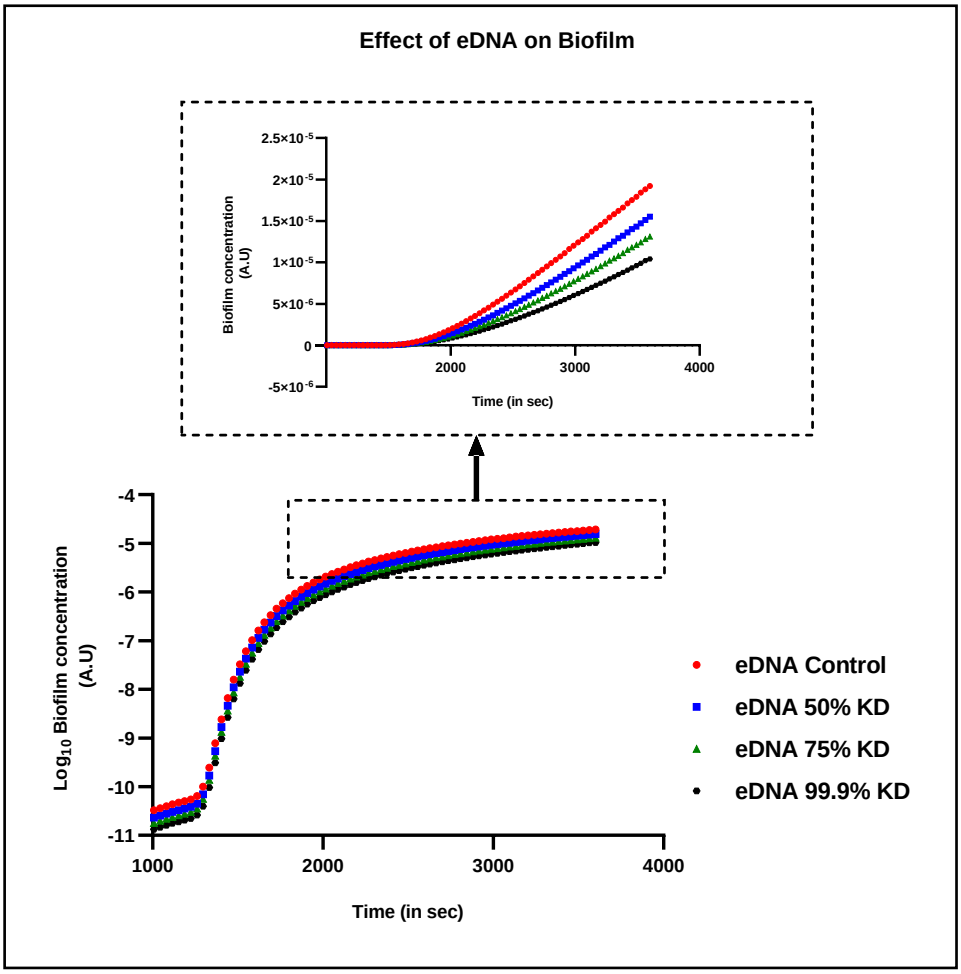

Figure 5.11 Role of extra-cellular DNA (eDNA) in biofilm formation. eDNA is an integral component of the biofilm matrix and the same has been validated in the model by running simulations with a graded reduction (50% KD, 75% KD and 99.9% KD) in

the overall levels of eDNA with respect to Control levels. As evident, a graded reduction in the levels of eDNA in the system resulted in a decline in biofilm formation. The plots represented here are the simulation output from the *in silico* platform as a result of the graded knockdown of eDNA levels in the model. (**Inset**: The effect of eDNA graded perturbation on biofilm formation represented in a linear scale).

Control: represents wild-type (WT) or Control simulations; **50% KD**: 50% knockdown; **75% KD**: 75% knockdown**; 99.9% KD**: 99.9% knockdown (equivalent to knockout, KO), done with respect to Control levels. A logarithmic scale has been used for better representation of the data.

A.U: Arbitrary Unit; used for the representation of the relative levels of model output.

Further, this model was enhanced and populated with over 300 genes constituting the various components expected to influence the biofilm formation. This was followed up with systematic alignment and optimization, and then its robustness was established by comparing it against known published information. An interlinked network of all these genes was built to exactly reflect and bring about the synchronised regulatory and structural gene expression responsible for the self-encased multi-cellular biofilm. The major components considered for developing this *in silico* platform are enlisted in **Table S5.1** of the **Appendix** section. Some of the gene overexpression (OE) and knockouts (KOs) and their effect on biofilm levels are listed in **Table 5.2A** and **2B.** Most of the results, depending on the gene expression, followed the expected trend, although the magnitude of change did not at times exactly match as reported in the literature. This difference could be attributed to the system limitations associated with *in silico* modelling.

Table 5.2 Gene knockout studies and model validation

(A) Gene knockouts which increase biofilm formation

Gene	Percentage increase in biofilm with respect to WT (Control) levels *	Reference[#]
lrhA	83.7	(Blumer et al., 2005)
ycgR	29.8	(Pesavento et al., 2008)
csrA	728.9	(X. Wang et al., 2005)
yhjH	25.3	(Pesavento et al., 2008)

(B) Gene knockouts which decrease biofilm formation

Gene	Percentage decrease in Biofilm with respect to WT (Control) levels *	Reference[#]
ag43	68.6	(Danese, Pratt, Dove, et al., 2000)
bcsA	75.9	(Gualdi et al., 2008)
crp	92	(Hufnagel et al., 2016)
fimB	99.9	(Blumer et al., 2005)
fis	99.9	(Sheikh et al., 2001)
hns	99.9	(Battesti et al., 2012; Belik et al., 2008)
bolA	79.6	(Vieira et al., 2004)
mlrA	46.4	(Weber et al., 2006)
nhaR	99.8	(Goller et al., 2006)
pgaA	92.9	(X. Wang et al., 2004)

*Percentage increase or decrease was calculated with respect to the levels of biofilm biomass produced under control / unperturbed system.

[#]References listed were used for model alignment and validation purposes. Only the qualitative nature of impact and not the exact magnitude was considered.

5.3.2 *In silico* to *in vitro* translation: Predictive studies, target identification and validation of their role in biofilm formation

The objective of developing this model was to create a network of all genes and their regulators involved in biofilm formation. Extending this approach, perturbations that cause changes in their levels were introduced, and any effect on biofilm formation was assessed. Based on the model output, a few new secondary and tertiary-level regulators were identified, and the corresponding KO strains were tested for biofilm formation *in vitro*. From the predictive studies of the model, the genes *miaA*, *ydeO*, and *ygiV* (tertiary-level regulators) were identified to influence biofilm formation. Each of these targets has its own regulatory network through which it influences the overall process of biofilm formation (**Figure 5.12**). The *in vitro* evaluation and validation of the results of the *in silico* simulations were done in two ways. To begin, a set of KOs of *E. coli BW25113* from the Keio collection (Baba et al., 2006) were chosen based on *in silico* predictions, and their biofilm-forming capacities were validated in a crystal violet staining-based biofilm assay. Second, and more importantly, UPEC KOs generated via P1 transduction were subjected to a similar evaluation.

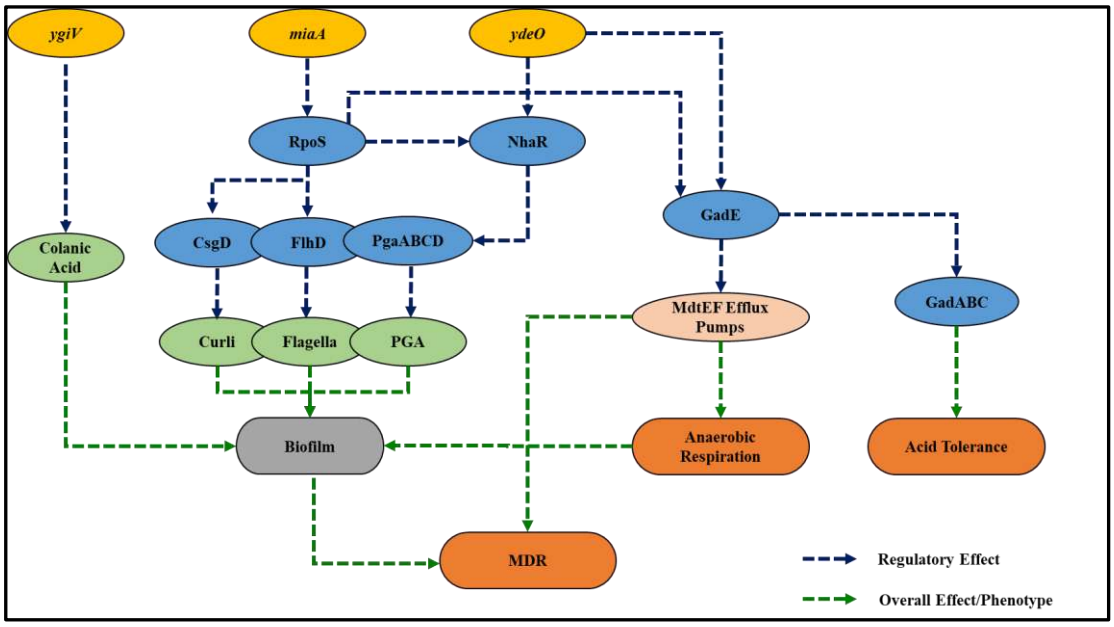

Figure 5.12 Regulatory network and the overall effect of the target genes *miaA*, *ydeO*, and *ygiV* on *E. coli* biofilm formation and multi-drug resistance (MDR). The three genes *miaA*, *ydeO*, and *ygiV* were identified as novel targets via predictive studies with the *in silico* platform. They were further validated for their roles in biofilm formation in *E. coli* clinical isolates (see text for details). MiaA affects the expression

of RpoS, which, in turn, is a global regulator for the expression of multiple genes associated with biofilm formation, such as structural proteins (curli). YdeO regulates the synthesis of PGA adhesin (PGA_Cyt represents cytosolic PGA), an essential component of the biofilm matrix. (YgiV is directed towards the release of colanic acid. The illustration represents the regulatory network (with their representative components) for the three genes that involve different components of biofilm and multi-drug resistance.

MiaA (dimethylallyl diphosphate: tRNA transferase) is a tRNA modifying enzyme that has been associated with the expression and efficient translation of RpoS and IraP (Aubee et al., 2016; Thompson & Gottesman, 2014). The alternate sigma factor RpoS, in turn, is known to regulate gene expression in the stationary phase and under various stress conditions (Schellhorn, 2020). IraP, on the other hand, is an anti-adaptor protein that stabilises RpoS levels by preventing RssB-mediated degradation of RpoS (Micevski et al., 2015). Furthermore, MiaA regulates the expression of multiple genes involved in the synthesis of essential components such as flagella, fimbriae (**Figure 5.3**), and curli in *E. coli* biofilms via RpoS. (**Figure 5.12**). Earlier research on *Pseudomonas aeruginosa* has also shown that the absence of MiaA results in smaller cellular aggregates, lower biomass, and poor biofilm development (Schinner et al., 2020). As a result, the role of MiaA in the model was investigated by simulating loop runs and introducing graded knockdowns of MiaA levels. Such a change resulted in a gradual decrease in biofilm levels (**Figure 5.13A** and **Appendix** section **Table S5.3**). The translation of *in silico* findings to *in vitro* was demonstrated by testing biofilm formation in *E. coli BW25113* and UPEC mutants lacking *miaA*. Both strains were unable to form ideal biofilms (**Figure 5.14**).

(A)

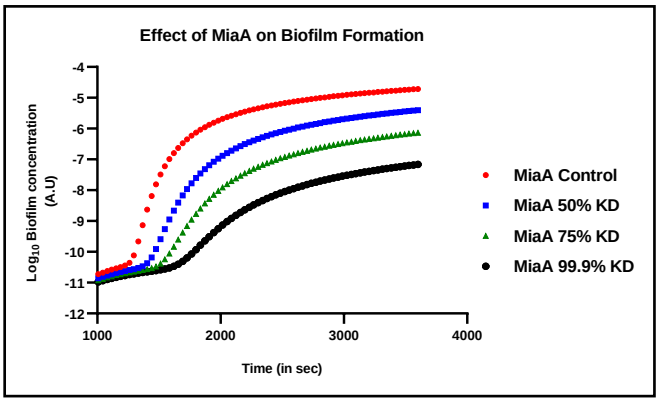

(B)

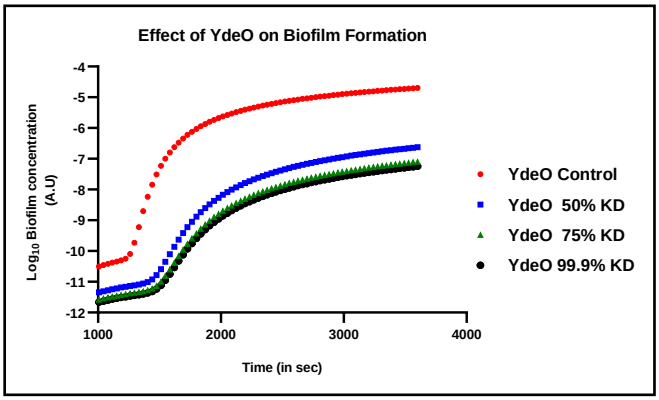

(C)

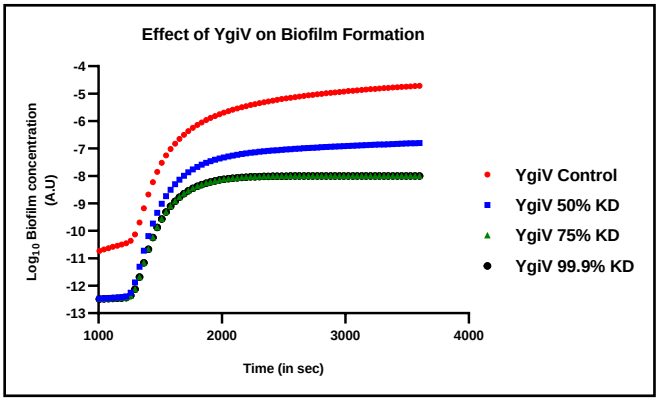

Figure 5.13 Effect of MiaA, YdeO and YgiV perturbation on biofilm formation. The role of the three novel targets *miaA*, *ygiV* and *ydeO* on biofilm formation was validated in the model by simulating the model with a graded knockdown (KD) of 50%, 75% and 99.9% (equivalent to knockout-KO) in comparison to the Control wild-type levels. A graded decrease in the levels of (A) MiaA, (B) YdeO and (C) YgiV in the system resulted in a concomitant decrease in biofilm levels. The plots represented here

are the simulation output from the *in silico* platform as a result of the graded knockdown of the protein levels in the model. A logarithmic scale has been used for better representation of the data.

Control: represents wild-type (WT) or Control simulations; **50% KD**: 50% knockdown; **75% KD**: 75% knockdown**; 99.9% KD**: 99.9% knockdown (equivalent to knockout, KO), done with respect to Control levels. A logarithmic scale has been used for better representation of the data.

A.U: Arbitrary Unit; used for the representation of the relative levels of model output.

YdeO is a transcription factor in *E. coli* belonging to the AraC/XylS family, which is associated with the activation of the downstream genes involved in cellular responses to acid resistance (Ma et al., 2004; Masuda & Church, 2002, 2003). It also regulates the synthesis of PGA adhesin, which is another essential component of the biofilm matrix. Furthermore, this transcription factor has also been reported to play a significant role in the expression of RND efflux pumps MdtEF, which in turn contributes to multi-drug resistance and tolerance to anaerobic conditions in *E. coli* (**Figure 5.12)** (Y. Zhang et al., 2011). Knockout of *ydeO* reduces cell stability under acidic and alkaline stress, along with the levels of PGA formed via NhaR signalling, resulting in a reduction in the levels of biofilm formation. Simulating graded reductions in YdeO levels in the model resulted in a decrease in biofilm-forming capacities (**Figure 5.13B** and **Appendix** section **Table S5.4**). However, upon *in vitro* measurement, the extent of reduction in biofilm formation varied between the two types of *E. coli* strains. UPEC *ydeO* KO had the greatest reduction, whereas *E. coli BW25113 ydeO* KO had only a 20% reduction in biofilm formation (**Figure 5.14**).

Reports on the role of **YgiV** in the toxin-antitoxin (TA) system (Kasari et al., 2010) and biofilm development are still limited, although our findings on this regulator attribute its important role in pathogenic strains. In the model, perturbations, or graded knockdown of YgiV levels, resulted in decreased colanic acid production and release via McbA and McbR (**Figure 5.12**), resulting in a decrease in overall EPS levels and thus biofilm (**Figure 5.13C** and **Appendix** section **Table S5.5**). However, deleting *ygiV* in *E. coli* had completely different results, with the outcome being determined by the bacterial host. UPEC *ygiV* KOs had a lower biofilm formation capacity than *ygiV* KOs in *E. coli BW25113*, which had a slightly higher biofilm formation capacity, as

represented in **Figure 5. 14**. YgiV (*b3023*) (Keseler et al., 2017; X. S. Zhang et al., 2008) is a DNA-binding transcriptional repressor that regulates biofilm formation and mucoidy by repressing McbR, which in turn regulates McbA (encoded by ybiM). McbA modulates the export of colanic acid into the extracellular polymeric matrix, and excessive colonic acid production inhibits biofilm formation due to mucoidy. As b3023 was identified as a repressor, the findings with *E. coli BW25113 ygiV* KO were perfectly aligned with our predictions (X. S. Zhang et al., 2008). However, the same study also reported that the phenotype is dependent on the bacterial host, which could explain why we observed complete inhibition of biofilm formation in *ygiV* KO UPEC. To fully understand this difference, further evaluation, especially differences, if any, in genome organisation and/or regulation in a laboratory versus a pathogenic strain, is needed.

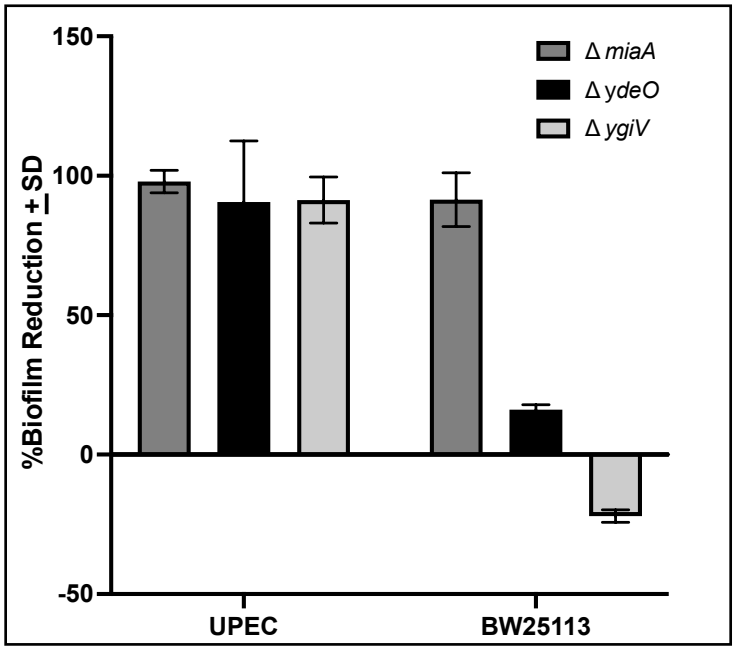

Figure 5.14 Inhibition of biofilm formation with specific UPEC and *E. coli BW25113* target KOs. Knockout strains of *miaA*, *ydeO* and *ygiV*, generated in UPEC and *E. coli BW25113* from Keio Collection (Baba et al., 2006) were assessed for biofilm formation using the crystal violet biofilm assay. % Reduction was calculated based on biofilm formation seen with the host strains, UPEC and *E. coli BW25113*, respectively. The data presented is the mean (%) ± SD of biofilm formation as measured in the crystal violet assay with replicates.

Overall, the *in vitro* confirmation of the roles of a few targets predicted *in silico*, particularly with pathogenic strains, strengthened the model's predictive capacity and established the validity of the model findings. The findings of the extended study with UPEC KOs are critical because they provide information on the target proteins whose absence or inhibition would prevent biofilm formation in virulent strains. This provides opportunities towards the development of inhibitors that could supplement traditional antibiotic therapies for the treatment of biofilm-associated chronic infections and the prevention of biofilm formation in medical implants.

Differential gene expression and its effect on *E. coli* biofilm formation

The expression profiles of the same genes in clinical isolates of *E. coli* (SEC54, SEC59) were examined using qRT-PCR. These isolates were obtained from patients suspected of urinary tract infections at St. John's Medical Hospital. The isolates were tested for biofilm formation, and any link and influence on transcript levels of *miaA*, *ydeO*, and *ygiV* were verified. UPEC CFT073 was also tested in the same assays and served as a positive control. Among the three, UPEC and SEC54 formed biofilms, whereas SEC59 was a non-biofilm former. For the qRT-PCR studies, the expression levels of *miaA*, *ydeO*, and *ygiV* were quantified following normalization with a housekeeping gene (dnaK).

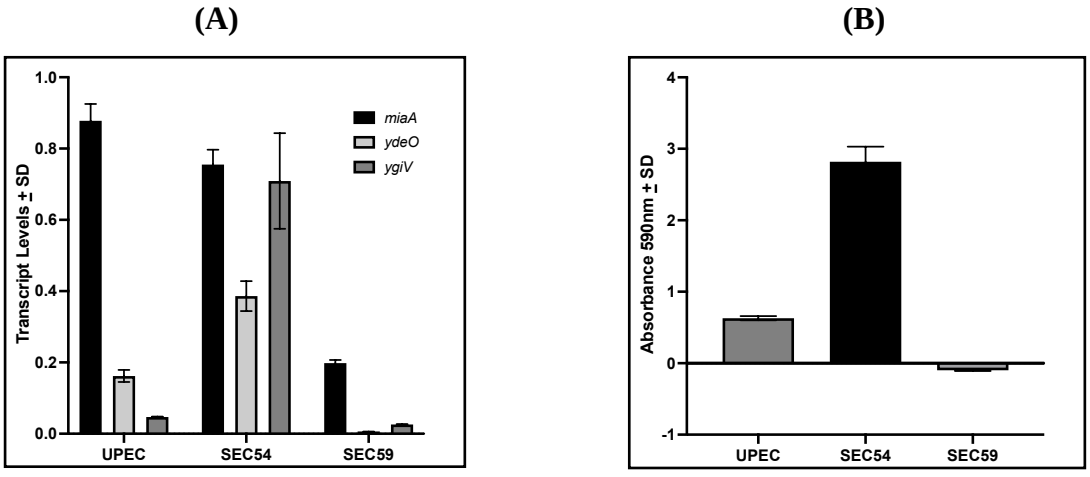

Figure 5.15 Expression levels of target genes and biofilm formation. (A) The relative gene (mean± SD) expression levels (run in triplicate) of the target genes in clinical isolates of *E. coli* and UPEC were determined by qRT-PCR. The data presented is the relative abundance of each of the gene transcripts normalized with respect to the housekeeping gene, *dnaK*. (B) Biofilm formation, as estimated by Crystal Violet assay

with the clinical isolates (SEC54 and SEC59) and UPEC. The data presented is the mean (%) ± SD of biofilm formation, as measured in the crystal violet assay with replicates. The biofilm-forming ability of the strains is directly correlated to the increased levels of the target gene transcripts in the UPEC and the clinical isolates.

The differential expression profiles of the key regulatory genes showed a direct correlation with the biofilm-forming ability of the clinical *E. coli* strains, as shown by the qRT-PCR data (**Figure 5.15A and 5.15B**). Genes such as *miaA, ydeO,* and *ygiV* are essential for the regulation of biofilm formation events. These genes are expressed at a higher level in strains such as UPEC and SEC54, which contributes to their enhanced biofilm formation. However, the expression levels of these genes were insignificant in SEC59, a poor biofilm-forming isolate. Overall, this demonstrates the coordinated regulatory effects of these multiple genes in driving the biofilm formation process.

5.3.3 Role of efflux pumps in biofilm formation: A heterologous overexpression study

The formation of biofilm is usually driven by multiple components, and efflux pumps play a pivotal role in this phenomenon (Soto, 2013). The inhibition of these efflux pumps has been reported to abolish the formation of biofilm in *E. coli* (Kvist et al., 2008). Further, to ascertain the role of efflux pumps in biofilm formation in *E. coli,* the different strains with overexpressed efflux pumps of heterologous origins were evaluated (**Chapter 2, Table 2.2**). For these assays, the common lab strain *E. coli BW25113* was chosen as the model system because of its recognition as a moderate biofilm-forming strain (Król et al., 2019). The constitutively expressed double complementation systems *pEcoAB* (AcrA-AcrB), *pMexAB* (MexA-MexB), and *pOqxAB* (OqxA-OqxB) were expressed in the efflux-deficient variant *E. coli BW25113 ΔacrA-ΔacrB* (**Chapter 2, Table 2.1**), and the overall biofilm formation was estimated.

As evident from **Figure 5.16**, the *E. coli BW25113* wild-type strain exhibited some biofilm formation, whereas the loss of efflux pumps resulted in a minor decline in the total biofilm yield. These results aligned perfectly with the observations reported earlier (Matsumura et al., 2011). Although the overexpression of the native AcrA-AcrB in *E. coli BW25113 ΔacrA-ΔacrB* enhanced biofilm formation, the overall effect was not very profound. Interestingly, the overexpression of the heterologous efflux pump

components significantly enhanced the biofilm-forming ability of the host strain, with values around 2 to 3-fold for MexA-MexB and 4 to 5-fold in OqxA-OqxB overexpressed systems, in comparison to the native wild-type levels. This finding further confirmed the role of the heterologously overexpressed/reconstituted efflux pumps in promoting enhanced biofilm formation in *E. coli*.

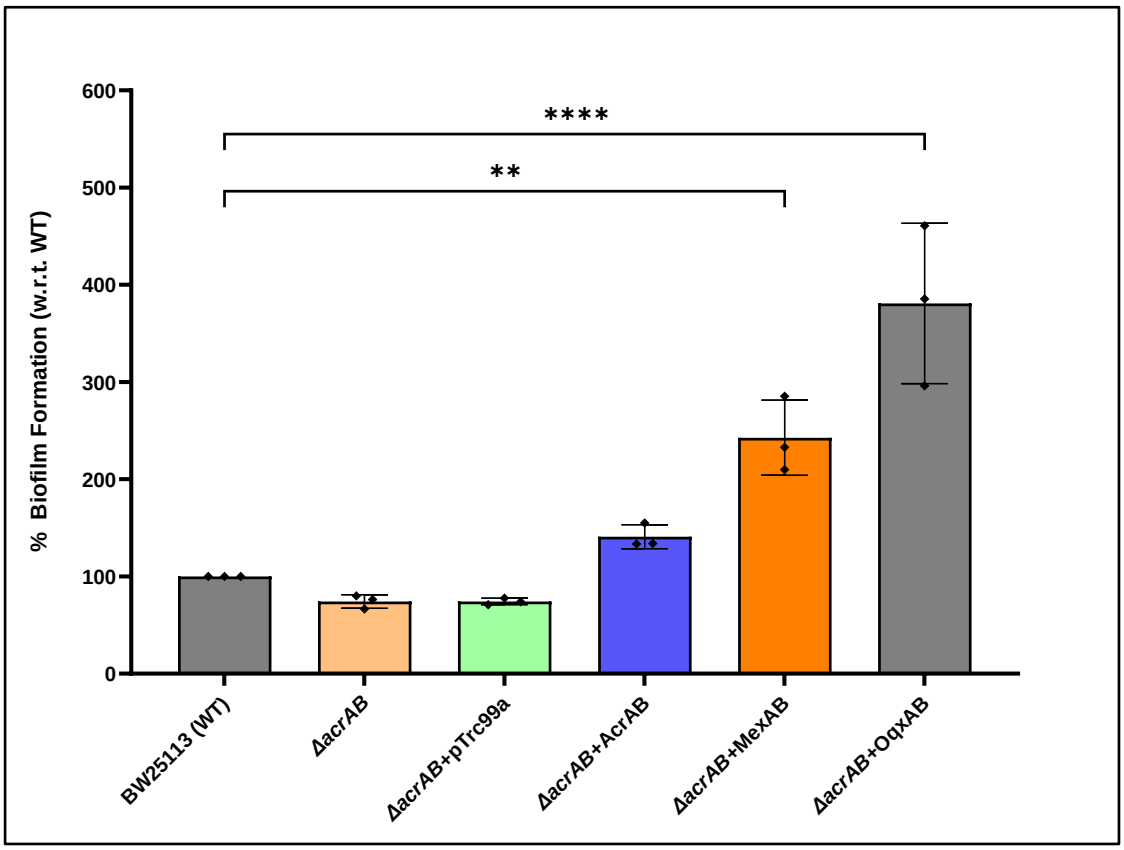

Figure 5.16 Biofilm formation in *E. coli BW25113 (ΔacrAB)* double KO background with different heterologous overexpression systems. The biofilm formation was estimated in either *E. coli BW25113* (WT) or its efflux deficient variant (*ΔacrA-ΔacrB*) with different heterologous systems, overexpressing the target genes AcrA-AcrB, MexA-MexB or OqxA-OqxB. Data presented is the mean (%) ± SD of biofilm formation, as measured in the crystal violet assay with replicates, compared to the wild-type system without any complementation, as observed from three independent biological experiments (n=3) in technical triplicates.

E. coli BW25113 (WT: wild-type) and its *ΔacrA-ΔacrB* variant with different double complementation systems were used.; *pTrc99a* (empty vector), *pEcoAB* (+ AcrAB), *pMexAB* (+MexAB), *pOqxAB* (+OqxA*B*) : complementation with plasmid carrying the respective genes.

5.4 Discussion

The present work on the development of a validated *in silico E. coli* biofilm model was done using multiple networks of interlinked pathways involved in biofilm formation. The model is structured for a better understanding of the functional role of several gene products, their regulators, and the structural components that support the transition of *E. coli* from a simple planktonic motile organism to a multicellular sessile three-dimensional form. However, the current model, like all previous approaches used to replicate and simulate a biological system, has its own set of limitations. It may yield results that are inconsistent with the reported outcomes. Misalignment can manifest as (a) no effect, (b) a result that contradicts what has been shown in the literature, or (c) a difference in the magnitude of the effect. This disparity could be attributed to a lack of adequate information, the inherent limitations of biological systems and their modelling as a result of considered approximations and assumptions for defining fluxes, reaction kinetics, unknown interactions within the system, or differences in genomic organisation in wild-type *E. coli* laboratory strains versus clinical isolates.

Despite the fact that the components of the biofilm network were aligned, optimised, and validated using the most recent literature information, the model's trend or outcomes were not always consistent with the reported values. The developed model accounts for the validations of more than 80% of the genes or components for their contributions or effects on biofilm in the current approach to understanding *E. coli* biofilm. Although all the genes used in the model development were chosen for their significant contributions, lowering the levels of a few of them did not affect the overall biofilm formation. This sensitivity may be due to systemic redundancy, which occurs when different components within the system perform the same function. As a result, it was critical to subject the platform to various perturbations such as acid stress or genetic changes such as modulating target gene expression levels (OE & KO) and then study their impact on biofilm formation.

Furthermore, according to the simulations, genes predicted to cause loss of biofilm formation upon deletion were also evaluated *in vitro*, using corresponding KOs for their biofilm-forming capacities. Even though the trend matched, we observed a difference in actual extent, which could be attributed to model limitations and host strain variations. In addition, qRT-PCR revealed that the transcript profiles of the genes *miaA*, *ydeO*, and *ygiV* in a biofilm-forming clinical isolate derived from a UTI case had elevated levels when compared to a non-former. The model's validity could be

established because its predictions matched well with UPEC target gene KO strains and the qRT-PCR data with the clinical isolate. The current model is the first comprehensive approach to gaining a holistic understanding of the structural and functional aspects of *E. coli* biofilm. This model has the potential to be expanded in the future as newer components are added, allowing for predictive studies to identify new targets and the possibility of extending to other biofilm-forming pathogens. The targets identified here are involved in processes that aid in adjusting to a different environment and transitioning to minimal growth with altered physiology just sufficient to survive until conditions improve for dispersal and reversion to a planktonic lifestyle.

Multiple genetic switches must operate at the transcriptional or post-transcriptional levels to ensure adequate RpoS expression during the transition from planktonic to stationary phase or biofilms. At this point, MiaA's role in maintaining steady-state RpoS levels and ensuring translational fidelity could be critical. Following environmental cues, MiaA-modified tRNAs may act as co-regulators to various global regulators, influencing pathogenicity traits, energy conservation during oxygen limitation (Basta et al., 2017), and fine-tuning and influencing key downstream events such as type IV pili biogenesis (Panayidou et al., 2020). YdeO and YgiV, the two other identified targets, are also important for biofilm development because the former is required to adapt to changes in environmental conditions. In contrast, YgiV, because of its connection to the TA system and biofilm formation via mucoidy, it could have a role in regulating the growth of the bacteria. According to published reports, YdeO may also help with survival under anaerobic conditions (Yamanaka et al., 2014). Such stressors are extremely likely to be encountered by the pathogen within the host. Furthermore, YdeO has been shown to increase *E. coli* multi-drug resistance by activating the MdtEF multi-drug efflux pump (Nishino et al., 2009), which is regulated and known to be most active during the stationary phase (Kobayashi et al., 2006). These findings, along with the model outcomes, further strengthen the cross-talks and the involvement of efflux pumps in the events of biofilm formation. Thus, the genes *miaA*, *ydeO*, and *ygiV* are important targets whose inhibition could halt and interfere with the events of biofilm development and survival processes, particularly during chronic infections. Inhibition of some of these targets may also reduce efflux-mediated resistance and refractoriness, which is common in biofilm-mediated infections.

Additionally, the findings that overexpression of efflux pumps of heterologous origins led to enhanced biofilm formation in *E. coli* further established the role of efflux

pumps in increasing biofilm formation. Such observations indicated the potential and possibilities of increased transmission of AMR traits across different bacterial species and that this is not limited only to the extrusion of toxic substrates, including antibiotics, but could be further extended to enhanced biofilm-forming abilities as well.

Although the discovery of new antibiotics would help address the global threat of AMR, it is possible that this would be limited to only resistant planktonic forms. On the other hand, preventing chronic infections or drug resistance caused by sessile bacterial communities may make it easier to combine conventional antibiotic therapy with inhibitors against biofilm targets identified through such modelling approaches. A strategy like this could lead to additional benefits, such as the enhanced susceptibility of otherwise resistant microbes, particularly those with polymicrobial origins.

5.5 Code Availability

The complete source code and the models built to simulate the knockout (KO) and overexpression (OE) studies presented in the manuscript can be downloaded from the GitHub repository (https://github.com/sreenathrajagopal/Biofilm_ODE.git). The README file contains a detailed description of the usage of the scripts. The **model_build** and **bulk_build** script allows the user to generate R models for single/multiple Knockout/overexpression studies. **Run** script evaluates the changes in the levels for each species over time and generates the .csv files (containing the data points). **Image** and **image_bulk** scripts help visualise the changes in species of interest from the results obtained through simulations of single/multiple perturbation models. All accompanying information related to model outputs and raw data for the studies could be accessed via the GitHub repository.

Chapter 6

Conclusion and Discussion

The success of any drug discovery process relies primarily on our understanding and knowledge of the intended cellular target, apart from the design of a novel molecule against it that is efficacious yet safe for humans. Even antibiotics are not an exception in this regard! As the bacterial systems exploit multiple resistance mechanisms, an in-depth understanding of the cellular components within the bacterial systems that are being targeted would aid not only in selecting the most optimal among them but also provide the much-needed boost to the overall process of drug development. The discovery of an effective antibacterial agent involves inhibition of either one or more essential targets which causes inhibition of growth and consequently affects its survival. To escape such a deleterious action of an antibiotic, the pathogen develops resistance through multiple avenues. Among the different mechanisms that bacteria employ to overcome the action of antibiotics, efflux pumps and biofilm formation contribute substantially. Both phenomena benefit the bacteria to avoid antimicrobial action and promote antimicrobial resistance (AMR) akin to 'two peas in a pod', as they are often found to be associated together with incidence of multi-drug resistance in clinical isolates that cause hospital-acquired infections. The current work is an attempt to unravel the workings of these constantly evolving efflux pumps and the extensive changes that bacteria undergo to persist and become tolerant to anti-bacterial drugs. In the case of the former, an inhibitor would interfere with the efflux pump activity, thereby making them sensitive to antibiotics, whereas in the case of the latter, any disruption of multi-cellular structures could lead to reduced virulence and improved susceptibility. In both cases, the pathogen is now ill-equipped to escape the efficient growth inhibitory action of an antibiotic within the host either by itself or when combined with a biofilm disruptor or efflux pump inhibitor.

Owing to the action of efflux pumps, there have been instances of premature termination of the progression of many potent target inhibitors and projects failing to take off and traverse the entire drug discovery journey due to a lack of cellular activity. When it comes to drug-resistant hospital-acquired infections and the transmission of AMR, the members of the RND efflux pump families have emerged as one of the predominant contributors. Therefore, a detailed understanding of the structural aspects and functional mechanisms of efflux pumps is crucial in drug discovery. Firstly, understanding the structural details of efflux pumps can help identify potential binding sites, unravel the transport of drugs and devise strategy to design inhibitors that prevent drug efflux. Finally, understanding the diversity of efflux pumps across different

bacterial species and strains is crucial in developing new antibiotics that can overcome this entire range.

The complexity of the AMR situation rises manifold with biofilms due to their complex architecture. Efflux pumps also play a crucial role in developing these community based resistance levels in biofilms. Moreover, planktonic cells through quorum sensing cause coordinated gene expression, chemotactic movements, swarming motility, exopolysaccharide production, virulence, cell aggregation etc. This phenomenon has been captured in the development of the *E. coli* biofilm model using all the components and the inter-connected pathways including efflux pumps like Mtr and AcrEF which were found to be involved in the extrusion of signalling molecules like indole, AHL, AI-2, etc. The latter are known to drive a series of multiple events that cause transition of planktonic to sessile forms. The significance of efflux pumps in biofilm formation could be emphasized further with the fact that while addressing the complications associated with biofilms, anti-biofilm treatments are often combined with efflux pump inhibitors to yield better results.

Therefore, in light of our current understanding and the information available in the published literature, we have considered these distinct yet significant contributors to AMR across bacterial systems. The set research objectives and findings thereof would certainly help in a better understanding of the structural and functional characterization of different members of the RND efflux pump family and the plausible mechanisms involved in the transmission of AMR across different bacterial systems. The outcomes of the first objective shed light towards the promiscuity of the different RND permeases. It clearly indicates that despite sharing low homology in their sequences, efflux pump components from evolutionarily distant groups are structurally similar in their organization and can form functional complexes to extrude a broad spectrum of antibiotics. Finally, the *in silico* model for *E. coli* biofilm provides an overall view of the interconnecting networks and pathways contributing to biofilm formation. The model successfully identified and validated three novel target genes in *E. coli*, namely *miaA, ydeO,* and *ygiV,* for their potential role in biofilm formation and plausible mechanisms of tolerance to harsh environments and resistance. The biofilm platform is available in the public domain as an "open-source plug-and-play" model and provides an excellent opportunity for further upgradation. This platform also offers scope for enhancements with the availability of more information, allowing researchers an improved assessment of the role of cellular metabolites, signalling pathways, key

structural and regulatory components and efflux pumps during biofilm formation and antimicrobial resistance (AMR). The link to efflux pumps reiterates the importance of this key strategy used by pathogens to better survive stressful environments. The present research would significantly aid in designing agents that could interfere with efflux pump inhibition and/or disruption of biofilms, with specific applications in different industrial sectors, including healthcare.

In summary, the output of this thesis work would certainly add value to ongoing scientific research directed towards understanding bacterial strategies involving mechanisms of resistance development. Such insights would aid in devising countermeasures to tackle AMR and for effective treatment of multi-drug-resistant infections, thus greatly contributing to improved patient care globally.

Bibliography

Abushaheen, M. A., Muzaheed, Fatani, A. J., Alosaimi, M., Mansy, W., George, M., Acharya, S., Rathod, S., Divakar, D. D., Jhugroo, C., Vellappally, S., Khan, A. A., Shaik, J., & Jhugroo, P. (2020). Antimicrobial resistance, mechanisms and its clinical significance. *Disease-a-Month*, *66*(6), 100971.

Acemel, R. D., Govantes, F., & Cuetos, A. (2018). Computer simulation study of early bacterial biofilm development. *Scientific Reports*, *8*(1).

Akinduti, P. A., George, O. W., Ohore, H. U., Ariyo, O. E., Popoola, S. T., Adeleye, A. I., Akinwande, K. S., Popoola, J. O., Rotimi, S. O., Olufemi, F. O., Omonhinmin, C. A., & Olasehinde, G. I. (2023). Evaluation of Efflux-Mediated Resistance and Biofilm formation in Virulent *Pseudomonas aeruginosa* Associated with Healthcare Infections. *Antibiotics (Basel, Switzerland)*, *12*(3).

Al-Abdely, H., AlHababi, R., Dada, H. M., Roushdy, H., Alanazi, M. M., Alessa, A. A., Mohamed Gad, N., Alasmari, A. M., Radwan, E. E., Al-Dughmani, H., Koura, B., Bader, M. M., Al Deen, H. M., Bueid, A., Elgaher, K. M., Alghoribi, M. F., Albarrag, A. M., & Somily, A. M. (2021). Molecular characterization of carbapenem-resistant *Enterobacterales* in thirteen tertiary care hospitals in Saudi Arabia. *Annals of Saudi Medicine*, *41*(2), 63–70.

Alav, I., Bavro, V. N., & Blair, J. M. A. (2022). A role for the periplasmic adaptor protein AcrA in vetting substrate access to the RND efflux transporter AcrB. *Scientific Reports 2022 12:1*, *12*(1), 1–13. https://doi.org/10.1038/s41598-022-08903-9

Alav, I., Sutton, J. M., & Rahman, K. M. (2018). Role of bacterial efflux pumps in biofilm formation. *The Journal of Antimicrobial Chemotherapy*, *73*(8), 2003–2020.

Alvarez-Ortega, C., Olivares, J., & Martínez, J. L. (2013). RND multidrug efflux pumps: What are they good for? *Frontiers in Microbiology*, *4*(FEB), 7.

Amaral, L., Martins, A., Spengler, G., & Molnar, J. (2014). Efflux pumps of Gram-negative bacteria: What they do, how they do it, with what and how to deal with them. *Frontiers in Pharmacology*, *4 JAN*, 168.

Årdal, C., Røttingen, J. A., Opalska, A., Van Hengel, A. J., & Larsen, J. (2017). Pull Incentives for Antibacterial Drug Development: An Analysis by the Transatlantic

Task Force on Antimicrobial Resistance. *Clinical Infectious Diseases*, *65*(8), 1378–1382.

Arenz, S., & Wilson, D. N. (2016). Bacterial Protein Synthesis as a Target for Antibiotic Inhibition. *Cold Spring Harbor Perspectives in Medicine*, *6*(9).

Aron, Z., & Opperman, T. J. (2016). Optimization of a novel series of pyranopyridine RND efflux pump inhibitors. *Current Opinion in Microbiology*, *33*, 1–6.

Ashkenazy, H., Abadi, S., Martz, E., Chay, O., Mayrose, I., Pupko, T., & Ben-Tal, N. (2016). ConSurf 2016: an improved methodology to estimate and visualize evolutionary conservation in macromolecules. *Nucleic Acids Research*, *44*(W1), W344–W350.

Asri, N. A. M., Ahmad, S., Mohamud, R., Hanafi, N. M., Zaidi, N. F. M., Irekeola, A. A., Shueb, R. H., Yee, L. C., Noor, N. M., Mustafa, F. H., Yean, C. Y., & Yusof, N. Y. (2021). Global Prevalence of Nosocomial Multidrug-Resistant *Klebsiella pneumoniae*: A Systematic Review and Meta-Analysis. *Antibiotics*, *10*(12), 1508.

Aubee, J. I., Olu, M., & Thompson, K. M. (2016). The i6A37 tRNA_MiaA modification is essential for proper decoding of UUX-Leucine codons during *rpoS* and *iraP* translation. *RNA*, *22*(5), 729–742.

Avalos Vizcarra, I., Hosseini, V., Kollmannsberger, P., Meier, S., Weber, S. S., Arnoldini, M., Ackermann, M., & Vogel, V. (2016). How type 1 fimbriae help *Escherichia coli* to evade extracellular antibiotics. *Scientific Reports*, *6*(1), 1–13. https://doi.org/10.1038/srep18109

Baba, T., Ara, T., Hasegawa, M., Takai, Y., Okumura, Y., Baba, M., Datsenko, K. A., Tomita, M., Wanner, B. L., & Mori, H. (2006). Construction of *Escherichia coli K-12* in-frame, single-gene knockout mutants: The Keio collection. *Molecular Systems Biology*, *2*, 2006–0008.

Ballén, V., Cepas, V., Ratia, C., Gabasa, Y., & Soto, S. M. (2022). Clinical *Escherichia coli*: From Biofilm Formation to New Antibiofilm Strategies. *Microorganisms*, *10*(6).

Band, V. I., & Weiss, D. S. (2021). Heteroresistance to beta-lactam antibiotics may often be a stage in the progression to antibiotic resistance. *PLOS Biology*, *19*(7),

e3001346.

Baran, A., Kwiatkowska, A., & Potocki, L. (2023). Antibiotics and Bacterial Resistance—A Short Story of an Endless Arms Race. *International Journal of Molecular Sciences*, *24*(6).

Barve, A., Gupta, A., Solapure, S. M., Kumar, A., Ramachandran, V., Seshadri, K., Vali, S., & Datta, S. (2010). A kinetic platform for *in silico* modeling of the metabolic dynamics in *Escherichia coli. Advances and Applications in Bioinformatics and Chemistry*, *3*(1), 97–110.

Bassetti, M., Righi, E., Carnelutti, A., Graziano, E., & Russo, A. (2018). Multidrug-resistant *Klebsiella pneumoniae*: challenges for treatment, prevention and infection control. *Expert Review of Anti-Infective Therapy*, *16*(10), 749–761.

Basta, D. W., Bergkessel, M., & Newman, D. K. (2017). Identification of Fitness Determinants during Energy-Limited Growth Arrest in *Pseudomonas aeruginosa*. *mBio*, *8*(6), 1170–1187.

Battesti, A., Tsegaye, Y. M., Packer, D. G., Majdalani, N., & Gottesman, S. (2012). H-NS Regulation of IraD and IraM antiadaptors for control of RpoS degradation. *Journal of Bacteriology*, *194*(10), 2470–2478.

Bayles, K. W. (2007). The biological role of death and lysis in biofilm development. *Nature Reviews Microbiology*, *5*(9), 721–726.

Belik, A. S., Tarasova, N. N., & Khmel', I. A. (2008). Regulation of biofilm formation in *Escherichia coli K12*: Effect of mutations in the genes *hns*, *stpA*, *lon* and *rpoN*. *Molecular Genetics, Microbiology and Virology*, *23*(4), 159–162.

Beloin, C., Valle, J., Latour-Lambert, P., Faure, P., Kzreminski, M., Balestrino, D., Haagensen, J. A. J., Molin, S., Prensier, G., Arbeille, B., & Ghigo, J. M. (2004). Global impact of mature biofilm lifestyle on *Escherichia coli K-12* gene expression. *Molecular Microbiology*, *51*(3), 659–674.

Bharatham, N., Bhowmik, P., Aoki, M., Okada, U., Sharma, S., Yamashita, E., Shanbhag, A. P., Rajagopal, S., Thomas, T., Sarma, M., Narjari, R., Nagaraj, S., Ramachandran, V., Katagihallimath, N., Datta, S., & Murakami, S. (2021). Structure and function relationship of OqxB efflux pump from *Klebsiella*

pneumoniae. *Nature Communications*, *12:1*, *12*(1), 1–12.

Bhowmik, P., Rajagopal, S., Hmar, R. V., Singh, P., Saxena, P., Amar, P., Thomas, T., Ravishankar, R., Nagaraj, S., Katagihallimath, N., Sarangapani, R. K., Ramachandran, V., & Datta, S. (2022). Validated *In Silico* Model for Biofilm Formation in *Escherichia coli*. *ACS Synthetic Biology*, *11*(2), 713–731.

Bialek-Davenet, S., Lavigne, J. P., Guyot, K., Mayer, N., Tournebize, R., Brisse, S., Leflon-Guibout, V., & Nicolas-Chanoine, M. H. (2015). Differential contribution of AcrAB and OqxAB efflux pumps to multidrug resistance and virulence in *Klebsiella pneumoniae*. *Journal of Antimicrobial Chemotherapy*, *70*(1), 81–88.

Bisht, K., & Ann Wakeman, C. (2019). Discovery and therapeutic targeting of differentiated biofilm subpopulations. In *Frontiers in Microbiology* (Vol. 10, Issue AUG, p. 1908). Frontiers Media S.A.

Blair, J. (2017). Making magic bullets. *Nature Microbiology 2017 2:8*, *2*(8), 1–1.

Blair, J. M. A., Bavro, V. N., Ricci, V., Modi, N., Cacciotto, P., Kleinekathöfer, U., Ruggerone, P., Vargiu, A. V., Baylay, A. J., Smith, H. E., Brandon, Y., Galloway, D., & Piddock, L. J. V. (2015). AcrB drug-binding pocket substitution confers clinically relevant resistance and altered substrate specificity. *Proceedings of the National Academy of Sciences of the United States of America*, *112*(11), 3511–3516.

Blanco, P., Hernando-Amado, S., Reales-Calderon, J. A., Corona, F., Lira, F., Alcalde-Rico, M., Bernardini, A., Sanchez, M. B., & Martinez, J. L. (2016). Bacterial Multidrug Efflux Pumps: Much More Than Antibiotic Resistance Determinants. *Microorganisms*, *4*(1), 14.

Blumer, C., Kleefeld, A., Lehnen, D., Heintz, M., Dobrindt, U., Nagy, G., Michaelis, K., Emödy, L., Polen, T., Rachel, R., Wendisch, V. F., & Unden, G. (2005). Regulation of type 1 fimbriae synthesis and biofilm formation by the transcriptional regulator LrhA of *Escherichia coli*. *Microbiology*, *151*(10), 3287–3298.

Bohnert, J. A., Karamian, B., & Nikaido, H. (2010). Optimized Nile Red Efflux Assay of AcrAB-TolC Multidrug Efflux System Shows Competition between Substrates. *Antimicrob Agents Chemother.*, *54*(9), 3770–3775.

Braman, J., Papworth, C., & Greener, A. (1996). Site-directed mutagenesis using double-stranded plasmid DNA templates. *Methods in Molecular Biology (Clifton, N.J.)*, *57*, 31–44.

Branda, S. S., Vik, Å., Friedman, L., & Kolter, R. (2005). Biofilms: The matrix revisited. *Trends in Microbiology*, *13*(1), 20–26.

Brown, J. R., Jurcisek, J., Lakhani, V., Snedden, A., Ray, W. C., Mokrzan, E. M., Bakaletz, L. O., & Das, J. (2019). *In Silico* Modeling of Biofilm Formation by Nontypeable *Haemophilus influenzae In Vivo* . *mSphere*, *4*(4).

Brown, P. N., Byrne, G. D., & Hindmarsh, A. C. (1989). VODE: A Variable-Coefficient ODE Solver. *SIAM Journal on Scientific and Statistical Computing*, *10*(5), 1038–1051.

Bruchmann, S., Dötsch, A., Nouri, B., Chaberny, I. F., & Häussler, S. (2013). Quantitative contributions of target alteration and decreased drug accumulation to *Pseudomonas aeruginosa* fluoroquinolone resistance. *Antimicrobial Agents and Chemotherapy*, *57*(3), 1361–1368.

Byrd, B. A., Zenick, B., Rocha-Granados, M. C., Englander, H. E., Hare, P. J., LaGree, T. J., DeMarco, A. M., & Mok, W. W. K. (2021). The AcrAB-TolC Efflux Pump Impacts Persistence and Resistance Development in Stationary-Phase *Escherichia coli* following Delafloxacin Treatment. *Antimicrob Agents Chemother.* *65*(8), e0028121.

Carmel, O., Rahav-Manor, O., Dover, N., Shaanan, B., & Padan, E. (1997). The Na^+-specific interaction between the LysR-type regulator, NhaR, and the *nhaA* gene encoding the Na^+/H^+ antiporter of *Escherichia coli*. *EMBO Journal*, *16*(19), 5922–5929.

Castañeda-Barba, S., Top, E. M., & Stalder, T. (2023). Plasmids, a molecular cornerstone of antimicrobial resistance in the One Health era. *Nature Reviews Microbiology 2023 22:1*, *22*(1), 18–32.

Cerca, N., & Jefferson, K. K. (2008). Effect of growth conditions on poly-N-acetylglucosamine expression and biofilm formation in *Escherichia coli*. *FEMS Microbiology Letters*, *283*(1), 36–41.

Cha, H. J., Müller, R. T., & Pos, K. M. (2014). Switch-loop flexibility affects transport of large drugs by the promiscuous AcrB multidrug efflux transporter. *Antimicrobial Agents and Chemotherapy*, *58*(8), 4767–4772.

Characklis, W. G. (1981). Bioengineering report: Fouling biofilm development: A process analysis. *Biotechnology and Bioengineering*, *23*(9), 1923–1960.

Chatterjee, N., Banerjee, T., & Datta, S. (2012). Accurate estimation of nucleic acids by amplification efficiency dependent PCR. *PLoS ONE*, *7*(8), e42063.

Christie, P. J., & Vogel, J. P. (2000). Bacterial type IV secretion: conjugation systems adapted to deliver effector molecules to host cells. *Trends in Microbiology*, *8*(8), 354.

CLSI. (2018). Methods for Dilution Antimicrobial Susceptibility Tests for Bacteria That Grow Aerobically (11th ed.). *CLSI Standard M07*. Wayne, PA: Clinical and Laboratory Standards Institute.

Coculescu, B. I. (2009). Antimicrobial resistance induced by genetic changes. *Journal of Medicine and Life*, *2*(2), 114.

Collignon, P. J., & McEwen, S. A. (2019). One Health—Its Importance in Helping to Better Control Antimicrobial Resistance. *Tropical Medicine and Infectious Disease*, *4*(1).

Cudkowicz, N. A., & Schuldiner, S. (2019). Deletion of the major *Escherichia coli* multidrug transporter AcrB reveals transporter plasticity and redundancy in bacterial cells. *PLoS ONE*, *14*(6).

Danese, P. N., Pratt, L. A., Dove, S. L., & Kolter, R. (2000). The outer membrane protein, Antigen 43, mediates cell-to-cell interactions within *Escherichia coli* biofilms. *Molecular Microbiology*, *37*(2), 424–432.

Danese, P. N., Pratt, L. A., & Kolter, R. (2000). Exopolysaccharide production is required for development of *Escherichia coli K-12* biofilm architecture. *Journal of Bacteriology*, *182*(12), 3593–3596.

Darby, E. M., Trampari, E., Siasat, P., Gaya, M. S., Alav, I., Webber, M. A., & Blair, J. M. A. (2022). Molecular mechanisms of antibiotic resistance revisited. *Nature Reviews Microbiology 2022*, 1–16.

Das, J., Mokrzan, E., Lakhani, V., Rosas, L., Jurcisek, J. A., Ray, W. C., & Bakaletz, L. O. (2017). Extracellular DNA and type IV pilus expression regulate the structure and kinetics of biofilm formation by nontypeable *Haemophilus influenzae*. *mBio*, *8*(6).

Datsenko, K. A., & Wanner, B. L. (2000). One-step inactivation of chromosomal genes in *Escherichia coli K-12* using PCR products. *Proc. Natl Acad. Sci. USA*, *97*(12), 6640–6645.

Daury, L., Orange, F., Taveau, J. C., Verchère, A., Monlezun, L., Gounou, C., Marreddy, R. K. R., Picard, M., Broutin, I., Pos, K. M., & Lambert, O. (2016). Tripartite assembly of RND multidrug efflux pumps. *Nature Communications*, *7*.

de Kraker, M. E. A., Stewardson, A. J., & Harbarth, S. (2016). Will 10 Million People Die a Year due to Antimicrobial Resistance by 2050? *PLoS Medicine*, *13*(11), 1002184.

De Oliveira, D. M. P., Forde, B. M., Kidd, T. J., Harris, P. N. A., Schembri, M. A., Beatson, S. A., Paterson, D. L., & Walker, M. J. (2020). Antimicrobial Resistance in ESKAPE Pathogens. *Clin Microbiol Rev.* 33(3):e00181-19.

DeLano, W. L. (2002). *The PyMOL Molecular Graphics System, Schrödinger, LLC.* http://www.pymol.org/.

Denissen, J., Reyneke, B., Waso-Reyneke, M., Havenga, B., Barnard, T., Khan, S., & Khan, W. (2022). Prevalence of ESKAPE pathogens in the environment: Antibiotic resistance status, community-acquired infection and risk to human health. *International Journal of Hygiene and Environmental Health*, *244*, 114006.

Domka, J., Lee, J., Bansal, T., & Wood, T. K. (2007). Temporal gene-expression in *Escherichia coli K-12* biofilms. *Environmental Microbiology*, *9*(2), 332–346.

Du, D., Wang, Z., James, N. R., Voss, J. E., Klimont, E., Ohene-Agyei, T., Venter, H., Chiu, W., & Luisi, B. F. (2014). Structure of the AcrAB-TolC multidrug efflux pump. *Nature*, *509*(7501), 512–515.

Ducret, V., Gonzalez, M. R., Leoni, S., Valentini, M., & Perron, K. (2020). The CzcCBA Efflux System Requires the CadA P-Type ATPase for Timely Expression Upon Zinc Excess in *Pseudomonas aeruginosa*. *Frontiers in Microbiology*, *11*,

530550.

El-Halfawy, O. M., & Valvano, M. A. (2015). Antimicrobial heteroresistance: an emerging field in need of clarity. *Clinical Microbiology Reviews*, *28*(1), 191–207.

Elkins, C. A., & Nikaido, H. (2003). Chimeric analysis of AcrA function reveals the importance of its C-terminal domain in its interaction with the AcrB multidrug efflux pump. *J Bacteriol*.;185(18):5349-56.

Etebu, E., & Arikekpar, I. (2016). Antibiotics: Classification and mechanisms of action with emphasis on molecular perspectives. *IJAMBR*, *4*, 90–101.

Evans, M. L., & Chapman, M. R. (2014). Curli biogenesis: Order out of disorder. *Biochimica et Biophysica Acta - Molecular Cell Research*, *1843*(8), 1551–1558.

Ferreira, R. L., Da Silva, B. C. M., Rezende, G. S., Nakamura-Silva, R., Pitondo-Silva, A., Campanini, E. B., Brito, M. C. A., Da Silva, E. M. L., De Melo Freire, C. C., Da Cunha, A. F., & Da Silva Pranchevicius, M. C. (2019). High Prevalence of Multidrug-Resistant *Klebsiella pneumoniae* Harboring Several Virulence and β-Lactamase Encoding Genes in a Brazilian Intensive Care Unit. *Front Microbiol.* 22;9:3198.

Flemming, H. C., Neu, T. R., & Wozniak, D. J. (2007). The EPS matrix: The "House of Biofilm Cells." *Journal of Bacteriology*, *189*(22), 7945–7947.

Flemming, H. C., Wingender, J., Szewzyk, U., Steinberg, P., Rice, S. A., & Kjelleberg, S. (2016). Biofilms: An emergent form of bacterial life. *Nature Reviews Microbiology*, *14*(9), 563–575.

García-Betancur, J. C., Moreno, A. G., Horger, T., Schott, M., Sharan, M., Eikmeier, J., Wohlmuth, B., Zernecke, A., Ohlsen, K., Kuttler, C., & Lopez, D. (2017). Cell differentiation defines acute and chronic infection cell types in *Staphylococcus aureus*. *eLife*, *6*.

Gervasoni, S., Malloci, G., Bosin, A., Vargiu, A. V., Zgurskaya, H. I., & Ruggerone, P. (2022). Recognition of quinolone antibiotics by the multidrug efflux transporter MexB of *Pseudomonas aeruginosa*. *Physical Chemistry Chemical Physics*, *24*(27), 16566–16575.

Ghosh, A., Jayaraman, N., & Chatterji, D. (2020). Small-Molecule Inhibition of

Bacterial Biofilm. *ACS Omega, 5*(7), 3108–3115.

Ghosh, P., Ben-Jacob, E., & Levine, H. (2013). Modeling cell-death patterning during biofilm formation. *Physical Biology, 10*(6).

Ghosh, P., Mondal, J., Ben-Jacob, E., & Levine, H. (2015). Mechanically-driven phase separation in a growing bacterial colony. *Proc Natl Acad Sci U S A.*, *112*(17), E2166–E2173.

Global AMR R&D Hub & WHO. (2023). Incentivising the development of new antibacterial treatments 2023. Progress Report by *Global AMR R&D Hub & WHO*, 1-16.

Goller, C., Wang, X., Itoh, Y., & Romeo, T. (2006). The cation-responsive protein NhaR of *Escherichia coli* activates *pgaABCD* transcription, required for production of the biofilm adhesin poly-β-1,6-N-acetyl-D-glucosamine. *Journal of Bacteriology*, *188*(23), 8022–8032.

González Barrios, A. F., Zuo, R., Hashimoto, Y., Yang, L., Bentley, W. E., & Wood, T. K. (2006). Autoinducer 2 controls biofilm formation in *Escherichia coli* through a novel motility quorum-sensing regulator (MqsR, B3022). *Journal of Bacteriology*, *188*(1), 305–316.

Green, A. B., Chiaraviglio, L., Truelson, K. A., Zulauf, K. E., Cui, M., Zhang, Z., Ware, M. P., Flegel, W. A., Haspel, R. L., Yu, E. W., & Kirby, J. E. (2023). RND Pump-Mediated Efflux of Amotosalen, a Compound Used in Pathogen Inactivation Technology to Enhance Safety of Blood Transfusion Products, May Compromise Its Gram-Negative Anti-Bacterial Activity. *mSphere*, 8(2):e0067322.

Gualdi, L., Tagliabue, L., Bertagnoli, S., Ieranò, T., De Castro, C., & Landini, P. (2008). Cellulose modulates biofilm formation by counteracting curli-mediated colonization of solid surfaces in *Escherichia coli*. *Microbiology, 154*(7), 2017–2024.

Guttenplan, S. B., & Kearns, D. B. (2013). Regulation of flagellar motility during biofilm formation. *FEMS Microbiology Reviews*, *37*(6), 849–871.

Guzmán-Soto, I., McTiernan, C., Gonzalez-Gomez, M., Ross, A., Gupta, K., Suuronen, E. J., Mah, T. F., Griffith, M., & Alarcon, E. I. (2021). Mimicking biofilm

formation and development: Recent progress in *in vitro* and *in vivo* biofilm models. *iScience*, *24*(5), 102443.

Hall-Stoodley, L., Costerton, J. W., & Stoodley, P. (2004). Bacterial biofilms: From the natural environment to infectious diseases. *Nature Reviews Microbiology*, *2*(2), 95–108.

Hameed P, S., Bharatham, N., Katagihallimath, N., Sharma, S., Nandishaiah, R., Shanbhag, A. P. A. P., Thomas, T., Narjari, R., Sarma, M., Bhowmik, P., Amar, P., Ravishankar, R., Jayaraman, R., Muthan, K., Subbiah, R., Ramachandran, V., Balasubramanian, V., & Datta, S. (2018). Nitrothiophene carboxamides, a novel narrow spectrum antibacterial series: Mechanism of action and Efficacy. *Scientific Reports*, *8*(1), 1–18.

Hansen, L., Jensen, L., Sørensen, H., & Sørensen, S. (2007). Substrate specificity of the OqxAB multidrug resistance pump in *Escherichia coli* and selected enteric bacteria. *Journal of Antimicrobial Chemotherapy*, *60*(1), 145–147.

Hardie, K. R., & Fenn, S. J. (2022). JMM profile: rifampicin: a broad-spectrum antibiotic. *Journal of Medical Microbiology*, *71*(8).

Harrison, F., Roberts, A. E. L., Gabrilska, R., Rumbaugh, K. P., Lee, C., & Diggle, S. P. (2015). A 1,000-Year-Old Antimicrobial Remedy with Antistaphylococcal Activity. *MBio*, *6*(4), 1129–1144.

Hartmann, R., Singh, P. K., Pearce, P., Mok, R., Song, B., Díaz-Pascual, F., Dunkel, J., & Drescher, K. (2019). Emergence of three-dimensional order and structure in growing biofilms. *Nature Physics*, *15*(3), 251–256.

Hauryliuk, V., Atkinson, G. C., Murakami, K. S., Tenson, T., & Gerdes, K. (2015). Recent functional insights into the role of (p)ppGpp in bacterial physiology. *Nature Reviews Microbiology*, *13*(5), 298–309.

Hayashi, K., Nakashima, R., Sakurai, K., Kitagawa, K., Yamasaki, S., Nishino, K., & Yamaguchi, A. (2016). AcrB-AcrA Fusion Proteins That Act as Multidrug Efflux Transporters. *Journal of Bacteriology*, *198*(2), 332.

Henderson, P. J. F., Maher, C., Elbourne, L. D. H., Eijkelkamp, B. A., Paulsen, I. T., & Hassan, K. A. (2021). Physiological Functions of Bacterial “multidrug” Efflux

Pumps. *Chemical Reviews*, *121*(9), 5417–5478.

Hengge, R. (2013). Novel tricks played by the second messenger c-di-GMP in bacterial biofilm formation. *EMBO Journal*, *32*(3), 322–323.

Hernando-Amado, S., Blanco, P., Alcalde-Rico, M., Corona, F., Reales-Calderón, J. A., Sánchez, M. B., & Martínez, J. L. (2016). Multidrug efflux pumps as main players in intrinsic and acquired resistance to antimicrobials. *Drug Resistance Updates : Reviews and Commentaries in Antimicrobial and Anticancer Chemotherapy*, *28*, 13–27.

Hobbs, J. K., & Boraston, A. B. (2019). (p)ppGpp and the Stringent Response: An Emerging Threat to Antibiotic Therapy. *ACS Infectious Diseases*, *5*(9), 1505–1517.

Holmes, A. H., Moore, L. S. P., Sundsfjord, A., Steinbakk, M., Regmi, S., Karkey, A., Guerin, P. J., & Piddock, L. J. V. (2016). Understanding the mechanisms and drivers of antimicrobial resistance. *Lancet*, *387*(10014), 176–187.

Hong, B. K., Wang, M., Chi, H. P., Kim, E. C., Jacoby, G. A., & Hooper, D. C. (2009). oqxAB encoding a multidrug efflux pump in human clinical isolates of *Enterobacteriaceae*. *Antimicrobial Agents and Chemotherapy*, *53*(8), 3582–3584.

Horiyama, T., & Nishino, K. (2014). AcrB, AcrD, and MdtABC Multidrug Efflux Systems Are Involved in Enterobactin Export in *Escherichia coli*. *PLOS ONE*, *9*(9), e108642.

Horn, H., & Lackner, S. (2014). Modeling of biofilm systems: A review. *Advances in Biochemical Engineering/Biotechnology*, *146*, 53–76.

Huang, L., Wu, C., Gao, H., Xu, C., Dai, M., Huang, L., Hao, H., Wang, X., & Cheng, G. (2022). Bacterial Multidrug Efflux Pumps at the Frontline of Antimicrobial Resistance: An Overview. *Antibiotics*, *11*(4), 520.

Hufnagel, D. A., Depas, W. H., & Chapman, M. R. (2015). The Biology of the *Escherichia coli* Extracellular Matrix. *Microbiology Spectrum*, *3*(3), 1–14.

Hufnagel, D. A., Evans, M. L., Greene, S. E., Pinkner, J. S., Hultgren, S. J., & Chapman, M. R. (2016). The catabolite repressor protein-cyclic AMP complex regulates CsgD and biofilm formation in uropathogenic *Escherichia coli*. *Journal of*

Bacteriology, *198*(24), 3329–3334.

Hung, C., Zhou, Y., Pinkner, J. S., Dodson, K. W., Crowley, J. R., Heuser, J., Chapman, M. R., Hadjifrangiskou, M., Henderson, J. P., & Hultgren, S. J. (2013). *Escherichia coli* biofilms have an organized and complex extracellular matrix structure. *mBio*, *4*(5), 645–658.

Hutchings, M., Truman, A., & Wilkinson, B. (2019). Antibiotics: past, present and future. *Current Opinion in Microbiology*, *51*, 72–80.

Itou, J., Eguchi, Y., & Utsumi, R. (2009). Molecular mechanism of transcriptional cascade initiated by the EvgS/EvgA system in *Escherichia coli K-12*. *Bioscience, Biotechnology and Biochemistry*, *73*(4), 870–878.

Jackson, D. W., Simecka, J. W., & Romeo, T. (2002). Catabolite repression of *Escherichia coli* biofilm formation. *Journal of Bacteriology*, *184*(12), 3406–3410.

Jackson, D. W., Suzuki, K., Oakford, L., Simecka, J. W., Hart, M. E., & Romeo, T. (2002). Biofilm formation and dispersal under the influence of the global regulator CsrA of *Escherichia coli*. *Journal of Bacteriology*, *184*(1), 290–301.

Jamshidi, S., Sutton, J. M., & Rahman, K. M. (2016). An overview of bacterial efflux pumps and computational approaches to study efflux pump inhibitors. *Future Med Chem.*8(2):195-210.

Jaskolski, M., Dauter, Z., & Wlodawer, A. (2014). A brief history of macromolecular crystallography, illustrated by a family tree and its Nobel fruits. *FEBS J*, *281*(18), 3985–4009.

Jefferson, K. K. (2004). What drives bacteria to produce a biofilm? *FEMS Microbiology Letters*, *236*(2), 163–173.

Jian, Z., Zeng, L., Xu, T., Sun, S., Yan, S., Yang, L., Huang, Y., Jia, J., & Dou, T. (2021). Antibiotic resistance genes in bacteria: Occurrence, spread, and control. *Journal of Basic Microbiology*, *61*(12), 1049–1070.

Jim O'Neil. (2014). Antimicrobial Resistance: Tackling a crisis for the health and wealth of nations. *The Review on Antimicrobial Resistance*, *20*, 1–16.

Jingjing Zhao, Chen, Z., Chen, S., Deng, Y., Liu, Y., Tian, W., Huang, X., Wu, C., Sun,

Y., Sun, Y., Zeng, Z., & Liu, J.-H. (2010). Prevalence and dissemination of OqxAB in *Escherichia coli* isolates from animals, farmworkers, and the environment. *Antimicrobial Agents and Chemotherapy*, *54*(10), 4219–4224.

Joao B Xavier, Picioreanu, C., & Loosdrecht, M. C. M. van. (2005). A framework for multidimensional modelling of activity and structure of multispecies biofilms. *Environmental Microbiology*, *7*(8), 1085–1103.

Johannesen, L. H. H. E., Burmølle, M., Sørensen, A. H., & Sørensen, S. J. (2004). Plasmid-encoded multidrug efflux pump conferring resistance to olaquindox in *Escherichia coli*. *Antimicrobial Agents and Chemotherapy*, *48*(9), 3332–3337.

Kalia, D., Merey, G., Nakayama, S., Zheng, Y., Zhou, J., Luo, Y., Guo, M., Roembke, B. T., & Sintim, H. O. (2013). Nucleotide, c-di-GMP, c-di-AMP, cGMP, cAMP, (p)ppGpp signaling in bacteria and implications in pathogenesis. *Chemical Society Reviews*, *42*(1), 305–341.

Kapoor, G., Saigal, S., & Elongavan, A. (2017). Action and resistance mechanisms of antibiotics: A guide for clinicians. *J Anaesthesiol Clin Pharmacol.*, *33*(3), 300.

Kasari, V., Kurg, K., Margus, T., Tenson, T., & Kaldalu, N. (2010). The *Escherichia coli mqsR* and *ygiT* genes encode a new toxin-antitoxin pair. *Journal of Bacteriology*, *192*(11), 2908–2919.

Kawamura-Sato, K., Shibayama, K., Horii, T., Iimuma, Y., Arakawa, Y., & Ohta, M. (1999). Role of multiple efflux pumps in *Escherichia coli* in indole expulsion. *FEMS Microbiology Letters*, *179*(2), 345–352.

Keseler, I. M., Mackie, A., Santos-Zavaleta, A., Billington, R., Bonavides-Martínez, C., Caspi, R., Fulcher, C., Gama-Castro, S., Kothari, A., Krummenacker, M., Latendresse, M., Muñiz-Rascado, L., Ong, Q., Paley, S., Peralta-Gil, M., Subhraveti, P., Velázquez-Ramírez, D. A., Weaver, D., Collado-Vides, J., … Karp, P. D. (2017). The EcoCyc database: Reflecting new knowledge about *Escherichia coli K-12*. *Nucleic Acids Research*, *45*(D1), D543–D550.

Kikuchi, T., Mizunoe, Y., Takade, A., Naito, S., & Yoshida, S. I. (2005). Curli fibers are required for development of biofilm architecture in *Escherichia coli K-12* and enhance bacterial adherence to human uroepithelial cells. *Microbiology and Immunology*, *49*(9), 875–884.

Kim, H. M., Xu, Y., Lee, M., Piao, S., Sim, S. H., Ha, N. C., & Lee, K. (2010). Functional relationships between the AcrA hairpin tip region and the TolC aperture tip region for the formation of the bacterial tripartite efflux pump AcrAB-TolC. *Journal of Bacteriology*, *192*(17), 4498–4503.

Kim, J., & Park, W. (2015). Indole: a signaling molecule or a mere metabolic byproduct that alters bacterial physiology at a high concentration? *Journal of Microbiology*, 53(7), 421–428.

Klapper, I., & Dockeryt, J. (2010). Mathematical description of microbial biofilms. In *Society for Industrial and Applied Mathematics (SIAM) Review*, 52(2), 221–265.

Kobayashi, A., Hirakawa, H., Hirata, T., Nishino, K., & Yamaguchi, A. (2006). Growth phase-dependent expression of drug exporters in *Escherichia coli* and its contribution to drug tolerance. *Journal of Bacteriology*, *188*(16), 5693–5703.

Koo, H., Allan, R. N., Howlin, R. P., Stoodley, P., & Hall-Stoodley, L. (2017). Targeting microbial biofilms: Current and prospective therapeutic strategies. In *Nature Reviews Microbiology*, 15(12), 740–755.

Koshy-Chenthittayil, S., Archambault, L., Senthilkumar, D., Laubenbacher, R., Mendes, P., & Dongari-Bagtzoglou, A. (2021). Agent based models of polymicrobial biofilms and the micro-biome—a review. *Microorganisms*, *9*(2), 1–23.

Kostakioti, M., Hadjifrangiskou, M., & Hultgren, S. J. (2013). Bacterial biofilms: Development, dispersal, and therapeutic strategies in the dawn of the postantibiotic era. *Cold Spring Harbor Perspectives in Medicine*, *3*(4).

Krishnamoorthy, G., Tikhonova, E. B., & Zgurskaya, H. I. (2008). Fitting periplasmic membrane fusion proteins to inner membrane transporters: Mutations that enable Escherichia coli AcrA to function with *Pseudomonas aeruginosa* MexB. *Journal of Bacteriology*, *190*(2), 691–698.

Król, J. E., Hall, D. C., Balashov, S., Pastor, S., Sibert, J., McCaffrey, J., Lang, S., Ehrlich, R. L., Earl, J., Mell, J. C., Xiao, M., & Ehrlich, G. D. (2019). Genome rearrangements induce biofilm formation in *Escherichia coli C* - an old model organism with a new application in biofilm research. *BMC Genomics*, *20*(1).

Kvist, M., Hancock, V., & Klemm, P. (2008). Inactivation of efflux pumps abolishes bacterial biofilm formation. *Applied and Environmental Microbiology*, *74*(23), 7376–7382.

Laverty, G., Gorman, S. P., & Gilmore, B. F. (2014). Biomolecular mechanisms of *Pseudomonas aeruginosa* and *Escherichia coli* biofilm formation. *Pathogens*, *3*(3), 596–632.

Lazar, V. (2011). Quorum sensing in biofilms - How to destroy the bacterial citadels or their cohesion/power? *Anaerobe*, *17*(6), 280–285.

Ledger, E. V. K., Sabnis, A., & Edwards, A. M. (2022). Polymyxin and lipopeptide antibiotics: membrane-targeting drugs of last resort. *Microbiology*, *168*(2), 1136.

Lee, J. H., & Lee, J. (2010). Indole as an intercellular signal in microbial communities. *FEMS Microbiology Reviews*, *34*(4), 426–444.

Lee, J., Jayaraman, A., & Wood, T. K. (2007). Indole is an inter-species biofilm signal mediated by SdiA. *BMC Microbiology*, 18;7:42.

Lee, J., Maeda, T., Hong, S. H., & Wood, T. K. (2009). Reconfiguring the quorum-sensing regulator SdiA of *Escherichia coli* to control biofilm formation via indole and N-acylhomoserine lactones. In *Applied and Environmental Microbiology* 75 (6), 1703–1716).

Li, J., Attila, C., Wang, L., Wood, T. K., Valdes, J. J., & Bentley, W. E. (2007). Quorum sensing in *Escherichia coli* is signaled by AI-2/LsrR: Effects on small RNA and biofilm architecture. *Journal of Bacteriology*, *189*(16), 6011–6020.

Li, J., Zhang, H., Ning, J., Sajid, A., Cheng, G., Yuan, Z., & Hao, H. (2019). The nature and epidemiology of OqxAB, a multidrug efflux pump. *Antimicrobial Resistance and Infection Control*, *8*(1), 1–13.

Li, Q., Xia, P. F., Tao, Z. Y., & Wang, S. G. (2017). Modeling biofilms in water systems with new variables: A review. *Water (Switzerland)*, *9*(7), 1–12.

Li, Y. H., & Tian, X. (2012). Quorum sensing and bacterial social interactions in biofilms. *Sensors*, *12*(3), 2519–2538.

Liang, Z., Li, L., Wang, Y., Chen, L., Kong, X., Hong, Y., Lan, L., Zheng, M., Guang-

Yang, C., Liu, H., Shen, X., Luo, C., Li, K. K., Chen, K., & Jiang, H. (2011). Molecular Basis of NDM-1, a New Antibiotic Resistance Determinant. *PLoS ONE*, *6*(8), 23606.

Liangxing Fang, Li, X., Li, L., Li, S., Liao, X., Sun, J., & Liu, Y. (2016). Co-spread of metal and antibiotic resistance within ST3-IncHI2 plasmids from *E. coli* isolates of food-producing animals. *Sci Rep*, *6*, 25312.

Liu, C., Sun, D., Zhu, J., Liu, J., & Liu, W. (2020). The Regulation of Bacterial Biofilm Formation by cAMP-CRP: A Mini-Review. *Frontiers in Microbiology*, 14;11:802, 1–7.

Livak, K. J., & Schmittgen, T. D. (2001). Analysis of relative gene expression data using real-time quantitative PCR and the $2^{-\Delta\Delta CT}$ method. *Methods*, *25*(4), 402–408.

Lu, W., Zhong, M., Chai, Q., Wang, Z., Yu, L., & Wei, Y. (2014). Functional Relevance of AcrB Trimerization in Pump Assembly and Substrate Binding. *PLoS ONE*, *9*(2), e89143.

Ma, Z., Masuda, N., & Foster, J. W. (2004). Characterization of EvgAS-YdeO-GadE branched regulatory circuit governing glutamate-dependent acid resistance in *Escherichia coli*. *Journal of Bacteriology*, *186*(21), 7378–7389.

Ma, Z., Richard, H., & Foster, J. W. (2003). pH-Dependent Modulation of Cyclic AMP Levels and GadW-Dependent Repression of RpoS Affect Synthesis of the GadX Regulator and *Escherichia coli* Acid Resistance. *Journal of Bacteriology*, *185*(23), 6852–6859.

MacNair, C. R., Rutherford, S. T., & Tan, M.-W. (2023). Alternative therapeutic strategies to treat antibiotic-resistant pathogens. *Nature Reviews Microbiology 2023*, 1–14.

Martinez, J. L., Sánchez, M. B., Martínez-Solano, L., Hernandez, A., Garmendia, L., Fajardo, A., & Alvarez-Ortega, C. (2009). Functional role of bacterial multidrug efflux pumps in microbial natural ecosystems. *FEMS Microbiology Reviews*, *33*(2), 430–449.

Masuda, N., & Church, G. M. (2002). *Escherichia coli* gene expression responsive to levels of the response regulator EvgA. *Journal of Bacteriology*, *184*(22), 6225–

6234.

Masuda, N., & Church, G. M. (2003). Regulatory network of acid resistance genes in Escherichia coli. *Molecular Microbiology*, *48*(3), 699–712.

Matsumura, K., Furukawa, S., Ogihara, H., & Morinaga, Y. (2011). Roles of multidrug efflux pumps on the biofilm formation of *Escherichia coli K-12*. *Biocontrol Science*, *16*(2), 69–72.

Matsunaga, Y., Yamane, T., Terada, T., Moritsugu, K., Fujisaki, H., Murakami, S., Ikeguchi, M., & Kidera, A. (2018). Energetics and conformational pathways of functional rotation in the multidrug transporter AcrB. *eLife*, 6:7:e31715.

Mattei, M. R., Frunzo, L., D'Acunto, B., Pechaud, Y., Pirozzi, F., & Esposito, G. (2018). Continuum and discrete approach in modeling biofilm development and structure: a review. *Journal of Mathematical Biology*, *76*(4), 945–1003.

McKinney, W. (2010). Data Structures for Statistical Computing in Python. In *Proceedings of the 9th Python in Science Conference*. SciPy.

Micevski, D., Zammit, J. E., Truscott, K. N., & Dougan, D. A. (2015). Anti-adaptors use distinct modes of binding to inhibit the RssB-dependent turnover of RpoS (σS) by ClpXP. *Front Mol Biosci. 2015 Apr 23;2:15*.

Mikolosko, J., Bobyk, K., Zgurskaya, H. I., & Ghosh, P. (2006). Conformational flexibility in the multidrug efflux system protein AcrA. *Structure (London, England : 1993)*, *14*(3), 577–587.

Minagawa, S., Inami, H., Kato, T., Sawada, S., Yasuki, T., Miyairi, S., Horikawa, M., Okuda, J., & Gotoh, N. (2012). RND type efflux pump system MexAB-OprM of *Pseudomonas aeruginosa* selects bacterial languages, 3-oxo-acyl-homoserine lactones, for cell-to-cell communication. *BMC Microbiology*, 10;12:70.

Miroux, B., & Walker, J. E. (1996). Over-production of proteins in *Escherichia coli*: mutant hosts that allow synthesis of some membrane proteins and globular proteins at high levels. *J Mol Biol. 260*(3), 289–298.

Moore-Machacek, A., Gloe, A., O'Leary, N., & Reen, F. J. (2023). Efflux, Signaling and Warfare in a Polymicrobial World. *Antibiotics 2023, 12*(4), 731.

Mulani, M. S., Kamble, E. E., Kumkar, S. N., Tawre, M. S., & Pardesi, K. R. (2019). Emerging Strategies to Combat ESKAPE Pathogens in the Era of Antimicrobial Resistance: A Review. *Frontiers in Microbiology*, 1;10:539.

Munita, J. M., & Arias, C. A. (2016). Mechanisms of Antibiotic Resistance. *Microbiology Spectrum*, *4*(2).

Murakami, S. (2008). Multidrug efflux transporter, AcrB-the pumping mechanism. *Current Opinion in Structural Biology*, *18*(4), 459–465.

Murakami, S. (2016). Structures and Transport Mechanisms of RND Efflux Pumps. In: Li, XZ., Elkins, C., Zgurskaya, H. (eds) Efflux-Mediated Antimicrobial Resistance in Bacteria. Adis, Cham.

Murakami, S., Nakashima, R., Yamashita, E., Matsumoto, T., & Yamaguchi, A. (2006). Crystal structures of a multidrug transporter reveal a functionally rotating mechanism. *Nature*, *443*(7108), 173–179.

Murakami, S., Nakashima, R., Yamashita, E., & Yamaguchi, A. (2002). Crystal structure of bacterial multidrug efflux transporter AcrB. *Nature*, *419*(6907), 587–593.

Murata, T., Kuwagaki, M., Shin, T., Gotoh, N., & Nishino, T. (2002). The substrate specificity of tripartite efflux systems of *Pseudomonas aeruginosa* is determined by the RND component. *Biochemical and Biophysical Research Communications*, *299*(2), 247–251.

Murray, C. J., Ikuta, K. S., Sharara, F., Swetschinski, L., Robles Aguilar, G., Gray, A., Han, C., Bisignano, C., Rao, P., Wool, E., Johnson, S. C., Browne, A. J., Chipeta, M. G., Fell, F., Hackett, S., Haines-Woodhouse, G., Kashef Hamadani, B. H., Kumaran, E. A. P., McManigal, B., … Naghavi, M. (2022). Global burden of bacterial antimicrobial resistance in 2019: a systematic analysis. *The Lancet*, *399*(10325), 629–655.

Nair, A. V., Lee, K. W., & van Veen, H. W. (2016). Structural and Functional Landscape of MFS and MATE Efflux Pumps. *Efflux-Mediated Antimicrobial Resistance in Bacteria*, 29–44.

Nakashima, R., Sakurai, K., Yamasaki, S., Hayashi, K., Nagata, C., Hoshino, K.,

Onodera, Y., Nishino, K., & Yamaguchi, A. (2013). Structural basis for the inhibition of bacterial multidrug exporters. *Nature*, *500*(7460), 102–106.

Neuberger, A., Du, D., & Luisi, B. F. (2018). Structure and mechanism of bacterial tripartite efflux pumps. *Research in Microbiology*, *169*(7–8), 401–413.

Ni, R. T., Onishi, M., Mizusawa, M., Kitagawa, R., Kishino, T., Matsubara, F., Tsuchiya, T., Kuroda, T., & Ogawa, W. (2020). The role of RND-type efflux pumps in multidrug-resistant mutants of *Klebsiella pneumoniae*. Scientific Reports, 10(1), 1–10.

Niba, E. T. E., Naka, Y., Nagase, M., Mori, H., & Kitakawa, M. (2007). A genome-wide approach to identify the genes involved in biofilm formation in *E. coli*. *DNA Research*, *14*(6), 237–246.

Nicolaou, K. C., & Rigol, S. (2017). A brief history of antibiotics and select advances in their synthesis. *The Journal of Antibiotics 2018 71:2*, *71*(2), 153–184.

Nijland, R., Hall, M. J., & Grant Burgess, J. (2010). Dispersal of biofilms by secreted, matrix degrading, Bacterial DNase. *PLoS ONE*, *5*(12), 1–7.

Nikaido, H. (2009). Multidrug Resistance in Bacteria. *Annual Review of Biochemistry*, *78*, 119.

Nikaido, H. (2011). Structure and mechanism of RND-type multidrug efflux pumps. *Adv. Enzymol. Relat. Areas*. Mol. Biol. *77*, 1.

Nikaido, H., & Pagès, J. M. (2012). Broad-specificity efflux pumps and their role in multidrug resistance of Gram-negative bacteria. *FEMS Microbiol. Rev.*, *36*(2), 340–363.

Nikaido, H., & Takatsuka, Y. (2009). Mechanisms of RND multidrug efflux pumps. *Biochimica et Biophysica Acta - Proteins and Proteomics*, *1794*(5), 769–781.

Nikaido, H., & Zgurskaya, H. I. (2001). AcrAB and related multidrug efflux pumps of *Escherichia coli*. *J Mol Microbiol Biotechno*, *3*(2), 215–218.

Nishino, K., Senda, Y., Hayashi-Nishino, M., & Yamaguchi, A. (2009). Role of the AraC–XylS family regulator YdeO in multi-drug resistance of *Escherichia coli*. *The Journal of Antibiotics 2009 62:5*, *62*(5), 251–257.

O'Toole, G. A. (2011). Microtiter Dish Biofilm Formation Assay. *Journal of Visualized Experiments : JoVE*, *47*.

Okada, U., & Murakami, S. (2022). Structural and functional characteristics of the tripartite ABC transporter. *Microbiology (Reading, England)*, *168*(11).

Okshevsky, M., Regina, V. R., & Meyer, R. L. (2015). Extracellular DNA as a target for biofilm control. *Current Opinion in Biotechnology*, *33*, 73–80.

Orelle, C., & Jault, J.-M. (2016). Structures and Transport Mechanisms of the ABC Efflux Pumps. In H. Li, XZ., Elkins, C., Zgurskaya (Ed.), Efflux-Mediated Antimicrobial Resistance in Bacteria. *Adis, Cham.* Springer International Publishing.

Ornik-Cha, A., Wilhelm, J., Kobylka, J., Sjuts, H., Vargiu, A. V., Malloci, G., Reitz, J., Seybert, A., Frangakis, A. S., & Pos, K. M. (2021). Structural and functional analysis of the promiscuous AcrB and AdeB efflux pumps suggests different drug binding mechanisms. *Nature Communication*, *12*(1), 1–14.

Ovung, A., & Bhattacharyya, J. (2021). Sulfonamide drugs: structure, antibacterial property, toxicity, and biophysical interactions. *Biophysical Reviews*, *13*(2), 259.

Padan, E., Gerchman, Y., Rimon, A., Rothman, A., Dover, N., & Carmel-Harel, O. (1999). The molecular mechanism of regulation of the NhaA Na^+/H^+ antiporter of *Escherichia coli*, a key transporter in the adaptation to Na^+ and H^+. *Novartis Foundation Symposium*, *221*, 183–196.

Pagès, J. M., James, C. E., & Winterhalter, M. (2008). The porin and the permeating antibiotic: a selective diffusion barrier in Gram-negative bacteria. *Nature Reviews Microbiology 2008 6:12*, *6*(12), 893–903.

Pak-Leung Ho, Ng, K.-Y., Wai-U Lo, P., Law, Y., Lai, E. L.-Y., Wang, Y., & Chow, K.-H. (2016). Plasmid-mediated OqxAB is an important mechanism for nitrofurantoin resistance in *Escherichia coli*. *Antimicrobial Agents and Chemotherapy*, *60*(1), 537–543.

Panayidou, S., Georgiades, K., Christofi, T., Tamana, S., Promponas, V. J., & Apidianakis, Y. (2020). *Pseudomonas aeruginosa* core metabolism exerts a widespread growth-independent control on virulence. *Scientific Reports*, *10*(1), 1–

19.

Pandey, R., Swamy, K. V., & Khetmalas, M. B. (2013). Indole: A novel signaling molecule and its applications. *Indian Journal of Biotechnology*, *12*(3), 297–310.

Peleg, A. Y., & Hooper, D. C. (2010). Hospital-Acquired Infections Due to Gram-Negative Bacteria. *New England Journal of Medicine*, *362*(19), 1804–1813.

Pendleton, J. N., Gorman, S. P., & Gilmore, B. F. (2013). Clinical relevance of the ESKAPE pathogens. *Expert Rev Anti Infect Ther.*, *11*(3), 297–308.

Pesavento, C., Becker, G., Sommerfeldt, N., Possling, A., Tschowri, N., Mehlis, A., & Hengge, R. (2008). Inverse regulatory coordination of motility and curli-mediated adhesion in *Escherichia coli*. *Genes and Development*, *22*(17), 2434–2446.

Peters, B. M., Jabra-Rizk, M. A., O'May, G. A., William Costerton, J., & Shirtliff, M. E. (2012). Polymicrobial interactions: Impact on pathogenesis and human disease. *Clinical Microbiology Reviews*, *25*(1), 193–213.

Plotly Technologies Inc. (2015). Collaborative data science. Plotly Technologies Inc.; *Plotly Technologies Inc.* https://plot.ly

Pos, K. M. (2009). Drug transport mechanism of the AcrB efflux pump. *Biochim Biophys Acta.*, *1794*(5), 782–793.

Potrykus, K., & Cashel, M. (2008). (p)ppGpp: Still magical? *Annual Review of Microbiology*, *62*, 35–51.

Prajapati, J. D., Kleinekathöfer, U., & Winterhalter, M. (2021). How to Enter a Bacterium: Bacterial Porins and the Permeation of Antibiotics. *Chemical Reviews*, *121*(9), 5158–5192.

Pratt, L. A., & Kolter, R. (1998). Genetic analysis of *Escherichia coli* biofilm formation: Roles of flagella, motility, chemotaxis and type I pili. *Molecular Microbiology*, *30*(2), 285–293.

Prüß, B. M., Besemann, C., Denton, A., & Wolfe, A. J. (2006). A complex transcription network controls the early stages of biofilm development by *Escherichia coli*. *Journal of Bacteriology*, *188*(11), 3731–3739.

Quinn, R. A., Comstock, W., Zhang, T., Morton, J. T., Da Silva, R., Tran, A., Aksenov,

A., Nothias, L. F., Wangpraseurt, D., Melnik, A. V., Ackermann, G., Conrad, D., Klapper, I., Knight, R., & Dorrestein, P. C. (2018). Niche partitioning of a pathogenic microbiome driven by chemical gradients. *Science Advances*, *4*(9), eaau1908.

R Core Team, V. A. (2014). *R: A Language and Environment for Statistical Computing*. http://www.r-project.org/

Rahmati, S., Yang, S., Davidson, A. L., & Zechiedrich, E. L. (2002). Control of the AcrAB multidrug efflux pump by quorum-sensing regulator SdiA. *Molecular Microbiology*, *43*(3), 677–685.

Ramachandran, S., Kota, P., Ding, F., & Dokholyan, N. V. (2011). Automated minimization of steric clashes in protein structures. *Proteins*, *79*(1), 261–270.

Rampioni, G., Pillai, C. R., Longo, F., Bondì, R., Baldelli, V., Messina, M., Imperi, F., Visca, P., & Leoni, L. (2017). Effect of efflux pump inhibition on *Pseudomonas aeruginosa* transcriptome and virulence. *Scientific Reports 2017 7:1*, *7*(1), 1–14.

Rehman, S. (2023). A parallel and silent emerging pandemic: Antimicrobial resistance (AMR) amid COVID-19 pandemic. *Journal of Infection and Public Health*, *16*(4), 611.

Rice, L. B. (2010). Progress and Challenges in Implementing the Research on ESKAPE Pathogens. *Infection Control & Hospital Epidemiology*, *31*(S1), S7–S10.

Roch, M., Sierra, R., & Andrey, D. O. (2023). Antibiotic heteroresistance in ESKAPE pathogens, from bench to bedside. *Clinical Microbiology and Infection*, *29*(3), 320–325.

Rodríguez-Martínez, J. M., Alba, P. D. de, Briales, A., J Machuca, Lossa, M., Fernández-Cuenca, F., Baño, J. R., Martínez-Martínez, L., & Pascual, Á. (2013). Contribution of OqxAB efflux pumps to quinolone resistance in extended-spectrum-β-lactamase-producing *Klebsiella pneumoniae*. *J Antimicrob Chemother.*, 68(1), 68–73.

Römling, U., & Balsalobre, C. (2012). Biofilm infections, their resilience to therapy and innovative treatment strategies. *Journal of Internal Medicine*, *272*(6), 541–561.

Rosas, N. C., & Lithgow, T. (2022). Targeting bacterial outer-membrane remodelling

to impact antimicrobial drug resistance. *Trends in Microbiology*, *30*(6), 544–552.

Rossum, G. Van, & Drake, F. L. (2009). *Python 3 Reference Manual*. CreateSpace.

Ruggerone, P., Vargiu, A. V., Collu, F., Fischer, N., & Kandt, C. (2013). Molecular Dynamics Computer Simulations of Multidrug RND Efflux Pumps. *Computational and Structural Biotechnology Journal*, *5*(6), e201302008.

Ruiz, J. (2003). Mechanisms of resistance to quinolones: target alterations, decreased accumulation and DNA gyrase protection. *Journal of Antimicrobial Chemotherapy*, *51*(5), 1109–1117.

Sabnis, N. A., Yang, H., & Romeo, T. (1995). Pleiotropic regulation of central carbohydrate metabolism in *Escherichia coli* via the gene *csrA*. *Journal of Biological Chemistry*, *270*(49), 29096–29104.

Sakhtah, H., Koyama, L., Zhang, Y., Morales, D. K., Fields, B. L., Price-Whelan, A., Hogan, D. A., Shepard, K., & Dietrich, L. E. P. (2016). The *Pseudomonas aeruginosa* efflux pump MexGHI-OpmD transports a natural phenazine that controls gene expression and biofilm development. *Proc Natl Acad Sci U S A*, *113*(25), E3538–E3547.

Sakurai, K., Yamasaki, S., Nakao, K., Nishino, K., Yamaguchi, A., & Nakashima, R. (2019). Crystal structures of multidrug efflux pump MexB bound with high-molecular-mass compounds. *Scientific Reports 2019 9:1*, *9*(1), 1–9.

Salverda, M. L. M., Koomen, J., Koopmanschap, B., Zwart, M. P., & De Visser, J. A. G. M. (2017). Adaptive benefits from small mutation supplies in an antibiotic resistance enzyme. *Proc Natl Acad Sci U S A*, *114*(48), 12773–12778.

Santajit, S., & Indrawattana, N. (2016). Mechanisms of Antimicrobial Resistance in ESKAPE Pathogens. *Biomed Res Int. 2016:2475067.*

Sapula, S.A., Brown, M.H. (2016). Antimicrobial Drug Efflux Pumps in *Staphylococcus aureus* . In: Li, XZ., Elkins, C., Zgurskaya, H. (eds) *Efflux-Mediated Antimicrobial Resistance in Bacteria*. Adis, Cham.

Sarkar, P., Yarlagadda, V., Ghosh, C., & Haldar, J. (2017). A review on cell wall synthesis inhibitors with an emphasis on glycopeptide antibiotics. *MedChemComm*, *8*(3), 516.

Sauer, K., Stoodley, P., Goeres, D. M., Hall-Stoodley, L., Burmølle, M., Stewart, P. S., & Bjarnsholt, T. (2022). The biofilm life cycle: expanding the conceptual model of biofilm formation. *Nature Reviews Microbiology 20*(10), 608–620.

Schellhorn, H. E. (2020). Function, Evolution, and Composition of the RpoS Regulon in *Escherichia coli*. *Front Microbiol.* 17;11:560099.

Schembri, M. A., Kjærgaard, K., & Klemm, P. (2003). Global gene expression in *Escherichia coli* biofilms. *Molecular Microbiology*, *48*(1), 253–267.

Schinner, S., Engelhardt, F., Preusse, M., Thöming, J. G., Tomasch, J., & Häussler, S. (2020). Genetic determinants of *Pseudomonas aeruginosa* fitness during biofilm growth. *Biofilm*, *2*, 100023.

Schmittgen, T. D., & Livak, K. J. (2008). Analyzing real-time PCR data by the comparative C(T) method. *Nature Protocols*, *3*(6), 1101–1108.

Schuster, S., Kohler, S., Buck, A., Dambacher, C., König, A., Bohnert, J. A., & Kern, W. V. (2014). Random mutagenesis of the multidrug transporter AcrB from *Escherichia coli* for identification of putative target residues of efflux pump inhibitors. *Antimicrobial Agents and Chemotherapy*, *58*(11), 6870–6878.

Schuster, S., Vavra, M., Köser, R., Rossen, J. W. A., & Kern, W. V. (2021). New Topoisomerase Inhibitors: Evaluating the Potency of Gepotidacin and Zoliflodacin in Fluoroquinolone-Resistant *Escherichia coli* upon TolC Inactivation and Differentiating Their Efflux Pump Substrate Nature. *Antimicrobial Agents and Chemotherapy*, *65*(2).

Seeger, M. A., Schiefner, A., Eicher, T., Verrey, F., Diederichs, K., & Pos, K. M. (2006). Structural asymmetry of AcrB trimer suggests a peristaltic pump mechanism. *Science*, *313*(5791), 1295–1298.

Sennhauser, G., Bukowska, M. A., Briand, C., & Grütter, M. G. (2009). Crystal Structure of the Multidrug Exporter MexB from *Pseudomonas aeruginosa*. *Journal of Molecular Biology*, *389*(1), 134–145.

Šeputiene, V., Daugelavičius, A., Sužiedelis, K., & Sužiedeliene, E. (2006). Acid response of exponentially growing *Escherichia coli K-12*. *Microbiological Research*, *161*(1), 65–74.

Seyer, K., Lessard, M., Piette, G., Lacroix, M., & Saucier, L. (2003). *Escherichia coli* heat shock protein DnaK: production and consequences in terms of monitoring cooking. *Applied and Environmental Microbiology*, *69*(6), 3231–3237.

Shalá, A. A., Restrepo, S., & González Barrios, A. F. (2011). A network model for biofilm development in *Escherichia coli K-12*. *Theoretical Biology and Medical Modelling*, *8*(1), 34.

Shannon, P., Markiel, A., Ozier, O., Baliga, N. S., Wang, J. T., Ramage, D., Amin, N., Schwikowski, B., & Ideker, T. (2003). Cytoscape: A Software Environment for Integrated Models of Biomolecular Interaction Networks. *Genome Research*, *13*(11), 2498–2504.

Sharma, D., Misba, L., & Khan, A. U. (2019). Antibiotics versus biofilm: an emerging battleground in microbial communities. *Antimicrobial Resistance & Infection Control 2019 8:1*, *8*(1), 1–10.

Sheikh, J., Hicks, S., Dall'Agnol, M., Phillips, A. D., & Nataro, J. P. (2001). Roles for Fis and YafK in biofilm formation by enteroaggregative *Escherichia coli*. In *Molecular Microbiology* (Vol. 41, Issue 5, pp. 983–997).

Shigemura, K., Osawa, K., Kato, A., Tokimatsu, I., Arakawa, S., Shirakawa, T., & Fujisawa, M. (2015). Association of overexpression of efflux pump genes with antibiotic resistance in *Pseudomonas aeruginosa* strains clinically isolated from urinary tract infection patients. *The Journal of Antibiotics 2015 68:9*, *68*(9), 568–572.

Sievers, F., Wilm, A., Dineen, D., Gibson, T. J., Karplus, K., Li, W., Lopez, R., McWilliam, H., Remmert, M., Söding, J., Thompson, J. D., & Higgins, D. G. (2011). Fast, scalable generation of high-quality protein multiple sequence alignments using Clustal Omega. *Molecular Systems Biology*, *7*.

Singh, M., Yau, Y. C. W., Wang, S., Waters, V., & Kumar, A. (2017). MexXY efflux pump overexpression and aminoglycoside resistance in cystic fibrosis isolates of *Pseudomonas aeruginosa* from chronic infections. *Can J Microbiol.*, *63*(12), 929–938.

Singh, R., Ramachandran, V., Shandil, R., Sharma, S., Khandelwal, S., Karmarkar, M., Kumar, N., Solapure, S., Saralaya, R., Nanduri, R., Panduga, V., Reddy, J.,

Prabhakar, K. R., Rajagopalan, S., Rao, N., Narayanan, S., Anandkumar, A., Balasubramanian, V., & Dattaa, S. (2015). *In Silico*-based high-throughput screen for discovery of novel combinations for tuberculosis treatment. *Antimicrobial Agents and Chemotherapy*, *59*(9), 5664–5674.

Sjuts, H., Vargiu, A. V., Kwasny, S. M., Nguyen, S. T., Kim, H.-S. S., Ding, X., Ornik, A. R., Ruggerone, P., Bowlin, T. L., Nikaido, H., Pos, K. M., & Opperman, T. J. (2016). Molecular basis for inhibition of AcrB multidrug efflux pump by novel and powerful pyranopyridine derivatives. *Proc Natl Acad Sci U S A*, *113*(13), 3509–3514.

Skalet, A. H., Cevallos, V., Ayele, B., Gebre, T., Zhou, Z., Jorgensen, J. H., Zerihun, M., Habte, D., Assefa, Y., Emerson, P. M., Gaynor, B. D., Porco, T. C., Lietman, T. M., & Keenan, J. D. (2010). Antibiotic Selection Pressure and Macrolide Resistance in Nasopharyngeal *Streptococcus pneumoniae*: A Cluster-Randomized Clinical Trial. *PLOS Medicine*, *7*(12), e1000377.

Sköld, O. E., & Swedberg, G. (2017). Sulfonamides and Trimethoprim. *Antimicrobial Drug Resistance*, 345–358.

Soetaert, K., Petzoldt, T., & Setzer, R. W. (2010). Solving differential equations in R: Package deSolve. *Journal of Statistical Software*, *33*(9), 1–25.

Sondermann, H., Shikuma, N. J., & Yildiz, F. H. (2012). You've come a long way: C-di-GMP signaling. *Current Opinion in Microbiology*, *15*(2), 140–146.

Soto, S. M. (2013). Role of efflux pumps in the antibiotic resistance of bacteria embedded in a biofilm. *Virulence*, *4*(3).

Soto, S. M. (2014). Importance of Biofilms in Urinary Tract Infections: New Therapeutic Approaches. *Advances in Biology*, *2014*, 1–13.

Soto, S. M., Smithson, A., Horcajada, J. P., Martinez, J. A., Mensa, J. P., & Vila, J. (2006). Implication of biofilm formation in the persistence of urinary tract infection caused by uropathogenic *Escherichia coli*. *Clinical Microbiology and Infection*, *12*(10), 1034–1036.

Spengler, G., Kincses, A., Gajdács, M., & Amaral, L. (2017). New Roads Leading to Old Destinations: Efflux Pumps as Targets to Reverse Multidrug Resistance in

Bacteria. *Molecules 2017, Vol. 22, Page 468*, *22*(3), 468.

Stephens, L. J., Werrett, M. V., Sedgwick, A. C., Bull, S. D., & Andrews, P. C. (2020). Antimicrobial innovation: a current update and perspective on the antibiotic drug development pipeline. *Future Medicinal Chemistry*, *12*(22), 2035–2065.

Stojowska-swędrzyńska, K., Łupkowska, A., Kuczyńska-wiśnik, D., & Laskowska, E. (2022). Antibiotic Heteroresistance in *Klebsiella pneumoniae*. *International Journal of Molecular Sciences*, *23*(1).

Stoodley, P., Sauer, K., Davies, D. G., & Costerton, J. W. (2002). Biofilms as complex differentiated communities. *Annual Review of Microbiology*, *56*, 187–209.

Su, C. C., Morgan, C. E., Kambakam, S., Rajavel, M., Scott, H., Huang, W., Emerson, C. C., Taylor, D. J., Stewart, P. L., Bonomo, R. A., & Yu, E. W. (2019). Cryo-electron microscopy structure of an *Acinetobacter baumannii* multidrug efflux pump. *mBio*, 10(4):e01295-19.

Sugawara, E., & Nikaido, H. (2014). Properties of AdeABC and AdeIJK efflux systems of *Acinetobacter baumannii* compared with those of the AcrAB-TolC system of *Escherichia coli*. *Antimicrobial Agents and Chemotherapy*, *58*(12), 7250–7257.

Sun, D., Jeannot, K., Xiao, Y., & Knapp, C. W. (2019). Editorial: Horizontal Gene Transfer Mediated Bacterial Antibiotic Resistance. *Front. in Microbiol.* 27;10:1933.

Sun, J., Deng, Z., & Yan, A. (2014). Bacterial multidrug efflux pumps: mechanisms, physiology and pharmacological exploitations. *Biochem. Biophys. Res. Commun.*, *453*(2), 254–267.

Sutherland, I. W. (2001). The biofilm matrix - An immobilized but dynamic microbial environment. *Trends in Microbiology*, *9*(5), 222–227.

Sutrina, S. L., Daniel, K., Lewis, M., Charles, N. T., Anselm, C. K. E., Thomas, N., & Holder, N. (2015). Biofilm Growth of *Escherichia coli* Is Subject to cAMP-Dependent and cAMP-Independent Inhibition. *Journal of Molecular Microbiology and Biotechnology*, *25*(2–3), 209–225.

Symmons, M. F., Marshall, R. L., & Bavro, V. N. (2015). Architecture and roles of periplasmic adaptor proteins in tripartite efflux assemblies. *Front Microbiol.*,

28;6:513.

Tacconelli, E., Carrara, E., Savoldi, A., Harbarth, S., Mendelson, M., Monnet, D. L., Pulcini, C., Kahlmeter, G., Kluytmans, J., Carmeli, Y., Ouellette, M., Outterson, K., Patel, J., Cavaleri, M., Cox, E. M., Houchens, C. R., Grayson, M. L., Hansen, P., Singh, N., … Zorzet, A. (2018). Discovery, research, and development of new antibiotics: the WHO priority list of antibiotic-resistant bacteria and tuberculosis. *The Lancet. Infectious Diseases*, *18*(3), 318–327.

Takatsuka, Y., Chen, C., & Nikaido, H. (2010). Mechanism of recognition of compounds of diverse structures by the multidrug efflux pump AcrB of *Escherichia coli*. *Proc. Natl. Acad. Sci. USA*, *107*(15), 6559–6565.

Tamura, N., Murakami, S., Oyama, Y., Ishiguro, M., & Yamaguchi, A. (2005). Direct interaction of multidrug efflux transporter AcrB and outer membrane channel TolC detected via site-directed disulfide cross-linking. *Biochemistry*, *44*(33), 11115–11121.

Tan, Y. S., Zhang, R. K., Liu, Z. H., Li, B. Z., & Yuan, Y. J. (2022). Microbial Adaptation to Enhance Stress Tolerance. *Frontiers in Microbiology*, *13*, 1205.

Taneja, N., Sethi, S., Tahlan, A. K., Yashwant, & Kumar. (2019). Introductory Chapter: Stepping into the Post-Antibiotic Era— Challenges and Solutions. In Y. Kumar (Ed.), *Antimicrobial Resistance - A Global Threat*. IntechOpen.

Thomen, P., Valentin, J. D. P., Bitbol, A. F., & Henry, N. (2020). Spatiotemporal pattern formation in: E. coli biofilms explained by a simple physical energy balance. *Soft Matter*, *16*(2), 494–504.

Thompson, K. M., & Gottesman, S. (2014). The MiaA tRNA modification enzyme is necessary for robust RpoS expression in *Escherichia coli*. *Journal of Bacteriology*, *196*(4), 754–761.

Tikhonova, E. B., Wang, Q., & Zgurskaya, H. I. (2002). Chimeric analysis of the multicomponent multidrug efflux transporters from gram-negative bacteria. *Journal of Bacteriology*, *184*(23), 6499–6507.

Toesca, I., Perard, C., Bouvier, J., Gutierrez, C., & Conter, A. (2001). The transcriptional activator NhaR is responsible for the osmotic induction of *osmCp1*,

a promoter of the stress-inducible gene *osmC* in *Escherichia coli*. *Microbiology*, *147*(10), 2795–2803.

Trampari, E., Prischi, F., Vargiu, A. V., Abi-Assaf, J., Bavro, V. N., & Webber, M. A. (2023). Functionally distinct mutations within AcrB underpin antibiotic resistance in different lifestyles. *Npj Antimicrobials and Resistance*, *1*(1), 1–13.

Tsutsumi, K., Yonehara, R., Ishizaka-Ikeda, E., Miyazaki, N., Maeda, S., Iwasaki, K., Nakagawa, A., & Yamashita, E. (2019). Structures of the wild-type MexAB–OprM tripartite pump reveal its complex formation and drug efflux mechanism. *Nature Communications*, *10*(1), 1–10.

Uddin, T. M., Chakraborty, A. J., Khusro, A., Zidan, B. R. M., Mitra, S., Emran, T. Bin, Dhama, K., Ripon, M. K. H., Gajdács, M., Sahibzada, M. U. K., Hossain, M. J., & Koirala, N. (2021). Antibiotic resistance in microbes: History, mechanisms, therapeutic strategies and future prospects. *Journal of Infection and Public Health*, *14*(12), 1750–1766.

Untergasser, A., Cutcutache, I., Koressaar, T., Ye, J., Faircloth, B. C., Remm, M., & Rozen, S. G. (2012). Primer3-new capabilities and interfaces. *Nucleic Acids Research*, *40*(15), e115–e115.

Uruén, C., Chopo-Escuin, G., Tommassen, J., Mainar-Jaime, R. C., & Arenas, J. (2020). Biofilms as Promoters of Bacterial Antibiotic Resistance and Tolerance. *Antibiotics 2021, Vol. 10, Page 3*, *10*(1), 3.

van Eijk, E., Wittekoek, B., Kuijper, E. J., & Smits, W. K. (2017). DNA replication proteins as potential targets for antimicrobials in drug-resistant bacterial pathogens. *Journal of Antimicrobial Chemotherapy*, *72*(5), 1275. h

Van Epps, J. S., & Younger, J. G. (2016). Implantable device-related infection. *Shock*, *46*(6), 597–608.

Van Houdt, R., & Michiels, C. W. (2005). Role of bacterial cell surface structures in *Escherichia coli* biofilm formation. *Research in Microbiology*, *156*(5–6), 626–633.

Vargiu, A. V., Ramaswamy, V. K., Malvacio, I., Malloci, G., Kleinekathöfer, U., & Ruggerone, P. (2018). Water-mediated interactions enable smooth substrate

transport in a bacterial efflux pump. *BBA-General Subjects*, *1862*(4), 836–845.

Vargiu, A. V., & Nikaido, H. (2012). Multidrug binding properties of the AcrB efflux pump characterized by molecular dynamics simulations. *Proc Natl Acad Sci U S A*, *109*(50), 20637–20642.

Vargiu, A. V., Ruggerone, P., Opperman, T. J., Nguyen, S. T., & Nikaido, H. (2014). Molecular Mechanism of MBX2319 Inhibition of *Escherichia coli* AcrB Multidrug Efflux Pump and Comparison with Other Inhibitors. *Antimicrobial Agents and Chemotherapy*, *58*(10), 6224.

Vestby, L. K., Grønseth, T., Simm, R., & Nesse, L. L. (2020). Bacterial Biofilm and its Role in the Pathogenesis of Disease. *Antibiotics (Basel, Switzerland)*, *9*(2).

Vieira, H. L. A., Freire, P., & Arraiano, C. M. (2004). Effect of *Escherichia coli* morphogene *bolA* on biofilms. *Applied and Environmental Microbiology*, *70*(9), 5682–5684.

Vijay, S., Bansal, N., Rao, B. K., Veeraraghavan, B., Rodrigues, C., Wattal, C., Goyal, J. P., Tadepalli, K., Mathur, P., Venkateswaran, R., Venkatasubramanian, R., Khadanga, S., Bhattacharya, S., Mukherjee, S., Baveja, S., Sistla, S., Panda, S., & Walia, K. (2021). Secondary Infections in Hospitalized COVID-19 Patients: Indian Experience. *Infection and Drug Resistance*, *Volume 14*, 1893–1903.

Vorkapic, D., Pressler, K., & Schild, S. (2016). Multifaceted roles of extracellular DNA in bacterial physiology. *Current Genetics*, *62*(1), 71–79.

Vu, B., Chen, M., Crawford, R. J., & Ivanova, E. P. (2009). Bacterial extracellular polysaccharides involved in biofilm formation. *Molecules*, *14*(7), 2535–2554.

Wang, C. H., Hsieh, Y. H., Powers, Z. M., & Kao, C. Y. (2020). Defeating Antibiotic-Resistant Bacteria: Exploring Alternative Therapies for a Post-Antibiotic Era. *International Journal of Molecular Sciences*, 21(3), 1061.

Wang, X., Dubey, A. K., Suzuki, K., Baker, C. S., Babitzke, P., & Romeo, T. (2005). CsrA post-transcriptionally represses pgaABCD, responsible for synthesis of a biofilm polysaccharide adhesin of *Escherichia coli*. *Molecular Microbiology*, *56*(6), 1648–1663.

Wang, X., Preston, J. F., & Romeo, T. (2004). The *pgaABCD* Locus of *Escherichia coli*

Promotes the Synthesis of a Polysaccharide Adhesin Required for Biofilm Formation. *Journal of Bacteriology*, *186*(9), 2724–2734.

Wang, Z., Fan, G., Hryc, C. F., Blaza, J. N., Serysheva, I. I., Schmid, M. F., Chiu, W., Luisi, B. F., & Du, D. (2017). An allosteric transport mechanism for the AcrAB-TolC multidrug efflux pump. *eLife*, *6*, e24905.

Wang, Z., Zhong, M., Lu, W., Chai, Q., & Wei, Y. (2015). Repressive mutations restore function-loss caused by the disruption of trimerization in *Escherichia coli* multidrug transporter AcrB. *Frontiers in Microbiology*, 22;6:4.

Webber, M. A., & Piddock, L. J. V. (2003). The importance of efflux pumps in bacterial antibiotic resistance. *Journal of Antimicrobial Chemotherapy*, *51*(1), 9–11.

Weber, H., Pesavento, C., Possling, A., Tischendorf, G., & Hengge, R. (2006). Cyclic-di-GMP-mediated signalling within the σS network of *Escherichia coli*. *Molecular Microbiology*, *62*(4), 1014–1034.

Wehrli, W. (1983). Rifampin: Mechanisms of Action and Resistance. *Reviews of Infectious Diseases*, *5*(Supplement_3), S407–S411.

Wenzel, R. P. (2007). Health care-associated infections: Major issues in the early years of the 21st century. *Clinical Infectious Diseases*, 45(Supplement_1), S85–S88.

Whitchurch, C. B., Tolker-Nielsen, T., Ragas, P. C., & Mattick, J. S. (2002). Extracellular DNA required for bacterial biofilm formation. *Science*, *295*(5559), 1487.

Wiegand, I., Hilpert, K., & Hancock, R. E. W. (2008). Agar and broth dilution methods to determine the minimal inhibitory concentration (MIC) of antimicrobial substances. *Nature Protocols 2008 3:2*, *3*(2), 163–175.

Wilson, D. N. (2013). Ribosome-targeting antibiotics and mechanisms of bacterial resistance. *Nature Reviews Microbiology 2013 12:1*, *12*(1), 35–48.

World Health Organization. (2017, February 27). *WHO publishes list of bacteria for which new antibiotics are urgently needed*. https://www.who.int/news/item/27-02-2017-who-publishes-list-of-bacteria-for-which-new-antibiotics-are-urgently-needed.

World Health Organization. (2023, November 21). *Antimicrobial resistance*. https://www.who.int/news-room/fact-sheets/detail/antimicrobial-resistance.

Wright, G. D. (2005). Bacterial resistance to antibiotics: enzymatic degradation and modification. *Advanced Drug Delivery Reviews*, *57*(10), 1451–1470.

Wyres, K. L., & Holt, K. E. (2018). *Klebsiella pneumoniae* as a key trafficker of drug resistance genes from environmental to clinically important bacteria. *Current Opinion in Microbiology*, *45*, 131–139.

Xiong, W., Sun, Y., Ding, X., Wang, M., & Zeng, Z. (2015). Selective pressure of antibiotics on ARGs and bacterial communities in manure-polluted freshwater-sediment microcosms. *Frontiers in Microbiology*, *11;6:194*.

Xu, C., Bilya, S. R., & Xu, W. (2019). *adeABC* efflux gene in *Acinetobacter baumannii*. *New Microbes and New Infections*, *30*, 100549.

Xu, Q., Jiang, J., Zhu, Z., Xu, T., Sheng, Z. K., Ye, M., Xu, X., & Wang, M. (2019). Efflux pumps AcrAB and OqxAB contribute to nitrofurantoin resistance in an uropathogenic *Klebsiella pneumoniae* isolate. *Int. J. Antimicrob. Agents*, *54*(2), 223–227.

Xu, S., Chen, G., Liu, Z., Xu, D., Wu, Z., Li, Z., & Hong, M. (2020). Site-Directed Mutagenesis Reveals Crucial Residues in *Escherichia coli* Resistance-Nodulation-Division Efflux Pump OqxB. *Microbial Drug Resistance (Larchmont, N.Y.)*, *26*(6), 550–560.

Yamanaka, Y., Oshima, T., Ishihama, A., & Yamamoto, K. (2014). Characterization of the YdeO regulon in *Escherichia coli. PLoS ONE*, *9*(11).

Yoneyama, H., Ocaktan, A., Gotoh, N., Nishino, T., & Nakae, T. (1998). Subunit Swapping in the Mex-Extrusion Pumps in *Pseudomonas aeruginosa*. *Biochemical and Biophysical Research Communications*, *244*(3), 898–902. h

Yousef, K. P., Streck, A., Schütte, C., Siebert, H., Hengge, R., & von Kleist, M. (2015). Logical-continuous modelling of post-translationally regulated bistability of curli fiber expression in *Escherichia coli*. *BMC Systems Biology*, *9*(1), 1–17.

Yuan, J., Xu, X., Guo, Q., Zhao, X., Ye, X., Guo, Y., & Wang, M. (2012). Prevalence of the *oqxAB* gene complex in *Klebsiella pneumoniae* and *Escherichia coli* clinical

isolates. *Journal of Antimicrobial Chemotherapy*, *67*(7), 1655–1659.

Zgurskaya, H. I., Krishnamoorthy, G., Ntreh, A., & Lu, S. (2011). Mechanism and Function of the Outer Membrane Channel TolC in Multidrug Resistance and Physiology of *Enterobacteria*. *Frontiers in Microbiology*, 16;2:189.

Zhang, T. (2017). Modeling biofilms: From genes to communities. *Processes*, 5(1):5.

Zhang, X. S., García-Contreras, R., & Wood, T. K. (2007). YcfR (BhsA) influences *Escherichia coli* biofilm formation through stress response and surface hydrophobicity. *Journal of Bacteriology*, *189*(8), 3051–3062.

Zhang, X. S., García-Contreras, R., & Wood, T. K. (2008). *Escherichia coli* transcription factor YncC (McbR) regulates colanic acid and biofilm formation by repressing expression of periplasmic protein YbiM (McbA). *ISME Journal*, *2*(6), 615–631.

Zhang, Y., Xiao, M., Horiyama, T., Zhang, Y., Li, X., Nishino, K., & Yan, A. (2011). The multidrug efflux pump MdtEF protects against nitrosative damage during the anaerobic respiration in *Escherichia coli*. *The Journal of Biological Chemistry*, *286*(30), 26576–26584.

Zhao, J., Wang, Q., Li, M., Heijstra, B. D., Wang, S., Liang, Q., & Qi, Q. (2013). *Escherichia coli* toxin gene *hipA* affects biofilm formation and DNA release. *Microbiology (United Kingdom)*, *159*(PART3), 633–640.

Zhou, Q., Sun, S. P., Chan, J. G. Y., Wang, P., Barraud, N., Rice, S. A., Wang, J., Li, J., & Chan, H. K. (2015). Novel Inhaled Combination Powder Containing Amorphous Colistin and Crystalline Rifapentine with Enhanced Antimicrobial Activities against Planktonic Cells and Biofilm of *Pseudomonas aeruginosa* for Respiratory Infections. *Molecular Pharmaceutics*, *12*(8), 2594–2603.

Zowawi, H. M., Forde, B. M., Alfaresi, M., Alzarouni, A., Farahat, Y., Chong, T. M., Yin, W. F., Chan, K. G., Li, J., Schembri, M. A., Beatson, S. A., & Paterson, D. L. (2015). Stepwise evolution of pandrug-resistance in *Klebsiella pneumoniae*. *Scientific Reports*, *5*(1), 1–8.

Zuo, Z., Weng, J., & Wang, W. (2016). Insights into the inhibitory mechanism of D13-9001 to the multidrug transporter AcrB through molecular dynamics simulations.

J. Phys. Chem. B, *120*(9), 2145–2154.

Zwama, M., & Nishino, K. (2021). Ever-adapting rnd efflux pumps in gram-negative multidrug-resistant pathogens: A race against time. *Antibiotics*, *10*(7), 774.

Appendix

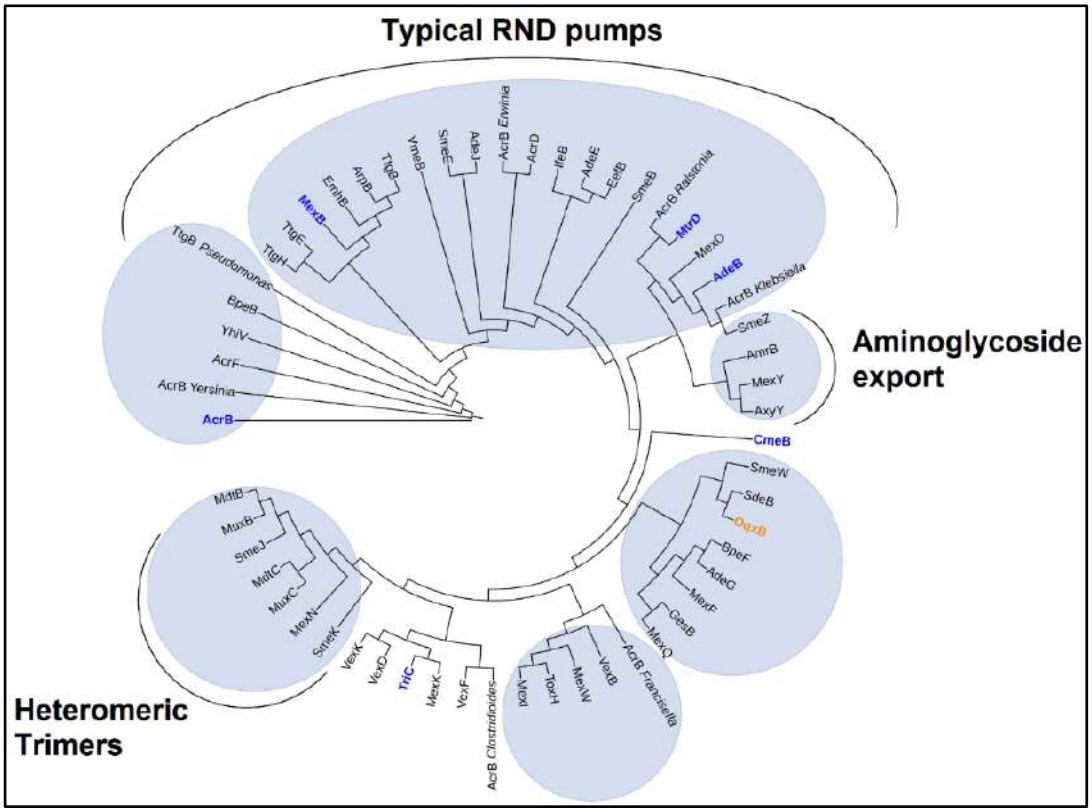

Figure S2.1 Diversity among different members of RND efflux pumps. The multi-drug resistance influencing OqxB (labelled in orange) is distant from the typical RND efflux pump. Structurally characterized members are marked in blue. The list of RND transporters is considered from 2.A.6.2.xx [categorized as the Hydrophobe/Amphiphile Efflux-1 (HAE1) Family] transporter classification database by Milton Saier, UCSD (http://www.tcdb.org/search/result.php?tc=2.A.6) to generate a phylogenetic tree (Bharatham et al., 2021).

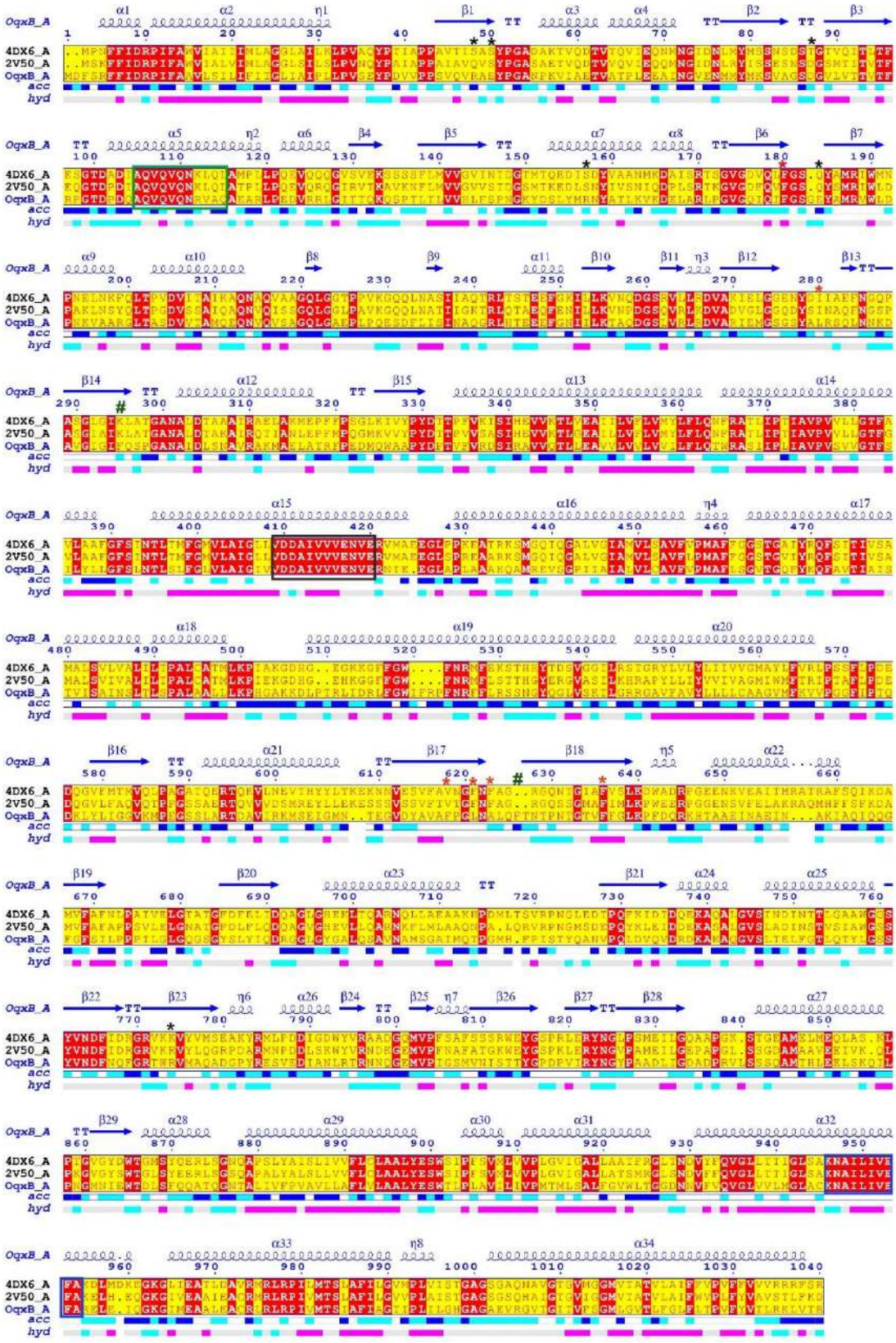

Figure S2.2 Structure-based sequence alignment of OqxB with other RND pumps. The OqxB sequence aligned with AcrB (4DX6_A) and MexB (2V50_A) using ENDscript webserver (https://espript.ibcp.fr/ESPript/cgi-bin/ENDscript.cgi) to

compare the similarities and differences. Important hydrophobic residues and hydrophilic residues of the OqxB substrate-binding pocket are highlighted with red and black asterisks, respectively. Aromatic residues unique in OqxB substrate-binding pocket are emphasised with green colour #. The conserved central α-helix, TM4 and TM10 are highlighted with green, black, and blue boxes, respectively.

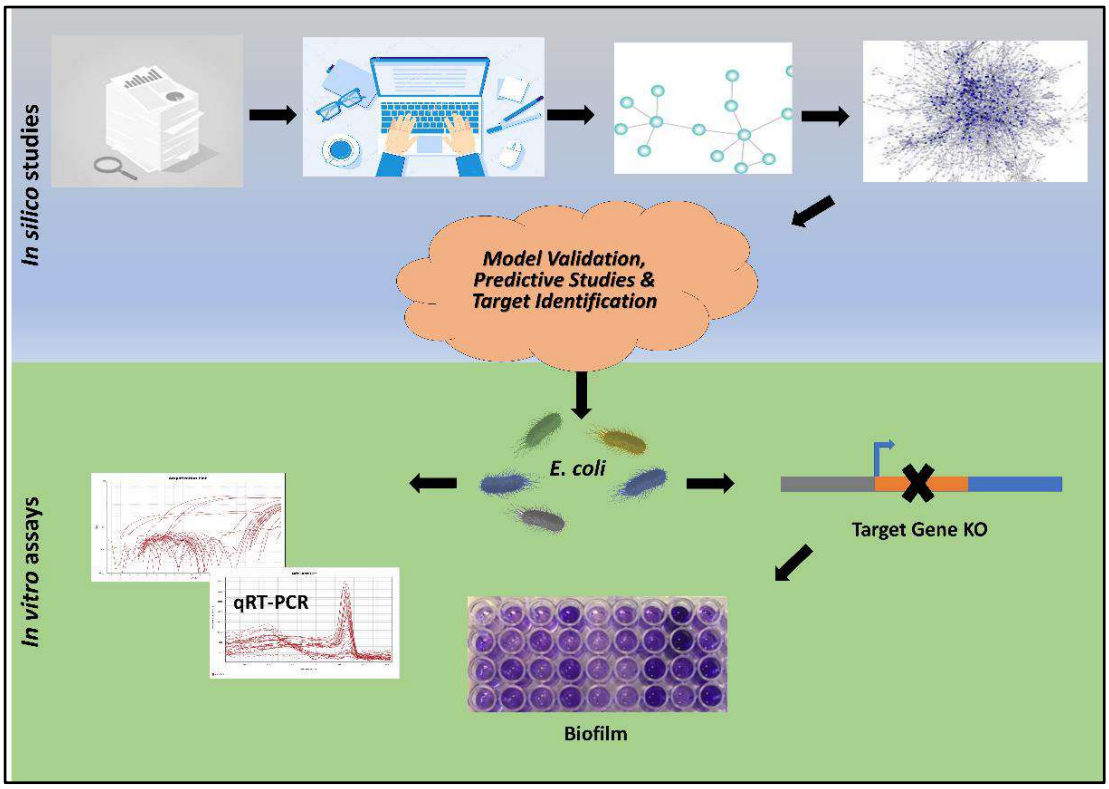

Figure S5.1 Abstract figure for the strategy followed in model development and target identification for *E. coli* biofilm. Following the curation of data from published literature, static base models are developed and aligned to form an integrated static map network of different biofilm components. Kinetic equations are defined for each of the fluxes to develop an ODE-based dynamic *in silico* network. The model is validated by running simulations with gene perturbations and validated for their roles for the known model components. Thereafter, predictive studies were simulated by identifying novel targets and further confirmed via *in vitro* assays for their roles in biofilm formation.

Supplementary Note (Bhowmik et al., 2022)

S5.1 Strategy for *in silico* model development, alignment and validation

The development of an Ordinary Differential Equations (ODE) model for biofilm is a sequential procedure which involves the following stages:

- **Scoping**: It includes an extensive literature survey of the published reports and databases to extract information related to the various aspects of biofilm-forming components, the signalling and the regulatory pathways involved in biofilm formation.
- **Base Model Development**: This is the development of a static map containing the sequential and interconnected network of enzymes and metabolites, which leads to the formation of the end product in a particular pathway.
- **Static to Dynamic Conversion and Model Integration:** The "standalone static maps" were then converted to "dynamic standalone models" by defining individual fluxes with ODE using an R- based platform. ODE calculates the rate of change of concentrations of metabolites over a given period. These independent dynamic standalone models were then integrated to create the complete, interconnected biofilm model with over 300 gene products.
- **Model Optimization & Validation:** The various kinetic parameters of the models were used to optimize and validate the model as per the information already published in scientific journals.

S5.2 Model Terminology

The *in silico* model of biofilm consists of several contributing factors, each playing a specific role in the overall process of biofilm development. Based on their roles, each of the components is referred to as one of the following:

- **Species:** In a dynamic model, it refers to any entity, which can be a metabolite, enzyme, transcriptional regulator, sRNAs, tRNAs, DNA, etc.
- **Activator:** Any species that activates the formation of a particular product in a reaction.
- **Inhibitor:** Any species that inhibits the formation of a particular product in a reaction.

- **Flux:** The rate at which substrates are converted into products is called “flux”. Different proteins/enzymes act as activators or inhibitors on a particular flux and determine the overall rate of conversion of substrates into products.
- **Control:** It is synonymous with a wild-type bacterial cell. In this, all the species have achieved a state of homeostasis.
- **Perturbation** refers to any alteration in the homeostatic condition of the system. These could be internal factors (like gene knockdown, gene knockout/deletion or overexpression) or external factors such as environmental stimuli.

Standalone models were built for gene transcription-translation machinery for all the regulatory and structural proteins in the model. The concentration of these proteins in the model is the cumulative effect of the various regulators acting at the transcriptional and translational levels. The model is aligned with data reported from literature and optimized to achieve a state of homeostasis for all the species (metabolites, activators, inhibitors, etc.).

- **Transcriptional level:** Transcription factors, RNA polymerase, Sigma factors (depending upon growth phase, the nutritional state of the cell or stress response), along with other regulators, can either activate or inhibit a particular flux.
- **Translational level:** 70S Ribosome, small regulatory RNAs or other activators and inhibitors, post-translational regulations, etc., that can modulate the activity of the flux.

S5.3 Hierarchy of structural components and their regulators in the biofilm network

The entire network of the biofilm formation is the resultant effect of a multi-factorial, concerted series of events, each driven by a specific subset of components. Therefore, all model components (structural and regulators) were organized into a multi-tiered hierarchy based on their biological roles in biofilm formation. This mode of organization was followed throughout the model. This classification into various levels was based on each species' roles and contribution to the overall biofilm formation process. Level 0 comprises all the structural components directly contributing to either of the two major components, namely the structural proteins or the exopolysaccharides in biofilm formation. The factors acting upstream of these structural components at the

transcriptional and translational levels were broadly categorized as Levels I, II, III and IV, respectively (**Figure S5.2**).

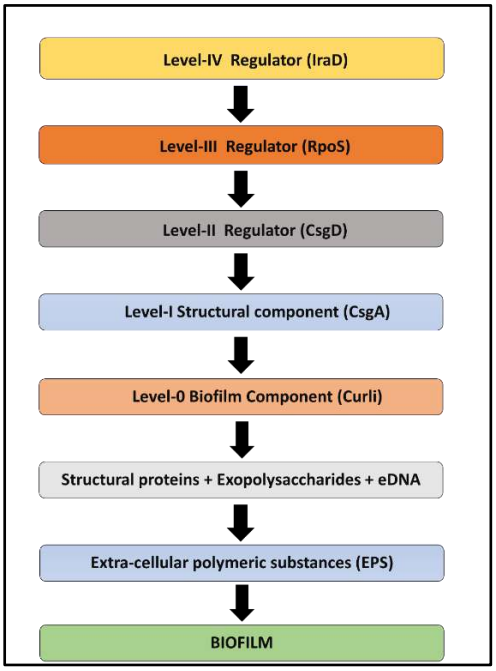

Figure S5.2 Hierarchy levels of different model components in biofilm formation. The complete model development for *E. coli* biofilm formation was done by categorizing the role of each of the regulators (activators/inhibitors) into one of the five levels based on the stage at which their function impacts biofilm.

While the underlying idea for the conceptualization of such a structural organization is discussed below, a detailed listing of all the species considered for developing the *E. coli* biofilm model into one of these four levels is provided in **Table S5.1** of the **Appendix** section.

- **Level 0:** The assembly of the biofilm architecture is majorly contributed by two major components, structural proteins and exopolysaccharides, which constitute the extra-cellular polymeric substances (EPS) of the biofilm. All significant components directly contributing to the assembly of either of these two components are categorized under Level 0. For example, components like curli and fimbriae are critical components of the structural proteins, whereas cellulose, PGA, and colanic acid contribute to the formation of exopolysaccharides in the biofilm architecture.

- **Level I:** Each of the components of Level 0 is formed by the association of several structural subunits. Each of these subunits is grouped under Level I. For example, Structural components like extra-cellular DNA (eDNA), genes encoding the structural proteins like FlhA, FlhB (the structural constituents of flagellar assembly) and CsgA, CsgB, CsgE (which encodes various proteins for curli assembly) are under Level I. Similarly, genes like BcsA, BcsB (associated with cellulose biosynthesis) and PgaABCD (associated with PGA biosynthesis) are also categorized as Level I. This species group includes the structural subunits or components, which directly contribute to the assembly of one of the major constituents of the biofilm matrix.
- **Level II**: The expression of the structural components under Level I is governed by the cumulative effect of several regulators, both at the transcriptional and translational levels. All these vital regulatory components are considered under Level II. For instance, CsgD is a well-known master regulator which governs the expression of the structural genes associated with curli biogenesis. FimB and FimE act as regulatory switches for the expression of the genes related to fimbriae biosynthesis. Similarly, FlhDC regulates the expression of genes for flagellar biosynthesis. All these key regulatory proteins are considered under Level II.
- **Level III**: The components of Level III comprise primarily the biofilm network components, which regulate the expression of Level I and Level II components and exert a multi-level regulatory impact on the different processes of biofilm formation. For instance, the RpoS sigma factor (σ38) is one of the critical regulatory factors that drive the expression of *E. coli* genes operating in the stationary phase and under various stress or adverse environmental conditions. Other proteins like RpoH (heat shock and carbon starvation), RpoN (nitrogen starvation), RpoE (exocytoplasmic stress response), etc., also regulate the expression of genes under various stress conditions. Similarly, proteins like CsrA exert their global regulatory effect at the post-transcriptional level. Therefore, this hierarchy level includes all the global regulators involved (at both transcription and translation levels) in biofilm formation.
- **Level IV**: This final level of characterization includes all the remaining components of the biofilm network and majorly comprises all the second and tertiary levels regulators, signal transduction system for stress, and chaperones,

which exert their effects upstream of the components of the remaining three levels discussed above. For example, members of the two-component signal transduction systems (e.g., EvgA-EvgS, PhoP-PhoQ), proteases (e.g., ClpXP, Lon, DegS), secondary and tertiary level regulators (e.g., MqsA, GadE, GadX, IraD), RNA degrading proteins (e.g., RNaseE and RNase III) are all characterized under Level IV.

S5.3 Model Validation

The model was tested against various experimental results reported in the literature to check its robustness. Specific perturbations like gene overexpression (OE), knockdown (KD) or knockout (KO) were simulated in the model and compared with the published data to check and validate the robustness of the model. In cases of mismatch, kinetic parameters and action values were optimized to achieve the desired outcome. This process ensures reliability in the predicted results. Only the qualitative and not the quantitative change is considered in this whole model alignment and validation process, which is an iterative process done to ascertain the biological accuracy of the model. The following modes of model perturbations were used for model alignment, validation and predictive simulations:

- **Knockdown.** The stepwise gradient knockdown of a gene implies a decrease in its concentration by a certain percentage, consequently leading to a gradual reduction in its activity. Knockdown studies help in identifying the genetic vulnerability of a particular gene. A genetically vulnerable gene can be considered a putative target, which, when reduced by genetic means, leads to a decrease in biofilm formation.
- **Knockout**. The concentration of the gene under study is made negligible in the model, and the simulation is run to see its effect on biofilm formation. If a gene knockout leads to a significant decline in biofilm biomass, it can be a putative target for biofilm prevention.
- **Overexpression.** Gene overexpression is done by increasing the gene concentration in the model by 2-fold or more. If gradual overexpression of a gene leads to a simultaneous decrease/increase in biofilm formation, the gene can be considered to possess a critical role / as a vulnerable target for an inhibitor/activator of biofilm formation, respectively.

- **Stress.** The model can be subjected to stress by increasing the stress factors which then trigger a series of responses like 2-component signalling, gene induction, upregulation or downregulation of genes (e.g., flagellar genes) leading to an impact on biofilm formation.
- **Loop Runs.** The model is simulated with loop runs, which refers to the simulations done with gradual alterations in the gene level to check for its effect on biofilm. Each of the loop runs includes a control or unperturbed system, 50%, 75% and 99.9% knockdown of the gene levels in the model. The loop runs were performed to check the sensitivity and robustness of the model.

After model optimization and validation, predictive studies (specific target knockdown, knockout and overexpression simulations) were carried out on the model, followed by *in vitro* testing for biofilm formation with target gene deleted (KO) of *E. coli BW25113* and *UPEC*. Confirmatory studies using qRT-PCR was also done with clinical isolates.

S5.4 Model Assumptions.

The current model captures the events contributing to the early phases of biofilm formation. As the transition of the planktonic phase to the sessile phase is governed by the sequential expression of various structural and regulatory components, only some of them have been considered. For example, flagellar motility is essential in the initial phase but interferes with the later phases of biofilm development. Similarly, colanic acid is a major component of matrix maturation, but overproduction of colanic acid also interferes with initial phases of adhesion by causing mucoidy. Therefore, flagella has been considered as a component of structural protein, whereas, colonic acid is considered for its contribution in the EPS matrix. Additionally, a feedback regulation has been included as well in the model to account for the inhibitory role of colonic acid. Also, the model does not include any metabolic pathways but takes into consideration all the various regulatory pathways. Therefore, the levels of different metabolites have been assumed to be from a Source, which is nothing but a continuous supply point for them from the other cellular processes. Similarly, the concept of Sink was introduced as a recycling mode to represent the degradation of individual components, maintain steady-state levels, and remove excess unwanted products to avoid undesirable effects due to their excessive accumulation. Although the generation of ATP using proton motive force was not considered, the overall levels of ATP, ADP, and AMP were kept

constant by including fluxes that mediate their interconversion. For the sake of modelling simplicity and to bypass the need for complex kinetic parameters (which are required for complex Michaelis – Menten kinetics), modified Reversible Mass Action (RMA) / Irreversible Mass Action (IRMA) kinetics were followed. For the development of the base models for gene expression, it was assumed that DNA is the source of mRNA, which in turn gets translated to protein. DNA has been kept at a constant concentration, thus providing a source of gene expression. Although the exact molecular mechanism of DNA replication, transcription, and translation has not been considered for the modelling, the effect has been modelled by regulations both at the transcriptional and post-transcriptional levels. For the perturbations in the system, the time runs which were applied for simulation did not take into consideration the actual bacterial generation time.

Table S1.1 Different classes of antibiotics, their sources, targets and mechanisms of action

Class	Antibiotics from	Example (and producing organism)	Molecular target
Aminoglycosides	**Actinomycetes**	Kanamycin A (*Streptomyces kanamyceticus*)	Protein synthesis: 30S ribosomal subunit
Tetracyclines		Tetracycline (*Streptomyces aureofaciens*)	Protein synthesis: 30S ribosomal subunit
Amphenicols		Chloramphenicol (*Streptomyces venezuelae*)	Protein synthesis: 50S ribosomal subunit
Macrolides		Erythromycin (*Saccharopolyspora erythraea*)	Protein synthesis: 50S ribosomal subunit
Tuberactinomycins		Viomycin (*Streptomyces puniceus*)	Protein synthesis: 30S and 50S ribosomal subunits (binds to the intersubunit bridge B2a)
Glycopeptides		Vancomycin (*Amycolatopsis orientalis*)	Cell wall synthesis: D-Ala-D-Ala termini of lipid II
Lincosamides		Clindamycin; Semi-synthetic derivative of lincomycin (*Streptomyces lincolnensis*)	Protein synthesis: 50S ribosomal subunit
Ansamycins		Rifamycin SV; Semi-synthetic derivative of rifamycin (*Amycolatopsis rifamycinica*)	Nucleic acid synthesis: RNA polymerase
Cycloserines		Seromycin (*Streptomyces orchidaceus*)	Cell wall synthesis: inhibition of alanine racemase and D-alanine-D-alanine ligase
Streptogramins		Pristinamycin (*Streptomyces pristinaespiralis*)	Protein synthesis: 50S ribosomal subunit
Phosphonates		Fosfomycin (*Streptomyces fradiae*)	Cell wall synthesis: MurA (UDP-GlcNAc-3-enol-

			pyruvyl-transferase) inhibition
Carbapenems		Meropenem; Synthetic molecule based on thienamycin (*Streptomyces cattleya*)	Cell wall synthesis: penicillin-binding proteins
Lipopeptides		Daptomycin (*Streptomyces roseosporus*)	Cell wall: cell membrane disruption.
Lipiarmycins		Fidaxomicin (*Dactylosporangium aurantiacum subsp. hamdenesis*)	Nucleic acid synthesis: RNA polymerase
Polypeptides	**Other Bacteria**	Gramicidin A (*Bacillus brevis*)	Cell wall: forms ion channels that increase the permeability of the bacterial cell membrane.
Bacitracin		Bacitracin A (*Bacillus subtilis*)	Cell wall synthesis: inhibition of dephosphorylation of C_{55} - isoprenyl pyrophosphate
Polymyxins		Colistin (*Paenibacillus polymyxa*)	Cell wall: cell membrane disruption
Mupirocin		Mupirocin (*Pseudomonas fluorescens*)	Protein synthesis: isoleucyl t-RNA synthetase
Monobactams		Aztreonam; Synthetic molecule based on SQ 26,180 (*Chromobacterium violaceum*)	Cell wall synthesis: penicillin-binding proteins
Penicillins	**Fungi**	Semi-synthetic derivative of penicillin (*Penicillium chrysogenum*)	Cell wall synthesis: penicillin-binding proteins
Fusidic acid		Fusidic acid (*Fusidium coccineum*)	Protein synthesis: elongation factor G
Enniatins[a]		Fusafungine (*Fusarium lateritium*)	Cell wall: cell membrane disruption

Class	Antibiotics from	Example (and producing organism)	Molecular target
Cephalosporins	**Fungi**	Cefacetrile; Semi-synthetic derivative of cephalosporin C (*Acremonium chrysogenum*)	Cell wall synthesis: penicillin-binding proteins
Pleuromutilins		Retapamulin; Semi-synthetic derivative of pleuromutilin (*Pleurotus mutilus*)	Protein synthesis: 50S ribosomal subunit
Arsphenamines[b]	**Synthetic antibiotics**	Salvarsan	Unknown
Sulfonamides		Mafenide	Folate synthesis: inhibition of dihydropteroate synthetase
Salicylates[c]		4-Aminosalicylic acid	Folate synthesis: prodrug that inhibits dihydrofolate reductase
Sulfones		Dapsone	Folate synthesis: inhibition of dihydropteroate synthetase
Pyridinamides		Isoniazid	Cell wall: prodrug that inhibits the synthesis of mycolic acids
Nitrofurans		Nitrofurantoin	DNA synthesis: DNA damage
Azoles[d]		Metronidazole	DNA synthesis: DNA damage
(Fluoro)quinolones		Ciprofloxacin	DNA synthesis: inhibition of DNA gyrase, and topoisomerase IV
Diaminopyrimidines		Trimethroprim	Folate synthesis: inhibition of dihydrofolate reductase
Ethambutol	**Synthetic antibiotics**	Ethambutol	Cell wall: arabinosyl transferase inhibition

Class	Antibiotics from	Example (and producing organism)	Molecular target
Thioamides		Ethionamide	Cell wall: prodrug that inhibits the synthesis of mycolic acids
Phenazines[d]		Clofazimine	DNA synthesis: binds to guanine bases
Oxazolidinones		Linezolid	Protein synthesis: 50S ribosomal subunit
Diarylquinolines		Bedaquiline	ATP synthesis: proton pump inhibition

The categorization of the antibiotic classes is based on the origin, structure and mechanism of action, which are the characteristic and distinguishing features for members of each class (Hutchings et al., 2019).

[a] The European Medicines Agency recommended the withdrawal of fusafungine from the market in February 2016.

[b] Salvarsan is no longer in clinical use.

[c] Salicylic acids are found in nature, but this was not the source of this class of antibiotic.

[d] Compound synthesis was inspired by natural antibiotic classes.

Table S2.1 Sequence identity and similarity between OqxB and other RND pumps

RND pump	Identity	Strongly similar	Weakly similar	Different
OqxB vs AcrB	**40.34%**	**25.26%**	**11.4%**	**23%**
OqxB vs MexB	**41.68%**	**23.63%**	**12.29%**	**22.4%**
AcrB vs MexB	**69.71%**	**15.05%**	**6.76%**	**8.48%**

ClustalW sequence alignment method utilized to calculate the identity metrics.

Table S2.2 Cloning primers for PCR amplification of inserts for single complementation overexpression

Insert Amplified	Primers	Primer Sequence (5' → 3')	Restriction Endonuclease (RE)
E. coli acrB	Eco_acrB_FP	5' ACGCCATATGATGCCTAATTTCTTTATC 3'	NdeI
	Eco_acrB_RP	5' AGCGCTCGAGATGATGATCGACAGTATGGC 3'	XhoI
P. aeruginosa mexB	Pae_mexB_FP	5' ACGCCATATGTCGAAGTTTTTCATTGAT 3'	NdeI
	Pae_mexB_RP	5' AGCGCTCGAGTTGCCCCTTTTCGACGGACGC 3'	XhoI
K. pneumoniae oqxB	Kpn_oqxB_FP	5' ACGCCATATGGACTTTTCCCGCTTTTTTA 3'	NdeI
	Kpn_oqxB_RP	5' AGCGCTCGAGGGCGGGCAGATCCTCCTGGA 3'	XhoI

Table S2.3 Cloning primers for PCR amplification of inserts for double complementation overexpression

Insert Amplified	Primers	Primer Sequence (5' → 3')	Restriction Endonuclease (RE)
E. coli acrA-acrB	Eco_acrAB_FP	5'GATACATATGCTGTTTACGATTAATCATCCGGCTCGTATAATGTGTGGTCACACAGGAAACAGACCATGAACAAAACAGAGGGTTTAC 3'	NdeI
	Eco_acrAB_RP	5' CCCAAGCTTTCAATGATGATCGACAGTATG 3'	HindIII
P. aeruginosa mexA-mexB	Pae_mexAB_FP	5'GATACATATGGAGCTGTTTACGATTAATCATCCGGCTCGTATAATGTGTGGTCACACAGGAAACAGACCATGCAACGAACGCCAGCCATG 3'	NdeI
	Pae_mexAB_RP	5'CCCAAGCTTTCATTGCCCCTTTTCGACGGAC 3'	HindIII
K. pneumoniae oqxA-oqxB	Kpn_oqxAB_FP	5'GATACATATGGAGCTGTTTACGATTAATCATCCGGCTCGTATAATGTGTGGTCACACAGGAAACAGACCATGAGCCTGCAAAAAACCTGGGGAAACAT 3'	NdeI
	Kpn_oqxAB_RP	5' CCCAAGCTTCTAGGCGGGCAGATCCTCCTGGAC 3'	HindIII

Table S2.4 Primer pairs for qRT-PCR to confirm overexpression in complementation systems

Species	Gene Name	Product Size (in bp)	Primer	Primer Sequence
E. coli	*acrA*	237	Eco_AcrA_RT_FP1	5’ ATTGATCCTGCGACCTATCA 3’
			Eco_AcrA_RT_RP1	5’GGTGTAAGCCAGATTGATCC 3’
	acrB	214	acrB_RT_FP_2	5’ CGTTGATTCCGACCATTGCC 3’
			acrB_RT_RP_2	5’ CCCATCGACTTACGGGTAGC 3’
	dnaK	130	dnaK_RT_Fwd	5’GTGCGAAACTGGAAAGCCT 3’
			dnaK_RT_Rev	5’GAGTCTGACCACCAACGAGG 3’
P. aeruginosa	*mexA*	212	Pae_MexA_RT_FP2	5’ GAATTCTCCGAGGTTTCCGT 3’
			Pae_MexA_RT_RP2	5’ GTGAACGCGCAGAACAA 3’
	mexB	210	Pae_MexA_RT_FP2	5’ GAATTCTCCGAGGTTTCCGT 3’
			Pae_MexA_RT_RP2	5’ GTGAACGCGCAGAACAA 3’

Species	Gene Name	Product Size (in bp)	Primer	Primer Sequence
K. pneumoniae	*oqxA*	207	Kpn_OqxA_RT_FP	5’’-GTAACCTGGTCACCGCGGGC 3′
			Kpn_OqxA_RT_RP	5’TGCCCTGGTGGGGGTAACCC 3’
	oqxB	267	oqxB_RT-2_FP	5’ATCGACAGGCCGATTTTCGC 3’
			oqxB_ RT-2_RP	5’GAAGGTGACGGTGGTGACCAGC 3’

Table S2.5 Ct Values for the quantification of *acrB, mexB* and *oqxB* overexpression by qRT-PCR in a single complementation system in *C43(DE3) ΔacrB* background

Strain	Gene	Ct1	Ct2	Ct3	Average Ct	ΔCt (Ct_{gene}-Ct_{dnaK})	Fold Change = 2^-ΔCt Normalization w.r.t. DnaK	Relative Expression levels w.r.t. WT AcrB
C43(DE3)	*acrB*	17.00	16.63	16.65	16.76	-0.46	1.38	1.00
	dnaK	17.26	17.27	17.14	17.22	0.00	1	
C43(DE3) ΔacrB (ΔacrB)	*acrB*	23.02	23.10	23.07	23.06	6.99	0.008	0.0057
	dnaK	16.11	16.01	16.11	16.08	0.00	1	
ΔacrB+AcrB	*acrB*	14.03	14.21	14.11	14.12	-3.04	8.24	5.98
	dnaK	17.37	17.26	16.84	17.16	0	1	
ΔacrB+MexB	*mexB*	14.00	13.12	13.77	13.63	-2.73	6.64	4.82
	dnaK	16.37	16.48	16.23	16.36	0	1	
ΔacrB+OqxB	*oqxB*	13.87	14.06	13.98	13.97	-3.26	9.58	6.95
	dnaK	17.15	17.34	17.20	17.23	0	1	

(Ct1, Ct2, Ct3: Ct values for technical triplicates)

Table S2.6 Ct Values for the quantification of the gene overexpression by qRT-PCR in a double complementation system in *BW25113 ΔacrAB* background. (A) Genes encoding MPFs (*acrA, mexA and oqxA)* (B) Genes encoding RND permeases (*acrB, mexB* and *oqxB)*

(A) Ct1, Ct2, Ct3: Ct values for technical triplicates

Strain	Gene	Ct1	Ct2	Ct3	Average Ct	ΔCt (Ct_{gene}-Ct_{dnaK})	Fold Change = 2^-ΔCt Normalization w.r.t. DnaK	Relative Expression levels w.r.t. WT AcrB
BW25113 (WT)	*acrA*	20.76	20.87	20.78	20.80	4.07	0.06	1
	dnaK	16.80	16.70	16.70	16.73	0	1	
BW25113 ΔacrAB	*acrA*	27.59	27.48	27.58	27.55	11.14	0.0004	0.007
	dnaK	16.24	16.73	16.25	16.41	0	1	
ΔacrAB +pEcoAB	*acrA*	18.99	19.31	18.76	19.02	1.42	0.37	6.3
	dnaK	17.70	17.60	17.50	17.60	0	1	
ΔacrAB +pMexAB	*mexA*	18.49	18.77	18.16	18.47	1.56	0.34	5.72
	dnaK	16.84	16.88	17.03	16.92	0	1	
ΔacrAB +pOqxAB	*oqxA*	12.61	12.57	12.99	12.72	0.52	0.70	11.7
	dnaK	12.60	12.20	11.80	12.20	0	1	

(B) Ct1, Ct2, Ct3: Ct values for technical triplicates

Strain	Gene	Ct1	Ct2	Ct3	Average Ct	ΔCt (Ct_{gene}-Ct_{dnaK})	Fold Change = 2^-ΔCt Normalization w.r.t. DnaK	Relative Expression levels w.r.t. WT AcrB
BW25113 (WT)	*acrB*	22.1	21.9	21.9	21.97	5.23	0.03	1
	dnaK	16.8	16.7	16.7	16.73	0	1	
BW25113 ΔacrAB	*acrB*	28.2	28.4	28.8	28.46	12.06	0.0002	0.009
	dnaK	16.2	16.7	16.2	16.4	0	1	
ΔacrAB +pEcoAB	*acrB*	19.3	20.0	20.1	19.8	2.88	0.14	5.12
	dnaK	16.8	16.9	17.0	16.9	0	1	
ΔacrAB +pMexAB	*mexB*	18.9	18.2	19.1	18.7	2.59	0.17	6.24
	dnaK	16.5	15.8	16.2	16.2	0	1	
ΔacrAB +pOqxAB	*oqxB*	18.0	17.4	17.6	17.7	1.57	0.34	12.70
	dnaK	16.2	16.2	16.0	16.1	0	1	

Table S3.1 Ct Values for the quantification of the gene overexpression by qRT-PCR in double complementation system in *BW25113 (WT)* background for genes encoding RND permeases (*acrB* and *oqxB)*

Strain	Gene	Ct1	Ct2	Ct3	Average Ct	ΔCt (Ct_{gene} - Ct_{dnaK})	Fold Change = 2^-ΔCt Normalization w.r.t. DnaK	Relative Expression levels w.r.t. WT AcrB
BW25113	***acrB***	**22.1**	**21.9**	**21.9**	**21.97**	**5.23**	**0.03**	**1**
(WT)	***dnaK***	**16.8**	**16.7**	**16.7**	**16.73**	**0**	**1**	
BW25113	***acrB***	**28.2**	**28.4**	**28.8**	**28.46**	**12.06**	**0.0002**	**0.009**
ΔacrAB	***dnaK***	**16.2**	**16.7**	**16.2**	**16.4**	**0**	**1**	
BW25113	***acrB***	**20.4**	**20.3**	**20.3**	**20.33**	**2.73**	**0.15**	**5.66**
+pEcoAB	***dnaK***	**17.7**	**17.6**	**17.5**	**17.6**	**0**	**1**	
BW25113	***oqxB***	**13.7**	**13.4**	**13.1**	**13.4**	**1.2**	**0.44**	**16.37**
+pOqxAB	***dnaK***	**12.6**	**12.2**	**11.8**	**12.2**	**0**	**1**	

Ct1, Ct2, Ct3: Ct values for technical triplicates

Supplementary Note

Estimation of the over-expression of *acrA*/*acrB, mexA*/*mexB* and *oqxA*/ *oqxB* by qRT-PCR in single and double complementation systems.

The overexpression of the different efflux pump components i.e. the RND permeases (*acrB, mexB and oqxB) and the MFPs (acrA, mexA and oqxA)* were confirmed by estimating the mRNA expression of these genes in the respective host strains, *E. coli C43(DE3)* and *E. coli K-12 BW25113* and their overexpressing counterparts for *acrA*/*acrB*, *mexA*/*mexB* and *oqxA*/ *oqxB*. The Ct values were compared and normalized with the house-keeping gene *dnaK*, which is constitutively overexpressed at around 38000 copies per cell (Seyer et al., 2003). The expression levels for each of the genes were then estimated using the relative Ct method, as discussed elsewhere (Schmittgen & Livak, 2008). The relative fold change in the expression levels for these genes were than compared with respect to the *acrA/acrB* levels in the respective wild-types (WT).

Table S3.2 Minimum Inhibitory Concentrations (MIC) of ciprofloxacin against *E. coli* clinical isolates and mutation mapping of QRDR by sequencing[§]

Strain	**MIC (μg/mL)**	***Ec*GyrA[*]**		***Ec*ParC[*]**			
E. coli	**Ciprofloxacin**	**S83L**	**D87N**	**S80I**	**S80R**	**E84V**	**E84G**
SEC001	>8	+	+	+			
SEC002	>8	+	+	+			
SEC003	>8	+	+	+			
SEC004	>8	+	+	+			
SEC005	>8	+	+				
SEC006	>8	+	+	+			
SEC007	>8	+	+				+
SEC008	>8	+	+	+			
SEC009	>8	+	+	+			
SEC010	0.25	+	+				
SEC011	>8	+	+	+			
SEC012	>8		+	+			
SEC013	>8	+	+	+			
SEC014	>8	+	+	+			
SEC015	>8	+	+				
SEC016	>8	+	+	+			
SEC018	>8	+	+	+			
SEC019	>8	+	+	+			
SEC020	>8		+	+			
SEC021	>8	+		+		+	
SEC022	>8	+	+	+		+	
SEC023	>8	+	+				
SEC024	>8	+	+	+			
SEC025	>8	+	+				
SEC026	>8	+	+	+			
SEC027	>8	+	+				
SEC028	>8	+	+	+		+	
SEC029	>8	+	+	+		+	

SEC030	>8	+	+	+		+	
SEC031	>8	+	+	+		+	
SEC032	0.03						
SEC033	>8	+	+				
SEC034	>8	+	+	+			
SEC035	>8			+			
SEC036	>8	+	+	+			
SEC037	0.015						
SEC038	>8	+	+	+		+	
SEC039	>8	+	+	+			
SEC040	>8	+	+	+			
SEC041	>8	+	+	+			+
SEC042	>8	+	+	+			
SEC043	>8	+	+	+		+	
SEC044	>8	+	+	+			
SEC045	0.06	+					
SEC046	>8	+	+				
SEC047	>8		+	+			
SEC048	>8	+	+	+			
SEC049	>8	+	+	+			
SEC050	>8			+		+	
SEC051	0.25	+	+	+			
SEC052	0.25	+		+			
SEC053	>8	+	+	+			
SEC054	>8	+					
SEC055	>8	+					
SEC056	0.25	+					
SEC057	>8	+	+		+		
SEC058	>8	+	+				
SEC059	>8	+		+			
SEC061	>8	+	+	+			
SEC062	>8		+				
SEC063	0.125						

SEC064	>8	+	+	+			
SEC065	>8	+	+	+		+	
SEC066	>8	+					
SEC067	>8	+	+	+			
SEC068	>8	+	+	+			
SEC069	>8	+	+	+		+	
SEC070	>8	+	+	+			
SEC071	>8			+			
SEC072	>8	+	+	+			
SEC073	>8	+	+	+		+	
SEC074	>8	+	+	+		+	
SEC075	>8	+	+	+			
SEC076	>8	+	+	+		+	
SEC077	>8	+	+	+			+
SEC078	>8	+	+	+			+
SEC079	>8	+	+	+		+	
SEC081	>8	+	+	+			
SEC082	>8	+	+	+			
SEC084	>8	+	+	+			
SEC085	>8	+	+	+		+	
SEC086	0.015						
SEC087	>8	+	+	+			
SEC088	>8	+	+	+		+	

*Ciprofloxacin targets GyrA and ParC were sequenced and variations in key interacting residues were identified. Mutations in QRDR (Quinolone-resistance determining region) are highlighted with + symbol.

(§ Data from St. Johns Research Institute, Bengaluru, Karnataka, India)

Table S3.3 Minimum Inhibitory Concentrations (MIC) of ciprofloxacin with and without AcrB inhibitor PAβN[§]

Strains	CIP (µg/mL) [#]		LZD (µg/mL) [#]		*Ec*GyrA[*]		*Ec*ParC*			
	- PAβN	+ PAβN	- PAβN	+ PAβN	S83L	D87N	S80I	S80R	E84V	E84G
SEC010	0.25	0.25	400	40	+	+				
SEC030	200	100	400	40	+	+	+		+	
SEC032	0.06	0.015	400	40						
SEC037	0.015	0.015	200	20						
SEC045	0.25	0.125	200	20	+					
SEC052	0.25	0.25	200	20	+		+			
SEC056	0.25	0.25	200	10	+					
SEC063	0.25	0.25	400	20						
SEC086	0.008	0.008	200	20						
BW25113	0.015	0.015	200	5						
acrB KO	0.008	0.008	5	5						
*tol*C KO	0.004	0.004	5	5						

[#]MIC values for CIP (Ciprofloxacin) and LZD (Linezolid) in absence or presence (-/+) of PAβN

*Ciprofloxacin targets GyrA and ParC were sequenced and variations in key interacting residues were identified. Mutations in QRDR (Quinolone-resistance determining region) are highlighted with + symbol. Linezolid is the positive control.

([§] Data from St. Johns Research Institute, Bengaluru, Karnataka, India)

Table S3.4 Profiling of clinical strains by colony PCR method to verify the presence of *oqxB* [§]

Strains	CIP (µg/mL) [#]		LZD (µg/mL) [#]		*oqxB*	*Ec*GyrA*		*Ec*ParC*			
	- PAβN	+ PAβN	- PAβN	+ PAβN		S83L	D87N	S80I	S80R	E84V	E84G
SEC027	>320	160	320	20	-	+	+				
SEC029	160	80	160	5	-	+	+	+		+	
SEC046	40	40	160	5	-	+	+				
SEC028	160	160	320	10	#	+	+	+		+	
SEC033	80	40	320	40	#	+	+				
SEC058	10	10	160	40	#	+	+				

[#]MIC values for CIP (Ciprofloxacin) and LZD (Linezolid) in absence or presence (-/+) of PAβN

*Ciprofloxacin targets GyrA and ParC were sequenced and variations in key interacting residues were identified. The presence of *oqxB* in the clinical isolates is highlighted with # symbol. Mutations in QRDR (Quinolone-resistance determining region) are highlighted with + symbol. Linezolid is the positive control.

([§] Data from St. Johns Research Institute, Bengaluru, Karnataka, India)

Table S3.5 Ct Values for the quantification of *acrB* and *oqxB* overexpression by qRT-PCR in *E. coli BW25113* wild-type

Strain	Gene	Ct1	Ct2	Ct3	Average Ct	ΔCt (Ct_{gene}-Ct_{dnaK})	Fold Change = 2^-ΔCt Normalization w.r.t. DnaK	Relative Expression levels w.r.t. WT AcrB
BW25113	***acrB***	**22.1**	**21.9**	**21.9**	**21.95**	**5.20**	**0.03**	**1**
(WT)	***dnaK***	**16.8**	**16.7**	**16.7**	**16.75**	**0.00**	**1.00**	
BW25113	***acrB***	**20.4**	**20.3**	**20.3**	**20.35**	**2.77**	**0.15**	**5.38**
+pEcoAB	***dnaK***	**17.7**	**17.6**	**17.5**	**17.58**	**0.00**	**1.00**	
BW25113	***oqxB***	**13.7**	**13.4**	**13.1**	**13.39**	**1.21**	**0.43**	**15.85**
+pOqxAB	***dnaK***	**12.6**	**12.2**	**11.8**	**12.18**	**0.00**	**1.00**	

Ct1, Ct2, Ct3: Ct values for technical triplicates

The overexpression of the different efflux pump components AcrB and OqxB were confirmed by estimating the mRNA expression of these genes in the three strains: *E. coli K-12 BW25113* wild-type (WT), and its overexpressing counterparts for AcrAB and OqxAB. The Ct values were compared and normalized with the house-keeping gene *dnaK*, which is constitutively overexpressed at around 38000 copies per cell (Seyer et al., 2003). The expression levels for each of the genes were then estimated using the relative Ct method, as discussed elsewhere (Schmittgen & Livak, 2008). The relative fold change in the expression levels for these genes was then compared with respect to the *acrB* levels in *BW25113* (WT). Upon comparison, the quantification of the target gene mRNA revealed a 5-6-fold increase in the expression of AcrB in the WT with *pEcoAB* strain and a 2.5-fold increase of OqxB levels in the WT with *pOqxAB* strain, as compared to the levels of AcrB in the WT with *pEcoAB* strain (**Figure 3.4**). Overall, these values confirm the overexpression of AcrB and OqxB in the recombinant expression system in *E. coli.*

Table S4.1 Primers for OqxB site-directed mutagenesis (SDM)

Primer name	OqxB SDM	Sequence
OqxB R48A FP	R48A	5’ GAGCGTCCAGGTGGCGGCGGAGTATCCCG 3’
OqxB R48A RP	R48A	5’ CGGGATACTCCGCCGCCACCTGGACGCTC 3’
OqxB E50A FP	E50A	5’ AGGTGCGCGCGGCGTATCCCGGCGCCAAC 3’
OqxB E50A RP	E50A	5’ CGCCGGGATACGCCGCGCGCACCTGGAC 3’
OqxB D87A FP	D87A	5’ GTCGCTGGCTCCGCGGCGTGCTGGTCACCAC 3’
OqxB D87A RP	D87A	5’ GTGGTGACCAGCACGCCGCGGAGCCAGCGAC 3’
OqxB R157A FP	R157A	5’ GCTGTATATGGCGAACTACGCCACGCTG 3’
OqxB R157A RP	R157A	5’ CGTGGCGTAGTTCGCCATATACAGCGAGTC 3’
OqxB F180A FP	F180A	5’GCCAGATCCAGATTGCGGGCTCCGGTGAATATGC 3’
OqxB F180A RP	F180A	5’ GCATATTCACCGGAGCCCGCAATCTGGATCTGGC 3’
OqxB E184A FP	E184A	5’GGCTCCGGTGCGTATGCGATGCGCGTCTG 3’
OqxB E184A RP	E184A	5’ CAGACGCGCATCGCATACGCACCGGAGCC 3’
OqxB L280A FP	L280A	5’GGTTCCGGCAGCTATGGCGTGCGCTCCCAGC 3’
OqxB L280A RP	L280A	5’GCTGGGAGCGCACGCCATAGCTGCCGGAACC 3’
OqxB L621A FP	L621A	5’ GTCGCTTTCCCGGGGGCGAATGCGCTGCAG 3’

Primer name	OqxB SDM	Sequence
OqxB L621A RP	L621A	5’ CTGCAGCGCATTCGCCCCCGGGAAAGCGAC 3’
OqxB F626A FP	F626A	5’ GCTTAATGCGCTGCAGGCGACCAACACGCC 3’
OqxB F626A RP	F626A	5’ GGCGTGTTGGTCGCCTGCAGCGCATTAAGC 3’
OqxB R774A FP	R774A	5’ CGGGCGTACCTGGGCGGTGATGGCCCAG 3’
OqxB R774A RP	R774A	5’ CTGGGCCATCACCGCCCAGGTACGCCCG 3’

Table S5.1: List of components included in the *E. coli* biofilm *in silico* model

Species / Component	Hierarchy Level/ Category	Gene Name	b number	Alternate name	Function/Details
EPS	Complex	-	-	-	Exopolysaccharide / Exopolymeric substance component of Biofilm Matrix
SP (Structural Proteins)	Complex	-	-	-	Structural Protein component of Biofilm Matrix
Biofilm	**Final Output**	-	-	-	**Biofilm**
Ag43	Level 0	*flu*	b2000	*agn43*, *yzzX*, *yeeQ*, *agn*, *flu*	CP4-44 prophage; self recognizing antigen 43 (Ag43) autotransporter
CA	Level 0	-	-	-	Colanic Acid
Cellodextrin	Level 0	-	-	-	Cellodextrin
Cellulose	Level 0	-	-	-	Cellulose
Curli	Level 0	-	-	-	Curli
eDNA	Level 0	-	-	-	Extracellular DNA
Fimbriae	Level 0	-	-	-	Fimbriae
Flagellum	Level 0	-	-	-	Flagellum
LPS	Level 0	-	-	-	Lipopolysaccharide
PGA	Level 0	-	-	-	adhesin poly-beta-1,6-N-acetyl-D-glucosamine
CsgA	Level I	*csgA*	b1042	-	curlin, major subunit
CsgB	Level I	*csgB*	b1041	-	curlin, minor subunit
CsgC	Level I	*csgC*	b1043	*ycdE*	putative curli production protein
CsgD	Level I	*csgD*	b1040	-	CsgD DNA-binding transcriptional dual regulator
CsgE	Level I	*csgE*	b1039	-	curli assembly component CsgE
CsgF	Level I	*csgF*	b1038	-	curli assembly component CsgF
CsgG	Level I	*csgG*	b1037	-	curli secretion channel

Dam	Level I	*dam*	b3387	-	DNA adenine methyltransferase
FimA	Level I	*fimA*	b4314	*fimD, pilA, pilC*	type 1 fimbriae major subunit
FimC	Level I	*fimC*	b4316	*pilB*	periplasmic chaperone, required for type 1 fimbriae
FimD	Level I	*fimD*	b4317	*fimD_1, fimD_2*	FimD monomer
FimF	Level I	*fimF*	b4318	-	type 1 fimbriae minor subunit FimF
FimG	Level I	*fimG*	b4319	-	type 1 fimbriae minor subunit FimG
FimH	Level I	*fimH*	b4320	*pilE*	minor fimbrial subunit, D-mannose specific adhesin
FimI	Level I	*fimI*	b4315	-	putative fimbrial protein FimI
FlgA	Level I	*flgA*	b1072	*flaU*	flagellar biosynthesis; assembly of basal-body periplasmic P ring
FlgB	Level I	*flgB*	b1073	*flbA*	flagellar basal-body rod protein FlgB
FlgC	Level I	*flgC*	b1074	*flaFIII, flaW*	flagellar basal-body rod protein FlgC
FlgD	Level I	*flgD*	b1075	*flaFIV, flaV*	flagellar biosynthesis, initiation of hook assembly
FlgE	Level I	*flgE*	b1076	*flaFV, flaK*	flagellar hook protein FlgE
FlgF	Level I	*flgF*	b1077	*flaFVI, flaX*	flagellar basal-body rod protein FlgF
FlgG	Level I	*flgG*	b1078	*flaFVII, flaL*	flagellar basal-body rod protein FlgG
FlgH	Level I	*flgH*	b1079	*flaFVIII, flaY*	flagellar L-ring protein FlgH; basal-body outer-membrane L (lipopolysaccharide layer) ring protein

FlgI	Level I	*flgI*	b1080	*flaFIX, flaM*	flagellar P-ring protein FlgI
FlgJ	Level I	*flgJ*	b1081	*flaZ*	putative peptidoglycan hydrolase FlgJ
FlgK	Level I	*flgK*	b1082	*flaS*	flagellar biosynthesis, hook-filament junction protein 1
FlgL	Level I	*flgL*	b1083	*flaT*	flagellar biosynthesis; hook-filament junction protein
FlgM	Level I	*flgM*	b1071	-	anti-sigma factor for FliA (σ²⁸)
FlgN	Level I	*flgN*	b1070	-	flagellar biosynthesis protein FlgN
FlhA	Level I	*flhA*	b1879	*flaH*	flagellar biosynthesis protein FlhA
FlhB	Level I	*flhB*	b1880	*yecQ, flaG*	flagellar biosynthesis protein FlhB
FliC	Level I	*fliC*	b1923	*H, flaF, hag*	flagellar biosynthesis; flagellin, filament structural protein
FliD	Level I	*fliD*	b1924	*flbC, rfs*	flagellar cap protein FliD; filament capping protein; enables filament assembly
FliE	Level I	*fliE*	b1937	*fla, flaAI, flaN*	flagellar basal-body protein FliE
FliF	Level I	*fliF*	b1938	*flaAII.1, flaBI*	flagellar M-ring protein FliF; basal-body MS(membrane and supramembrane)-ring and collar protein
FliG	Level I	*fliG*	b1939	*flaAII.2, flaBII*	flagellar motor switch protein FliG
FliH	Level I	*fliH*	b1940	*flaAII.3, flaBIII*	flagellar biosynthesis protein FliH
FliI	Level I	*fliI*	b1941	*fla, flaAIII, flaC*	flagellum-specific ATP synthase FliI

FliJ	Level I	*fliJ*	b1942	*flaO*	flagellar biosynthesis protein FliJ
FliK	Level I	*fliK*	b1943	*flaE*	flagellar hook-length control protein FliK
FliL	Level I	*fliL*	b1944	*flaQI, flaAI, cheC1*	flagellar biosynthesis
FliM	Level I	*fliM*	b1945	*flaQ, fla, flaQII, flaAII, flaA, cheC2*	flagellar motor switch protein FliM
FliN	Level I	*fliN*	b1946	*motD*	flagellar motor switch protein FliN
FliO	Level I	*fliO*	b1947	*flbD*	flagellar biosynthesis protein FliO
FliP	Level I	*fliP*	b1948	*flaR*	flagellar biosynthesis protein FliP
FliQ	Level I	*fliQ*	b1949	*flaQ*	flagellar biosynthesis protein FliQ
FliR	Level I	*fliR*	b1950	*flaP*	flagellar biosynthesis protein FliR
FliS	Level I	*fliS*	b1925	-	flagellar biosynthesis protein FliS
FliT	Level I	*fliT*	b1926	-	flagellar biosynthesis protein FliT
PgaA	Level I	*pgaA*	b1024	*hmsH, ycdS*	partially N-deacetylated poly-β-1,6-N-acetyl-D-glucosamine outer membrane porin
PgaB	Level I	*pgaB*	b1023	*hmsF, ycdR*	poly-β-1,6-N-acetyl-D-glucosamine N-deacetylase
PgaC	Level I	*pgaC*	b1022	*hmsR, ycdQ*	poly-β-1,6-N-acetyl-D-glucosamine synthase - PgaC subunit
PgaD	Level I	*pgaD*	b1021	*hmsS, ycdP*	poly-β-1,6-N-acetyl-D-glucosamine synthase - PgaD subunit

WcaA	Level I	*wcaA*	b2059	-	predicted colanic acid biosynthesis glycosyl transferase
WcaB	Level I	*wcaB*	b2058	-	predicted colanic acid biosynthesis acyl transferase
WcaC	Level I	*wcaC*	b2057	-	predicted colanic acid biosynthesis glycosyl transferase
WcaD	Level I	*wcaD*	b2056	-	predicted colanic acid polymerase
WcaE	Level I	*wcaE*	b2055	-	predicted colanic acid biosynthesis glycosyl transferase
WcaF	Level I	*wcaF*	b2054	-	predicted acyl transferase
WcaI	Level I	*wcaI*	b2050	*yefD*	predicted colanic biosynthesis glycosyl transferase
WcaJ	Level I	*wcaJ*	b2047	-	UDP-glucose:undecaprenyl-phosphate glucose-1-phosphate transferase
WcaL	Level I	*wcaL*	b2044	*yefL*	predicted colanic biosynthesis glycosyl transferase
Wza	Level I	*wza*	b2062	-	outer membrane polysaccharide export protein
Wzb	Level I	*wzb*	b2061	-	protein-tyrosine phosphatase
Wzc	Level I	*wzc*	b2060	-	protein-tyrosine kinase
Wzx	Level I	*wzx*	b2046	*wzx*	WzxC
YpdI	Level I	*ypdI*	b2376	-	YpdI colanic acid synthesis lipoprotein
BcsA	Level I	*bcsA*	*b3533*	*yhjP, yhjO*	*cellulose synthase, catalytic subunit*
BcsB	Level I	*bcsB*	b3532	*yhjN*	cellulose synthase, periplasmic subunit

BcsC	Level I	*bcsC*	b3530	*yhjL*	cellulose biosynthesis protein
BcsE	Level I	*bcsE*	b3536	*yhjS*	c-di-GMP-binding protein
BcsF	Level I	*bcsF*	b3537	*yhjT*	predicted protein
BcsG	Level I	*bcsG*	b3538	*yhjU*	predicted inner membrane protein
BcsQ	Level I	*bcsQ*	b3534	*yhjQ*	cellulose biosynthesis protein, pseudogene lacking N-terminal amino acids
BcsZ	Level I	*bcsZ*	b3531	*bcsC, yhjM*	endo-1,4-D-glucanase
Basal_Body_Hook	Level I / Complex	-	-	-	Complex of Basal Body Hook in Flagellum assembly
BcsA_c_di_GMP	Level I / Complex	-	-	-	Complex of BcsA with cyclic-di-GMP
BcsAB_c_di_GMP	Level I / Complex	-	-	-	Complex of BcsAand BcsB with cyclic-di-GMP
BcsE_c_di_GMP	Level I / Complex	-	-	-	Complex of BcsE with cyclic-di-GMP
Flagellar_Export_Apparatus	Level I / Complex	-	-	-	Type III Export Gate Complex for export of Flagellar proteins and assembly
Flagellar_Motor_Complex	Level I / Complex	-	-	-	Motor proteins complex associated with Flagellar assembly and functioning
Motor_Switch_Complex	Level I / Complex	-	-	-	Motor proteins complex associated with Flagellar assembly and functioning
PgaCD_c_di_GMP	Level I / Complex	-	-	-	poly-β-1,6-N-acetyl-D-glucosamine synthase complex with c-di-GMP

Rib70S	Level I / Complex	-	-	-	Ribosomal complex in Translational machinery
RNAP	Level I / Complex	-	-	-	RNA Polymerase complex in Transcription machinery
WCA	Level I / Complex	-	-	-	Complex of wca genes associated with synthesis of Colanic Acid
DsbA	Level II	*dsbA*	b3860	*dsf, iarA, ppfA*	protein disulfide oxidoreductase - DsbA
DsbB	Level II	*dsbB*	b1185	*ycgA, roxB, dsbX, iarB, rosB*	protein disulfide oxidoreductase - DsbB
FlhC	Level II	*flhC*	b1891	*flaI*	DNA-binding transcriptional dual regulator FlhC
FlhD	Level II	*flhD*	b1892	*flbB*	DNA-binding transcriptional dual regulator FlhD
Fnr	Level II	*fnr*	b1334	*frdB, nirA, nirR, ossA, oxrA*	DNA-binding transcriptional dual regulator FNR
HipA	Level II	*hipA*	b1507	-	serine/threonine-protein kinase toxin HipA
HipB	Level II	*hipB*	b1508	-	HipB antitoxin / DNA-binding transcriptional repressor
McbA	Level II	*mcbA*	b0806	*ybiM*	protein involved in colanic acid production
MicA	Level II	*micA*	b4442	*sraD, psrA10*	small regulatory RNA MicA
MicM	Level II	*micM*	b4585	*sroB, rybC, chiX*	small regulatory RNA MicM
MotA	Level II	*motA*	b1890	*flaJ*	MotA protein, proton conductor component

					of motor; no effect on switching
MotB	Level II	*motB*	b1889	*flaJ*	MotB protein, enables flagellar motor rotation, linking torque machinery to cell wall
RfaH	Level II	*rfaH*	b3842	*hlyT, sfrB*	RfaH transcriptional anti-terminator
YcgR	Level II	*ycgR*	b1194	-	molecular brake that regulates flagellar motility in response to c-di-GMP
FimB	Level II	*fimB*	b4312	*pil*	regulator for fimA
FimE	Level II	*fimE*	b4313	*hyp, pilH*	regulator for fimA
FlhDC	Level II / Complex	-	-	-	FlhDC DNA-binding transcriptional dual regulator
FlhDC_YdiV	Level II / Complex	-	-	-	Complex of FlhDC with YgiV
HipA_HipB	Level II / Complex	-	-	-	HipAB toxin/antitoxin complex
YcgR_c_di_GMP	Level II / Complex	-	-	-	Complex of YcgR and cyclic-di-GMP
BolA	Level III	*bolA*	b0435	-	BolA DNA-binding transcriptional dual regulator
BssR	Level III	*bssR*	b0836	*yliH*	regulator of biofilm formation
BssS	Level III	*bssS*	b1060	*yceP*	regulator of biofilm formation
Cra	Level III	*cra*	b0080	*fruR, fruC, shl*	Cra DNA-binding transcriptional dual regulator
Crp	Level III	*crp*	b3357	*cap, csm, gurB*	CRP transcriptional dual regulator
CsrA	Level III	*csrA*	b2696	*zfiA*	carbon storage regulator; pleiotropic regulatory protein for carbon source metabolism

CyaR	Level III	*cyaR*	b4438	-	small regulatory RNA CyaR
DsrA	Level III	*dsrA*	b1954	-	small regulatory RNA DsrA
FliZ	Level III	*fliZ*	b1921	*yedH*	FliZ DNA-binding transcriptional regulator
GcvA	Level III	*gcvA*	b2808	-	GcvA DNA-binding transcriptional dual regulator
GcvB	Level III	*gcvB*	b4443	*psrA, IS 145*	small regulatory RNA GcvB
Hfq	Level III	*hfq*	b4172	-	RNA-binding protein
IhfA	Level III	*ihfA*	b1712	*hid, himA*	integration host factor (IHF), α subunit
IhfB	Level III	*ihfB*	b0912	*hip, himD*	integration host factor (IHF), β subunit
LrhA	Level III	*lrhA*	b2289	*genR*	LrhA DNA-binding transcriptional dual regulator
Lrp	Level III	*lrp*	b0889	*rblA, oppI, mbf, lstR, alsB, ihb, livR, lrs, lss*	Lrp transcriptional dual regulator
LsrA	Level III	*lsrA*	b1513	*ego, ydeX*	AI-2 ABC transporter - ATP binding subunit
LsrB	Level III	*lsrB*	b1516	*yneA*	Autoinducer-2 ABC transporter - periplasmic binding protein
LsrC	Level III	*lsrC*	b1514	*ydeY*	Autoinducer-2 ABC transporter - membrane subunit
LsrD	Level III	*lsrD*	b1515	*ydeZ*	Autoinducer-2 ABC transporter - membrane subunit
LsrF	Level III	*lsrF*	b1517	*yneB*	predicted class I aldolase
LsrG	Level III	*lsrG*	b1518	*yneC*	Autoinducer 2-degrading protein

LsrK	Level III	*lsrK*	b1511	*ydeV*	autoinducer-2 kinase
LsrR	Level III	*lsrR*	b1512	*ydeW*	LsrR Transcriptional regulator
LuxS	Level III	*luxS*	b2687	*ygaG*	Ribosylhomocysteine lyase
MatA	Level III	*matA*	b0294	*ykgK, ecpR*	MatA DNA-binding transcriptional dual regulator
McaS	Level III	*mcaS*	b4426	*IS061, isrA*	small regulatory RNA McaS
McbR	Level III	*mcbR*	b1450	*yncC*	McbR DNA-binding transcriptional dual regulator
MdoH	Level III	*mdoH*	b1049	*mdoA, opgH*	membrane glycosyltransferase: synthesis of osmo-regulated periplasmic glucans (OPGs)
MlrA	Level III	*mlrA*	b2127	*yehV*	MlrA DNA binding transcriptional activator
MqsA	Level III	*mqsA*	b3021	*ygiT*	MqsA antitoxin of the MqsRA toxin-antitoxin system and DNA-binding transcriptional repressor
MqsR	Level III	*mqsR*	b3022	*ygiU*	mRNA interferase, toxin of the MqsR-MqsA toxin-antitoxin system
Nac	Level III	*nac*	b1988	-	Nac DNA-binding transcriptional dual regulator
NagC	Level III	*nagC*	b0676	*nagR*	NagC DNA-binding transcriptional dual regulator
NanR	Level III	*nanR*	b3226	*yhcK*	NanR DNA-binding transcriptional dual regulator

NhaR	Level III	*nhaR*	b0020	*antO, yaaB*	NhaR transcriptional activator
OmrA	Level III	*omrA*	b4444	*psrA12, rygA, PAIR2a, t59, sraE*	small regulatory RNA OmrA
OmrB	Level III	*omrB*	b4445	*PAIR2b, t59, rygB*	small regulatory RNA OmrB
QseB	Level III	*qseB*	b3025	*ygiX*	QseB-Phosphorylated DNA-binding transcriptional activator
QseC	Level III	*qseC*	b3026	*ygiY*	QseC sensory histidine kinase - phosphorylated
RcdA	Level III	*rcdA*	b0846	*ybjK*	RcdA DNA-binding transcriptional regulator
RcsA	Level III	*rcsA*	b1951	*cpsR*	positive DNA-binding transcriptional regulator of capsular polysaccharide synthesis, activates its own expression
RcsB	Level III	*rcsB*	b2217	-	DNA-binding transcriptional activator RcsB
RpoD	Level III	*rpoD*	b3067	*alt*	RNA polymerase, sigma 70 (sigma D) factor
RpoE	Level III	*rpoE*	b2573	*sigE*	RNA polymerase, sigma 24 (sigma E) factor
RpoF	Level III	*rpoF*	b1922	*fliA, flaD*	RNA polymerase, sigma 28 (sigma F) factor
RpoH	Level III	*rpoH*	b3461	*fam, hin, htpR*	RNA polymerase, sigma 32 (sigma H) factor

RpoN	Level III	*rpoN*	b3202	*glnF, ntrA*	RNA polymerase, sigma 54 (sigma N) factor
RpoS	Level III	*rpoS*	b2741	*sigS, otsX, abrD, appR, csi2, dpeB, katF, nur*	RNA polymerase, sigma S (sigma 38) factor
RprA	Level III	*rprA*	b4431	*psrA5, IS083*	small regulatory RNA RprA
RstA	Level III	*rstA*	b1608	*urpT*	RstA-Phosphorylated DNA-binding transcriptional regulator
RybB	Level III	*rybB*	b4430	*tpe7, IS082*	small regulatory RNA RydB
RydC	Level III	*rydC*	b4597	-	small regulatory RNA RydC
SdiA	Level III	*sdiA*	b1916	-	SdiA DNA-binding transcriptional dual regulator
SlyA	Level III	*slyA*	b1642	-	SlyA DNA-binding transcriptional activator
YdaM	Level III	*ydaM*	b1341	*dgcM*	diguanylate cyclase
YdiV	Level III	*ydiV*	b1707	*rflP*	anti-FlhDC factor
ArcZ_Hfq	Level III / Complex	-	-	-	Complex of Hfq with ArcZ small regulatory RNA
Crp_cAMP	Level III / Complex	-	-	-	cAMP-activated global transcriptional regulator CRP
DsrA_DeaD	Level III / Complex	-	-	-	Complex of DsrA and DEAD-box RNA helicase
DsrA_Hfq	Level III / Complex	-	-	-	Complex of DsrA and RNA-binding protein Hfq
RpoE_RseA	Level III / Complex	-	-	-	Complex of RpoE with RseA

RpoE_RseAB	Level III / Complex	-	-	-	Complex of RpoE with RseA and RseB
RpoF_FlgM	Level III / Complex	-	-	-	Complex of RpoF with FlgM
RpoS_RssB_p	Level III / Complex	-	-	-	Complex of RpoS with RssB
YdaM_MlrA_act	Level III / Complex	-	-	-	Activated complex of YdaM and MlrA
GcvA_GcvR	Level III / Complex	-	-	-	Complex of GcvA and RNA-binding protein Hfq
GcvB_Hfq	Level III / Complex	-	-	-	Complex of GcvB and RNA-binding protein Hfq
Hfq_RydC	Level III / Complex	-	-	-	Complex of RydC and RNA-binding protein Hfq
Hfq_RyhB	Level III / Complex	-	-	-	Complex of RydB and RNA-binding protein Hfq
IHF	Level III / Complex	-	-	-	IHF DNA-binding transcriptional dual regulator
LrhA_Hfq	Level III / Complex	-	-	-	Complex of LrhA and RNA-binding protein Hfq
LsrABCD	Level III / Complex	-	-	-	AI-2 transporter complex, LsrABCD
McaS_Hfq	Level III / Complex	-	-	-	Complex of McaS and RNA-binding protein Hfq
MicA_Hfq	Level III / Complex	-	-	-	Complex of MicA and RNA-binding protein Hfq
MqsR_MqsA	Level III / Complex	-	-	-	MqsA-MqsR antitoxin/toxin complex
NhaR_Na_Act	Level III / Complex	-	-	-	Activated NhaR under alkaline stress conditions

OxyS_Hfq	Level III / Complex	-	-	-	Complex of OxyS and RNA-binding protein Hfq
RcsA_RcsB_p	Level III / Complex	-	-	-	RcsAB DNA-binding transcriptional dual regulator (phophorylated)
RprA_Hfq	Level III / Complex	-	-	-	Complex of RprA and RNA-binding protein Hfq
AcrE	Level IV	*acrE*	b3265	*envC*	multidrug efflux pump membrane fusion lipoprotein AcrE
AcrF	Level IV	*acrF*	b3266	*envD*	multidrug efflux pump RND permease AcrF
ArcA	Level IV	*arcA*	b4401	*sfrA, cpxC, dye, fexA, msp, seg*	ArcA-Phosphorylated DNA-binding transcriptional dual regulator
ArcB	Level IV	*arcB*	b3210	-	ArcB sensory histidine kinase
ArcZ	Level IV	*arcZ*	b4450	*psrA16, sraH, ryhA*	Small regulatory RNA ArcZ
ArrS	Level IV	*arrS*	b4704	*6H57*	Small regulatory RNA ArrS
BarA	Level IV	*barA*	b2786	*airS(S.t.)*	BarA sensory histidine kinase - his302 phosphorylated
BasR	Level IV	*basR*	b4113	*pmrA*	BasR-Phosphorylated transcriptional regulator
BasS	Level IV	*basS*	b4112	*pmrB*	BasS sensory histidine kinase - phosphorylated
ClpP	Level IV	*clpP*	b0437	*lopP*	ClpP, Proteolytic component of the ATP-dependent ClpXP Protease

ClpX	Level IV	*clpX*	b0438	*lopC*	ATP-dependent Clp protease ATP-binding subunit ClpX
CpxA	Level IV	*cpxA*	b3911	*rssE, ecfB, eup, ssd, ecf*	CpxA sensory histidine kinase - phosphorylated
CpxP	Level IV	*cpxP*	b4484	*yiiO*	regulator of the Cpx response and possible chaperone involved in resistance to extracytoplasmic stress
CpxQ	Level IV	*cpxQ*	B4716	-	Small regulatory RNA CpxQ
CpxR	Level IV	*cpxR*	b3912	*yiiA*	CpxR-Phosphorylated
CreB	Level IV	*creB*	b4398	*yjjE, ORF2*	CreB-Phosphorylated DNA-binding transcriptional regulator
CreC	Level IV	*creC*	b4399	*phoM*	CreCB Two-Component Signal Transduction System
CspA	Level IV	*cspA*	b3556	-	cold shock protein CspA
CsrB	Level IV	*csrB*	b4408	-	small regulatory RNA CsrB
CsrC	Level IV	*csrC*	b4457	-	small regulatory RNA CsrC
CsrD	Level IV	*csrD*	b3252	*yhdA*	regulator of CsrB and CsrC decay
CysB	Level IV	*cysB*	b1275	-	DNA-binding transcriptional dual regulator CysB
CytR	Level IV	*cytR*	b3934	-	DNA-binding transcriptional repressor CytR
DeaD	Level IV	*deaD*	b3162	*csdA, mssB, rhlD*	DeaD, DEAD-box RNA helicase
DegS	Level IV	*degS*	b3235	*hhoB, htrH*	DegS serine endoprotease

DgcX	Level IV	*dgcX*	-	-	predicted diguanylate cyclase
DgcY	Level IV	*dgcY*	-	-	predicted diguanylate cyclase
DksA	Level IV	*dksA*	b0145	*msmA*	RNA polymerase-binding transcription factor DksA
DnaA	Level IV	*dnaA*	b3702	-	DNA-binding transcriptional dual regulator DnaA
DnaK	Level IV	*dnaK*	b0014	*groPF, groPC, seg, grpF, grpC, groPAB*	chaperone protein DnaK
EnvZ	Level IV	*envZ*	b3404	*tpo, perA, ompB*	Sensor histidine kinase EnvZ
EvgA	Level IV	*evgA*	b2369	-	EvgA-Phosphorylated DNA-binding transcriptional activator
EvgS	Level IV	*evgS*	b2370	-	EvgS sensory histidine kinase - his721 phosphorylated
Fis	Level IV	*fis*	b3261	*nbp*	DNA-binding protein Fis
FtsK	Level IV	*ftsK*	b0890	*dinH*	essential cell division protein FtsK
Fur	Level IV	*fur*	b0683	-	DNA-binding transcriptional dual regulator Fur
GadE	Level IV	*gadE*	b3512	*yhiE, yhiT*	GadE DNA-binding transcriptional activator
GadW	Level IV	*gadW*	b3515	*yhiW*	GadW DNA-binding transcriptional dual regulator
GadX	Level IV	*gadX*	b3516	*yhiX*	GadX DNA-binding transcriptional dual regulator

GcvR	Level IV	*gcvR*	b2479	*yffD*	GcvR predicted transcriptional regulator
GlnB	Level IV	*glnB*	b2553	-	nitrogen regulatory protein PII-1
HdfR	Level IV	*hdfR*	b4480	*yifA, yifD*	HdfR DNA-binding transcriptional dual regulator
HNS	Level IV	*hns*	b1237	*B1, H1, virR, topX, topS, pilG, osmZ, msyA, irk, hnsA, bglY, cur, drc, drdX, drs, fimG*	H-NS DNA-binding transcriptional dual regulator
HupA	Level IV	*hupA*	b4000	-	transcriptional dual regulator HU-α (HU-2)
HupB	Level IV	*hupB*	b0440	*dpeA, dbhB, hopD*	transcriptional dual regulator HU-β, NS1 (HU-1)
IraD	Level IV	*iraD*	b4326	*yjiD*	anti-adaptor protein IraD
IraM	Level IV	*iraM*	b1160	*elb1, ycgW, elbA*	anti-adaptor protein IraM
IraP	Level IV	*iraP*	b0382	*yaiB*	anti-adaptor protein IraP
LeuO	Level IV	*leuO*	b0076	-	LeuO DNA-binding transcriptional dual regulator
LexA	Level IV	*lexA*	b4043	*exrA, spr, tsl, umuA*	DNA-binding transcriptional repressor LexA
Lon	Level IV	*lon*	b0439	*capR, deg, dir, lopA, muc*	Lon Protease
MgrB	Level IV	*mgrB*	b1826	*yobG*	negative feedback regulator of the PhoQP system

MiaA	Level IV	*miaA*	b4171	*trpX*	tRNA(i^6 A37) synthase/ tRNA dimethyl allyl transferase
MicF	Level IV	*micF*	b4439	*stc*	small regulatory RNA MicF
Mtr	Level IV	*mtr*	b3161	-	tryptohan / indole:H+ symporter Mtr
NsrR	Level IV	*nsrR*	b4178	*yjjeB*	DNA-binding transcriptional dual regulator NsrR
NtrB	Level IV	*ntrB*	b3869	*glnR, glnL, NRII*	protein histidine kinase NtrB
NtrC	Level IV	*ntrC*	b3868	*glnT, glnG, NRI*	DNA-binding transcriptional dual regulator NtrC
OmpA	Level IV	*ompA*	b0957	*con, tolG, tut*	Outer membrane protein A
OmpR	Level IV	*ompR*	b3405	*cry, kmt, ompB*	OmrR dimer
OxyR	Level IV	*oxyR*	b3961	*momR, mor*	OxyR DNA-binding transcriptional dual regulator
OxyS	Level IV	*oxyS*	b4458	-	small regulatory RNA OxyS
PdeW	Level IV	*pdeW*	-	-	putative c-di-GMP phosphodiesterase
PdeX	Level IV	*pdeX*	-	-	putative c-di-GMP phosphodiesterase
PdeY	Level IV	*pdeY*	-	-	putative c-di-GMP phosphodiesterase
PhoB	Level IV	*phoB*	b0399	*phoRc, phoT*	PhoB-Phosphorylated DNA-binding transcriptional dual regulator
PhoP	Level IV	*phoP*	b1130	-	DNA-binding transcriptional dual regulator PhoP
PhoQ	Level IV	*phoQ*	b1129	-	PhoQ sensory histidine kinase

PhoR	Level IV	*phoR*	b0400	*R1pho, phoR1, nmpB*	sensor histidine kinase PhoR
PmrD	Level IV	*pmrD*	b2259	-	signal transduction protein
RcsC	Level IV	*rcsC*	b2218	-	RcsC sensory histidine kinase
RcsD	Level IV	*rcsD*	b2216	*yojP, yojQ, yojN*	RcsD phosphotransferase
RelA	Level IV	*relA*	b2784	*ppGpp synthetase I, PSI, ppGpp synthase I, (p)ppGpp synthetase I*	GDP/GTP pyrophosphokinase
RNAse_III (Rnc)	Level IV	*rnc)*	b2567	*ranA*	Ribonuclease 3; RNase III
RNAseE (Rne)	Level IV	*rne)*	b1084	*smbB, ams, hmp1*	Ribonuclease, RNase E
RseA	Level IV	*rseA*	b2572	*yfiJ, mclA*	anti-sigma factor
RseB	Level IV	*rseB*	b2571	-	anti-sigma factor stabilizing protein
RseP	Level IV	*rseP*	b0176	*ecfE, yaeL*	RseP zinc protease, signal peptide peptidase
RssB	Level IV	*rssB*	b1235	*ychL, sprE, hnr*	regulator of RpoS
RstB	Level IV	*rstB*	b1609	*uspT*	RstB sensory histidine kinase - phosphorylated
Rtn	Level IV	*rtn*	b2176	*pdeN*	putative c-di-GMP phosphodiesterase
RutR	Level IV	*rutR*	b1013	*ycdC*	RutR DNA-binding transcriptional dual regulator
RyhB	Level IV	*ryhB*	b4451	*psrA18, IS176, sraI*	small regulatory RNA
SafA	Level IV	*safA*	b1500	*yneN*	two-component system connector

SoxS	Level IV	*soxS*	b4062	-	SoxS DNA-binding transcriptional dual regulator
SpoT	Level IV	*spoT*	b3650	-	bifunctional (p)ppGpp synthase/hydrolase
SutR	Level IV	*sutR*	b1434	*ydcN*	DNA-binding transcriptional dual regulator
TnaA	Level IV	*tnaA*	b3708	*ind*, *tnaR*	tryptophanase
UvrY	Level IV	*uvrY*	b1914	*yecB*	UvrY- Phosphorylated transcriptional regulator
YahA	Level IV	*yahA*	b0315	*pdeL*	phosphodiesterase, c-di-GMP-specific
YaiC	Level IV	*yaiC*	b0385	*adrA*	predicted diguanylate cyclase
YcdT	Level IV	*ycdT*	b1025	*dgcT*	diguanylate cyclase
YcgG	Level IV	*ycgG*	b1168	*pdeG*	putative c-di-GMP phosphodiesterase
YciR	Level IV	*yciR*	b1285	*pdeR, gmr*	cyclic di-GMP phosphodiesterase
YddU	Level IV	*yddU*	b1489	*dos, pdeO, dosP*	c-di-GMP phosphodiesterase
YddV	Level IV	*yddV*	b1490	*dosC*	diguanylate cyclase
YdeH	Level IV	*ydeH*	b1535	*ydeG, dgcZ*	diguanylate cyclase
YdeO	Level IV	*ydeO*	b1499	-	YdeO DNA-binding transcriptional dual regulator
YdgG	Level IV	*ydgG*	b1601	*tqsA*	autoinducer 2 exporter
YeaG	Level IV	*yeaG*	b1783	-	protein kinase
YeaJ	Level IV	*yeaJ*	b1786	*dgcJ*	predicted diguanylate cyclase
YeaP	Level IV	*yeaP*	b1794	*dgcP*	diguanylate cyclase
YedQ	Level IV	*yedQ*	b1956	*dgcQ*	predicted diguanylate cyclase
YegE	Level IV	*yegE*	b2067	*dgcE*	predicted diguanylate cyclase
YfeA	Level IV	*yfeA*	b2395	*pdeA*	putative c-di-GMP phosphodiesterase

YfgF	Level IV	*yfgF*	b2503	*pdeF*	cyclic di-GMP phosphodiesterase
YfiN	Level IV	*yfiN*	b2604	*dgcN*	predicted diguanylate cyclase
YfiR	Level IV	*yfiR*	b2603	-	predicted periplasmic protein involved in swarming motility
YgiV	Level IV	*ygiV*	b3023	-	YgiV DNA-binding transcriptional repressor
YhjH	Level IV	*yhjH*	b3525	*pdeH*	c-di-GMP phosphodiesterase
YhjK	Level IV	*yhjK*	b3529	*pdeK*	predicted c-di-GMP phosphodiesterase
YjcC	Level IV	*yjcC*	b4061	*pdeC*	predicted c-di-GMP-specific phosphodiesterase
YjjQ	Level IV	*yjjQ*	b4365	-	DNA-binding transcriptional repressor
YlaB	Level IV	*ylaB*	b0457	*pdeB*	c-di-GMP phosphodiesterase
YliE	Level IV	*yliE*	b0833	*pdeI*	predicted c-di-GMP-specific phosphodiesterase
YliF	Level IV	*yliF*	b0834	*dgcI*	predicted diguanylate cyclase
YneF	Level IV	*yneF*	b1522	*dgcF*	predicted diguanylate cyclase
YoaD	Level IV	*yoaD*	b1815	*pdeD*	putative c-di-GMP phosphodiesterase
AcrEF	Level IV / Complex	-	-	-	AcrEF Efflux component complex
ClpXP	Level IV / Complex	-	-	-	ClpXP chaperone/protease complex
Fur_FeII	Level IV / Complex	-	-	-	Complex of Fur with Fe^{2+}

HU	Level IV / Complex	-	-	-	HU DNA-binding transcriptional dual regulator
PhoQ_MgrB_ inact	Level IV / Complex	-	-	-	Inactivated complex of PhoQ and MgrB
RseAB	Level IV / Complex	-	-	-	Complex of RseA and RseB
c_di_GMP	Secondary Metabolite	-	-	-	Cyclic di-guanosine monophosphate
cAMP	Secondary Metabolite	-	-	-	Cyclic Adenosine Monophosphate
ppGpp	Secondary Metabolite	-	-	-	guanosine tetraphosphate and guanosine pentaphosphate
Acidic_pH	Stress / External Stimuli	-	-	-	Representative Species for Stress Under low pH or Acidic Conditions
Aliphatic_ Carboxylic_Acids	Stress / External Stimuli	-	-	-	Stress Component
Alkali_Metal_ Stress	Stress / External Stimuli	-	-	-	Stress Component
Alkaline_pH_ Stress	Stress / External Stimuli	-	-	-	Stress Component
Antibiotic_Stress	Stress / External Stimuli	-	-	-	Stress Component
Ca_II	Stress / External Stimuli	-	-	-	Stress Component
Cold_Shock	Stress / External Stimuli	-	-	-	Stress Component
Envelope_Stress	Stress / External Stimuli	-	-	-	Stress Component

Fe_III	Stress / External Stimuli	-	-	-	Stress Component
Heat_Shock	Stress / External Stimuli	-	-	-	Stress Component
Mg_II	Stress / External Stimuli	-	-	-	Stress Component
N_Stress	Stress / External Stimuli	-	-	-	Stress Component
OCL	Stress / External Stimuli	-	-	-	Qurom Sensing
Osmotic_Shock	Stress / External Stimuli	-	-	-	Stress Component
Oxidative_Stress	Stress / External Stimuli	-	-	-	Stress Component
uOMP	Stress / External Stimuli	-	-	-	Unfolded / Misfolded Membrane Proteins; Stress Component
Zn_II	Stress / External Stimuli	-	-	-	Stress Component
AHL_ec	Stress / External Stimuli; Quorum Sensing Molecule	-	-	-	Exogenous N-acyl-L-homoserine lactone; Quorum Sensing molecule
AI2	Stress / External Stimuli; Quorum Sensing Molecule	-	-	-	Auto-Inducer 2; Quorum Sensing molecule

Indole	Stress / External Stimuli; Quorum Sensing Molecule	-	-	-	Qurom Sensing molecule

Table S5.2. Primers used for quantification of target gene transcript levels by qRT-PCR

Gene Primers	Primer sequence 5' → 3'
dnaK Fwd	GTGCGAAACTGGAAAGCCTG
dnaK Rev	GAGTCTGACCACCAACGAGG
miaA Fwd	AGCAACAGGCGGCAGAGC
miaA Rev	ATGCACCTGATACGGTAGAG
ydeO Fwd	AGTGACGGTGCCTGTTCC
ydeO Rev	CAGAAACGGATAGCACACC
ygiV Fwd	AATGGTGAACTTACCGGTGG
ygiV Rev	GTTTCCAGTCGCTGCTCTG

Table S5.3: Effect of graded KD of MiaA on biofilm formation: raw data from model simulations (in AU)

Time	Control	MiaA 50% KD	MiaA 75% KD	MiaA 99.9% KD
0	0	0	0	0
36	2.36E-14	2.36E-14	2.36E-14	2.36E-14
72	4.55E-14	4.55E-14	4.55E-14	4.55E-14
108	6.59E-14	6.59E-14	6.59E-14	6.59E-14
144	8.49E-14	8.48E-14	8.48E-14	8.48E-14
180	1.03E-13	1.03E-13	1.03E-13	1.03E-13
216	1.19E-13	1.19E-13	1.19E-13	1.19E-13
252	1.35E-13	1.35E-13	1.35E-13	1.35E-13
288	1.53E-13	1.52E-13	1.52E-13	1.52E-13
324	1.76E-13	1.74E-13	1.73E-13	1.73E-13
360	2.12E-13	2.08E-13	2.06E-13	2.04E-13
396	2.74E-13	2.64E-13	2.60E-13	2.55E-13
432	3.77E-13	3.57E-13	3.47E-13	3.37E-13
468	5.39E-13	5.00E-13	4.81E-13	4.63E-13
504	7.78E-13	7.09E-13	6.76E-13	6.43E-13
540	1.11E-12	9.97E-13	9.42E-13	8.90E-13
576	1.56E-12	1.38E-12	1.29E-12	1.21E-12
612	2.14E-12	1.85E-12	1.73E-12	1.61E-12
648	2.85E-12	2.44E-12	2.25E-12	2.08E-12
684	3.72E-12	3.13E-12	2.87E-12	2.64E-12
720	4.74E-12	3.93E-12	3.59E-12	3.28E-12
756	5.92E-12	4.84E-12	4.39E-12	3.98E-12
792	7.28E-12	5.86E-12	5.28E-12	4.76E-12
828	8.80E-12	6.98E-12	6.24E-12	5.60E-12
864	1.05E-11	8.19E-12	7.28E-12	6.50E-12
900	1.23E-11	9.49E-12	8.39E-12	7.45E-12
936	1.44E-11	1.09E-11	9.55E-12	8.44E-12
972	1.65E-11	1.23E-11	1.08E-11	9.47E-12
1008	1.88E-11	1.39E-11	1.20E-11	1.05E-11

1044	2.12E-11	1.54E-11	1.33E-11	1.16E-11
1080	2.38E-11	1.71E-11	1.47E-11	1.27E-11
1116	2.64E-11	1.87E-11	1.60E-11	1.38E-11
1152	2.92E-11	2.04E-11	1.74E-11	1.49E-11
1188	3.21E-11	2.22E-11	1.87E-11	1.60E-11
1224	3.58E-11	2.39E-11	2.01E-11	1.71E-11
1260	4.41E-11	2.57E-11	2.15E-11	1.82E-11
1296	7.68E-11	2.75E-11	2.28E-11	1.93E-11
1332	2.16E-10	2.99E-11	2.42E-11	2.04E-11
1368	7.32E-10	3.38E-11	2.56E-11	2.15E-11
1404	2.34E-09	4.26E-11	2.73E-11	2.25E-11
1440	6.50E-09	6.52E-11	2.96E-11	2.36E-11
1476	1.55E-08	1.23E-10	3.36E-11	2.47E-11
1512	3.24E-08	2.57E-10	4.15E-11	2.60E-11
1548	6.01E-08	5.46E-10	5.73E-11	2.77E-11
1584	1.02E-07	1.12E-09	8.82E-11	3.01E-11
1620	1.60E-07	2.16E-09	1.46E-10	3.39E-11
1656	2.36E-07	3.94E-09	2.48E-10	3.98E-11
1692	3.32E-07	6.75E-09	4.19E-10	4.92E-11
1728	4.48E-07	1.09E-08	6.91E-10	6.37E-11
1764	5.85E-07	1.68E-08	1.11E-09	8.57E-11
1800	7.41E-07	2.48E-08	1.71E-09	1.18E-10
1836	9.18E-07	3.52E-08	2.55E-09	1.64E-10
1872	1.11E-06	4.83E-08	3.69E-09	2.27E-10
1908	1.33E-06	6.42E-08	5.18E-09	3.11E-10
1944	1.55E-06	8.33E-08	7.08E-09	4.21E-10
1980	1.80E-06	1.06E-07	9.43E-09	5.62E-10
2016	2.06E-06	1.31E-07	1.23E-08	7.38E-10
2052	2.33E-06	1.60E-07	1.57E-08	9.55E-10
2088	2.62E-06	1.93E-07	1.97E-08	1.22E-09
2124	2.91E-06	2.29E-07	2.43E-08	1.52E-09
2160	3.22E-06	2.69E-07	2.96E-08	1.89E-09
2196	3.54E-06	3.12E-07	3.55E-08	2.31E-09

2232	3.87E-06	3.59E-07	4.21E-08	2.78E-09
2268	4.20E-06	4.09E-07	4.94E-08	3.32E-09
2304	4.55E-06	4.62E-07	5.74E-08	3.93E-09
2340	4.90E-06	5.19E-07	6.61E-08	4.60E-09
2376	5.26E-06	5.79E-07	7.55E-08	5.34E-09
2412	5.62E-06	6.42E-07	8.56E-08	6.15E-09
2448	5.99E-06	7.07E-07	9.64E-08	7.03E-09
2484	6.37E-06	7.76E-07	1.08E-07	7.98E-09
2520	6.75E-06	8.48E-07	1.20E-07	9.00E-09
2556	7.13E-06	9.22E-07	1.33E-07	1.01E-08
2592	7.52E-06	9.99E-07	1.46E-07	1.13E-08
2628	7.91E-06	1.08E-06	1.60E-07	1.25E-08
2664	8.31E-06	1.16E-06	1.75E-07	1.38E-08
2700	8.70E-06	1.25E-06	1.90E-07	1.52E-08
2736	9.11E-06	1.33E-06	2.06E-07	1.66E-08
2772	9.51E-06	1.42E-06	2.23E-07	1.81E-08
2808	9.92E-06	1.51E-06	2.40E-07	1.97E-08
2844	1.03E-05	1.61E-06	2.57E-07	2.13E-08
2880	1.07E-05	1.70E-06	2.76E-07	2.30E-08
2916	1.12E-05	1.80E-06	2.94E-07	2.48E-08
2952	1.16E-05	1.90E-06	3.14E-07	2.66E-08
2988	1.20E-05	2.00E-06	3.33E-07	2.85E-08
3024	1.24E-05	2.10E-06	3.54E-07	3.04E-08
3060	1.28E-05	2.21E-06	3.74E-07	3.24E-08
3096	1.32E-05	2.31E-06	3.95E-07	3.45E-08
3132	1.37E-05	2.42E-06	4.17E-07	3.66E-08
3168	1.41E-05	2.53E-06	4.39E-07	3.88E-08
3204	1.45E-05	2.64E-06	4.62E-07	4.10E-08
3240	1.49E-05	2.75E-06	4.85E-07	4.33E-08
3276	1.54E-05	2.87E-06	5.08E-07	4.56E-08
3312	1.58E-05	2.98E-06	5.32E-07	4.80E-08
3348	1.62E-05	3.10E-06	5.56E-07	5.04E-08
3384	1.67E-05	3.22E-06	5.80E-07	5.29E-08

3420	1.71E-05	3.33E-06	6.05E-07	5.54E-08
3456	1.75E-05	3.46E-06	6.31E-07	5.80E-08
3492	1.80E-05	3.58E-06	6.56E-07	6.06E-08
3528	1.84E-05	3.70E-06	6.82E-07	6.32E-08
3564	1.88E-05	3.82E-06	7.09E-07	6.60E-08
3600	1.93E-05	3.95E-06	7.35E-07	6.87E-08

Control: represents wild-type (WT) or Control simulations; **50% KD**: 50% knockdown; **75% KD**: 75% knockdown; **99.9% KD**: 99.9% knock down (equivalent to knockout, KO); all KD were done with respect to Control levels.

Simulation Time: in seconds

AU: Arbitrary Unit; used for representation of the relative levels of model output.

Table S5.4: Effect of graded KD of YdeO on biofilm formation: raw data from model simulations (in AU)

Time	Control	YdeO 50% KD	YdeO 75% KD	YdeO 99.9% KD
0	0	0	0	0
36	2.36E-14	2.36E-14	2.36E-14	2.36E-14
72	4.55E-14	4.55E-14	4.55E-14	4.55E-14
108	6.59E-14	6.59E-14	6.59E-14	6.59E-14
144	8.49E-14	8.49E-14	8.49E-14	8.49E-14
180	1.03E-13	1.03E-13	1.03E-13	1.03E-13
216	1.22E-13	1.19E-13	1.19E-13	1.19E-13
252	1.46E-13	1.36E-13	1.35E-13	1.35E-13
288	1.87E-13	1.53E-13	1.51E-13	1.50E-13
324	2.61E-13	1.75E-13	1.68E-13	1.67E-13
360	3.92E-13	2.04E-13	1.89E-13	1.86E-13
396	6.05E-13	2.45E-13	2.16E-13	2.09E-13
432	9.29E-13	3.03E-13	2.51E-13	2.40E-13
468	1.39E-12	3.81E-13	2.98E-13	2.79E-13
504	2.01E-12	4.84E-13	3.58E-13	3.28E-13
540	2.80E-12	6.14E-13	4.32E-13	3.89E-13
576	3.79E-12	7.73E-13	5.23E-13	4.63E-13
612	4.98E-12	9.60E-13	6.29E-13	5.51E-13
648	6.39E-12	1.18E-12	7.51E-13	6.50E-13
684	8.01E-12	1.42E-12	8.89E-13	7.63E-13
720	9.84E-12	1.69E-12	1.04E-12	8.87E-13
756	1.19E-11	1.98E-12	1.21E-12	1.02E-12
792	1.42E-11	2.30E-12	1.38E-12	1.17E-12
828	1.66E-11	2.63E-12	1.57E-12	1.32E-12
864	1.93E-11	2.98E-12	1.77E-12	1.48E-12
900	2.21E-11	3.35E-12	1.98E-12	1.65E-12
936	2.51E-11	3.73E-12	2.19E-12	1.82E-12
972	2.82E-11	4.11E-12	2.40E-12	2.00E-12
1008	3.15E-11	4.51E-12	2.62E-12	2.18E-12
1044	3.49E-11	4.91E-12	2.85E-12	2.36E-12

1080	3.84E-11	5.31E-12	3.07E-12	2.54E-12
1116	4.19E-11	5.71E-12	3.30E-12	2.72E-12
1152	4.55E-11	6.11E-12	3.52E-12	2.90E-12
1188	4.96E-11	6.51E-12	3.74E-12	3.08E-12
1224	5.65E-11	6.90E-12	3.96E-12	3.26E-12
1260	8.05E-11	7.30E-12	4.18E-12	3.44E-12
1296	1.85E-10	7.70E-12	4.39E-12	3.61E-12
1332	6.01E-10	8.14E-12	4.62E-12	3.80E-12
1368	1.98E-09	8.74E-12	4.89E-12	4.01E-12
1404	5.76E-09	9.76E-12	5.28E-12	4.30E-12
1440	1.43E-08	1.19E-11	5.97E-12	4.80E-12
1476	3.08E-08	1.64E-11	7.35E-12	5.76E-12
1512	5.86E-08	2.58E-11	1.01E-11	7.64E-12
1548	1.01E-07	4.45E-11	1.54E-11	1.12E-11
1584	1.60E-07	7.88E-11	2.50E-11	1.78E-11
1620	2.38E-07	1.38E-10	4.16E-11	2.91E-11
1656	3.36E-07	2.34E-10	6.85E-11	4.74E-11
1692	4.56E-07	3.81E-10	1.10E-10	7.57E-11
1728	5.96E-07	5.96E-10	1.71E-10	1.17E-10
1764	7.57E-07	8.97E-10	2.57E-10	1.76E-10
1800	9.38E-07	1.30E-09	3.74E-10	2.56E-10
1836	1.14E-06	1.82E-09	5.27E-10	3.61E-10
1872	1.35E-06	2.48E-09	7.22E-10	4.95E-10
1908	1.59E-06	3.29E-09	9.64E-10	6.61E-10
1944	1.84E-06	4.25E-09	1.26E-09	8.64E-10
1980	2.10E-06	5.39E-09	1.60E-09	1.10E-09
2016	2.38E-06	6.71E-09	2.01E-09	1.39E-09
2052	2.67E-06	8.22E-09	2.48E-09	1.71E-09
2088	2.97E-06	9.92E-09	3.01E-09	2.08E-09
2124	3.28E-06	1.18E-08	3.61E-09	2.50E-09
2160	3.61E-06	1.39E-08	4.27E-09	2.96E-09
2196	3.94E-06	1.62E-08	5.01E-09	3.47E-09
2232	4.28E-06	1.87E-08	5.81E-09	4.03E-09

2268	4.63E-06	2.14E-08	6.68E-09	4.64E-09
2304	4.98E-06	2.43E-08	7.61E-09	5.30E-09
2340	5.35E-06	2.74E-08	8.62E-09	6.01E-09
2376	5.72E-06	3.06E-08	9.69E-09	6.76E-09
2412	6.09E-06	3.41E-08	1.08E-08	7.56E-09
2448	6.47E-06	3.78E-08	1.20E-08	8.41E-09
2484	6.86E-06	4.16E-08	1.33E-08	9.31E-09
2520	7.25E-06	4.56E-08	1.47E-08	1.03E-08
2556	7.64E-06	4.99E-08	1.61E-08	1.12E-08
2592	8.04E-06	5.42E-08	1.75E-08	1.23E-08
2628	8.44E-06	5.88E-08	1.91E-08	1.34E-08
2664	8.85E-06	6.35E-08	2.06E-08	1.45E-08
2700	9.26E-06	6.84E-08	2.23E-08	1.56E-08
2736	9.67E-06	7.35E-08	2.40E-08	1.69E-08
2772	1.01E-05	7.87E-08	2.58E-08	1.81E-08
2808	1.05E-05	8.41E-08	2.76E-08	1.94E-08
2844	1.09E-05	8.96E-08	2.95E-08	2.07E-08
2880	1.13E-05	9.53E-08	3.14E-08	2.21E-08
2916	1.18E-05	1.01E-07	3.34E-08	2.35E-08
2952	1.22E-05	1.07E-07	3.54E-08	2.50E-08
2988	1.26E-05	1.13E-07	3.75E-08	2.64E-08
3024	1.30E-05	1.19E-07	3.96E-08	2.80E-08
3060	1.35E-05	1.26E-07	4.18E-08	2.95E-08
3096	1.39E-05	1.32E-07	4.41E-08	3.11E-08
3132	1.43E-05	1.39E-07	4.64E-08	3.27E-08
3168	1.48E-05	1.46E-07	4.87E-08	3.44E-08
3204	1.52E-05	1.53E-07	5.11E-08	3.61E-08
3240	1.56E-05	1.60E-07	5.35E-08	3.78E-08
3276	1.61E-05	1.67E-07	5.60E-08	3.96E-08
3312	1.65E-05	1.74E-07	5.85E-08	4.14E-08
3348	1.70E-05	1.82E-07	6.10E-08	4.32E-08
3384	1.74E-05	1.89E-07	6.36E-08	4.50E-08
3420	1.78E-05	1.97E-07	6.63E-08	4.69E-08

3456	1.83E-05	2.05E-07	6.90E-08	4.88E-08
3492	1.87E-05	2.12E-07	7.17E-08	5.08E-08
3528	1.92E-05	2.20E-07	7.45E-08	5.28E-08
3564	1.96E-05	2.28E-07	7.73E-08	5.48E-08
3600	2.01E-05	2.37E-07	8.01E-08	5.68E-08

Control: represents wild-type (WT) or Control simulations; **50% KD**: 50% knockdown; **75% KD**: 75% knockdown; **99.9% KD**: 99.9% knock down (equivalent to knockout, KO); all KD were done with respect to Control levels.

Simulation Time: in seconds

AU: Arbitrary Unit; used for representation of the relative levels of model output.

Table S5.5 Effect of graded KD of YgiV on biofilm formation: raw data from model simulations (in AU)

Time	Control	YgiV 50% KD	YgiV 75% KD	YgiV 99.9% KD
0	0	0	0	0
36	2.36E-14	2.36E-14	2.36E-14	2.36E-14
72	4.55E-14	4.55E-14	4.55E-14	4.55E-14
108	6.59E-14	6.59E-14	6.59E-14	6.59E-14
144	8.48E-14	8.49E-14	8.49E-14	8.49E-14
180	1.03E-13	1.03E-13	1.03E-13	1.03E-13
216	1.19E-13	1.19E-13	1.19E-13	1.19E-13
252	1.35E-13	1.35E-13	1.35E-13	1.35E-13
288	1.53E-13	1.50E-13	1.50E-13	1.50E-13
324	1.76E-13	1.63E-13	1.63E-13	1.63E-13
360	2.12E-13	1.76E-13	1.76E-13	1.76E-13
396	2.73E-13	1.89E-13	1.89E-13	1.89E-13
432	3.74E-13	2.00E-13	2.00E-13	2.00E-13
468	5.34E-13	2.11E-13	2.11E-13	2.11E-13
504	7.71E-13	2.22E-13	2.22E-13	2.22E-13
540	1.10E-12	2.31E-13	2.31E-13	2.31E-13
576	1.54E-12	2.41E-13	2.41E-13	2.41E-13
612	2.11E-12	2.50E-13	2.50E-13	2.50E-13
648	2.82E-12	2.58E-13	2.58E-13	2.58E-13
684	3.67E-12	2.66E-13	2.66E-13	2.66E-13
720	4.68E-12	2.74E-13	2.74E-13	2.74E-13
756	5.85E-12	2.82E-13	2.82E-13	2.82E-13
792	7.18E-12	2.89E-13	2.89E-13	2.89E-13
828	8.68E-12	2.97E-13	2.96E-13	2.96E-13
864	1.03E-11	3.04E-13	3.03E-13	3.03E-13
900	1.22E-11	3.11E-13	3.09E-13	3.09E-13
936	1.41E-11	3.19E-13	3.16E-13	3.16E-13
972	1.63E-11	3.27E-13	3.22E-13	3.22E-13
1008	1.85E-11	3.35E-13	3.27E-13	3.27E-13
1044	2.09E-11	3.43E-13	3.33E-13	3.33E-13

1080	2.34E-11	3.51E-13	3.38E-13	3.38E-13
1116	2.61E-11	3.60E-13	3.43E-13	3.43E-13
1152	2.88E-11	3.69E-13	3.48E-13	3.48E-13
1188	3.16E-11	3.81E-13	3.54E-13	3.54E-13
1224	3.52E-11	4.12E-13	3.69E-13	3.68E-13
1260	4.32E-11	5.59E-13	4.37E-13	4.30E-13
1296	7.36E-11	1.33E-12	7.53E-13	7.35E-13
1332	2.01E-10	4.94E-12	2.08E-12	2.05E-12
1368	6.63E-10	1.89E-11	6.83E-12	6.82E-12
1404	2.11E-09	6.41E-11	2.12E-11	2.12E-11
1440	5.89E-09	1.85E-10	5.71E-11	5.72E-11
1476	1.42E-08	4.56E-10	1.33E-10	1.33E-10
1512	2.99E-08	9.74E-10	2.69E-10	2.69E-10
1548	5.61E-08	1.84E-09	4.84E-10	4.84E-10
1584	9.58E-08	3.15E-09	7.90E-10	7.89E-10
1620	1.51E-07	4.96E-09	1.19E-09	1.19E-09
1656	2.25E-07	7.30E-09	1.68E-09	1.68E-09
1692	3.18E-07	1.02E-08	2.24E-09	2.24E-09
1728	4.32E-07	1.35E-08	2.86E-09	2.86E-09
1764	5.66E-07	1.73E-08	3.52E-09	3.52E-09
1800	7.20E-07	2.13E-08	4.19E-09	4.19E-09
1836	8.94E-07	2.56E-08	4.85E-09	4.85E-09
1872	1.09E-06	3.00E-08	5.48E-09	5.48E-09
1908	1.30E-06	3.45E-08	6.08E-09	6.08E-09
1944	1.52E-06	3.89E-08	6.63E-09	6.63E-09
1980	1.77E-06	4.33E-08	7.13E-09	7.13E-09
2016	2.02E-06	4.75E-08	7.57E-09	7.57E-09
2052	2.30E-06	5.16E-08	7.97E-09	7.96E-09
2088	2.58E-06	5.55E-08	8.30E-09	8.30E-09
2124	2.88E-06	5.93E-08	8.60E-09	8.60E-09
2160	3.18E-06	6.29E-08	8.85E-09	8.85E-09
2196	3.50E-06	6.64E-08	9.06E-09	9.06E-09
2232	3.83E-06	6.97E-08	9.23E-09	9.23E-09

2268	4.16E-06	7.29E-08	9.38E-09	9.38E-09
2304	4.51E-06	7.59E-08	9.50E-09	9.50E-09
2340	4.86E-06	7.88E-08	9.60E-09	9.60E-09
2376	5.21E-06	8.16E-08	9.68E-09	9.68E-09
2412	5.58E-06	8.43E-08	9.74E-09	9.74E-09
2448	5.95E-06	8.70E-08	9.80E-09	9.79E-09
2484	6.32E-06	8.95E-08	9.84E-09	9.84E-09
2520	6.70E-06	9.20E-08	9.87E-09	9.87E-09
2556	7.09E-06	9.45E-08	9.90E-09	9.90E-09
2592	7.47E-06	9.69E-08	9.92E-09	9.92E-09
2628	7.87E-06	9.92E-08	9.94E-09	9.94E-09
2664	8.26E-06	1.02E-07	9.95E-09	9.95E-09
2700	8.66E-06	1.04E-07	9.96E-09	9.96E-09
2736	9.06E-06	1.06E-07	9.97E-09	9.97E-09
2772	9.47E-06	1.08E-07	9.98E-09	9.98E-09
2808	9.87E-06	1.11E-07	9.98E-09	9.98E-09
2844	1.03E-05	1.13E-07	9.99E-09	9.99E-09
2880	1.07E-05	1.15E-07	9.99E-09	9.99E-09
2916	1.11E-05	1.17E-07	9.99E-09	9.99E-09
2952	1.15E-05	1.20E-07	9.99E-09	9.99E-09
2988	1.19E-05	1.22E-07	9.99E-09	9.99E-09
3024	1.24E-05	1.24E-07	1.00E-08	1.00E-08
3060	1.28E-05	1.26E-07	1.00E-08	1.00E-08
3096	1.32E-05	1.28E-07	1.00E-08	1.00E-08
3132	1.36E-05	1.30E-07	1.00E-08	1.00E-08
3168	1.41E-05	1.33E-07	1.00E-08	1.00E-08
3204	1.45E-05	1.35E-07	1.00E-08	1.00E-08
3240	1.49E-05	1.37E-07	1.00E-08	1.00E-08
3276	1.53E-05	1.39E-07	1.00E-08	1.00E-08
3312	1.58E-05	1.41E-07	1.00E-08	1.00E-08
3348	1.62E-05	1.43E-07	1.00E-08	1.00E-08
3384	1.66E-05	1.45E-07	1.00E-08	1.00E-08
3420	1.71E-05	1.48E-07	1.00E-08	1.00E-08

3456	1.75E-05	1.50E-07	1.00E-08	1.00E-08
3492	1.79E-05	1.52E-07	1.00E-08	1.00E-08
3528	1.84E-05	1.54E-07	1.00E-08	1.00E-08
3564	1.88E-05	1.56E-07	1.00E-08	1.00E-08
3600	1.92E-05	1.58E-07	1.00E-08	1.00E-08

Control: represents wild-type (WT) or Control simulations; **50% KD**: 50% knockdown; **75% KD**: 75% knockdown; **99.9% KD**: 99.9% knock down (equivalent to knockout, KO); all KD were done with respect to Control levels.

Simulation Time: in seconds

AU: Arbitrary Unit; used for representation of the relative levels of model output.

Bibliography for Appendix

Bharatham, N., Bhowmik, P., Aoki, M., Okada, U., Sharma, S., Yamashita, E., Shanbhag, A. P., Rajagopal, S., Thomas, T., Sarma, M., Narjari, R., Nagaraj, S., Ramachandran, V., Katagihallimath, N., Datta, S., & Murakami, S. (2021). Structure and function relationship of OqxB efflux pump from *Klebsiella pneumoniae*. *Nature Communications*, 12(1), 1–12.

Bhowmik, P., Rajagopal, S., Hmar, R. V., Singh, P., Saxena, P., Amar, P., Thomas, T., Ravishankar, R., Nagaraj, S., Katagihallimath, N., Sarangapani, R. K., Ramachandran, V., & Datta, S. (2022). Validated *In Silico* Model for Biofilm Formation in *Escherichia coli*. ACS Synthetic Biology, 11(2), 713–731.

Hutchings, M., Truman, A., & Wilkinson, B. (2019). Antibiotics: past, present and future. Current Opinion in Microbiology, 51, 72–80.

Schmittgen, T. D., & Livak, K. J. (2008). Analyzing real-time PCR data by the comparative C(T) method. Nature Protocols, 3(6), 1101–1108.

Seyer, K., Lessard, M., Piette, G., Lacroix, M., & Saucier, L. (2003). *Escherichia coli* heat shock protein DnaK: production and consequences in terms of monitoring cooking. Applied and Environmental Microbiology, 69(6), 3231–3237.